이학박사학위논문

이리듐 복합체를 이용한 전기화학적 발광 기반의 화학센서의 개발에 관한 연구

Studies on the Development of Electrogenerated Chemiluminescent (ECL) Chemosensors Using Cyclometalated Ir(III) Complex

2017 년 2 월

서울대학교 대학원

화학부 유기화학전공

김 훈 준

Abstract

Studies on the Development of Electrogenerated Chemiluminescent (ECL) Chemosensors Using Cyclometalated Ir(III) Complex

Hoon Jun Kim

Major in Organic Chemistry

Department of Chemistry

Graduate School

Seoul National University

The development of effective chemosensors for detecting small-molecule biotargets has been attracted significant attention in biosensing researches for a long time. Among them, ECL-based chemosensors have several advantages over the conventional analytical techniques such as high sensitivity, good reproducibility, and simple analytic process.

Part I describes the development of fluorescent chemosensors for phosphate-containing anions and their application to ECL. Through these investigations, we confirmed that it is possible to apply the same principles of designing fluorescent chemosensors to ECL analysis. Moreover, these studies also showed the both high sensitivity and simplicity of ECL-based detecting systems.

First, coumarin-based fluorescent chemosensor **1**-2**Zn** was developed for the sensitive sensing of pyrophosphate (PPi). **1**-2**Zn** has bis(2-pyridylmethyl)amine (DPA)-Zn^{2+} complex as a selective recognition sites for PPi and a coumarin fluorophore as a signaling unit. **1**-2**Zn** showed an improved detection limit for PPi compared to that of the naphthyl-based PPi sensor due to the introduction of coumarin dye. In addition, it showed good selectivity for PPi over other anions. Additionally, the new chemosensor **2**-2**Zn** was developed for the discrimination of PPi, ATP, and GTP in aqueous solution. The fluorescence changes of **2**-2**Zn** for each phosphate-containing anions resulted from the structural change (excimer formation) and from photo-induced electron transfer (PET) quenching. **2**-2**Zn** induced a little red-shifted emission change when PPi was added, while it led to enhanced fluorescence and fluorescence quenching without a wavelength shifts upon the addition of ATP and GTP, respectively.

Lastly, the pyrene-based turn-on probe **3** for organophosphate nerve agents was developed. Probe **3** showed highly sensitive and rapid detection capabilities through intramolecular cyclization. In addition to PL study, we carried out the ECL experiment for diethyl chlorophosphate (DCP) for the first time. Though PET quenching efficiency of probe **3** in ECL analysis was lowered due to the oxidation of tertiary amine and the ECL efficiency of pyrene in oxidative reduction process was lower than previously known ECL

luminophores such as $Ru(bpy)_3^{2+}$, it was still possible to detect and quantify the nerve agents with high sensitivity.

In **Part II**, highly sensitive ECL chemodosimeters for small anions based on cyclometalated Ir(III) complex were presented. For high ECL efficiency, phenylisoquinoline (PIQ) unit which has ideal HOMO/LUMO energy levels was selected as a main ligand of Ir(III) complex.

Probe **4** was synthesized for ECL determination of homocysteine, which selectively reacts with Hcy then produces efficient light emission via an electrochemical process. Formyl groups in the main ligands of probe **4** underwent a ring-formation reaction with Hcy, triggering changes in the thermodynamic and photophysical properties of the probe itself. The level of Hcy was successfully monitored in 99.9% aqueous media with a linear correlation between 0-40 μM. The mechanistic explanation has also been suggested based on the electrochemical and theoretical studies. The ECL analytical method would enable point-of-care testing of Hcy levels and is potentially useful for precautionary diagnosis of cardiovascular diseases.

To improve the reactivity between probe **4** and Hcy, probes **5** and **6** were developed, bearing an additional methoxy group as an electron-donating group relative to the original probe **4**. Specifically, probe **5** showed improve properties compared to probe **4**, including a faster reaction time, higher sensitivity, and a higher turn-on ratio. The methoxy groups in probe **5** induced the destabilization of HOMO energy level, which resulted in the improved reaction rate and fully-quenched initial ECL intensity. Probe **5** showed 15-times lower detection limit and 1.9-times faster reaction time as compared to those of probe **4**. This study provided the new strategy with which to design Ir(III)-complex-based molecular probe with high sensitivity and reactivity via the modulation of energy levels with additional substituents.

In the next step, the ECL turn-on probe **7** for cyanide based on Ir(III) complex was designed and synthesized. Probe **7** possessed phenyl isoquionline groups as main ligands with dicyanovinyl groups as the reaction sites for cyanide. In the presence of cyanide, the red ECL emission of probe **7** was greatly increased with good selectivity. Probe **7** showed the linear correlation in the range of 0 to 0.4 mM when the probe concentration was 10 uM in an aqueous solution. We conducted a quantification test through a standard addition analysis in tap water successfully with high reliability and reproducibility. Theoretical studies were carried out for the rational design of probe by predicting the HOMO/LUMO energy levels and electronic distributions.

Lastly, Ir(III) complex **8** was developed for the selective sensing of sulfide. Probe **8** has two different parts of reaction sites, unsaturated acrylated and dinitrobenzenesulfornyl (DNBS) group. The unsaturated acrylate unit reacted with sulfide selectively, inducing phosphorescence and leading to an ECL enhancement in the blue-shifted region. In addition, the DNBS group was well-known PET quencher which could be cleaved by sulfide and other biothiols such as cysteine or homocysteine. Probe **8** showed high sensitivity and good selectivity by given the introduction of two reaction sites in a single molecule.

In **Part III**, the rational design and mechanistic study of Ir(III)-based ECL probes by tuning the LUMO level were presented. Because the LUMO energy level of emitter is closely related to ECL efficiency during TPA coreactant process, it is possible to develop ECL chemosensors in a new way that differs from the methods used to create fluorescent chemosensors by controlling LUMO level with a specific reaction site for the analyte. We selected the

$(ppy)_2Ir(acac)$ complex as a backbone molecule and introduced the specific functional groups to various position of phenylpyridine.

Three ppy-based Ir(III) complexes bearing formyl group as a reaction site for were developed. The formyl groups in pyridine rings strongly stabilized the LUMO level, and the additional substituents served to modulate the HOMO and LUMO levels while maintaining the HOMO-LUMO energy gap of each iridium complex. The OMe_acac complex showed different signal changes in PL and ECL upon the addition of cyanide. An obvious ratiometric change was observed in PL, whereas the ECL signal decreased. The electron-donating methoxy group meta substituted to coordinated Ir(III) metal in OMe_acac made the HOMO and LUMO energy level unstable, leading to the hard generation of excited states during ECL process. In contrast, H_acac and Br_acac showed similar results in terms of PL and ECL dure to their relatively stabilized LUMO levels.

Next, we used boronate groups to Ir(III) complexes as a reaction site for H_2O_2. In this case, the change of HOMO and LUMO levels depended on the substitution location. Probe **9** and **11** showed a phosphorescent change from yellow to green upon the addition of H_2O_2, whereas probe **10** showed a phosphorescent change from yellow to green under an identical condition. Probe **12** showed a phosphorescent change similar to those of **9** and **11**; however, the modification of pyridyl rings had a strong influence on the LUMO energy level, while the modification of the phenyl rings mainly affected to HOMO energy levels. The destabilization of the LUMO level of probe **12** upon the addition of H_2O_2 degraded the ECL efficiency by blocking the ECL electron transfer process. The ECL intensity of **12** was greatly decreased upon the addition of H_2O_2 compared to the results with other probes, demonstraing an outcome similar to that of the PL study. This work provided

the rational design of ECL probe based on ECL quenching route *via* the control of the LUMO level, which is a differentiated strategy for the development of general fluorescence-based probes.

Keywords: Electrogenerated chemiluminescence (ECL), Cyclometalated Ir(III) Complex, Chemosensor, Chemodosimeter, Homocysteine, Cyanide, Sulfide, Hydrogen peroxide (H_2O_2).

Student Number: 2008-22722.

Contents

Abstract ……..ii

Contents…….vii

Part I. Fluorescent and ECL Probes for Phosphate-containing Anions using Organic Luminophore

Background

1. The Fundamentals to Fluorescent molecular probes.....……2

2. The Fundamentals to ECL analysis……..15

Section 1. Highly Sensitive Chemosensor for Dectection of PPi with Improved Detection Limit

1. Introduction……31

2. Results……32

3. Conclusion……..36

4. Experimental Section……..……36

Section 2. Spectroscopic "All at Once" Dicrimination of PPi, ATP, and GTP with Naphthalene-based Fluorescent Probe

1. Introduction……42

2. Results……43

3. Conclusion……47

4. Experimental Section……..……47

Section 3. The Development of Pyrene-based Organophosphorus Nerve Agent Probe and Its ECL Application with High Sensitivity and Facile Synthesis

1. Introduction……52

2. Results……55

3. Conclusion……59

Part II. ECL Chemodosimeters for Small Anions Based on Cyclometalated Ir(III) Complex

Background

1. The examples of ECL-emitting Cyclometalated Ir(III) Complex……..62

2. The Requirements for good ECL-emitting Ir(III) Complex……66

3. ECL Chemosensors Based on Cyclometalated Ir(III) Complex…….69

Section 1. Electrochemiluminescent "Turn-on" Probe for Highly Sensitive and Selective Determination of Homocysteine

1. Introduction……74

2. Results……76

3. Conclusion…….84

4. Experimental Section……..……85

Section 2. The Development of Highly Sensitive ECL Probe for Homocysteine Based Cyclometalated Ir(III) Complex with Enhanced Reactivity by Controlling HOMO Level

1. Introduction……97

2. Results……98

3. Conclusion……..104

4. Experimental Section……..……105

Section 3. Highly Sensitive and Selective Electrochemiluminescent Probe for Cyanide via Chemodosimetric Approach Based on Cyclometalated Iridium(III) Complex

1. Introduction……114

2. Results……116

3. Conclusion……123

4. Experimental Section……134

Section 4. Electrogenerated Chemiluminescence Detection of sulfide with High selectivity based on Double-quenched Cyclometalated Ir(III) Complexes

1. Introduction……133

2. Results……135

3. Conclusion……147

4. Experimental Section……147

Part III. The Rational Design and Mechanistic Study of ECL Probes by Tuning LUMO Energy Level

Background

1. Tuning the HOMO and LUMO Energy Levels of Cyclometalated Ir(III) Complex by main ligand modification……156

Section 1. The Rational Design of ECL Probes for Cyanide based Cyclometalated Ir(III) Complexes by Controlling LUMO Energy Levels

1. Introduction……165

2. Results……168

3. Conclusion……..173

4. Experimental Section……..……174

Section 2. PL and ECL Dual-channel Sensing of Hydrogen Peroxide with Mechanistic Study Based on Borylated Ir(III) Complexes

1. Introduction……176

2. Results……178

3. Conclusion……..184

4. Experimental Section……..……185

References and Notes

1. Part I……..……..……190

2. Part II……..……...……199

3. Part III…….208

Part I

Fluorescent and ECL Probes for

Phosphate-containing Anions using

Organic Luminophore

Background

1. The Fundamentals to Fluorescent Molecular Probes

1.1. Design Principles of Fluorescent Molecular Probes[1]

Fluorescence sensing of chemical and biochemical analytes is an active area of research. This research is being driven by the desire to eliminate radioactive tracers, which are costly to use. Additionally, there is a need for rapid and low-cost testing methods for a wide range of clinical, bioprocess, and environmental applications.[2]

Luminescence can be defined as a spontaneous emission of radiation from an excited state. Depending on the mode of excitation, the terms chemoluminescence, electroluminescence, radioluminecsecnce, sonoluminescence, etc. are used. If we focus our attention in the emission process, the luminescence phenomenon can be classified as fluorescence when the excited molecule results in a new molecule with the same spin multiplicity and as phosphorescence when it involves luminescence with a change in spin multiplicity. What is observed in a fluorescence molecule is that absorption of light at a given wavelength results in an almost instantaneous emission of light at a longer wavelength. Fluorescence detection has been widely used as a versatile tool in analytical chemistry, biochemistry, cell biology, etc.[3] In reaction to the use of fluorescence for sensing or detecting, the principal advantage over other light-based methods such as absorbance is its high sensibility. This is so because the emission fluorescence signal is proportional to the substance concentration whereas in absorbance measurements the substance concentration is proportional to the absorbance,

which is related to the ratio between intensities measured before and after the beam passes through the sample. Therefore, in fluorescence, an increase of the intensity of the incident beam results in a larger fluorescence signal whereas this is not so for absorbance. Fluorescence techniques can measure concentrations even one million times smaller than absorbance techniques.

It is interesting to understand the basis of the nature of the photoinduced processes that are responsible for the photophysical changes upon anion coordination. These effects are specifically related with the use of the binding site-signaling subunit approach, the displacement approach and the chemodosimeter approach.

1.1.1. Photoinduced electron transfer (PET)

This photoinduced process has been extensively studied and widely used for sensing purposes of cations and anions.[4] Fluorescence in a molecule is observed when an excited electron, for instance in the lowest unoccupied molecular orbital (LUMO), goes to the highest occupied molecular orbital (HOMO), releasing the excess of energy as light. Over this scheme, it might

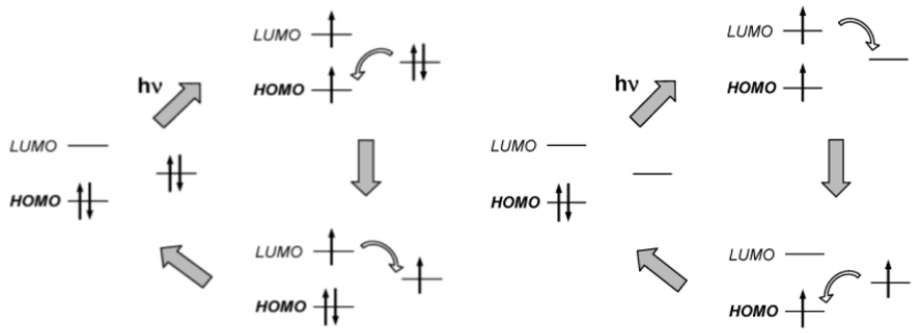

Figure 1-1. PET process with the participation of the HOMO and LUMO of the fluorophore and (left) an external molecular orbital (right) an empty external molecular orbital.

happen that an orbital from another part of the molecule or from another molecular entity could have energy between that of the HOMO and that of the LUMO of the fluorophore. When this "alien" orbital is full (for instance, if we have a donor group), a PET from this full orbital to the HOMO of the fluorophore can take place. A further electron transfer from the LUMO of the fluorophore to the external orbital retrieves the stable ground state. Following this sequence, fluorescence quenching occurs because the transition from the excited to the ground state takes place following a nonradiative path (Figure 1-1). What is macroscopically observed is a decrease of the emission intensity or no fluorescence at all.

A similar process can take place when there is an empty orbital from another part of the molecule or from another molecular entity between both the HOMO and the LUMO of the fluorophore. In this case, a PET from the excited LUMO to the empty orbital can occur, followed by a further electron transfer from this orbital to the HOMO of the fluorophore. Again, deexcitation occurs without radiation and fluorescence quenching is observed (Figure 1-2).

The design of anion chemosensors tries to take advantage of such PET effects in such a way that the presence of the anion should induce the appearance or the removal of energy levels between the HOMO and the LUMO of the fluorophore inducing quenching or enhancement of the fluorescence emission.

1.1.2. Electronic Energy Transfer (EET)

Another mechanism that may be responsible for the fluorescence quenching by certain molecular entities is the EET.[4] When the external molecular group has some empty or half-filled energy levels between the

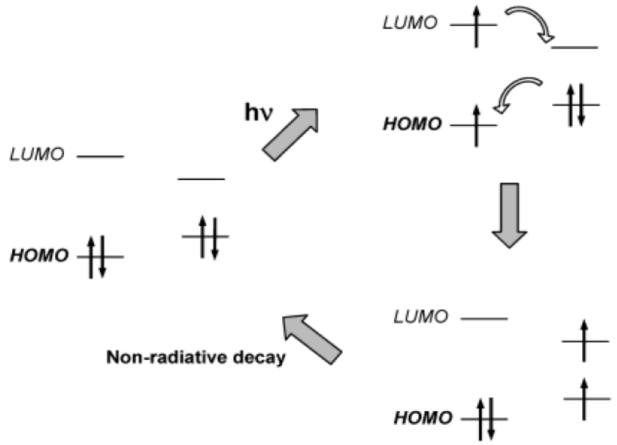

Figure 1-2. EET process with the participation of the HOMO and LUMO of the fluorophore and an external molecular orbital.

HOMO and the LUMO of the fluorophore, a simultaneous exchange of two electrons (from the LUMO to the foreign orbital and from the foreign orbital to the HOMO) can occur (Figure 1-2). The double electron exchange restores the fluorophore to its ground state following a nonradiative process therefore resulting in a fluorescence quenching. The occurrence of this double and simultaneous electron transfer requires a close contact between the fluorophore and the molecular group. Thus, flexible linkers may favor the occurrence of an intramolecular energy transfer process of this type.

1.1.3. Monomer-Excimer Formation

A phenomenon that can be observed when using fluorophores is the formation of excimers. An excimer can be defined as a complex formed by interaction of a fluorophore in the excited state with a fluorophore of in the excited state with a fluorophore of the same structure in the ground state.[4b] An important aspect is that the emission spectrum of the excimer is red-shifted with respect to that of the monomer, and in many cases, the dual emission of

the monomer and the excimer is observed. Therefore, excimer formation or excimer rupture upon anion addition results in anion sensing by simple monitoring of the emission excimer band. In general, it is assumed that flat highly π-delocalized systems such as pyrene and anthracene show greater tendency to form excimers. An additional requirement for excimer formation is that two monomers need to be in close proximity in order to give stacking interactions and the molecular excimer state. Figure 1-3 shows an example of anion-induced excimer formation in which anion coordination favors the

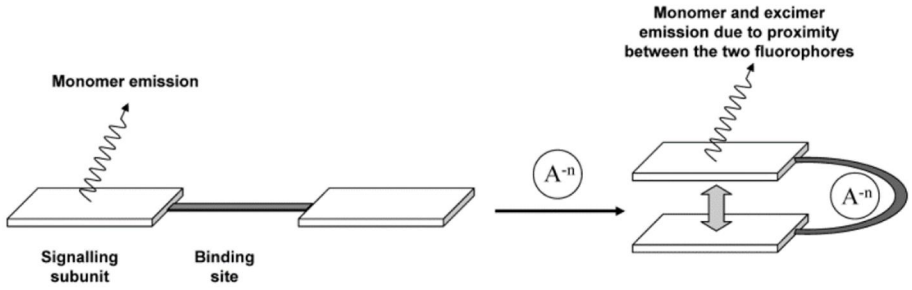

Figure 1-3. Receptor composed of a flexible coordinating subunit and two "flat" fluorophores. Coordination with an anion induced spatial proximity between the two fluorophores and dual emission from the monomer and the excimer.

proximity between two fluorophores.

1.1.4. Conformational Restriction Effect

Although there are doubts of the real existence of this effect, it has been many times employed to justify fluorescence enhancement upon anion coordination. As a consequence of the anion coordination, the rigidity of the formed complex increases making the nonradiative decay from the excited state less probable; consequently, the emission intensity increases.[5]

1.1.5. Förster Resonance Energy Transfer (FRET) [6]

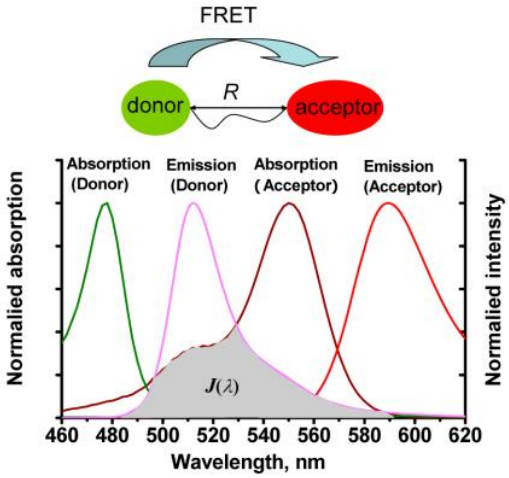

Figure 1-4. Schematic of Förster resonance energy transfer (FRET) process

FRET is a nonradiative process in which an excited dye donor trnasfers energy to a dye acceptor in the ground state through long-range dipole-dipole interactions (Figure 1-4). To design small-molecule based FRET ratiometric fluorescent probes, it is a prerequisite to formulate a FRET energy transfer platform, which consists of an energy donor, a linker, and an energy acceptor. The donor emission spectrum should have reasonable overlap with the acceptor absorption spectrum, and the HOMO and LUMO energy levels of the acceptor should be located within those of the donor to avoid quenching of the acceptor fluorescence by PET. Furthermore, the additional points should be considered for rational designs of probe: (i) the absorption spectrum of the donor should be well separated from that of the acceptor to ensure independent excitation at the absorption wavelengths of the donor and acceptor, respectively; (ii) the emission spectrum of the donor should be resolved from that of the acceptor for high accuracy in the measurement of fluorescence intensity ratios; (iii) the donor fluorophore and the acceptor dye should have comparable brightness, which may impart two well-separated

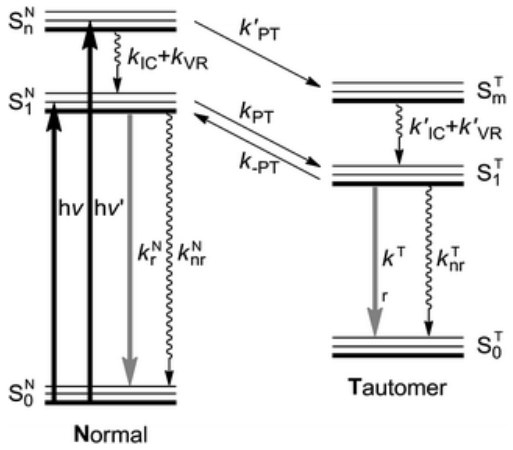

Figure 1-5. Schematic representation of the energy levels describing the formation of the tautomer (T) in the S^T_1 excited state caused by excitations into the S^N_1 and S^N_n states of the normal (N) form.

emission bands with comparable intensities before and after interaction with an analyte; (iv) appropriate linkers should be selected to avoid static fluorescence quenching due to close contact of donor and acceptor dyes in aqueous environment; (v) a near perfect energy transfer efficiency should be achieved in the energy transfer platform.

1.1.6. Excited State Proton Transfer (ESPT)

The strategy of linking a fluorophore with emission from an internal charge transfer (CT) excited state to an ion-binding domain, while widely used for cation sensing, has been rarely exploited for anion sensing.[7] Anion binding close to the fluorophore could lead to the stabilization of positive charge developed in the fluorophore excited state and to the opening of another fluorescence emission channel through intermolecular or intramolecular excited state proton transfer (ESPT) (Figure 1-5).[8]

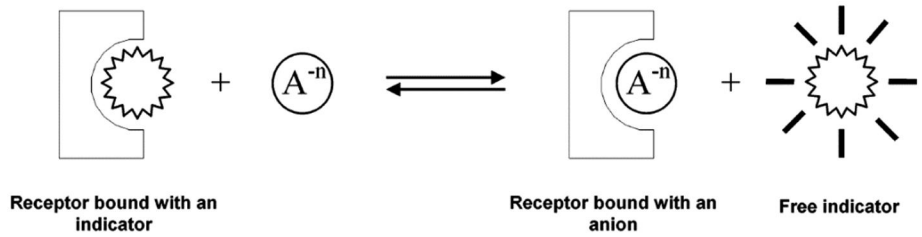

Figure 1-6. Anion chemosensors based on the displacement approach.

1.1.7. Displacement Approach

This approach involves the use of binding sites and signaling subunits. However, in this case, both subunits are not covalently attached but form a coordination complex (molecular ensemble). Then, when a target anlyte is added to the solution containing the binding site-signaling unit ensemble, there is a displacement reaction; the binding site coordinates the analyte whereas the signaling subunit returns to the solution retrieving its non-coordinated spectroscopic behavior (Figure 1-6). If the spectroscopic characteristics of the signaling subunit in the molecular ensemble are different to those in its non-coordinated state, then the anion binding process is coupled to a signaling event.[9]

1.1.8. Chemodosimetric Approach

This approach involves the use of specific chemical reactions (usually irreversible) induced by the presence of target anions that are coupled to a color or emission variation.[10] If the chemical reaction is irreversible, the use of the term chemosensor cannot strictly be used and we will refer to these

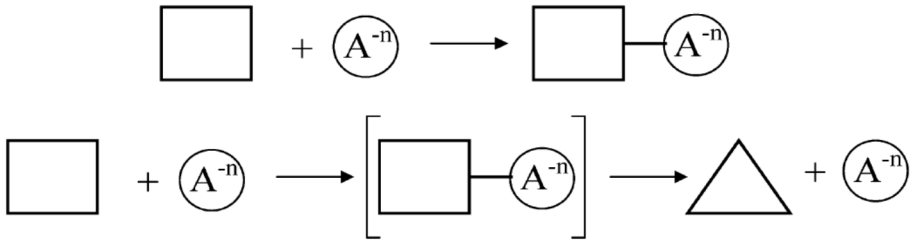

Figure 1-7. The schematic of Chemodosimeter. In the first sequences, the anion react with the chemodosimeter and remains covalently attached, and in the second sequence, the anion catalyzes a chemical reaction.

systems as chemodosimeters. The main difference between the reaction-based and more classic supramolecular-predicated approaches is that in the former the molecular specificity is derived from an analyte-specific reaction, rather than via anlayte-receptor complementarity. Currently, the field of reaction-based probes is still in its infancy. Nonetheless, it is already apparent that reaction-based sensory systems need to fulfill at least two key design requirements: (i) operate with high selectivity; (ii) produce products that can be used as a marker for the analyte in question.

1.2. Chemosensors for phosphate-containing analytes

1.2.1. Chemosensors for pyrophosphate (PPi) [11]

Pyrophosphate (PPi) is a biologically important anion produce by ATP hydrolysis under cellular conditions.[12] PPi is involved in a range of bioenergetic and metabolic processes such as gene duplication, gene

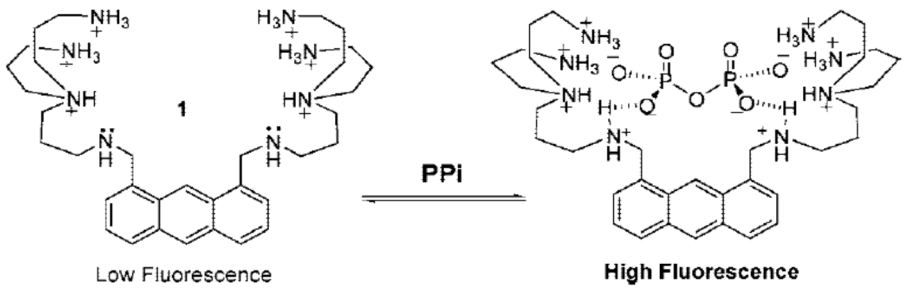

Figure 1-8. Fluorescent chemosensor for PPi.

transcription and signal transduction.[13] Additionally, PPi is closely related to diseases: Accumulations of calcium pyrophosphate dihydrate crystals are frequently found in patients with osteoarthropathy or psuedogout.[14]

The design of PPi chemosensors are mostly based on the supramolecular interaction between PPi and the recognition sites. PPi sensing normally requires selectivity versus other phosphate-containing biomolecules such as ATP and other NTPs in aqueous solution. So far, lots of PPi chemosensor have been developed, most of which are based on strong binding affinity between metal ions, such as Zn^{2+}, Cd^{2+}, and Cu^{2+}, and PPi. A. W. Czarnik et al. reported anthracene based chemosensor with polyamine unit as a recognition

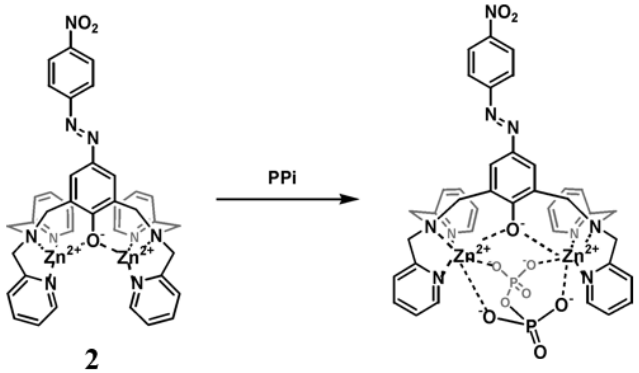

Figure 1-9. Azophenol based colorimetric probe for PPi.

site for PPi in a 100% aqueous condition.[15] Probe **1** shows dynamic fluorescent turn-on property in the presence of PPi. A real-time assay of PPi catalyzed by inorganic pyrophosphatase was also carried out using this fluorescent probe. (Figure 1-8)

Bis(2-pyridylmethyl)amine (DPA)-Zn^{2+} complex is a best well-known recognition unit that shows strong biding with PPi. For example, J.-I. Hong et al. reported an azophenol-based colorimetric probe **2** containing two Zn^{2+}-DPA units, which can selectively recognize PPi ($K_d = 6.6 \times 10^8\ M^{-1}$) among the various anions in water (Figure 1-9).[16]

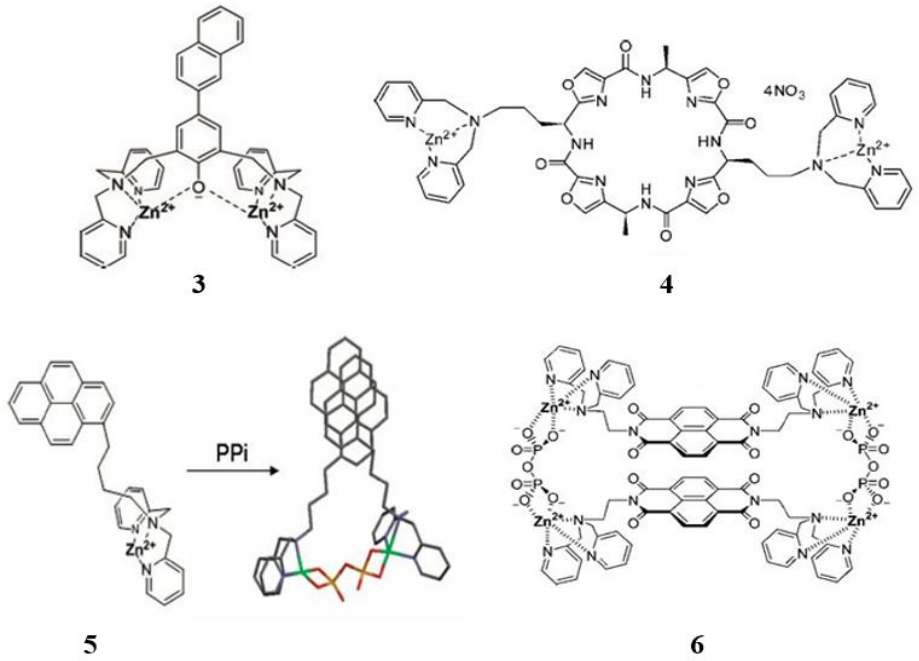

Figure 1-10. Naphthalene based fluorescent chemosensor **3** and other fluorescent chemosensors based Zn-DPA complex **4-6**.

In 2004, J.-I. Hong et al. reported another type of Zn^{2+}-DPA based PPi sensor based naphthalene fluorophore. A naphthalene derivative exhibited a selective florescence change upon the addition of PPi, as shown Figure 1-10.[17] A slight fluorescent enhancement was observed in the presence of ATP, however, it turned out that probe **3** can detect less than 1 equiv of PPi in the presence of 50- to 250-fold excess amounts of ATP. In addition to these examples, several PPi chemosensors have been reported based on Zn^{2+}-DPA unit, which show good selectivity over NTPs and high association constant.[18-20]

1.2.2. Chemosensors for Organophosphorus (OP) Nerve Agents

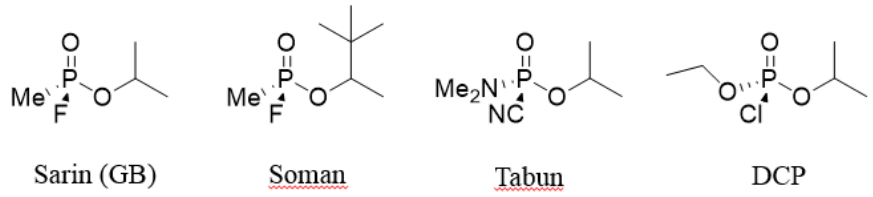

Figure 1-11. G-series nerve agents and simulant (DCP).

Due to the current increase of criminal terrorist attacks via chemical warfare agents (CWAs), there is an increasing interest to detect the lethal chemicals with high reliability in quick time. Among all these CWAs, organophosphorus (OP)-containing nerve agents including Sarin, Soman, and Tabun, also called G-series of nerve agents, are required more attention because of their odorless and colorless properties. Recently, the release of the nerve agent GB (sarin) on the Tokyo subway in 1996 demonstrates the threat posed by these materials. The toxicity of G-series of nerve agents is caused by the inhibition of the acetylcholinesterase (AChE), which is the critical central-nervous enzyme.[19]

There are two strategies to detecting organophosphorus using small molecule probe, supramolecular recognition [20] and chemodosimetric approach. The earliest example of supramolecular chemistry based chemosensor is reported by Van Hooidonk et al. in 1970. [21] They proposed the formation of α-cyclodextrin:GB complex under basic conditions, which was followed by nucleophilic attack by the CD secondary hydroxyl functional groups, resulting in a phosphonylated CD ring and liberation of HF. In the 1980s Desire and Saint-Andre reported on the catalyzed hydrolysis of GD by the b-cyclodextrin, which was postulated by the authors to present a good size matching for complexation.[22] Dimethyl methylphosphonate (DMMP) is also known to provide the recognition sites for G-series nerve agent and their mimics.[23]

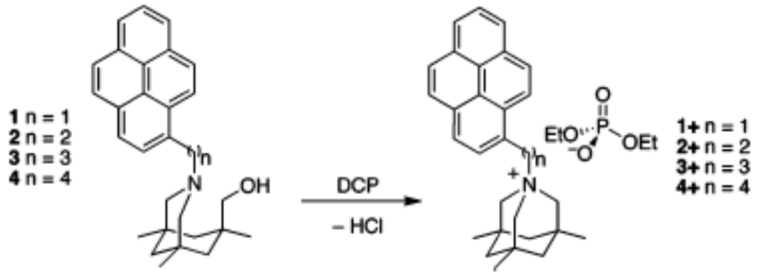

Figure 1-12. Pyrene based fluorescent chemodosimeter for DCP.

More recently, fluorescent chemodosimeters for organophosphate nerve agent have been developed due to their relative facile synthesis and high sensitivity. The design of G-series nerve agents probes based on chemodosimetic approaches is mostly based on the attack of nucleophilic probe to form phosphate ester, which mimics the reaction of AChE with the nerve agent. Rebek Jr. et al. reported the first chemodosimeter for DCP in 2006.[24] Probe **1-4** contains three components: (i) pyrene as the fluorescent acceptor, (ii) Kemp's triacid as the rigid linker, and (iii) primary hydroxyl group as the reaction site with DCP. Probe would be quenched via photoinduced electron transfer by the lone pair electron of tertiary amine and increased fluorescence would be observe upon conversion to its ammonium

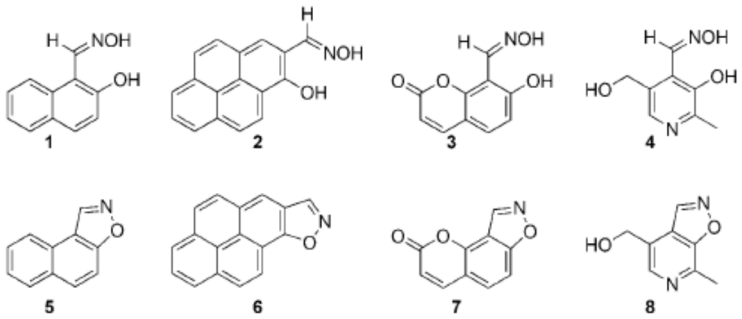

Figure 1-15. Hydroxy oxime based chemodosimeters for OP nerve agents.

salt. They also changed the fluorophore unit to coumarin, which showed similar turn-on fluorescence change.

In 2009, Rebek Jr. et el. reported the oxime-based fluorescent nerve agent probe, which shows the improved properties compared to their previous work.[25] The additional advantage of this oxime-based sensing system is access to more practical water-soluble system in aqueous condition.

2. The fundamentals of ECL analysis

2.1. Introduction to ECL

Electrogenerated chemiluminescence (Electrochemiuminescence, ECL) involves a light emission process through the electron transfer reactions between electrochemically generated radicals in a working electrode.[26] The application of a voltage to the working electrode in the presence of ECL luminophore such as $Ru(bpy)_3^{2+}$, iridium complex, and quantum dots (QDs) or carbon dots (C-Dots) results in strong light emission and allows the detection of biomolecules at very low concentrations. This In comparison to conventional analytical techniques, the ECL assay has a lot of advantages including high sensitivity, wide linear response range, and good reproducibility. For these reasons, ECL-based assays have been widely used in the bioanalytical areas such as immunoassay, DNA analysis, toxic chemical testing in food and water, and warfare agent detection. [27, 28] ECL-based commercial systems have been developed to detect many clinically important analytes including digoxin, α-fetoprotein, thyrotopin, proteins, and antibodies with high sensitivity and selectivity.[26]

Since the first detailed studies by Hercules and Bard et al, in the mid-1960s, [29, 30, 31] over 2000 papers, patents, and book chapters have been published on ECL, ranging from the very fundamental to the very applied.

The studies about ECL can be classified to two large categories. The bigger part is related to the biological applications, such as immunoassays based on antigen-antibody binding or DNA hybridization. In that case, well-known ECL luminophore (e.g. ruthenium complex, iridium complex, QDs, etc.) is used as tagging or labelling unit, which supplies to place of conventional isotope or fluorescent based units. Other researches related to enhance the ECL efficiency has been also studied steadily. The development of new ECL luminophores that have high quantum yield and good solubility is a very challengeable issue to detect the bioanalytes at lower concentrations. Although lots of good ECL luminophores and the modification methods of working electrode with carbon nanotube or other electron-transfer assisting materials already have been developed, it is still very much researches in progress.

Most of these analytical systems are based on $Ru(bpy)_3^{2+}$, representative ECL luminophore. The ECL of $Ru(bpy)_3^{2+}$ was first reported in 1972 in acetonitrile solution (MeCN) in the presence of tetrabutylammonium tetrfluoroborate as a supporting electrolyte. [32] In that case, ECL is generated by alternate pulsing of an electrode potential to form oxidized $Ru(bpy)_3^{3+}$ and reduced $Ru(bpy)_3^{+}$. The formed excited state of $Ru(bpy)_3^{2+}$* then decays to the ground state, producing the same luminescence as obtained from photoluminescence (PL) spectroscopy.

More generally, electrogenerated chemiluminescence (ECL) deal with emission at working electrode in electrochemical cells caused by energetic electron transfer (redox) reactions of electrogenerated species in solution. A typical system would involve an organic solution, acetronitrile (MeCN) in most cases, containing the reactant A, or sometimes containing the two reactants A and D with supporting electrolyte, for example, tetra-n-

butylammonium perchlorate (TBAP) or tetra-n-butylammonium hexafluorophosphate (TBAF). One example of the reaction sequence to generate an excited state and light emission in annihilation mechanism is as follows.

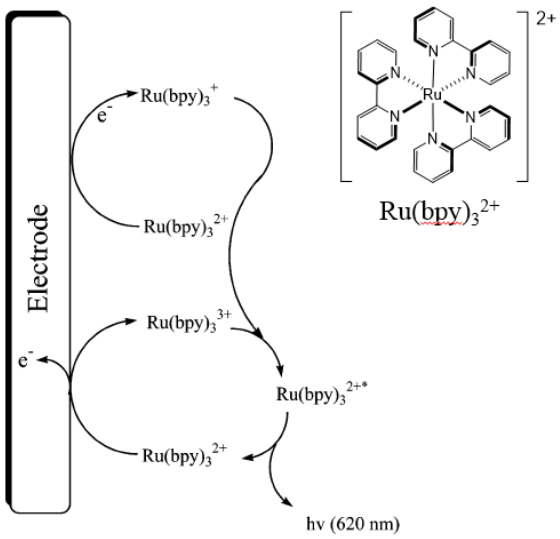

Figure 1-16. Structure of $Ru(bpy)_3^{2+}$ and mechanism for $Ru(bpy)_3^{3+}/Ru(bpy)_3^{+}$ ECL system.

$$A + e^- \rightarrow A^{-\cdot} \text{ (Reduction at electrode) (1)}$$

$$A - e^- \rightarrow A^{+\cdot} \text{ (Oxidation at electrode) (2)}$$

$$A^{-\cdot} + A^{+\cdot} \rightarrow A^* + A \text{ (Excited state formation by annihilation) (3)}$$

$$A^* \rightarrow A + h\nu \text{ (Light emission) (4)}$$

The term electrogenerated chemiluminescence (ECL) was coined to describe this class of reaction [33] and to distinguish it from other systems where light is emitted from an electrode in electrochemical cells.

In addition to ECL process, a number of different ways to emit a light during electrochemical reactions, and reports concerning such emission date

back at least to the 1880s.[34] It is also important to distinguish ECL form other emitting mechanisms (e.g. photoluminescence and chemiluminescence) that undergo highly energetic electron-transfer reactions. However, ECL is only initiated and controlled by switching an electrode voltage.

2.2. Electrochemistry fundamentals for ECL

A brief over view of the electrochemical concepts needs to understand the basis of ECL.[35]

2.2.1. Electrode potential

The standard electrode potential for $A/A^{-\cdot}$, abbreviated $E^0\,(A, A^{-\cdot})$, is the measure with respect to a given reference electrode, based on redox pair O/R.

$$A + e^- \rightarrow A^{-\cdot} \quad (5)$$

$$O + e^- \rightarrow R \quad (6)$$

$$A + R \rightarrow A^{-\cdot} + O \quad (7)$$

For aqueous solution, the standard electrode is the H^+/H_2 couple, with all reactants at unit activity. For practical purposes, other reference electrodes such as Ag/AgCl, Ag/Ag^+, or the saturated calomel electrode (SCE) are usually employed. For non-aqueous solution such as MeCN, DMF, and DCM, the reference redox couple is usually the Fc/Fc^+ couple. When measuring the

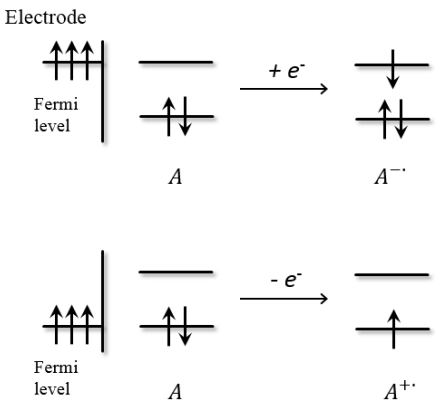

Figure 1-17. Molecular orbital representation of reduction and oxidation

difference of potential between two redox couples, as discussed below, the nature of the reference electrode is not important, so that a quasi-reference electrode, such as a silver wire immersed in the solution, can sometimes be used.

The potential of the couple represents the energy needed at equilibrium to ass an electron to A or to remove an electron from A^-. The more negative reduction potential means harder to reduce A, and the more negative oxidation potential means easier to oxidize A^-. A molecular orbital (MO) scheme of redox process is shown in figure 1-17, where one can identify the energy as that needed to place an electron in the lowest unoccupied MO (LUMO) of A

Similarly, the standard potential $E^0\ (A^{+\cdot}, A)$ of the electrode reaction

$$A^{+\cdot} + e^- \rightarrow A \quad (8)$$

Represents ΔG^0 for the reaction

$$A^{+\cdot} + \mathrm{R} \rightarrow \mathrm{A} + O \quad (9)$$

With respect to the reference electrode based on redox pair O/R, the potential represents the energy needed to remove an electrode from A or to add an electrode to A^+.

The more positive the potential, the more difficult it is oxidized A or the easier it is to reduce A^+. The MO scheme of oxidation process is shown in figure 1-17 identifies this potential as that needed to remove an electrode from highest occupied MO (HOMO) of A.

Of interest in ECL is the ΔG^0 of the reaction

$$A^{+\cdot} + A^{-\cdot} \rightarrow A + A \quad (10)$$

Which is given by

$$\Delta G^0 = -FE^0_{rex} \quad (11)$$

$$E^0_{rex} = E^0(A^{+\cdot}, A) - E^0(A, A^{-\cdot}) \quad (12)$$

The reaction entropy, ΔS^0, can be calculated from the temperature coefficient of the reaction potential :

$$\Delta S^0 = F^{\left(\frac{\partial E^0_{rxn}}{\partial T}\right)_p} \quad (13)$$

For ECL reaction, ΔG^0 is typically in the range of 2-3 eV (193-289 KJ/mol) and $T\Delta S^0$ is small, ≤ 0.1 eV.

2.2.2. Cyclic voltammetry

As a prelude to ECL studies, one usually investigates the electrochemical characteristics of system, and cyclic voltammetry (CV) is a powerful tool for a fast overview. Normally, routine voltammetric experiments are performed using a stationary working electrode, typically Pt or glassy carbon (GC), in organic solution with supporting electrolyte such as tetrabutylammonium perchlorate (TBAP). Starting from an initial potential E_i, a linear potential sweep is applied to this electrode. After reaching a switching potential E_λ, the sweep is reversed and potential returns linearly to its initial value at a scan rate v.[36] The resulting voltammogram shows characteristic peak showing the oxidation and reduction processes in the system in well-defined system, which shows the rapid electron transfer reactions at the electrode surface, stable product of the reaction during CV scanning. In the case of a reversible electrode reaction, the cathodic and anodic peak potentials depend in the following way on the formal potential for one-electron transfer reaction (n=1) when assuming reactant and product have the equal diffusion coefficients (D),

$$E_{pa} - E_{pc} = 2\left(1.109\frac{RT}{nF}\right) \approx 28.5\ mV\ at\ 25℃ \quad (14)$$

The latter relationship is a good indication of the reversibility of the electrode reaction, although some caution is necessary because a more complex electrode reaction may give the same difference.

During the reduction, current increases until it reaches a peak when all A^+ exposed to the surface of the electrode has been reduced to A. In a stirred solution, a Nernst diffusion layer ~10^{-2} cm thick, lies adjacent to the electrode surface. Because diffusion is limited to the narrow Nernst diffusion region, the reacting analytes cannot diffuse into the bulk solution, and therefore Nernstian equilibrium is still maintained. In this case, the peak current can be expressed the following equation,

$$i_p = (2.69 \times 10^5) S D_A^{1/2} V^{1/2} C_A^* \quad (15)$$

Where S is the surface area of the working electrode in cm^2, D is the diffusion coefficient, V is sweep rate, and C_A is the molar concentration of A in the bulk solution.[37] The stability of the products can be assessed from the CV waves. The existence of wave on scan reversal demonstrates that the product $A^{-\cdot}$ formed by reduction of A, is reoxidized on the reverse scan. If $A^{-\cdot}$ were unstable in the time it takes to traverse the wave would be absent.

2.2.3. Potential steps

During ECL experiments, the potential is often stepped (rather than swept)

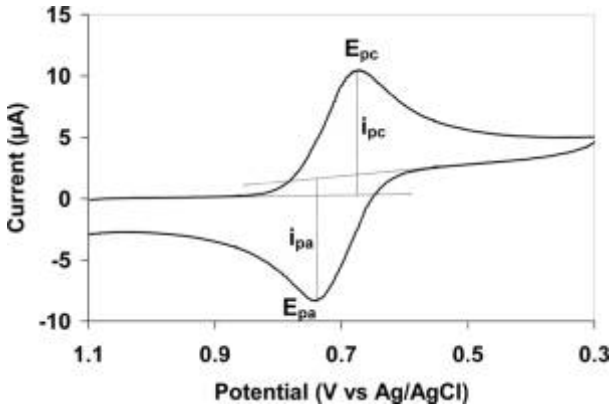

Figure 1-18. Cyclic voltammogram of a single electron oxidation-reduction

between potential where the redox processes occur. A first potential step from a potential where no reaction occurs to one well beyond E_p, produces a current I that decays with time t and follows the Cottrell equation,

$$i = FAC^* D^{\frac{1}{2}}/(\pi t)^{1/2} \quad (16)$$

The current decay with $t^{-1/2}$ represents a growing diffusion layer of formed product, $A^{-\cdot}$, A step toward positive potential to the region where equation (2) occurs is more complicated, because it involves oxidation of both $A^{-\cdot}$ and A and the occurrence of equation (3), and has been treated by digital simulation.

2.3. General reaction mechanisms of ECL

2.3.1. Self-Annihilation ECL

The first detailed studies on ECL involved electron-transfer reactions between an oxidized and a reduced species, both of which were generated at an electrode by alternate pulsing of the electrode potential. This process is

possible when the ECL emitter (A) can electrochemically produce both a sufficiently stable radical cation and anion. The general annihilation mechanism is outlined below.

$$\mathrm{A} + e^- \rightarrow A^{-\cdot} \text{ (Reduction at electrode) (1)}$$

$$\mathrm{A} - e^- \rightarrow A^{+\cdot} \text{ (Oxidation at electrode) (2)}$$

$$A^{-\cdot} + A^{+\cdot} \rightarrow A^* + \mathrm{A} \quad \text{(Excited state formation by annihilation) (3)}$$

$$A^* \rightarrow \mathrm{A} + h\nu \text{ (Light emission) (4)}$$

Depending on the energy available in an ion annihilation, the produced R^* could be either the lowest excited singlet state species ($^1R^*$) or the triplet state species ($^3R^*$). The energy available can be calculated from the electrode potentials as defined in below.

$$-\Delta H_{ann} = E_p(R, R^{+\cdot}) - E_p(R, R^{+\cdot}) - 0.16\ eV \quad (17)$$

Where $-\Delta H_{ann}$ is the enthalpy for ion annihilation, E_p is the peak potential for the electrochemical oxidation or reduction, and 0.1 eV is the entropy approximation term (TDS) at 25 ℃. If the estimated energy $(-\Delta H_{ann})$ is larger than the required energy to produce the lowest excited singlet state from the ground state, it is possible to directly generate $^1R^*$, and this system is called the energy-sufficient system or the S-route.

$$\text{S-route : } R^{+\cdot} + R^{-\cdot} \rightarrow R + {}^1R^* (18)$$

In contrast, if $-\Delta H_{ann}$ is smaller than E_s but larger than the triplet state energy (E_t), $^3R^*$ is initially formed, and then $^1R^*$ can be formed by the triplet-triplet annihilation. This is called the energy-deficient system or the T-route. However, the efficiency of direct emission from $^3R^*$ is usually very poor in a solution phase,

especially at low concentration, because of the long radiative lifetime of $^3R^*$ and its quenching by radical ions or other species, such as molecular oxygen.

$$\text{T-route}: \ R^{+\cdot} + R^{-\cdot} \rightarrow R + \ ^3R^* \quad (19)$$

$$^3R^* + \ ^3R^* \rightarrow R + \ ^1R^* \quad (20)$$

If $-\Delta H_{ann}$ is nearly marginal to E_s, The T-route can contribute to the formation of $^1R^*$ in addition to the S-route and it is called the ST-route. Although the T-route is inefficient in the presence of considerable S-route, it is still possible for the ST-route to exist.

It is also possible to use two different precursors to generate ECL, For example, the electron-transfer reaction and subsequent chemiluminescence between the anion radical of 9,10-diphenylanthracene (DPA) and the cation radical of N,N,N',N'-tetramethyl-p-phenylenediamine (Wurster;s Blue, TMPD) in dimethylformamide.

$$\mathrm{A} + \ e^- \rightarrow \ A^{-\cdot} \quad (21)$$

$$\mathrm{D} - \ e^- \rightarrow \ D^{+\cdot} \quad (22)$$

$$A^{-\cdot} + D^{+\cdot} \rightarrow \ A^* + \ \mathrm{D} \ (\text{or A} + \ D^*) \quad (23)$$

$$A^* (\text{or } D^*) \ \rightarrow \ \mathrm{A} \ (\text{or D}) + h\nu \quad (24)$$

2.3.2. Coreactant ECL

A coreactant is a compound that can produce a reactive intermediate (a strong reducing or oxidizing agent) by a reaction following the electrochemical or chemical electron transfer reaction. Although annihilation ECL process remains important for the exploration of fundamental properties of ECL systems and the development of ECL-based light-emitting devices,

annihilation based ECL mechanism has a limitation to applicate to bioanalysis by the relatively small potential window and poor ECL quantum yield in aqueous solutions, which generally prohibits the direct electrochemical generation of both the oxidized and reduced radical species. To overcome this limitation, Bard and co-workers developed coreactant ECL system using oxalate ($C_2O_4^{2-}$) as a reducing agent.[38,39] When $C_2O_4^{2-}$ is oxidized, it produces the strong reducing agent, $CO_2^{-\cdot}$ $(E^0 = -1.9V\ vs\ NHE)$, and CO_2. For example, water-soluble luminophore such as $Ru(bpy)_3^{2+}$ could be oxidized in the presence of oxalate, with the subsequent reaction between $Ru(bpy)_3^{2+}$ and $CO_2^{-\cdot}$ generating the radiative excited state.

$$Ru(bpy)_3^{2+} - e^- \rightarrow Ru(bpy)_3^{3+} \quad (25)$$

$$Ru(bpy)_3^{3+} - C_2O_4^{2-} \rightarrow Ru(bpy)_3^{3+} + C_2O_4^{-\cdot} \quad (26)$$

$$C_2O_4^{-\cdot} \rightarrow CO_2^{-\cdot} + CO_2 \quad (27)$$

$$Ru(bpy)_3^{3+} - CO_2^{-\cdot} \rightarrow Ru(bpy)_3^{2+*} + CO_2 \quad (28)$$

Tri-n-propylamine (TPA) is even more effective coreactant for oxidative ECL process.[40] Oxidation of TPA and related amines initially produces the corresponding aminium radical cation, which rapidly deprotonates to form a highly reductive α-amino alkyl radical,[41]

$$TPA - e^- \rightarrow TPA^{+\cdot} \quad (29)$$

$$TPA^{+\cdot} \rightarrow TPA^{\cdot} + H^+ \quad (30)$$

Figure 1-19 shows a comprehensive light-producing reaction pathways of the $Ru(bpy)_3^{2+}$-TPA ECL system.[40] These principles also can be extended to related ECL systems including other metal complexes or alternative coreactants.

The key reaction steps for general ECL lumionphores with TPA is as follows.

$$\mathrm{M} - e^- \rightarrow M^{+\cdot} \quad (31)$$

$$\mathrm{TPA} - e^- \rightarrow TPA^{+\cdot} \quad (32)$$

$$M^{+\cdot} + TPA \rightarrow M + TPA^{+\cdot} \quad (33)$$

$$TPA^{+\cdot} \rightarrow TPA^{\cdot} + H^+ \quad (34)$$

$$M^{+\cdot} + TPA^{\cdot} \rightarrow M^* + side\ product \quad (35)$$

$$M + TPA^{\cdot} \rightarrow M^{-\cdot} + side\ product \quad (36)$$

$$M^{-\cdot} + M^{+\cdot} \rightarrow M^* + M \quad (37)$$

$$M^{-\cdot} + TPA^{+\cdot} \rightarrow M^* + \mathrm{TPA} \quad (38)$$

$$M^* \rightarrow M + hv \quad (39)$$

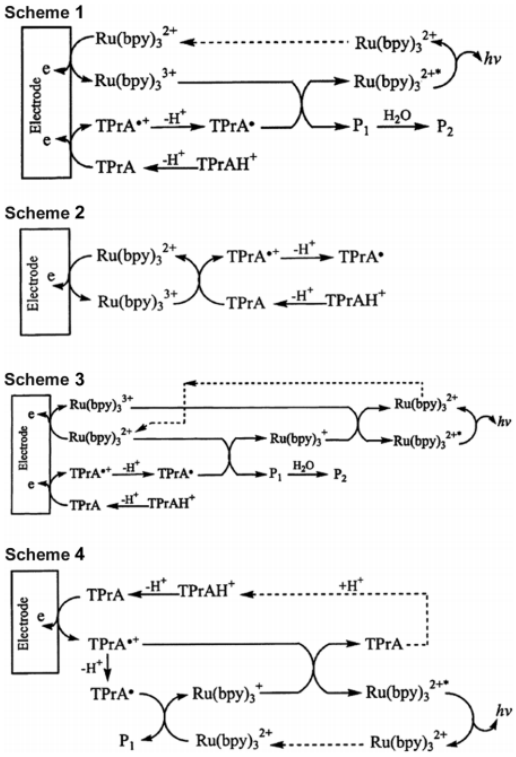

Figure 1-19. The mechanism of coreactant ECL for $Ru(bpy)_3^{2+}$ and TPA.

Because the phosphorescence and ECL emission are nearly identical in most cases, the emission process in ECL involves the MLCT state of Ru(II) or Ir(III) complexes. This state is formed by the electron transfer from TPA radical to ligands of metal complexes. Numerous other tertiary amine based coreactant have been developed such as DBAE (2-(dibutylamino)ethanol)[42], there are many attempts to enhance the coreactant efficiency.

Reductive-oxidative coreactants are also have been studied and showed the good ECL efficiency. Peroxydisulfate ($S_2O_8^{2-}$) [43] is representative coreactant in reduction ECL process, which produces the strong oxidant $SO_4^{-\cdot}$, which then undergoes an electron transfer reaction with an ECL luminophore such as $Ru(bpy)_3^{2+}$ to emit light.

$$Ru(bpy)_3^{2+} + e^- \rightarrow Ru(bpy)_3^{+} \quad (40)$$

$$S_2O_8^{2-} + e^- \rightarrow SO_4^{-\cdot} + SO_4^{2-} \quad (41)$$

$$Ru(bpy)_3^{2+} + SO_4^{-\cdot} \rightarrow Ru(bpy)_3^{2+*} + SO_4^{2-} \quad (42)$$

To be a good coreactant, the following conditions should be met: (i) the coreactant should be reasonably soluble in a solvent because the ECL intensity is generally proportional to the concentration of it, (ii) the electrochemically generated reactive intermediate species during oxidation or reduction CV scanning process should be stable enough for the duration of the ECL experiment, (iii) the coreactant should be easily oxidized or reduced with the ECL emitter at or near the electrode and undergo a rapid following chemical reaction to form a reactive intermediate, (iv) the rate of a reaction between the intermediate and the radical ion of an ECL emitter must be rapid, (v) the coreactant and its intermediate should have inert or weak quenching effect on ECL, (vi) the coreactant itself should not produce any light emission., and finally (vii) the appropriate energy levels of the coreactant and formed oxidative or reductive radical species compared to ECL luminophore for the smooth electron transfer reactions.

2.4. ECL luminophores

2.4.1. Organic ECL luminophores

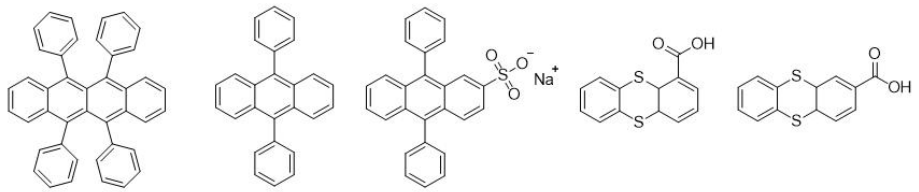

Figure 1-20. ECL-active polyaromatic hydrocarbons (PAHs)

The early studies for ECL involved polyaromatic hydrcarbons (PAHs) based organic systems such as anthracene and rubrene.[44] However, these compounds have some limitations to use the practical applications, which is their poor solubility in aqueous solution and the need for rigorously purified and deoxygenated non-aqueous solvents. 9,10-Diphenylanthracene (DPA) is the one of most well-known ECL emitter which shows good ECL property during annihilation process. To overcome the solubility problem, several anthracene derivatives including 9,10-diphenylanthracene-2-sulfonate (DPAS) and 1- and 2-thianthrenecarboxylic acid (1- and 2- THCOOH) have been developed and ECL behaviors of them were studied in aqueous solution using TPA as coreactant.[45] Fluorene-substituted PAHs have been investigated with enhanced ECL efficiency and stability.[46] Derivatives of DPA, pyrene, and anthracene were synthesized by using fluorine as a capping agent. These derivatives show the enhanced ECL properties due to their stable radical species.

More recently, non-PAHs have also been studied. For example, perylene diimide radical anion and cations were generated by pulsing the applied

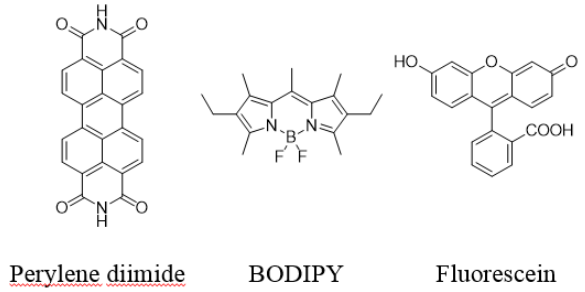

Figure 1-21. ECL-active fluorophores (Non-PAHs)

potential between the parent compound's first oxidation and reductive waves. [47] Especially, BODIPY (boron dipyrromethene) dyes also have been studied steadily. [48] They are unique materials with spectroscopic and electrochemical properties comparable to those of PAHs. Completely substituted BODIPY dyes produce stable, fairly intense ECL signals by both annihilation and oxidative reduction coreactant mechanisms. Besides, the ECL behaviors of widely used fluorophores such as fluorescein and rhodamine were studied under conventional cyclic voltammetric conditions. However, some fluorophores, for example coumarin and cyanine derivatives, could not show ECL properties due to their electrochemical instability or inadequate HOMO/LUMO energy levels despite their extraordinary PL quantum yield.

2.4.2. Inorganic ECL luminophores

The complexes and clusters containing Ag, Al, Au, Cd, Cr, Cu, Eu, Hg, Ir, Mo, W, Os, Pd, Pt, Re, Ru, Si, Tb, and Tl have been found to show ECL property. Among them, $Ru(bpy)_3^{2+}$ has been proved the first and most important inorganic complex to shows good ECL behavior. Many studies and applications to bioanalysis were performed based on this ruthenium complex. For examples, the first report of ECL with a coreactant in aqueous solution involved $Ru(bpy)_3^{2+}$. [49] $Ru(bpy)_3^{2+}$ has a number of advantages including its strong luminescence and solubility in a variety of aqueous and non-aqueous solvents at room temperature and its ability to undergo reversible one-electron transfer-reactions at relatively mild potentials. The mechanisms of $Ru(bpy)_3^{2+}$ based ECL have been extensively studied by many research groups,[50] especially it shows intense ECL emission with oxidative-reduction coreactant pathway at low concentration. Based on these well-defined studies, there has been widely used in bioanalytical applications. Other ruthenium complexes

such as $Ru(bpz)_3^{2+}$, $Ru(phen)_3^{2+}$, and $Ru(terpy)_3^{2+}$ also exhibit strong ECL emission.[51]

Cyclometalated Ir(III) complexes have attracted significant attention currently with superior ECL efficiencies and diverse emission colors compared to ruthenium complexes. Although the first study using $Ir(ppy)_3$ shows only a weak emission via annihilation, there has a large improvement through many studies about applied potential and solvent conditions. Furthermore, some red-emitting Ir(III) complexes such as $(pq)_2Ir(acac)$, $(pq)_2Ir(tmd)$, and $(piq)_2Ir(acac)$ showed higher ECL efficiencies in acetonitrile than that of $Ru(bpy)_3^{2+}$.[51] Francis et al. reported the blue-emitting Ir(III) complexes that have excellent ECL properties by controlling the HOMO/LUMO energy levels. [52]

Osmium polypyridine complexes have also been studied. Because osmium systems are more photostable than their ruthenium analogues and usually oxidize at less anodic potentials, the development of osmium-based ECL bioanalysis is very useful. The first report of ECL in osmium complex was $Os(Phen)_3^{2+}$ using $S_2O_8^{2-}$ reduction, and after then other osmium complexes such as $Os(bpy)_3^{2+}$ and $Os(phen)_2(dppene)^{2+}$ in aqueous and non-aqueous solutions. [53]

Quantum dots (QDs) [54] and carbon dots (C-dots) [55] have aroused interest for ECL studies. Many studies proved the good ECL properties of QDs including high ECL efficiency, good water solubility, and electrochemical stability. QD-based ECL immunoassays also have been reported steadily in recent years, which have emerged as a powerful substitute for $Ru(bpy)_3^{2+}$. The ECL emission of C-dots produced from the electrochemical oxidation of graphite was observed, and improved ECL efficiency was observed at single-walled carbon nanotube (SWCNT) modified working electrode.

Section 1.

Highly Sensitive Chemosensor for Detection of PPi with Improved Detection Limit

1.1. Introduction

The development of chemosensors for the detection of biologically significant anions is a growing research topic.[55] Chemosensor-based detection of pyrophosphate ($P_2O_7^{4-}$, PPi) is particularly important as PPi is involved in a range of bioenergetic and metabolic processes such as gene duplication, gene transcription and signal transduction.[56] Additionally, PPi is closely related to diseases: Accumulations of calcium pyrophosphate dihydrate crystals are frequently found in patients with osteoarthropathy or psuedogout.[57]

Approximately, 3 and 6 μM of PPi is normally present in human plasma and serum, respectively.[58] Thus, the PPi in biological samples can be detected using known PPi chemosensors because these sensors respond to micromolar concentrations of PPi. [59, 60, 61]

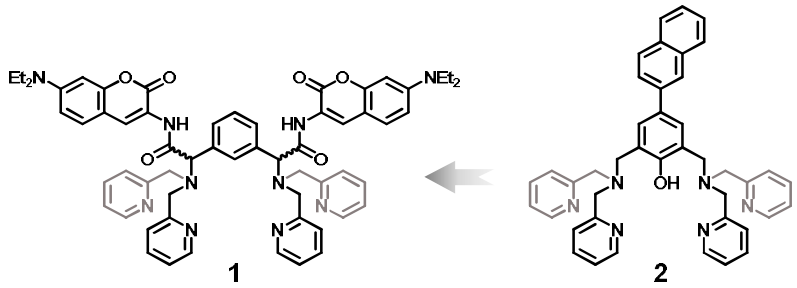

Scheme 1-1. Introduction of two coumarin units to improve the detection limit of PPi.

However, there is a need to develop highly sensitive PPi sensors with improved detection limits because enzymatic reactions that involve the release of this anion often result in subtle changes in the PPi concentration. Further, the improvement of the detection limit results in efficient pyrosequencing, which is one of the most promising methods of DNA sequencing. [16, 17, 62] In this communication, we propose a fluorescent chemosensor (1·2Zn) for the detection of PPi; the chemosensor has an improved detection limit as compared to that of existing PPi sensors and also shows selectivity for PPi over other anions including phosphate anions in aqueous media.

Generally, anion sensors consist of two basic elements.[55] The first one is the binding moiety, which overcomes strong hydration in an aqueous medium. The other element converts these binding-induced changes into optical signals via chromophores or fluorophores. Previously, we were able to improve the binding affinity of this sensor to PPi by more than hundred times that of 2·2Zn to PPi by introducing additional hydrogen bonds to this sensor.[61d] Although the introduction of additional hydrogen bonds results in a notable increase in the binding affinity, introducing a high quantum yield signaling motif is expected to increase the sensitivity of PPi chemosensors, leading to an improved detection limit. Therefore, two coumarin units were introduced in place of the naphthyl group used in 2·2Zn to amplify the fluorescent response caused by the addition of PPi (Scheme 1-1).

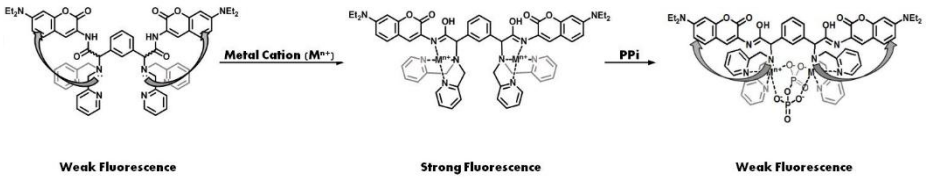

Figure 1-22. Proposed mechanism for controlling the fluorescence by blocking and restoring PET.

1.2. Result and Discussion

The synthesis of compound **1** is outlined in Scheme 2. The conversion of 1,3-phenylenediacetic acid to its acyl chloride facilitated α-bromination. The resulting halogenated acyl chloride was then hydrolyzed to the corresponding carboxylic acid, which was converted to its methyl ester product (compound 4). Compound **3** was obtained through the reaction between compound **4** and di-(2-picolyl)amine in the presence of potassium carbonate and potassium iodide. Hydrolysis of compound **3** followed by amide bond formation between the resulting diacid and 2 equiv of 3-amino-7-diethylaminocoumarin furnished compound **1**.

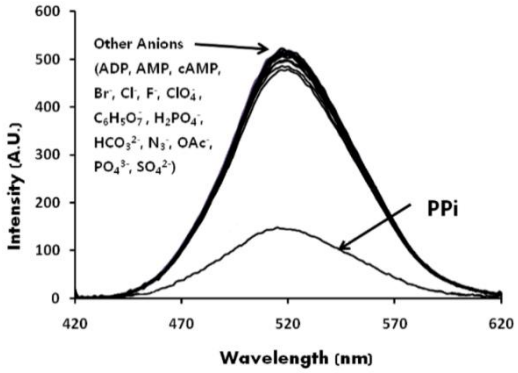

Figure 1-23. Fluorescence emission spectra of **1**·2**Zn** (10 μM) on addition of various anions (20 μM, sodium salts) in an aqueous HEPES buffer solution (10 mM, pH 7.4).

The effect of metal coordination on the emission spectra was measured through fluorescence spectroscopy (Supporting Information): By blocking the photo-induced electron transfer (PET), complexes with zinc and cadmium cations showed strong fluorescence emissions compared to the fluorescence emissions of other metal complexes.[64] Blocking of the PET process through coordination of a d^{10}-metal with an amine (reductive quencher) is commonly observed in fluorescence chemosensor studies. (Figure 1-22).[65] We expected that the addition of PPi would weaken the metal coordination with the

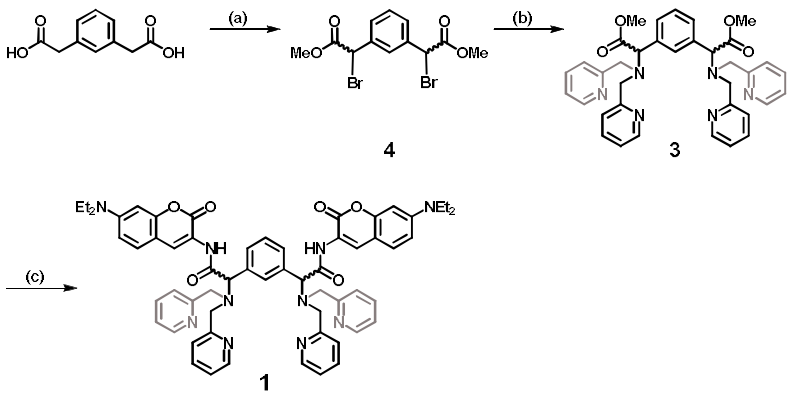

Scheme 1-2. (a) i. $(COCl)_2$, DMF, CH_2Cl_2 ii. Br_2, benzene iii. H_2O iv. cat. H_2SO_4, MeOH (b) di-(2-picolyl)amine, K_2CO_3, KI, MeCN (c) i. NaOH, MeOH/H_2O ii. 3-amino-7-diethylaminocoumarin, EDC-HCl, pyridine/ CH_2Cl_2

reductive quencher and lead to a significant change in the fluorescence intensity of **1**·2Zn and **1**·2Cd by restoring the PET pathway (Figure 1-22).

As expected, we found that the fluorescence of the complex (**1**·2Zn) between **1** and zinc cations was significantly reduced on the addition of PPi (Figure 1-23). The effect of other anions on the emission spectra of **1**·2Zn was examined by adding various anions to **1**·2Zn in a n aqueous 2-[4-(2-hydroxyethyl)-1-piperazinyl]ethanesulfonic acid (HEPES) buffer solution (0.01 M, pH 7.4) at 25°C.[12] However, other anions, including those of phosphate, showed no detectable changes in the fluorescence of **1**·2Zn (Figure 1-23). These results suggest that **1**·2Zn has a high selectivity for PPi over other anions.

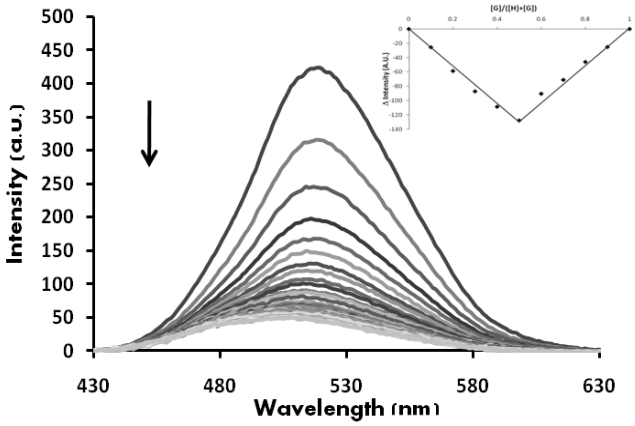

Figure 1-24. Change in the fluorescence of **1**·2Zn (10 μM) upon addition of PPi (0~33 μM) in aqueous HEPES buffer solutions (10 mM, pH 7.4).

To measure the change in the fluorescence of **1**·2Zn upon the addition of PPi, fluorescence titration was carried out in an aqueous HEPES buffer solution (10 mM, pH 7.4, 25°C). On addition of PPi, fluorescence decreased by a factor of 9.8 and was saturated at 3.3 equiv (Figure 1-24). 1:1 complexation between **1**·2Zn and PPi was confirmed by Job's plot (Figure 1-24 inset).

The emission spectra of **1**·2Zn containing coumarin dye was expected to vary significantly upon the addition of PPi, resulting in an improved detection limit. As depicted in Figure 1-25, the change in the fluorescence intensity of **1**·2Zn was 4.7 times greater than that of **2**·2Zn upon the addition of PPi under the same conditions. The detection limit was calculated to be three times of the standard deviation of the background noise. As expected, the detection limit of **1**·2Zn for PPi (49 nM) was better than that of **2**·2Zn (83 nM).[67] Considering the reduced binding affinity of **1**·2Zn compared to that of **2**·2Zn, t he improved detection limit of **1**·2Zn indicates that high quantum yield fluorophores may have a dominant effect on the determination of the detection limit.

1.3. Conclusion

In summary, we developed a new fluorescent chemosensor (**1**·2Zn) for the detection of PPi in an aqueous solution. The sensor system shows an

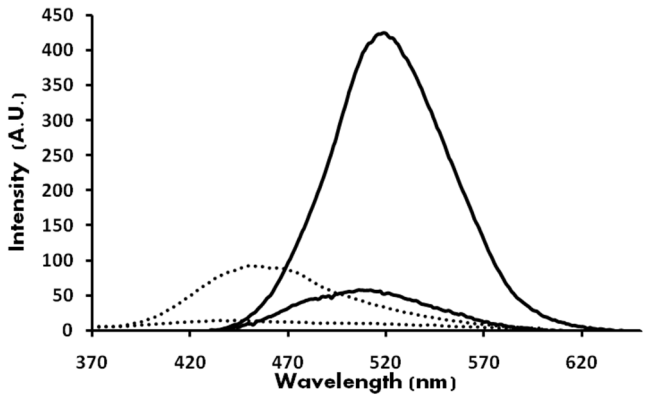

Figure 1-25. Fluorescence spectra of sensor **1**·2**Zn** (10 μM, solid lines) and **2**·2**Zn** (10 μM, dotted lines) before and after the addition of PPi (20 μM) in an aqueous buffer solution (10 mM HEPES, pH 7.4).

improved detection limit for PPi compared to that of the naphthyl-based PPi sensor by the introduction of coumarin dye. In addition, it shows good selectivity for PPi over other anions.

1.4. Experimental Section

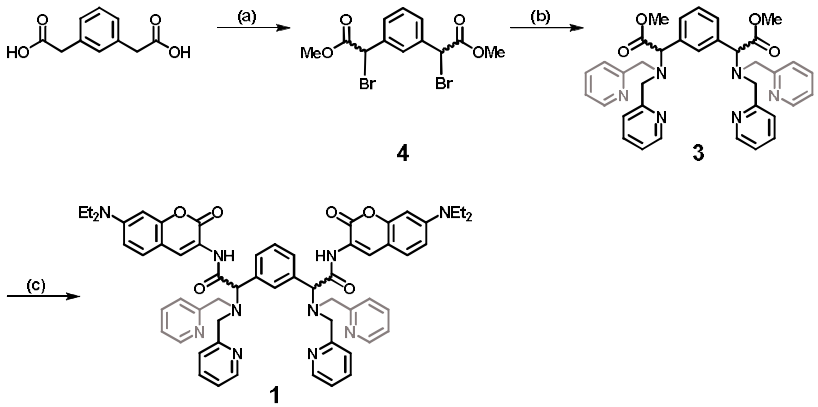

Scheme 1-2. (a) i. $(COCl)_2$, DMF, DCM ii. Br_2, Benzene iii. H_2O iv. cat. H_2SO_4, MeOH (b) Di-(2-picolyl)amine, K_2CO_3, KI, MeCN (c) i. NaOH, MeOH/H_2O ii. 3-amino-7-diethylaminocoumarin, EDC-HCl, Pyridine/DCM

Synthesis of 4: To a solution of 1,3-phenylenediacetic acid (1 g, 5.15 mmol) in methylene chloride (DCM), oxalyl chloride (~2 M in DCM, 10 mL) and a catalytic amount of dimethylformamide (DMF) was added. After 1.5 h, at wh ich time the reaction mixture was dissolved clearly in DCM, the reaction mixture was cooled in an ice bath and concentrated under reduced pressure. To that concentrated reaction mixture, bromine (0.8 mL) and benzene was added. After the reaction mixture had been moderately heated and refluxed overnight, all of its volatile components were evaporated and the residue was

partitioned between ethyl acetate and water. The organic phase was washed with water (×3), and then dried in Na_2SO_4.

To the resulting solution, 50 mL of methanol and a catalytic amount of sulfuric acid were added. After the reaction mixture had been moderately heated and refluxed for over 4 h, the reaction mixture was partitioned between DCM and water. The organic phase was washed with water (×3), and then dried in Na_2SO_4. Flash chromatographic purification (CH_2Cl_2: methanol = 100:1, v/v) afforded product **4** (520 mg) in 27% yield. ^{1}H NMR (300 MHz, acetone-d_6): 3.80 (6H, s), 5.36 (2H, s), 7.39 (1H, t, J=7.8 Hz), 7.58 (2H, t, J=8.5 Hz), 7.70 (1H, s). 13C NMR (300 MHz, CDCl3): δ 45.562, 45.623, 53.511, 76.733, 77.156, 77.355, 77.581, 128.927, 129.000, 129.429, 129.744, 135.968, 136.357, 168.519. HRMS (FAB): m/z calculated for $C_{36}H_{36}N_6O_4$ $[M+H]^+$ 378.9181, found 378.9174.

Synthesis of 3: To a solution of **4** (100 mg, 0.265 mmol) in 20 mL of acetonitrile were added 4 equiv. of KI (175 mg), 4 equiv. of K_2CO_3 (145 mg), and 2 equiv. of bis(2-pyridylmethyl)amine (104 mg, 0.47 mmol). After the reaction mixture had been moderately heated for over 12 h, insoluble inorganic salts were removed by filtration, and then all volatile components were evaporated. The mixture was partitioned between dichloromethane and water. The organic phase was washed with water (×3), and then dried in Na_2SO_4. Flash chromatographic purification (CH_2Cl_2: methanol = 20: 1, v/v) afforded 2 (108 mg) in 66% yield. ^{1}H NMR (300 MHz, acetone-d_6): 3.75 (6H, d, J=3.2 Hz), 3.98 (8H, dd, J=50.2 and 14.0 Hz), 4.81 (2H, d, J=3.0 Hz), 7.17-7.21 (4H, m), 7.39 (3H, d, J=0.8 Hz), 7.54 (4H, m), 7.68 (5H, m), 8.48 (4H, m). ^{13}C NMR (300 MHz, acetone-d_6): δ 28.192, 28.448, 28.704, 28.961, 29.217, 29.474, 29.730, 50.967, 50.980, 56.423, 66.925, 66.986, 121.961,

122.664, 122.728, 128.346, 128.429, 129.734, 129.942, 136.262, 137.065, 137.183, 148.857, 159.733, 171.888, 205.320. HRMS (FAB): m/z calculated for $C_{36}H_{36}N_6O_4$ $[M+H]^+$ 617.2876, found 617.2878.

Synthesis of 1: To a solution of **3** (42.1 mg, 0.068 mmol) in 4 mL of methanol were added 0.2 mL of 4 N NaOH. The reaction proceeded overnight at room temperature, after which all volatile components were evaporated. To that reaction mixture, N-(3-Dimethylaminopropyl)-N'-ethylcarbodiimide hydrochloride (40 mg, 0.13 mmol, EDC) and 3-amino-7-diethylaminocoumarin shown in Scheme 2 in 30% pyridine in CH2Cl2 (1.6 mL) were added. This mixture was left to react overnight at room temperature, after which the volatile components were evaporated, and the mixture was partitioned between dichloromethane and water. The organic phase was washed with water (×3), and then dried in Na2SO4. Flash chromatographic purification (CH_2Cl_2: methanol = 10:1, v/v) afforded **1** (15.8 mg) in 23% yield. ^{1}H NMR (300 MHz, acetone-d_6): 1.21 (12H, t), 3.50 (8H, m), 4.08-3.69 (8H, m), 4.84 (2H, d, J=2.8 Hz), 6.55 (2H, m), 6.75 (2H, d, J=12.0 Hz), 7.21 (4H, m), 7.38-7.70 (14H, m), 8.54-8.60 (6H, m), 10.64 (2H, s). ^{13}C NMR (300 MHz, acetone-d6): δ 11.878, 13.469, 28.192, 28.448, 28.705, 28.961, 29.218, 29.474, 29.731, 31.409, 44.279, 56.666, 56.750, 69.502, 59.555, 96.986, 108.111, 109.430, 119.568, 122.134, 123.156, 123.193, 125.112, 125.298, 127.654, 128.607, 129.846, 130.091, 132.224, 132.583, 134.720, 134.984, 136.449, 149.113, 146.427, 152.989, 158.574, 158.833, 158.917, 170.296, 170.330. HRMS (FAB): m/z calculated for $C_{60}H_{60}N_{10}O_6$ $[M+H]^+$ 1017.4776, found 1017.4764.

Synthesis of 1·2Zn: To a solution of **1** (1 mg) in 1 mL of MeOH, a methanolic solution of $Zn(ClO_4)_2 \cdot 6H_2O$ (1.3 mg) was added dropwise, and the mixture was stirred for 30 min at room temperature.

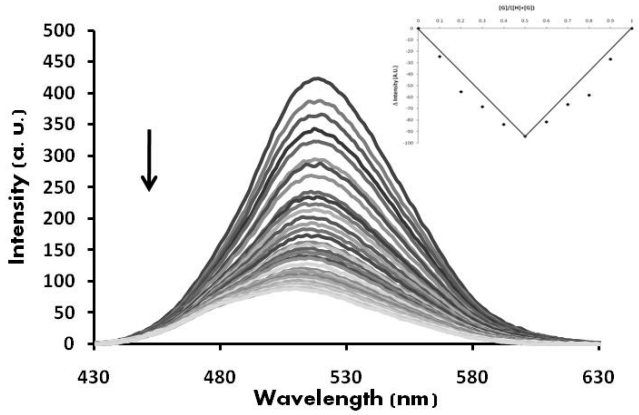

Figure 1-26. Fluorescence emission spectra of **1**-2**Zn** (10 μM) upon addition of 20 μM various cations (perchlorate salts) in an aqueous buffer solution (10 mM HEPES, pH 7.4).

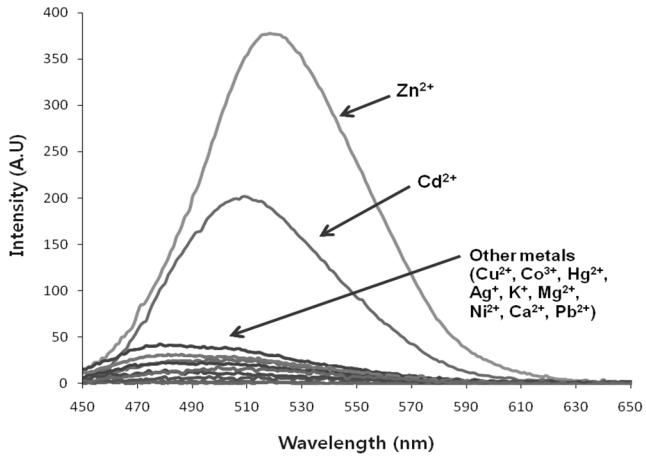

Figure 1-28. Changes in the fluorescence emission of **1**·2**Zn** (10μM) upon addition of ATP (0 ~ 46 μM) in aqueous buffer solutions (10 mM HEPES, pH 7.4). Upon addition of ATP, fluorescence emission was decreased 4.8-fold and saturated at 4.6 equiv.

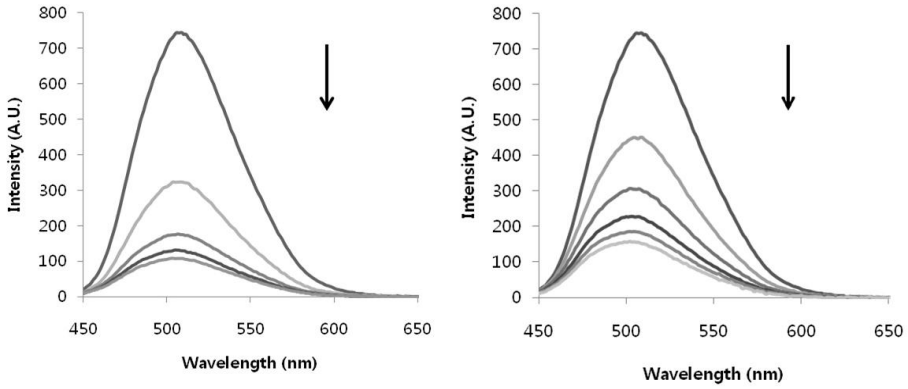

Figure 1-27. Changes in the fluorescence emission of **1**·2Cd (10 μM) upon addition of PPi (left, 0~33 μM) and ATP (right, 0~46 μM) in aqueous buffer solutions (10 mM HEPES, pH 7.4).

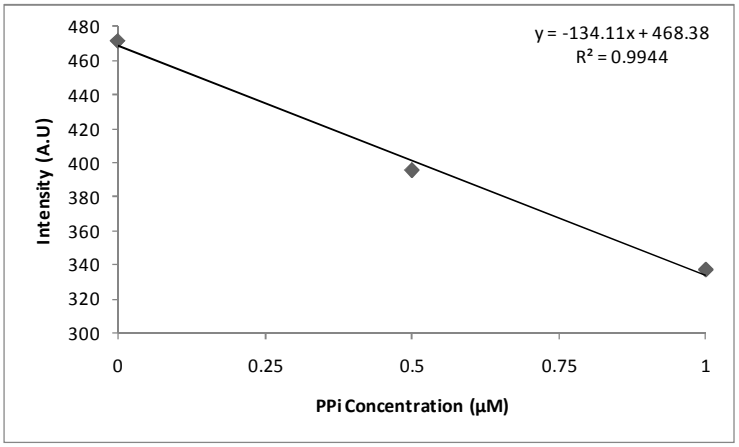

Figure 1-29. Changes in the fluorescence emission of sensor **1**·2Zn (10 μM) upon the addition of PPi (sodium salt) in HEPES buffer (pH 7.4) at 25 °C. The fluorescence intensity of **1**·2Zn at 511 nm decreases linearly with the concentration of PPi in the range of 0 ~ 1 μM (n=10, *k*=3). The detection limit is 49 nM.

Section 2.

Spectroscopic "All at Once" Discrimination of PPi, ATP, and GTP with Naphthalene-based Fluorescent Probe.

1.1. Introduction

Phosphate-containing compounds such as pyrophosphate anion (PPi) and NTPs play an important role in energy transduction in organisms and control metabolic processes by participation in enzymatic reactions.[68-73] For example, PPi regulates several metabolic processes such as gene duplication, gene transcription and signal transduction.[68] In addition, PPi is related to some diseases: The deposition of calcium pyrophosphate dehydrate in and around joints causes osteoarthropathy and calcium pyrophosphate deposition disease (CPDD), especially in articular cartilage and fibrocartilage.[69]

Adenosine-5'-triphosphate (ATP) and guanosine-5'-triphosphate (GTP) also play crucial roles in cell biology.[70-75] ATP is not only responsible for energy production and storage in living cells [70] but controls several metabolic processes, [4] whereas GTP is concerned with RNA synthesis, citric acid cycle, and acts as an energy source for protein synthesis.[72]

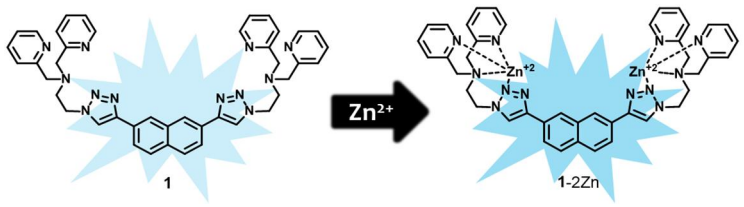

Scheme 1-3. The structures of **1** and **1**-2Zn.

So far, numerous fluorescent chemosensors have been developed for phosphate-containing anions, however, few chemosensors that can distinguish between PPi [73-74] and NTPs [75-76] have been reported. Therefore, the selective detection and precise discrimination of phosphate-containing anions still has been the main focus of the efforts of several research groups. Moreover, to construct more simple and convenient sensing system, it needs to develop the advanced small molecular probe that can discriminate several phosphate-containing biomolecules at once.

Herein, we developed a naphthalene-based Zn(II) complex, **1**-2Zn(II) for the discrimination of PPi, ATP, and GTP in aqueous media. Probe **1**-2Zn consist of three basic elements: (i) Naphthyl group, which is well-known blue-emissive fluorophore, as a signaling unit and (ii) Dipicolylamine (DPA)-Zn(II) complex as a binding site for phosphate-containing anions. (iii) Triazole unit has two sub-roles, one is the elongation of conjugation length of naphtyl group for red-shifted emission and another is the additional coordination site for Zn(II).

1.2. Results

The synthesis of **1** is outlined in Scheme 1-4. Firstly, we introduced terminal alkyne groups to 2,7-dibromonaphthalene by sonogashira coupling and desilylation. Azidoethyl-DPA (**3**) was obtained through the two SN2

reactions of 1,3-dibromoethane with sodium azide and 2,2'-dipicolylamine. Finally, we obtained compound **1** through Cu(I)-catalyzed azide-alkyne cycloaddition (CuAAC) between 2,7-diethynylnaphthalene (**2**) and **3.**

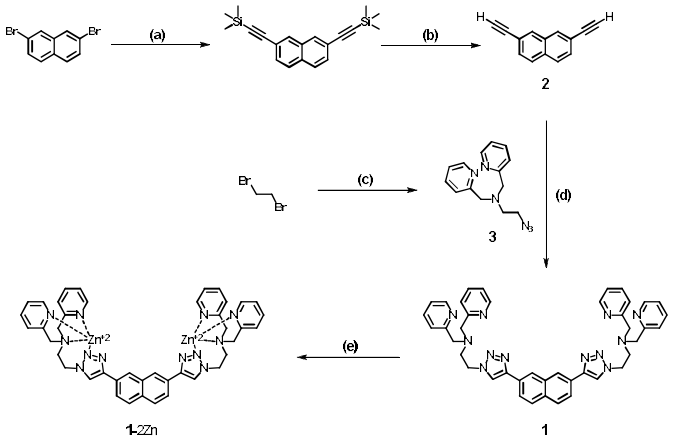

Scheme 1-4. (a) $Pd(PPh_3)_4$, CuI, TEA, Toluene, reflux, 6h (b) Tetrabutylammonium fluoride, THF, rt, 3h (c) i. NaN_3. Acetone ii. K_2CO_3, 2,2'-dipicolylamine (DPA), MeCN, rt, 12h (d) $CuSO_4$, sodium ascorbate, H_2O, t-BuOH, rt, 48h (e) $Zn(NO_3)_2$, MeOH, rt, 1h.

At first, probe **1** showed a weak emission around 370 nm in HEPES buffer (10 mM, pH 7.4) (λ_{ex}: 300 nm), which is due to photo-induced electron transfer (PET) from lone pair electron of tertiary amine (DPA moieties). When zinc cations (5 eq.) were added to **1**, as expected, 2.77 fold-increased PL intensity was observed. (Figure 1-30) This is due to the blocking the PET quenching effect through coordination of zinc cations with a tertiary amine,

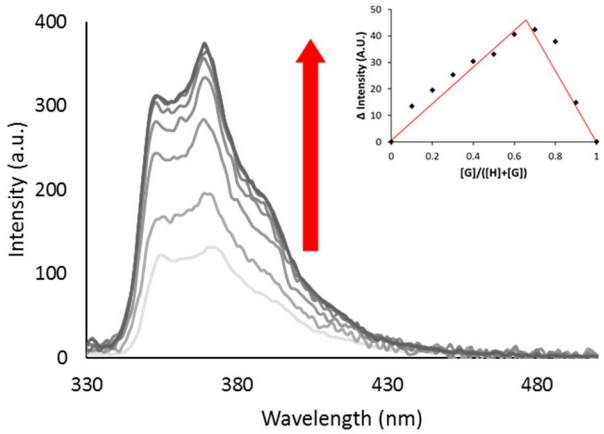

Figure 1-30. Change in the fluorescence of **1** (10 μM) upon addition of Zn^{2+} (0-5 equiv., perchlorate salt) in aqueous HEPES buffer solutions (10 mM, pH 7.4). (Inset) Job's plot for the complexation between **1** and Zn^{2+}.

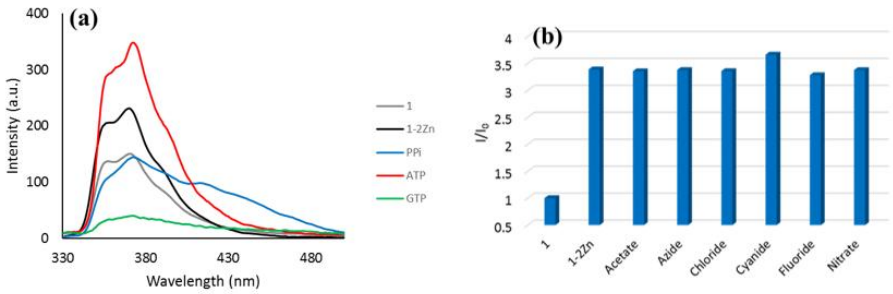

Figure 1-31. (a) Fluorescence emission spectra of **1**-2Zn (10 μM) upon addition of PPi, ATP, and GTP (50 μM each) in an aqueous buffer solution (10 mM HEPES, pH 7.4) (b) Relative fluorescent intensity of **1**-2Zn (10 μM) in the presence of non-phosphate-containing anions (500 μM).

which is common strategy for sensing d^{10}-metal cations.[77] We confirmed the 1:2 complexation between **1** and Zn^{2+} by Job's plot. (Figure 1-30 inset) Cadmium ions were also coordinated to probe **1**, however, only a little PL enhancing (1.22-fold) was observed. The addition of copper ions resulted in quenching of fluorescent by their paramagnetic property.

Then we carried out the fluorescence studies using the **1**-2Zn complex, which showed different fluorescent responses to each of phosphate-containing anions. (Figure 1-31a) For example, **1**-2Zn induced a 15 nm red-shift in PL emission when PPi was added, while it caused fluorescence enhancement and fluorescence quenching with a little red-shift or without any wavelength change upon the addition ATP and GTP, respectively. Other anions that do not contain phosphate groups did not any significant changes in the fluorescent intensity of **1**-2Zn at 370 nm, even at 10-times higher concentration. (Figure 1-31b)

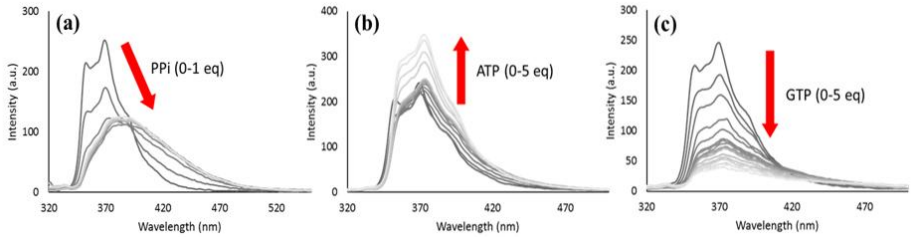

Figure 1-33. Changes in the fluorescence of **1**-2Zn (10 mM) upon addition of (a) PPi (0-10 mM), (b) ATP (0-50 mM), and (c) GTP (0-50 mM) in aqueous HEPES buffer solutions (10 mM, pH 7.4).

To observe the spectral change in more detail, we performed the titration experiment in each case (Figure 1-32). Firstly, when adding PPi (0-1 eq) to **1**-2Zn, it exhibited red-shifted and decreased PL emission gradually, similar to the shape of naphthalene excimer reported previously.[78] (Figure 1-32a) Yoon *et al.* reported naphthyldiimide-based PPi sensor that induced the unique 2+2 type excimer in the presence of PPi.[79] Judging from these points, it seems that probe **1** also formed the 2:2 excimer formation when reacting with ppi, in common with that of Yoon's group. Energy minimum calculation by Spartan 08' supported the 2:2 complexation between **1**-2Zn and PPi. When adding PPi over 1 equivalent (1-5 eq), PL spectra slightly recovered to blue-shifted emission. This phenomenon seems that some 2:2 complexes between **1**-2Zn and PPi converted to 1:2 complexation at high PPi concentration.

Upon increasing concentrations of ATP, a slightly red-shifted emission (~ 4 nm) and an additional increase in fluorescence (1.44 fold) were observed. These red-shifted and enhanced emission were attributed to the excimer formation between naphthalene and adenine unit of ATP, which is similar binding structure with previous ATP sensing study by Ghosh group.[8d] There is one interesting point that fluorescence of **1**-2Zn rather decreased when small amount of ATP was added (0-0.3 eq). This decreased PL intensity came from another effect of adding ATP, which would weaken the metal

coordination with the reductive quencher and lead restore the PET quenching pathway.

Lastly, we carried out the titration experiment with GTP to **1**-2Zn. fluorescence emission decreased gradually upon increasing GTP concentration. It is a well-known fact that guanine base of GTP acts a fluorescence quencher because of their proper energy level enough to induce PeT quenching for almost the whole fluorophores. [75a] We performed the DFT calculation to confirm the HOMO/LUMO energy levels of the naphthalene-triazole core unit of probe **1** and guanine base. This calculation results showed that the HOMO level of guanine was located between the HOMO level and LUMO level of naphthalene-triazole core unit. Guanosine-5'-diphosphate (GDP) was also quenched the fluorescence of **1**-2Zn, however, any fluorescence change occurred when adding guanosine-5'-monophosphate (GMP) due to its low binding affinity.

1.3. Conclusion

In summary, we developed a new fluorescent chemosensor (**1**-2Zn) for the discrimination of PPi, ATP, and GTP in an aqueous solution. The sensor system shows a different fluorescent signal change for PPi, ATP, and GTP respectively. Based on this design concept, we expect to develop improved fluorescent probes that exhibit more red-shifted emission and more drastic changes for each target anions.

1.4. Experimental Section

1.4.1. Synthesis

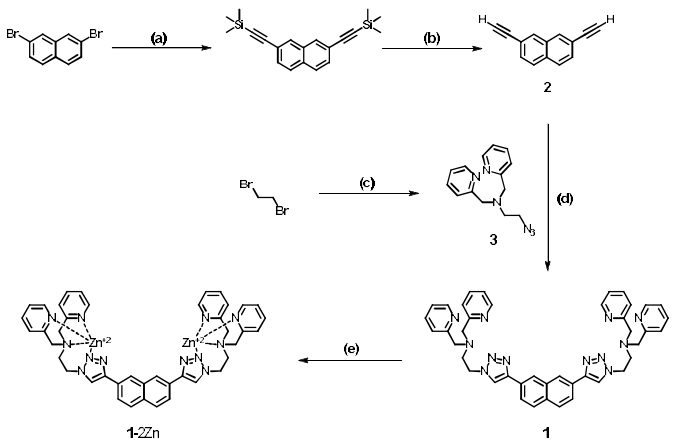

Scheme 1-4. (a) $Pd(PPh_3)_4$, CuI, TEA, Toluene, reflux, 6h (b) Tetrabutylammonium fluoride, THF, rt, 3h (c) i. NaN_3. Acetone ii. K_2CO_3, 2,2'-dipicolylamine (DPA), MeCN, rt, 12h (d) $CuSO_4$, sodium ascorbate, H_2O, t-BuOH, rt, 48h (e) $Zn(NO_3)_2$, MeOH, rt, 1h.

Synthesis of 2: Trimethylsilylacetylene (1.55 mL, 11 mmol), $Pd(PPh_3)_4$ (231 mg, 0.02 mmol), and CuI (76 mg, 0.04 mmol) were added sequentially to a solution of 2,7-dibromonaphthalene (1.43g, 5 mmol) in toluene (20 mL) and were refluxed for 6h. After cooling the room temperature, the reaction mixture was evaporated under reduced pressure. The residue was extracted with DCM and washed with water. The organic layer was dried with Na_2SO_4, and concentrated under reduced pressure. The resulting residue was purified by silica column chromatography (Hex:EA) to give an intermediate product (white powder, 1.48g, 91% yield).

Tetrabutylammonium fluoride was added to a solution of the intermediate silane in THF at room temperature. After 3h, the reaction mixture was evaporated under reduced pressure, and extracted with DCM and washed with water. The organic layer was dried with Na2SO4, the concentrated under reduced pressure. The resulting residue was purified by flash silica column chromatography (Hex/EA) to give **2** (pale red power 0.97g, 98% yield). ^1H NMR (300 MHz, $CDCl_3$): 7.99 (2H, s), 7.79 (2H, d, J = 8.44 Hz), 7.56 (2H,

dd, *J* = 8.46, 14.6 Hz), 3.19 (2H, s).

Synthesis of 3: Sodium azide (341 mg, 0.8 mmol) dissolved in water (2.5 mL) was added to a solution of 1,2-dibromoethane (0.086 mL, 1 mmol) in acetonitrile (5 mL) and heated at 50 C overnight. Then, bis(2-pyridylmethyl)amine (270 mg, 1.5 mmol) and potassium carbonate (553 mg, 4 mmol) was added to reaction mixture and heated at 50 C overnight. After cooling to the room temperature, the reaction mixture was evaporated under reduced pressure. The residue was extracted with DCM and washed with water. . The organic layer was dried with Na_2SO_4, and concentrated under reduced pressure. The resulting residue was purified by silica column chromatography (DCM: MeOH = 10: 1) to give a **3** (yellow liquid, 88 mg, 33% yield). ^{1}H NMR (300 MHz, $CDCl_3$): 8.54 (2H, d, *J* = 4.88 Hz), 7.66-7.72 (2H, m), 7.56 (2H, d, *J* = 7.34 Hz), 7.16-7.24 (2H, m), 3.89 (4H, s), 3.34 (2H, t, *J* = 5.88 Hz), 2.85 (2H, t, *J* = 5.92 Hz).

Synthesis of 1: Copper sulfate (3 mg, 0.011 mmol) and ascorbic acid sodium salt (2 mg, 0.011 mmol) were added to a solution of **2** (40 mg, 0.225 mmol) and **3** (134 mg, 0.5 mmol) in t-BuOH (2.5 mL) and H_2O (2.5 mL) at room temperature for 48h. Resulting residue was evaporated under reduced pressure, and extracted with ether. The organic layer was dried with Na_2SO_4, and concentrated under reduced pressure. The resulting residue was purified by silica column chromatography (DCM: MeOH = 10: 1) and high-performance liquid chromatography (HPLC) to give a **1** (pale-yellow liquid, 46 mg, 29% yield). ^{1}H NMR (300 MHz, Acetone-d_6): 8.63 (2H, s), 8.51 (4H, d, *J* = 3.70 Hz), 8.48 (2H, s), 8.03 (4H, dd, *J* = 8.81, 12.5 Hz), 7.59 (4H, t, *J* = 7.51 Hz), 7.34 (4H, d, *J* = 7.51 Hz), 7.18 (4H, t, *J* = 5.36 Hz), 4.71 (4H, t, *J* = 4.91 Hz), 3.92 (8H, s), 3.15 (4H, t, *J* = 4.78 Hz).

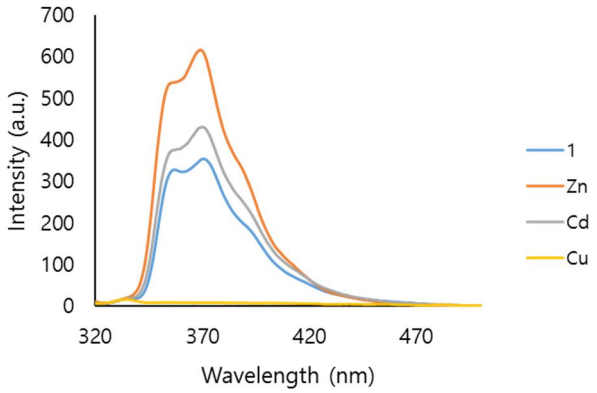

Figure 1-34. Fluorescence emission spectra of **1** (10 μM) upon addition of 50 μM Zn^{2+}, Cd^{2+}, and Cu^{2+} (perchlorate salts) in an aqueous buffer solution (10 mM HEPES, pH 7.4) (λ_{ex}: 300 nm)

Synthesis of 1·2Zn: To a solution of **1** (1 mg) in 1 mL of MeOH, a methanolic solution of $Zn(ClO_4)_2 \cdot 6H_2O$ (1.3 mg) was added dropwise, and the mixture was stirred for 30 min at room temperature.

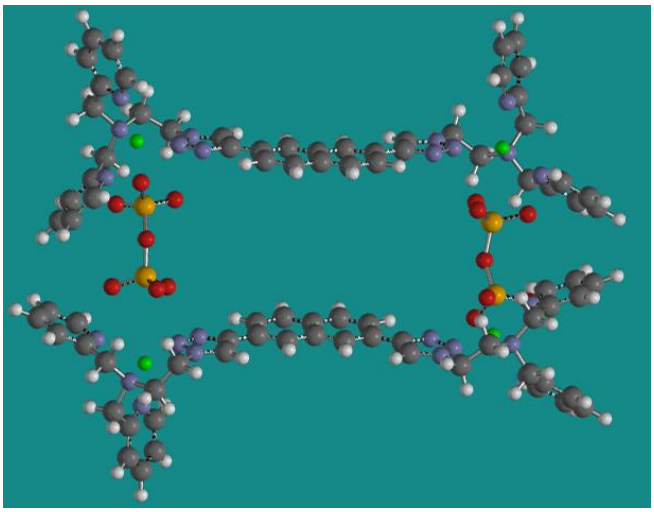

Figure 1-35. Energy minimum structure between **1** and PPi (2:2 complex) calculated by Spartan 08'

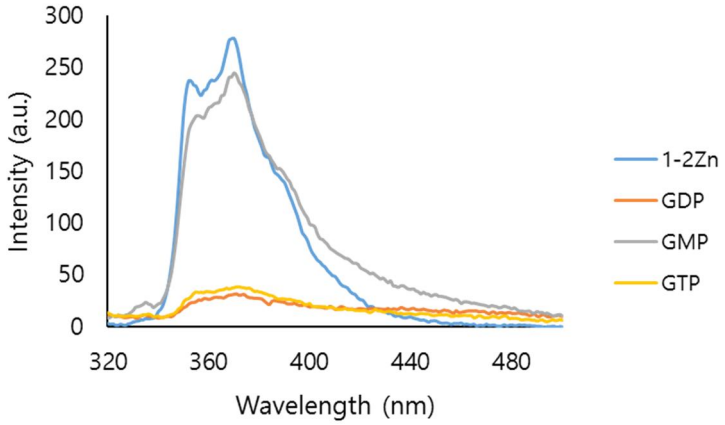

Figure 1-36. Fluorescence emission spectra of **1**-2Zn (10 μM) upon addition of 50 μM GTP, GDP, and GMP in an aqueous buffer solution (10 mM HEPES, pH 7.4) (λ_{ex}: 300 nm)

Section 3

The Development of Pyrene-based Organophosphorus Nerve Agent Probe and Its ECL Application with High Sensitivity and Facile Synthesis.

1.1. Introduction

Due to the current increase of criminal terrorist attacks *via* chemical warfare agents (CWAs), there is an increasing interest to detect the lethal chemicals with high reliability in quick time. Among all these CWAs, organophosphorus (OP)-containing nerve agents including Sarin, Soman, and Tabun, also called G-series of nerve agents, are required more attention because of their odorless and colorless properties.[68]

The toxicity of G-series of nerve agents is caused by the inhibition of the acetylcholinesterase (AChE), which is the critical central-nervous enzyme.[69, 70] When exposed to G-series of nerve agents, the hydroxyl groups in a serine residue on the active site of the enzyme undergo the esterification process through nucleophilic attack on the electrophilic phosphorus. The esterification of the alcohol makes the acetylcholinesterase (AChE) inoperative, resulting the accumulation of acetylcholine in the synaptic junctions that control the muscle relaxation.[70, 71]

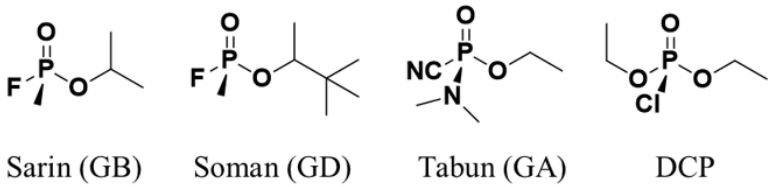

Scheme 1-5. The structure of G-type nerve agents and mimic.

Many detection methods for these nerve agents have been reported based on enzyme assays [72,73], potentiometry, [74,75,76] mass spectroscopy, [77] and interferometry. [78] However, these classical methods still have limitations, such as slow response, lack of specificity, limited selectivity, low sensitivity, operational complexity, and non-portability. In recent years, several fluorescent probes succeed to overcome lots of problems compared to traditional methods. Furthermore, small molecule based fluorescent probes afford a lot of advantages including easy production, relative low cost, and high sensitivity. [79-87] One promising strategy for detecting organophosphates is to utilize the esterification of the hydroxyl group. Because phosphate ester group formed by esterification is a highly reactive nucleophile, it subsequently undergoes cascade reaction to generate another reaction product. Rebek and co-workers developed the photo-induced electron transfer (PET) based fluorescent turn-on probe for organophosphorus based on intramolecular cyclization using tertiary amine group based on this strategy.[81] Several probes that possess hydroxyl group and tertiary amine in one molecule have been reported.[83, 84, 86]

In spite of many studies with enhanced property, there has still room for improvement to develop the sensing systems for nerve agent. One considering point for detecting the nerve agent is that enables the point-of-care (POC) detection. To recognize the toxic chemicals within few times and evacuate people from dangerous conditions, it is essential that constructs the direct

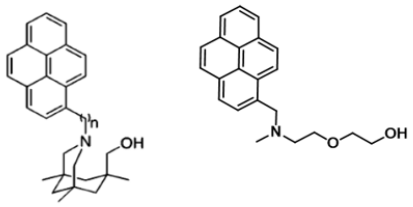

1 2

Scheme 1-6. The molecular structure of pyrene-based G-type nerve agent probes.

analysis system on the spot. Fluorescent assays have several advantages such as easy synthesis and low cost. However, they have a definite limit hard to applicate to POC detection, which needs to extra bulky equipment including external optical source. Another strategy to develop the point-of-care testing for organophosphorus is to induce dynamic color change, which enables naked-eye detection. Many researchers have reported the chromogenic probe and applicate to make the simple test kit using silica or filter paper.[84, 88, 89] However, chromogenic probes have lower sensitivity compared to fluorescence based probe, which is unsuitable to quantify a small amount of toxic chemicals.

ECL assays based on small molecule probes can be a good idea to take advantage of fluorescence based assay and chromogenic assay simultaneously. These methods not only have the excellent sensitivity over fluorescence based assays, but have a special merit to develop the disposable kits for field diagnosis easily because they are worked by electrical energy without extra bulky equipment or external optical source. Furthermore, in contrast with general ECL immunoassay systems, small-molecule based ECL systems introducing the chemodosimetric approach can identify the presence of targets with simpler manners that free from the additional washing process.

In this study, we designed and synthesized the probe **2** for organophosphorus. Probe **2** has the tertiary amine and alcohol group in pyrene,

on the same principle with previously reported probe by Rebek Jr. et al. (**1**).[81] We replaced the Kemp's triacid to flexible alkyl linker for low cost and facile synthesis. Going on step forwards, we performed the ECL experiment to detect and quantify the organophosphorus (OP) and check the possibility to utilize the precise POC detection.

1.2. Results

At first, we tested the fluorescence change in the presence of organophosphorus (OP). We choose the diethyl chlorophosphate (DCP) as the nerve agent simulant due to its similar reactivity and much less toxicity. Free probe **2** showed drastically decreased PL emission in acetonitrile via PET quenching of lone pair of tertiary amine. However, addition of DCP to probe **2** leaded to large fluorescence enhancement in a few minutes. The intramolecular cyclization of probe **2** induced the 24-fold fluorescence increasing at 378 nm, the monomer emission of pyrene. Compared to previous report, this result proves that the modifying of the flexible alkyl linker with easier synthesis ca uses almost no performance degradation. Because the rapid detection of toxic chemicals is very important, we measured a reaction time for PL saturation or probe **2** (10 μM) in the presence of 20 μM DCP in acetonitrile. The fluorescent intensity reached to its highest peak in 20 minute. This prompt detection of DCP shows suitability for sensing of toxic materials.

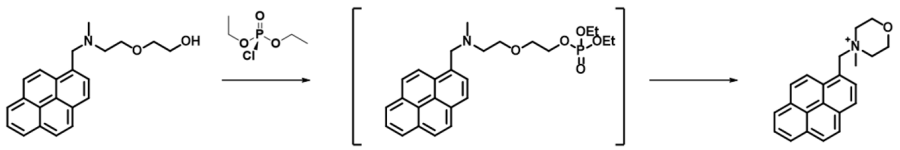

2 **2**-DCP

Scheme 1-7. Proposed mechanism of probe **2** with DCP

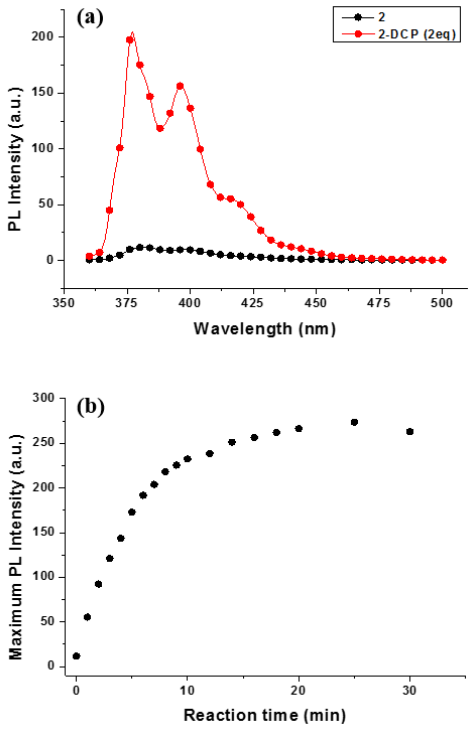

Figure 1-38. (a) Fluorescent emission spectra of **2** (10 μM) in the absence (black line) and presence (red line) of DCP (20 μM) in acetonitrile. (b) Time-course measurement of **2** (10 μM) in the presence of DCP (20 μM) in acetonitrile.

To test the sensitivity of probe **2** for DCP, we added DCP to probe **2** at different concentrations. All experiments were performed in acetonitrile and incubated at room temperature for 10 min. Figure 1-38a shows the gradual fluorescence enhancement at 378 nm upon the addition of 0-50 μM of DCP to probe **2** (10 μM). Especially, the fluorescent intensity at 378 nm increase linearly in the range of 0-25 μM, and when adding the 30 μM of DCP the saturated fluorescent emission is observed. The limit of detection (LOD) is calculated as 3.01 μM.

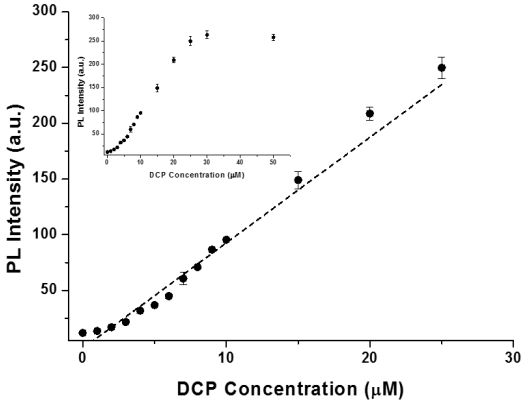

Figure 1-39. Isothermal binding curve of **2** (10 μM) obtained for PL titration upon the addition of DCP in acetonitrile.

Next, we measured the ECL signal of probe **2** in acetonitrile with tripropylamine (TPA) as a coreactant. Although pyrene has been reported as an ECL luminophore, [90,91] there are few examples based on oxidative reduction ECL mechanism.[92] Furthermore, in our best knowledge, no ECL based chemodosimer using pyrene has been reported so far. Firstly, CV experiment d uring 0-1.6V was carried out to confirm the electrochemical stability of pyrene-based probe **2**. In addition to large oxidation peak at 1.5V which is known to that of pyrene, the additional small oxidation peak was observed a round 0.8V (Figure 1-40). Judging from the similar oxidation potential to tripropylamine (TPA) and the disappearance after reacting with DCP, this oxidation peak is due to the tertiary amine of the reaction site of probe **2**.

Table 1. Electrochemical properties of **1**-DCP.

Compound	E^0_{ox} (V vs Fc/Fc^+)	HOMO (ev)	LUMO (ev)	ΔE (HOMO-LUMO)	Relative PL Intensity	Relative ECL Intensity
1-DCP	0.81	-5.62	-2.20	3.42	10.48	0.12
$Ru(bpy)_3^{2+}$	0.90	-5.73	-3.03	2.60	1	1

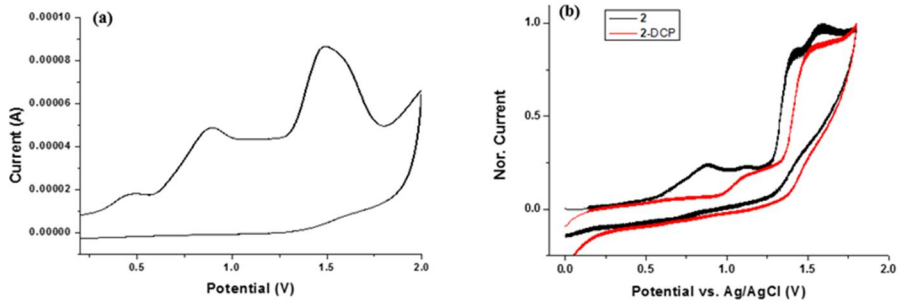

Figure 1-40. (a) Cyclic voltammetry curve of a solution of 100 μM **2** in acetonitrile containing 0.1M tetra-n-butylammonium perchlorate (TBAP). (b) Cyclic voltammetry curves of **2** (10 μM) before (black) and after (red) the addition of DCP in acetonitrile containing 0.1M TBAP.

Table 1 shows the HOMO/LUMO energy levels of pyrene obtained by CV experiment. Although the HOMO energy level is low enough to allow the electron transfer from TPA to the pyrene, wide HOMO/LUMO energy gap makes the destabilization of LUMO energy level, e ven higher than that of TPA radical (Scheme 1-8). [92, 93] This elevated LUMO makes it difficult to move the electron of TPA radical to pyrene, the process to form the excited states of pyrene. Consequently, the ECL efficiency of pyrene in oxidative process is very poor compared to $Ru(bpy)_3^{2+}$, the best well-known ECL luminophore.

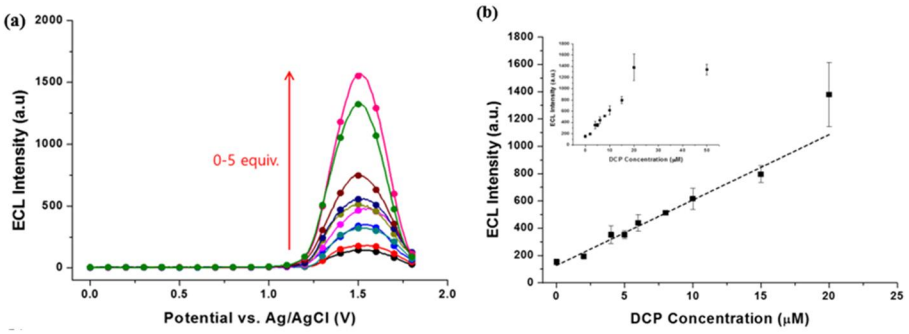

Figure 1-41. (a) ECL change of **2** (10 μM) upon the addition of DCP (0-50 μM) in acetonitrile. (b) Isothermal binding curve of **2** (10 μM) obtained for ECL titration upon the addition of DCP in acetonitrile.

Furthermore, the additional unexpected problem was found in ECL experiment. Contrary to PL intensity, the ECL intensity of probe **2** itself was almost quenched but weak signal was still remained. This decreased PET quenching efficiency is due to the oxidation of tertiary amine. The disappearance of the lone pair by formation of tertiary amine radical perturbs the PET mechanism. Consequently, weak initial ECL intensity still remains compared to PL, which reduces the turn-on ratio and sensitivity. Upon the addition of DCP, there was a large enhancement of the ECL signal at 1.5V. In the range of 0-20 μM, probe **2** showed the linear correlation. LOD is

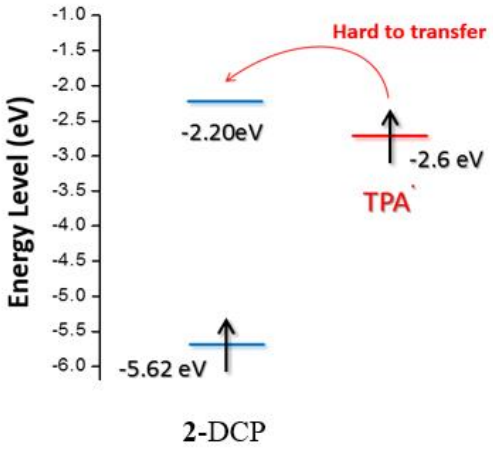

Scheme 1-8. The schematic explanation for low ECL efficiency of probe **2**.

calculated as 1.46 μM, the similar level to PL experiment in spite of the unexpected problems.

1.3. Conclusion

In summary, we developed the pyrene based turn-on probe **2** for organophosphate nerve agents. Probe **2** showed highly sensitive and rapid detection through intramolecular cyclization. In addition to PL study, we also carried out the ECL experiment for DCP for the first time. Furthermore, ECL-based small molecule probe **2** suggests a possible approach to develop of real-time POC detection and field analysis. Though PET quenching efficiency of probe **2** in ECL analysis is lowered due to the oxidation of tertiary amine, it is still possible to detect and quantify the nerve agents with high sensitivity. We anticipate this ECL based analysis becomes a basic concept to develop the POC detection system. At the same time, we prepare to advanced type of ECL nerve agent probe by replacing pyrene to another signal unit that has higher ECL efficiency and modification of the reaction site that induces full quenching of ECL intensity.

Part II

ECL Chemodosimeters for Small Anions Based on Cyclometalated Ir(III) Complex

1. ECL-emitting Cyclometalated Ir(III) Complexes

As depicted in part 1, most of ECL-based experiments have been performed with tris(2,2'-bipyridine)ruthenium(II) ($[Ru(bpy_3)^{2+}]$, Rubipy) and related poyimine-ruthenium(II) complexes, which show the characteristic orange red emissions. Over the last decade, however, numerous researchers have tried to develop the new ECL emitter with a wide range of electrochemical properties and emission maxima that can be tuned freely. Among the organometallic materials used in OLED (organic light emitting deveices) field such as Alq_3[94] and other metal complexes, cyclometalated Ir(III) species are one of the powerful candidates that can be substituted for the roles of conventional Ru(II) species. One of the great advantages of the Ir(III) complexes in ECL analysis is the easy tunability of emission wavelength by ligand modification. Furthermore, Ir(III) complexes generally have higher PL quantum yield than Ru(II) derivatives, suggesting a high possibility as good ECL luminophores.

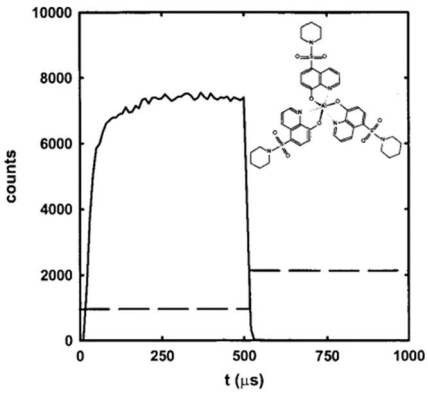

Figure 2-1. The structure and temporal ECL emission profile of $Al(qs)_3$.

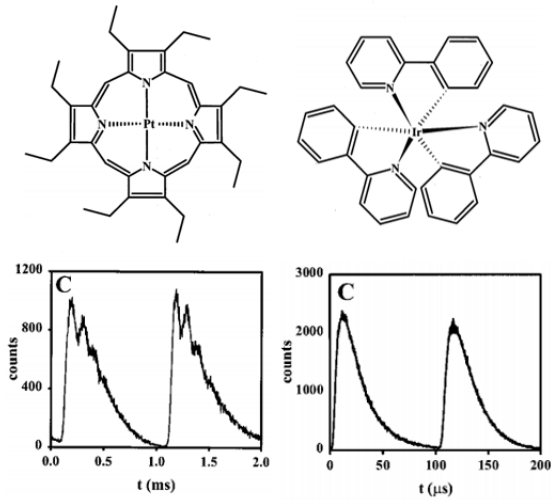

Figure 2-2. The structures and temporal ECL emissions of Pt(OEP) (left) and $Ir(ppy)_3$ (right).

So far, lots of ECL studies based on Ir(III) complexes have been carried out. Wightman, R. M. et al. studied the ECL efficiencies of Pt(OEP) and $Ir(ppy)_3$, known to OLED dopant materials on annihilation mechanism.[95] Richter, M. M. et al. also reported the ECL property of $Ir(ppy)_3$ with oxidative reduction mechanism more specifically in the same year.[96] However, contrary to the high ECL efficiency of $Ir(ppy)_3$ on annihilation mechanism, the ECL intensity on oxidative reduction mechanism with TPA gave a low ECL (about one-third of the value for $Ru(bpy)_3^{2+}$). This unexpected result is caused by the hard generation of the excited states required significantly greater energy than that of $Ru(bpy)_3^{2+}$. Because the coreactant ECL mechanism has a lot of advantages to applicate the bioanalysis and biosensing, such as high sensitivity at lower concentration and suitability for aqueous condition, many studies have been performed to develop the Ir(III) complexes with a high efficiency in oxidative reduction ECL process.

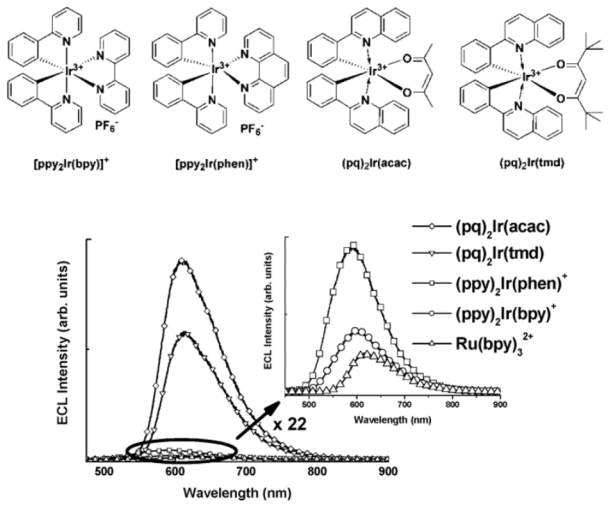

Figure 2-3. The structures and ECL spectra of Ir(III) complexes.

Kim, H. and Lee, J.-K. et al. reported the efficient ECL from diverse Ir(III) complexes with TPA on coreactant mechanism in 2005.[97] In that paper, they suggested the three ideal conditions for efficient ECL emission. Among them, $(pq)_2Ir(acac)$ and $(pq)_2Ir(tmd)$ with TPA gave very high ECL compared to a Ru- $(bpy)_3^{2+}$/ TPA system (77 and 49 times for $(pq)_2Ir(acac)$ and $(pq)_2Ir(tmd)$, respectively).

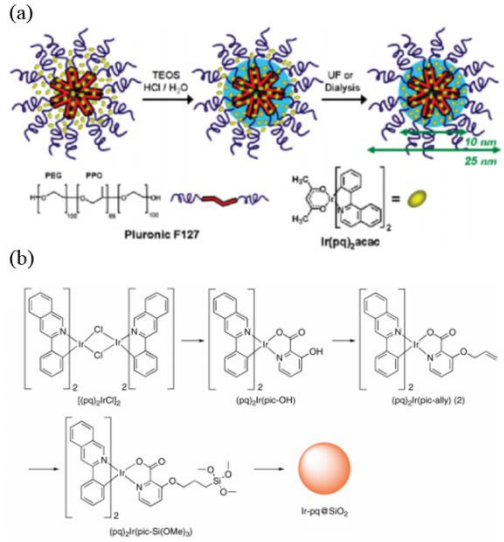

Figure 2-5. The examples of Ir(III) doped silica nanoparticles

In addition to red-emitting Ir(III) complexes, many researchers have tried to develop the high ECL efficiency in blue- or green- iridium(III) complexes to restore the merit of multi-color emission. Richter group reported the ECL properties of blue-emitting Ir(III) complex F(Ir)pic, however, its ECL property was much lower than that of $Ru(bpy)_3^{2+}$ and even $Ir(ppy)_3$.[98] The ECL of Ir(df-ppy)$_3$ [99] and Ir(df-ppy)$_2$(ptb)$^+$ [100] was also reported, which showed the 7.2% and 24% ECL intensity compared to that of $Ru(bpy)_3^{2+}$, respectively.

Enhancing water solubility of Ir(III) complex is also an important issue for

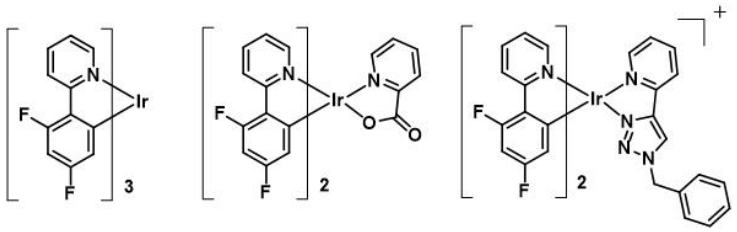

Figure 2-4. Ir(III) complexes as blue-emitting ECL luminophores.

many research groups. Although $(pq)_2Ir(acac)$ and $(pq)_2Ir(tmd)$ showed much stronger ECL intensity than ruthenium derivatives, those neutral-charged metal complexes have a poor solubility, especially in aqueous solution. To overcome this problem, Prodi, L. et al reported Ir(III) doped silica-PEG nanoparticles enabling electrochemiluminescence of neutral $(piq)_2Ir(acac)$ complex in aqueous media. Lee, J.-K. et al. also synthesized Ir(III)-doped silica nanoparticle which showed strong ECL intensity. In addition to synthesize a Ir(III) doped nanoparticle, the common strategies to increase the water solubility of Ir(III) complexes is the replacement of ancillary ligand with a neutral diamine (N^N) compound to impart an overall positive charge to the complex or a derivative containing highly polar sulfonate or saccharide groups. However, the introduction of a neutral diamine strongly effects on LUMO energy level of Ir(III) complex, which disturbs the design of blue- or green- emission of Ir(III) complexes.

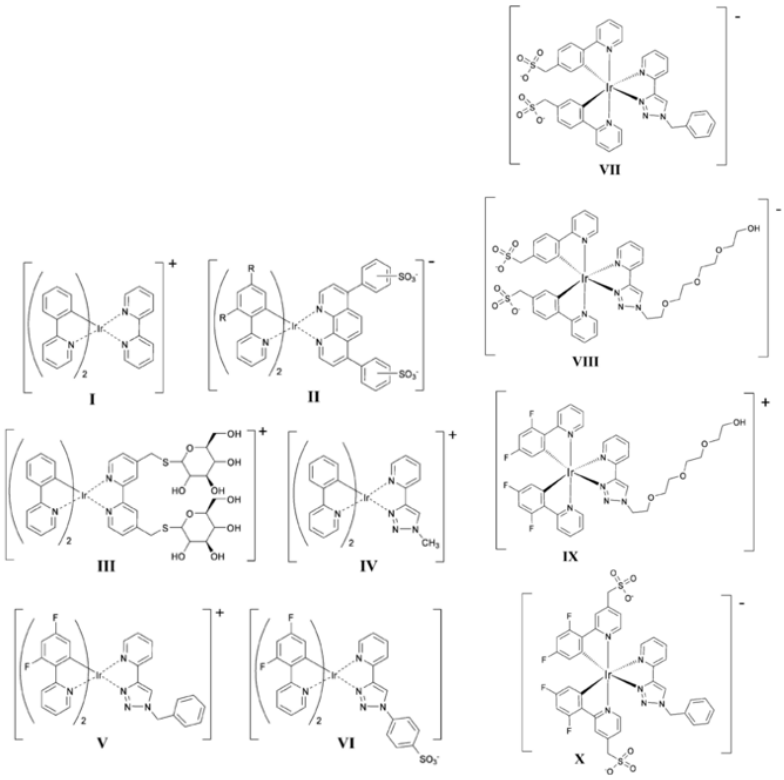

Figure 2-6. Water-soluble blue-emitting Ir(III) complexes

Very recently, Francis, P. S. et al.[100] reported blue ECL from water-soluble iridium complexes containing sulfonated phenylpyrinde or tetraethylene glycol derivatized triazolylpyridin ligands. Especially, complex IX containing tetraethylene glycol derivatized triazolypyridine as an ancillary ligand showed excellent ECL intensity, similar to that of $Ru(bpy)_3^{2+}$, and good solubility in water.

2. The requirements for good ECL-emitting Ir(III) complexes

The paper for efficient ECL from cyclometalated Ir(III) complexes, published by Lee, J.-K.'s group in 2005, [97] indicates us how to control the

HOMO and LUMO energy levels to enhance ECL efficiency of Ir(III) complexes. When an excess amount of TPA is employed as a coreactant, the excited species M* is produced as following reaction sequences.

$$\mathrm{M} - e^- \rightarrow M^{+\cdot} \quad (1)$$

$$\mathrm{TPA} - e^- \rightarrow TPA^{+\cdot} \quad (2)$$

$$M^{+\cdot} + TPA \rightarrow M + TPA^{+\cdot} \quad (3)$$

$$TPA^{+\cdot} \rightarrow TPA^{\cdot} + H^+ \quad (4)$$

$$M^{+\cdot} + TPA^{\cdot} \rightarrow M^* + side\ product \quad (5)$$

$$M + TPA^{\cdot} \rightarrow M^{-\cdot} + side\ product \quad (6)$$

$$M^{-\cdot} + M^{+\cdot} \rightarrow M^* + M \quad (7)$$

To realize high ECL efficiency, the electron-transfer reactions in reactions 3, 5, and 7 should occur effectively since direct oxidation of TPA on a Pt electrode (equation 2) usually occurs relatively slowly in a positive applied potential, contrary to the oxidation of the emitter could occur relatively fast. Therefore, it is important to additional oxidation process of TPA by the radical cation of emitter. In other words, the HOMO level of emitter should be higher than that of TPA for an efficient generation of TPA cation (Figure 2-7a).

Second, the most important process for ECL emitting is the electron transfer from TPA radical to the LUMO level of emitter (equation 5). The reducing power of TPA radical was reported by Bard's group, which studied by ECL quenching experiments in solution $(\epsilon^o(TPA^{\cdot}) = \sim -1.7\ V)$. [99] If the reduction potential of emitter is more negative than that of TPA radical, the ECL efficiency is lowered due to the poor generation of excited states M* (Figure 2-7b).

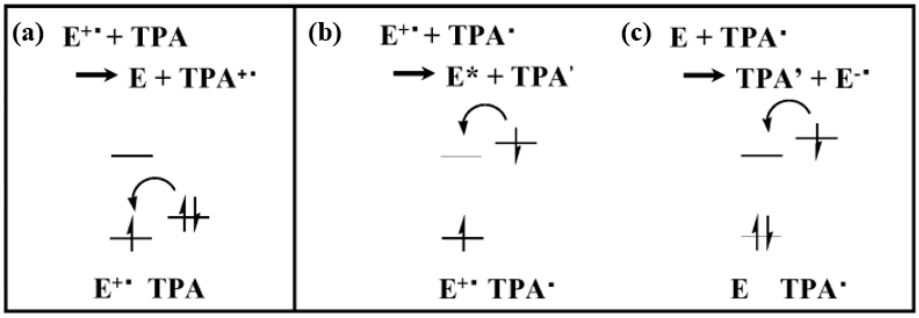

Figure 2-7. Postulated Efficient ECL route.

Finally, equation 6 expresses the generation of anion radical of emitter in oxidative process. The generation of anion radical enables to the additional emitting pathway, known to annihilation process. To enable the generation of anion radical of emitter, the potential of the TPA radical should be more negative than the reduction potential of the anion radical of emitter (Figure 2-7c). The three requirements could be summarized as following sentences: (i) the high oxidation potential ensures the efficient generation of TPA radicals by generating an emitter cation radial which in turn removes an electron form a HOMO level of TPA. (ii) The acceptor energy level (LUMO of M) should be lower than the potential of the TPA radical donor energy level.

In 2016, Francis, P. S. et al. reported the tutorial review about the chemical energy requirements of TPA coreactant pathway for the design of ECL-active Ir(III) complexes.[100] In that paper, they collected the conditions for good ECL emitters in four energetic requirements.

Firstly, when considering the generation of the excited state of emitter E* (equation 1, 2, 4, 5, and 7) the energy required to generate E* will be greater when the wavelength of emission is shorter ($E = hc/\lambda$). The critical values of E_{ox}° for each emission wavelength, which can be estimated from the requirement of a favorable free energy ($\Delta G < 0$) of the electron transfer reaction,

$$\Delta G = E^{\circ}(TPA^{\cdot}) - E^{\circ}_{ox} + E_{ES} \quad (8)$$

Where E_{ES} is the spectroscopic energy of the excited state (in eV) and $E^{\circ}(TPA^{\cdot})$ is the reduction potential of the TPA radical.

Second, in the catalytic route (equation 1, 3, and 4) the pathway could provide a more efficient TPA radical generation route, however it will only proceed if the potential of the M/M^{+} couple is more positive than the oxidation potential of the coreactant, TPA.

Third, the first reduction potential of the emitter $\left(E^{\circ}_{red}\right)$ is also an important factor in ECL efficiency. Iridium complex have to be capable of being reduced by the TPA radical intermediate (equation 6). In other words, the potential of the M/M^{-} couple must be less negative than that of TPA radical.

$$M^{-} + TPA^{+\cdot} \rightarrow M^{*} + TPA \quad (9)$$

Finally, another pathway in which the excited state of the emitter was generated by the reaction of emitter with TPA radical (equation 9). This process is dependent on favorable energetics for both the formation of M^{-} and the subsequent generation of the excited state species upon reaction with TAP cation radical. The energy required to generate the excited state in equation 9 will be greater when the wavelength of emission is shorter, and can be estimated by the following relationship:

$$\Delta G = E^{\circ}(M^{-}) - E^{\circ}(TPA^{+\cdot}) + E_{ES} \quad (10)$$

3. ECL Chemosensors Based on Cyclometalated Ir(III) Complex.

Although several Ir(III) complexes have been studied as ECL luminophores and phosphorescent probes for bioanalytes, ECL chemosensors based on cyclometalated Ir(III) complexes have been reported very rarely. As described in part 1, most ECL probes are based on ruthenium derivatives because of well-defined property, good solubility, and high ECL efficiency. Furthermore, most of ECL detection methods have been developed via specific

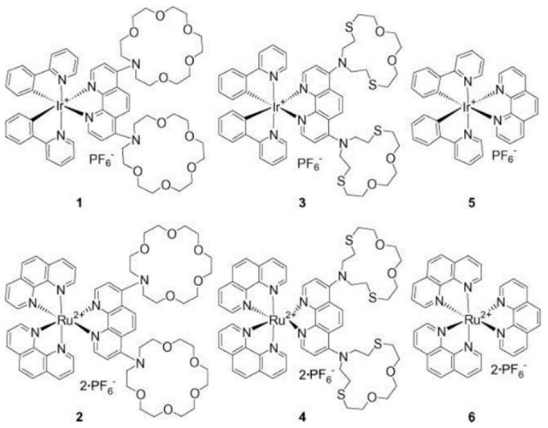

Figure 2- 8. Chemical structures of aza-crown metal complexes 1-6.

biomacromolecular recognition such as anti-body-antigen and DNA hybridization, ECL emitters have a limited role as a tagging or labelling unit.

Schmittel group reported several papers for ECL sensing based on cyclometalated Ir(III) complex. Firstly, they designed new Ir(III) and Ru(II) complexes by introducing azacrown ether moiety to ancillary ligand sensing metal cations in 2010.[101] In that paper, the comparison of Ir(III) and Ru(II) complexes were performed, and cyclometalated Ir(II) species showed the superior properties compared to Ru(II) species. Especially, Ir(III) complex 1 and 3 showed excellent selectivity and high ECL turn-on ratio for Ba^{+} and Ag^{+}, respectively.

In 2012, they reported a dual-channel lab-on-a-molecule for anion sensing based on iridium chloro-bridged dimer.[102] Iridium dimer itself did not show any PL and ECL signal, however, in the presence of specific anions such as

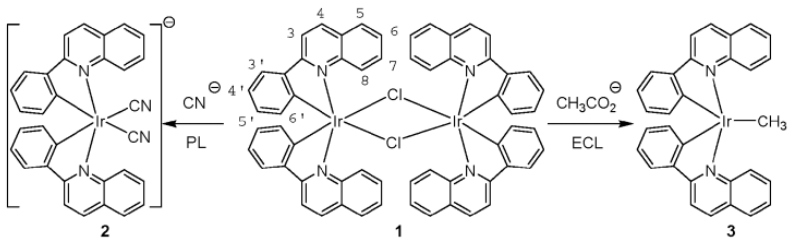

Figure 2-9. Iridium chloro-bridge dimer based anion sensing by PL and ECL dual channel.

cyanide and acetate PL and ECL intensity increased respectively.

They also reported bis(ferrocenyl)phenanthroline iridium(III) complex as a lab-on-a molecule for cyanide and fluoride in aqueous solution in 2012.[103] In that paper, the ECL intensity increased upon the addition of fluoride due to the complexation between ferrocene and fluoride. The formation of ferrocene-fluoride complex effects on the orbital energy level and electronic configuration of iridium complex, which induces the excited-state species.

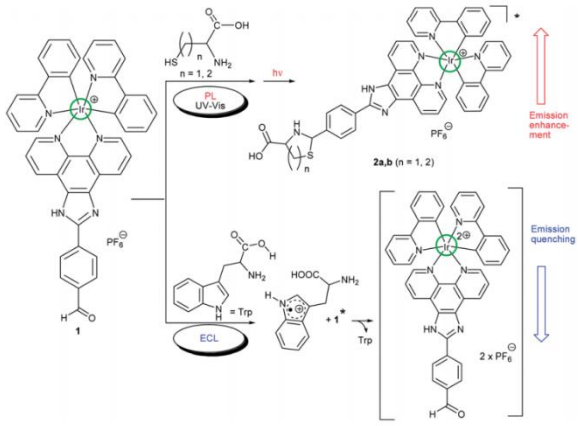

Figure 2-11. Ir(III) complex based ECL probe for amino acids.

Similar types of dual-channel or triple-channel probes reported steadily. In

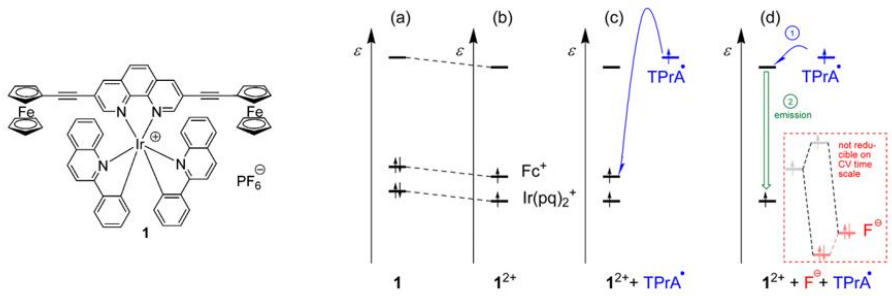

Figure 2-10. The structure and energy diagrams of Ir(III)-ferrocene probe 1.

2013, an iridium(III)-based lab-on-a-molecule for cysteine/homocysteine and tryptophan by triple channel was developed.[104] Cysteine and homocysteine react with formyl group of ancill ary ligand, which forms the five- and six-membered ring, respectively. These structural changes induce the PL enhancement, which can be distinguished with other amino acids. In the ECL channel, tryptophan was oxidized easily and quenched the ECL signal of iridium complex by disturbing the formation of exited state species.

Iridium(III)–imidazolium conjugate that can detect three different anions by UV, PL, and ECL triple channel was also developed in 2014.[105] The energy level of imidazolium located between the HOMO and LUMO levels of Ir(III) c omplex, which induces the PET quenching of PL intensity. However, the energy level of imidazolium increased in the presence of $H_2PO_4^-$, PET process was blocked. In ECL process, both the Ir^{4+}-based SOMO and the

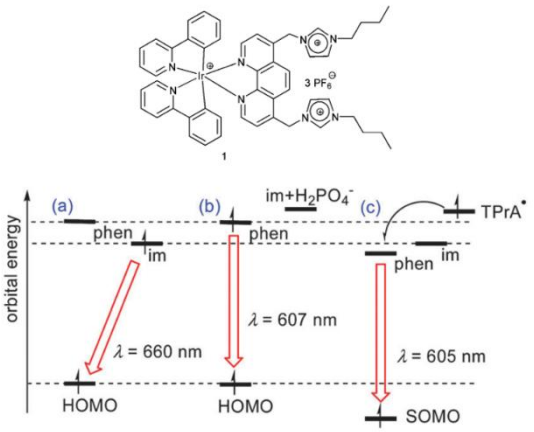

Figure 2-12. The structure of Ir-imidazolium conjugate probe 1 and energy level diagrams of (a) PL of 1 (b) PL of 1-$H_2PO_4^-$ (c) ECL.

phenanthroline-based LUMO are lowered in energy. As the latter falls below the energy level of the imidazolium unit, the ECL arises from a characteristic MLCT and is not affected PET process. Instead, the ECL of 1 enhanced in the presence of OAc^-, however this selective ECL response remained somewhat speculative.

Section 1

Electrochemiluminescent "Turn-on" Probe for Highly Sensitive and Selective Determination of Homocysteine

1.1. Introduction

Homocysteine (Hcy) is a naturally occurring, sulfur-containing amino acid produced by demethylation of methionine.[106] It is an essential amino acid found in both animal and plant proteins. A Hcy level between 5 and 15 μM in plasma is generally considered normal.[107] However, an elevated level of Hcy is strongly linked to cardiovascular disease,[106b,108] Alzheimer's disease,[109] neural tube defects, and osteoporosis [110] in humans. A previous study reported that the average Hcy level of Americans was 8 μM, and 20–30% of aged individuals (≥60 y) suffered from increased Hcy levels (>13 μM) during 1991–2004.[111] A routine, easy to use procedure for the determination of Hcy is highly desirable. Various methods are now available for Hcy analysis, such as high-performance liquid chromatography (HPLC),[112] and colorimetric,[113] radioactive,[114] and photoluminescence (PL)[115] immunoassay methods. Despite showing good performance for Hcy determination, these methods require rather fragile, bulky, and costly instruments, thereby restricting their use in clinical and laboratory-based research.

Electrochemiluminescent sensing platforms show important advantages over conventional analytical techniques; electrochemistry enables more cost- and time-efficient chemical analysis in a simpler manner without requiring

bulky equipment, additional reagents, or isotopes. In addition, as light emission can only be generated via an electrochemically triggered chemiluminescence process, the method is highly sensitive without

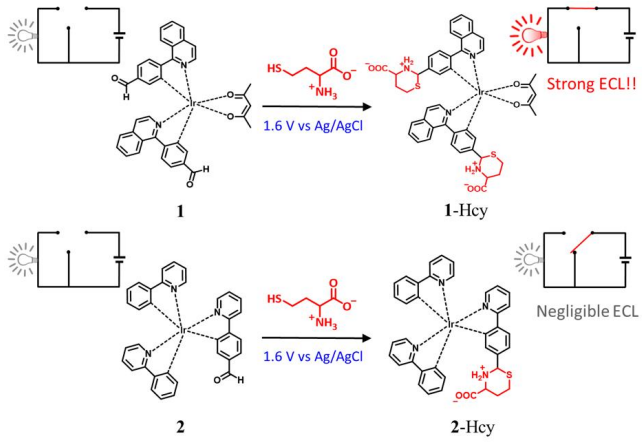

Scheme 2-1. Electrochemiluminescent sensing of homocysteine in aqueous solution

background fluorescent emission.[116]

Herein, we report a new sensing strategy for qualitative and quantitative analysis of Hcy (Scheme 1) in which a cyclometalated iridium complex-based probe (**1**) undergoes selective chemical reaction with two molecules of Hcy, and the resulting adduct (**1**–Hcy) subsequently produces efficient electrochemiluminescence (ECL) in aqueous media. The method is based on the following; (i) selective ring formation between a formyl group (−CHO) of **1** and Hcy, (ii) changes in the photophysical properties and energetic condition of the probe molecule due to the ring formation reaction, and finally (iii) the efficient ECL generated from the reaction adduct, **1**–Hcy. Probe **1** contains two aldehyde-functionalized phenylisoquinoline (piq) groups (–CHO–piq) as main ligands. The formyl group of **1** reacts with the free amine group of Hcy to form a **1**–Hcy containing six-membered 1,3-thiazinanes, where sp^2 carbonyl carbon converts to sp^3. The structural change in the main

ligand causes greatly enhanced ECL of **1**–Hcy at around 615 nm, whereas **1** showed almost no ECL. Throughout the study, we observed the thermodynamic changes in the probe molecule caused by ring formation with Hcy. Thus, we identified the thermodynamic conditions required for probe **1** to produce efficient ECL after Hcy recognition. The ECL intensity of probe **1** was gradually enhanced by selective response to the amount of Hcy. Our designed probe is able to quantify the level of Hcy with a linear correlation between 0–40 μM in 99.9% aqueous media. The approach provides a new proof-of-concept for point-of-care testing of Hcy levels based on ECL.

1.2. Results

We selected highly luminescent $(piq)_2Ir(acac)$ (piq = 1-phenylisoquinoline; acac = acetylacetonate, Φ_{PL} = 0.2, λ_{max} = 613 nm) as a model compound for **1**–Hcy. It showed almost Nernstian oxidation at an easily attainable potential ($E^{o'}_{ox}$ = 0.44 V vs Ag/Ag^+), and exhibited efficient orange-red ECL at around 615 nm with a tri-*n*-propylamine (TPA) coreactant under air-saturated conditions. The relative intensity of ECL emission from $(piq)_2Ir(acac)$/TPA was estimated to be 2 times higher than that from the electrochemical reaction between $Ru(bpy)_3^{2+}$ and TPA. Compared to $(piq)_2Ir(acac)$, probe **1**, which possesses an additional formyl group at the 4-position of the phenyl ring of each piq ligand, showed dramatically decreased PL (Φ_{PL} = ~0.001) in the red-shifted region (λ_{max} = 655 nm) due to the strong electron withdrawing ability of the formyl groups. However, largely enhanced PL (Φ_{PL} = 0.11), similar to that from $(piq)_2Ir(acac)$, was recovered owing to the disappearance of the formyl group when excess Hcy was added to the solution of **1** (λ_{max} = 613 nm). This blue-shifted emission is related to the increase in the HOMO-LUMO

energy gap of the organometallic complex; the loss of formyl groups via reaction with Hcy caused the LUMO level of the binding adduct to increase.

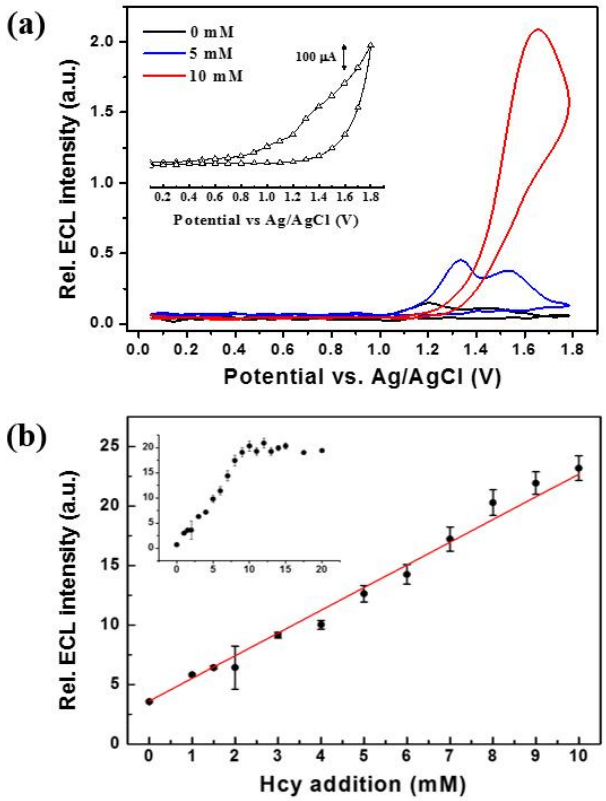

Figure 2-13. (a) ECL intensity of 50 µM **1** upon addition of Hcy in H_2O/MeCN (1:1 v/v, pH 7.4, 10 mM TPA, 10 mM HEPES, and 0.1 M $NaClO_4$ as the supporting electrolyte) as the potential is swept at a Pt disk electrode (diameter: 2 mm) over the range 0–1.8 V vs Ag/AgCl (scan rate: 0.1 V/s). (Inset: cyclic voltammogram of a solution of 50 µM 1 in the presence of 5 mM Hcy). (b) Isothermal binding curve obtained for ECL titration upon addition of Hcy in H_2O/MeCN (1:1 v/v, pH 7.4, 10 mM TPA, 10 mM HEPES, and 0.1 M $NaClO_4$ as the supporting electrolyte)

ECL measurements were performed in an aqueous mixture of 50 µM probe **1** and 10 mM TPA. During the cyclic voltammetry (CV) process, no significant ECL was observed from **1** in the aqueous media (pH 7.4, HEPES buffer/CH_3CN = 1:1 v/v), but the emission intensity gradually increased with addition of Hcy. The ECL emission profile of the probe solution is shown in Figure 2-13a; while no emission was observed in the absence of Hcy, ECL

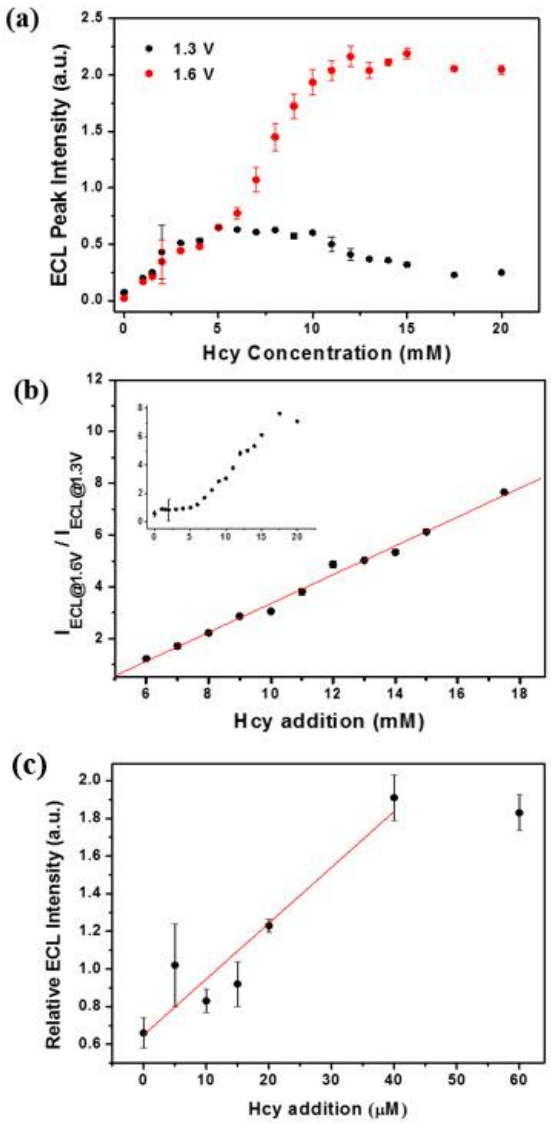

Figure 2-14. (a) ECL peak intensities at 1.3 and 1.6 V upon Hcy addition, and (b) ratio of the peak intensities between 1.3 and 1.6 V upon Hcy addition. (c) ECL intensity of 0.1 μM probe **1** upon addition of Hcy in H_2O/DMSO (99.9:0.1 v/v, pH 7.4, 10 mM TPA, 10 mM HEPES, and 0.1 M $NaClO_4$).

showed two maximum peak intensities at around 1.3 and 1.6 V (vs Ag/AgCl) upon addition of 5 mM Hcy, and a single-spiked, enhanced emission peak was observed at 1.6 V when 10 mM Hcy was added to the solution. A binding titration curve was obtained from a plot of the ECL intensity of **1** against

various concentrations of Hcy (Figure 1b). This indicates that the emission signal increases linearly with Hcy addition over the range 0–10 mM when the concentration of **1** is kept constant at 50 μM (R^2 = 0.995, $y = 2.0 \times 10^{-9}x + 1.7 \times 10^{-9}$). The estimated limit of detection (LOD) was 41 μM (signal-to-noise (S/N) ratio = 3, n = 5).

Interestingly, as shown in Figure 2-13a, the two emission peaks appear in the ECL titration profiles; during the first stage of Hcy addition, the two ECL emission peaks at 1.3 and 1.6 V gradually increase until 5 mM (100 equiv.) Hcy was added. Upon further addition of Hcy, the former peak decreases whereas the latter continues to increase. Figure 2-14a shows the variation in ECL peak intensity at 1.3 and 1.6 V. The signals at 1.3 and 1.6 V increase until addition of 100 equiv. Hcy (5 mM). Then, a new increment starts at 1.6 V, reaching saturation at 200 equiv. Hcy (10 mM), while the ECL intensity at 1.3 V decreases. Since **1** contains two formyl groups, it was expected to react with Hcy in a 1:1 molar ratio in the early stages of Hcy addition, followed by the formation of 1:2 adduct **1**–Hcy in the latter stages. So, the increase around 1.3 V is presumably due to the formation of a 1:1 product of **1** and Hcy, and the signal at 1.6 V originates from the final 1:2 product (**1**–Hcy). A ratiometric approach exploiting the two signals at 1.3 and 1.6 V provides a linear calibration curve over the range 6–17 mM (Figure 2b, R^2 = 0.996, $y = 0.56x - 2.2$).

Blood Hcy level is normally between 5–15 μM and approximately 5 μM Hcy should therefore be detectable in order to assess potential risks to patients. Our estimated LOD (41 μM) is higher than that required for practical determination of Hcy abnormalities.[106,108c] Thus, we fabricated a 25 μL volume ECL cell, modified from our previous flow cell system, in order to lower the detection limit for Hcy.[119] The cell was placed directly in front of a photon multiplier tube detector with a short path length of 1 mm, so that

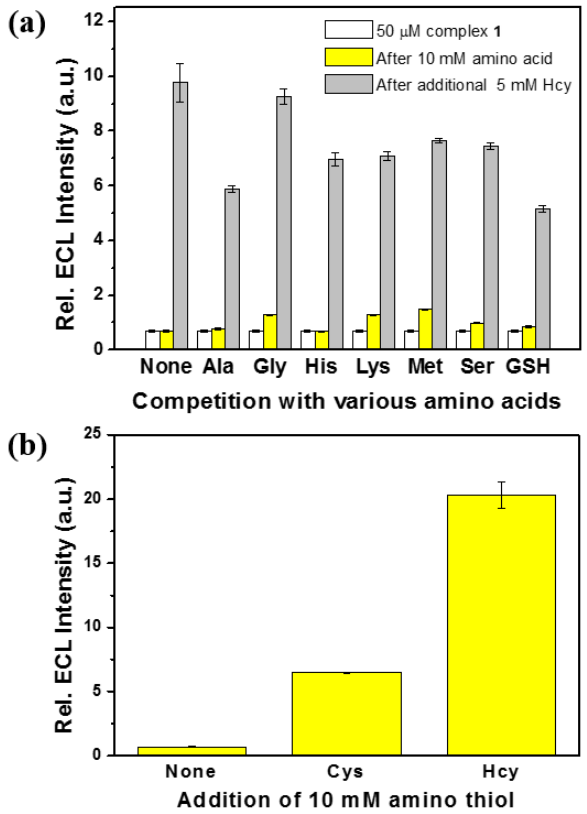

Figure 2-15. Competitive ECL binding assays performed with (a) addition of 5 mM Hcy to 50 μM probe **1** in the presence of 10 mM various amino acids, and (b) comparison of ECL intensity after addition of 10 mM Hcy and 10 mM Cys to 50 μM probe **1** in H_2O/MeCN (1:1 v/v, pH 7.4, 10 mM TPA, 10 mM HEPES, and 0.1 M $NaClO_4$.

higher sensitivity for ECL emission was expected. Using the new system, 0.1 μM **1** was incubated with various amounts of Hcy in 99.9% aqueous media, and finally a linear correlation between the ECL intensity and Hcy was obtained over the range 0−40 μM ($y = (3.0 \times 10^{-11})x + 6.5 \times 10^{-10}$), which almost covers the required range for clinical diagnosis (Figure 2c). The LOD of Hcy was estimated to be 7.9 μM (S/N ratio = 3, $n = 5$).

A competitive binding assay was carried out to evaluate the selectivity of **1** for Hcy recognition in the presence of other amino acids. Five mM Hcy was added to a solution of 50 μM **1** containing 10 mM other amino acids or

glutathione (GSH) (Figure 2-15a). The results show that the ECL intensity of **1** changes slightly upon addition of a 200-fold excess of other amino acids. However, a remarkable change in ECL intensity occurs when 5 mM (100 equiv.) Hcy was added to a solution of **1** and amino acids; despite the presence of a 200-fold excess of amino acids, the emission intensity approached 54–97% of that obtained in the absence of amino acids. PL competition assays showed similar results, indicating that **1** selectively recognizes Hcy without interference from other amino acids.

Only cysteine (Cys) can cause strong interference because of its structural similarity to Hcy. As shown in Figure 2-15b, an ECL signal was also observed upon addition of 10 mM Cys, indicating that **1** formed a binding adduct with Cys as well as Hcy. However, **1** shows 3.2 times stronger ECL intensity with Hcy (Figure 2-15b) than with Cys. These results correlate well with our previous findings, where a CHO-containing fluorescence probe showed 2.5 times higher selectivity to Hcy compared to Cys in fluorescence binding assays.[115a]

PL determination of Hcy with similar probes has been previously reported by us and other groups.[115,118] Huang *et al.* developed a –CHO-containing Ir(III) complex, $(pba)_2Ir(acac)$ (**3**, pba = 4-(2-pyridyl)benzaldehyde), which exhibited enhanced phosphorescence intensity with blue-shifted emission upon Hcy recognition.[10b] Recently, Schmittel *et al.* reported a similar approach, where enhanced PL intensity was achieved upon reaction of an Ir(III) complex with Hcy, but almost negligible ECL was observed after target recognition.[118]

From an electrochemical viewpoint, destabilization of the LUMO distribution of the probe as a result of –CHO breakdown causes its reduction potential to shift to a more negative value. Therefore, in the previous report,[115b] the binding adduct of $Ir(pba)_2(acac)$ (**3**) and Hcy was expected to

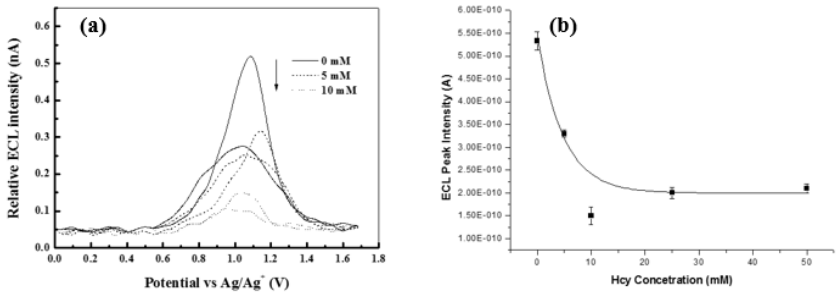

Figure 2-16. (a) ECL spectra of 2 (50 μM) in the absence and presence (5 mM and 10 mM, each) of Hcy. (b) ECL titration curve of 2 (50 μM) upon addition of Hcy. (HEPESbuffer/MeCN, 1:1 v/v, pH 7.4)

possess a considerably negative reduction potential. In the ECL process, however, the highly negative reduction potential prevented electron transfer from the TPA radical to the LUMO of the binding adduct, hardly generating the excited states.[97, 117] Iridium complexes possessing 2-phenylpyridine ligands are known to have similar or slightly more negative reduction potentials than the TPA radical,[12c,12d,12e] and therefore, elevation of the LUMO of **3** after reaction with Hcy would presumably quench its ECL signal by preventing energy transfer from the TPA radical to Ir(III) complex. (Scheme 2-2).

Taking this into consideration, we rationally designed Ir(III) complex (**1**) as an efficient ECL probe for Hcy determination. In other words, we changed pyridine to a more strongly electron withdrawing isoquinoline unit in the main ligand for stabilization of the LUMO, which would result in a turn-on ECL

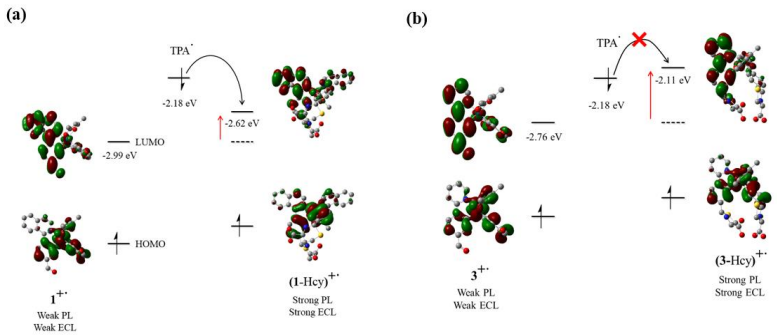

Scheme 2-2. Thermodynamic explanation for Hcy sensing of probes **1** and **3** obtained by DFT calculations.

signal of **1**–Hcy as in the PL experiments.

Density functional theory (DFT) calculations predicted that the LUMO energy level of **1**–Hcy is lower than that of the TPA radical HOMO, even after formation of the binding adduct **1**–Hcy, so that **1** is expected to generate efficient ECL in response to Hcy (Scheme 2-2a). On the other hand, the LUMO energy level of **3**, the probe used in Huang's report, is drastically elevated after binding with Hcy and is consequently higher than the HOMO level of the TPA radical (Scheme 2-2b). In this case, ECL generation could not proceed properly because electron transfer from the TPA radical to the LUMO of $(\mathbf{3}\text{–Hcy})^{+\cdot}$ would be unfavorable.

In order to confirm this experimentally, we synthesized two iridium complexes, $(pba)_2Ir(acac)$ (**3**) and $(ppy)_2Ir(pba)$ (probe **2**, Scheme 2-1). The former is that reported by Huang *et al.*, and the latter is a new Ir(III) complex possessing almost the same physicochemical properties as **3**. **2**–Hcy, the binding adduct of **2** with Hcy, showed largely enhanced PL intensity with a significant blue-shift, similar to that of **3**. As expected, the ECL intensity was gradually attenuated upon Hcy addition to **2** (Figure 2-16); the reaction

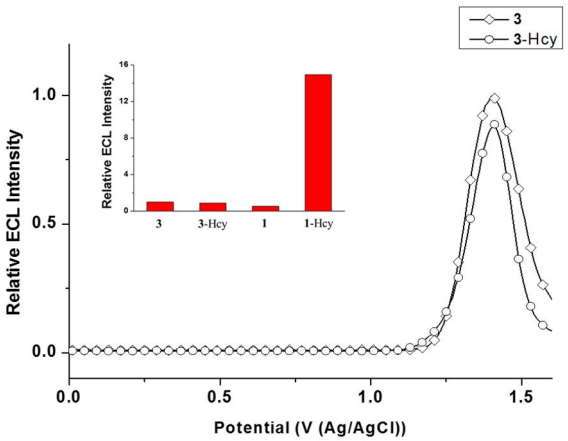

Figure 2-17. ECL spectra of **3** (50 μM) in the absence and presence (5 mM) of Hcy. (Inset) Relative ECL intensity of **3**, **3**-Hcy, **1**, and **1**-Hcy. (**1**, **3**: 50 μM, Hcy: 5 mM, each, HEPES buffer/MeCN, 1:1 v/v, pH 7.4)

mixture of 50 μM **2** and 10 mM Hcy showed further decreased ECL during CV (between 0−1.5 V at 0.1 V/s), while **2** showed weak ECL around 0.8 V before Hcy addition. The ECL properties of **3** and **3**–Hcy also showed similar tendencies to those of **2** and **2**–Hcy, respectively (Figure 2-17).

The CV studies further supported the theoretical predictions. As shown in Table S1, the reduction potential of $(ppy)_2Ir(pba)$ (**2**) is $E^{o'}_{red}$ = −1.66 V (vs SCE), which negatively shifts to −1.99 V after binding with Hcy. The reduction potential of the TPA radical is estimated as ~−1.7 V, [121] which provides an explanation as to why the binding adduct **2**–Hcy hardly produces the excited states via the ECL process. However, in the case of probe **1**, the binding adduct **1**–Hcy has a relatively mild reduction potential (E^{o}_{red} = −1.28 V), which is less negative than the reduction potential of the TPA radical (−1.7 V). Therefore, efficient production of excited states and ECL emission are expected.

1.3. Conclusion

In conclusion, we have demonstrated the first example of ECL-based Hcy analysis involving exclusive turn-on ECL emission after selective reaction with Hcy. In the presence of Hcy, the synthetic probe **1** exhibits strong light emission in aqueous solution by electrochemical triggering. The observed ECL of Hcy is distinguishable from that of Cys, GSH, and other amino acids. Monitoring of the emission profile against the applied potential provides additional mechanistic information on the reaction between **1** and Hcy which cannot be obtained in a typical PL study. We expect that our systematic chemodosimetric approach will emerge as a useful tool to develop various ECL probes based on Ir(III) complexes for small biotargets.

1.4. Experimental Section

1.4.1. Instrumentation

^{1}H and ^{13}C NMR spectra were recorded using a Bruker Advance DPX-300. Chemical shifts are given in parts per million using as internal reference the residual resonances of deuterated solvents. ESI-MS data were obtained using a QUATTRO LC Triple Quadrupole Tandem Mass Spectrometer and are reported in units of mass to charge (m/z). High-resolution mass spectroscopy (MALDI-TOF) was performed on a Voyager-DE STR Biospectrometry Workstation. Analytical thin layer chromatography was performed using Kieselgel 60F-254 plates from Merck. Column chromatography was carried out on Merck silica gel 60 (70-230 MESH) and Merck Aluminium oxide 60 (70-230 MESH ASTM).

1.4.2. Materials

All reagents were purchased from either Sigma-Aldrich (Sigma-Aldrich Corp., MO, USA) or TCI (Tokyo Chemical Industry, Tokyo, Japan) and used without any further purification. Deuterated solvents were acquired from CIL (Cambridge Isotopic Laboratories, MA, USA). All amino acids were purchased from Sigma-Aldrich or TCI.

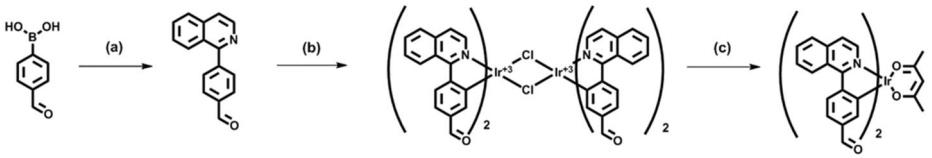

Scheme 2-3. Synthesis of Iridium(III) complex **1**. (a) 1-chloroisoquinoline, $Pd(PPh_3)_4$, K_2CO_3, THF, H_2O, reflux; (b) Iridium chloride hydrate, 2-ethoxyethanol, H_2O, reflux; (c) acetylacetone, Na_2CO_3, 2-ethoxyethanol, reflux

1.4.3. Synthesis of Ir(III) complex

Synthesis of 4-(isoquinolin-1-yl)benzaldehyde (5)

A mixture of 4-formylphenylboronic acid (1145 mg, 7 mmol), 1-chloroisoquinoline (1049 mg, 7 mmol), $Pd(PPh_3)_4$ (404 mg, 0.35 mmol) and potassium carbonate (1934mg, 14 mmol) in THF (40 mL) and H_2O (40 mL) was refluxed for 24 h. After cooling to room temperature, the reaction mixture was extracted with dichloromethane (MC), and the organic phase was washed with water, and dried over Na_2SO_4. The solvent was evaporated to give an white solid product (1372 mg, 84% yield), which was purified by silica gel column chromatography (eluent; EA/Hexane (Hex)=1:5).

300 MHz ^{1}H NMR (chloroform-d): δ 10.15 (s, 1H); 8.65 (d, 1H, J = 6.3 Hz); 8.02~8.08 (m, 3H); 7.93 (d, 1H, J = 10.1 Hz); 7.89 (d, 2H, J = 10.1 Hz); 7.73 (t, 1H, J = 7.8 Hz); 7.72 (d, 2H, J = 7.1 Hz); 7.58 (t, 1H, J = 8.0 Hz).

Synthesis of 6

A mixture of **5** (1g, 4.29 mmol) and Iridium chloride hydrate (576 mg, 1.93 mmol) in 2-ethoxyethanol (30 mL) and H_2O (10 mL) was refluxed for 12h. After cooling to room temperature, pouring cold water (~50 mL) to reaction mixture. Then a dark brown precipitate was filtered to crude cyclometalated Ir(III) chloro-bridged dimer.

Synthesis of 1

A mixture of crude cyclometalated Ir(III) dimer (**6,** 330 mg, 0.245 mmol), sodium carbonate (260 mg, 2.45 mmol) and acetylacetone (0.252 mL, 2.45

mmol) in 2-ethoxyethanol (10 mL) was refluxed 8h. After cooling to room temperature, the reaction mixture was extracted with dichloromethane (MC), and the organic phase was washed with water, and dried over Na_2SO_4. The solvent was evaporated to give a black solid product (229mg, 61% yield), which was purified by silica gel column chromatography (eluent; MC/methanol = 100:1).

300 MHz ^{1}H NMR (DMSO-d_6): δ 9.59 (s, 2H); 9.06 (d, 2H *J* = 8.85 Hz); 8.46 (m, 4H); 8.24 (d, 2H, *J* = 7.11 Hz); 7.98 (m, 6H); 7.40 (d, 2H, *J* = 8.25 Hz); 6.70 (s, 2H); 5.28 (s, 1H); 1.70 (s, 6H). 75 MHz ^{13}C ($CDCl_3$-d): δ 193.268, 185.179, 152.895, 151.009, 140.470, 137.315, 135.466, 134.930, 131.164, 129.581, 128.464, 127.605, 126.898, 126.500, 121.723, 121.592, 28.690. HRMS (FAB$^+$, *m*-NBA): *m/z* observed 756.1602 (calculated for

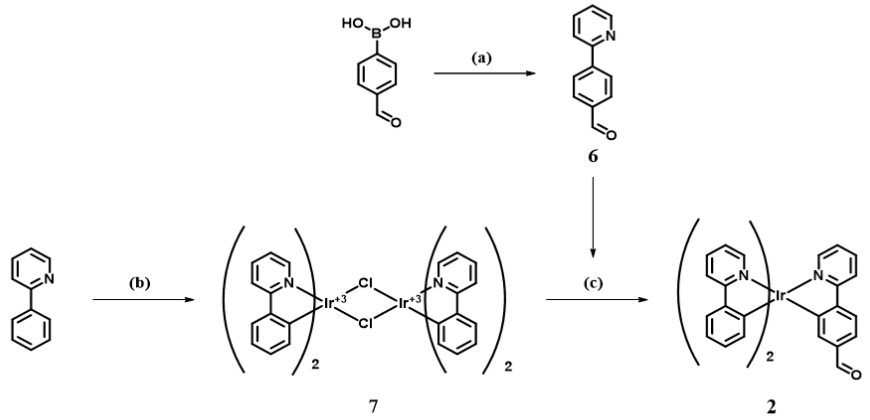

Scheme 2-4. Synthesis of Iridium(III) complex **2**. (a) 2-Bromopyridine, $Pd(PPh_3)_4$, K_2CO_3, THF, H_2O, reflux; (b) Iridium chloride hydrate, 2-ethoxyethanol, H_2O, reflux; (c) $AgCFSO_3$, diglyme, 110°C, 24h.

$C_{37}H_{27}N_2IrO_4$ $[M]^+$ 756.1600).

Synthesis of 6

A mixture of 4-formylphenylboronic acid (1145 mg, 7 mmol), 2-bromopyridine (0.667 mL, 7 mmol), $Pd(PPh_3)_4$ (404 mg, 0.35 mmol) and potassium carbonate (1934mg, 14 mmol) in THF (40 mL) and N_2-bubbled H_2O (40 mL) was refluxed for 24 h. After cooling to room temperature, the reaction mixture was extracted with dichloromethane (MC), and the organic phase was washed with water, and dried over Na_2SO_4. The solvent was evaporated to give an white solid product (826 mg, 76% yield), which was purified by silica gel column chromatography (eluent; MC/MeOH = 100:1 ~ 20:1).

Synthesis of 7 (crude form)

A mixture of **2** (1g, 6.44 mmol) and Iridium chloride hydrate (865 mg, 2.90 mmol) in 2-ethoxyethanol (45 mL) and H_2O (15 mL) was refluxed for 12h. After cooling to room temperature, pouring cold water (~100 mL) to reaction mixture. Then a yellow precipitate was filtered to crude cyclometalated Ir(III) chloro-bridged dimer.

Synthesis of 3

A mixture of **1** (360 mg, 2 mmol), **7** (214 mg, 0.2 mmol), silver trifluoromathanesulfonate (109 mg, 0.4 mmol) and diglyme (10 mL) was placed in reaction vessel and degassed. The reaction mixture was heated at 110 °C whilst under continuous stirring for 24 hours. The resulting dark orange-red solution was cooled to room temperature and water added. The suspension was filtered and the residue dissolved in dichloromethane. This solution was then chromatographed. The pure product was isolated as a red solid. (20% yield)

300 MHz ^{1}H NMR ($CDCl_3$): δ 9.64 (s, 1H); 8.01 (d, 1H J = 4.42 Hz); 7.92 (d, J = 4.42 Hz, 2H); 7378 (d, 1H, J = 8.7 Hz); 7.67 (m, 6H); 7.53 (q, 2H); 7.36 (d, J = 9.5 Hz 1H); 7.22 (d, J = 8.87 Hz 1H); 7.02 (m, 1H); 6.84 (m, 7H); 6.65 (m, 1H). HRMS (FAB^+, *m*-NBA): *m/z* observed 683.1538 (calculated for $C_{37}H_{27}N_2IrO_4$ $[M]^+$ 683.1548).

*$(ppy)_2Ir(acac)$ (**3**) [115b] and $(piq)_2Ir(acac)$ [122] were synthesized according to previous reports.

1.4.4. Electrochemical and electrogenerated chemiluminescent (ECL) measurements

Electrochemical study was performed with a CH Instruments 660 Electrochemical Analyzer (CH Instruments, Inc., TX, USA). In the electrochemical study, cyclic voltammetry (CV) and differential pulse voltammetry (DPV) was applied to the individual solutions in order to investigate electrochemical oxidative and reductive behaviors. Particularly, a CH Instruments 650B Electrochemical Analyzer was used in the ECL experiments to apply potential sweeps. ECL spectra was gained using a charge-coupled device (CCD) camera (LN/CCD 1752-PB/VSAR, Princeton Instruments, NJ, USA) cooled to below −120 ^oC using liquid N_2. The ECL intensity profile was obtained using a low-voltage photomultiplier tube module (H-6780, Hamamatsu photonics K. K., Tokyo, Japan) operated at 1.0 V. A 10 mL-sized ECL cell was directly mounted CCD or PMT module with home-made mounting support during the experiments. All the ECL data were collected upon the simultaneous cyclic voltammetry on the solution. The ECL solutions commonly contained 10 μM 1-2Zn, 10 mM TPrA (Sigma-Aldrich,

MO, USA) coreactant, and 0.1 M tetrabutylammonium hexafluorophosphate (TBAPF6, Sigma-Aldrich) supporting electrolyte in acetonitrile (MeCN, HPLC grade, Sigma-Aldrich) solution. Especially, TPrA was selected and used as an ECL coreactant as it has been widely studied and known on its electrochemical properties. The ECL solutions were prepared in a dry-box incorporating a N_2 atmosphere or were prepared in air, purged with N2, and then sealed in an air-tight cell. All the electrochemical and ECL experiments were referenced with respect to an Ag/Ag+ reference electrode. All potential values were calibrated against the saturated calomel electrode (SCE) by measuring the oxidation potential of 1 mM ferrocene (vs Ag/Ag+) as a standard (Eo(Fc+/Fc) = 0.424 V vs SCE). Cyclic voltammetry for ECL experiments was applied to Pt disk electrode (2 mm dia.) ranged between 0.3 ~ 1.3 V at the scan rate of 0.1 V/s. The electrochemical and ECL solutions were freshly prepared in each experiment, and Pt working electrode was polished with 0.05 M alumina (Buehler, IL, USA) on a felt pad following sonication in the 1:1 mixed solution of deionized water and absolute ethanol for 5 min. Then the electrode was blown by ultra pure N2 gas for 1 min. A single solution was only used for one experimental try, and discarded after collecting data. The reported ECL values were obtained by averaging the values from at least five tries with a good reliability in the MeCN solution.

Table 2-1. Electrochemical properties of Ir(III)-based Hcy probes

Compound	[a] $E_{ox}^{0'}$ (V vs SCE)	[b] $E_{red}^{0'}$ * (V vs SCE)	E_{0-0} * (eV)
3	0.40	-1.66	2.06
3-Hcy	0.37	-1.99	2.36
3-Cys	0.38	-1.98	2.36
1	0.77	-1.04	1.81
1-Hcy	0.74	-1.28	2.02
1-Cys	0.70	-1.32	2.02

[a]The oxidation potentials were measured using cyclic voltammetry at the scan rate of 0.1 V/s in acetonitrile (CH_3CN) solutions with 0.1M tetra-*n*-butylammonium perchlorate as the supporting electrolyte and then the values were calibrated against the oxidation of 1 mM ferrocene (Fc/Fc^+) as a standard and then referenced to SCE. [b]The values of the reduction potential were calculated from the excitation energies (E_{0-0}) and the oxidation potentials ($E_{ox}^{0'}$).

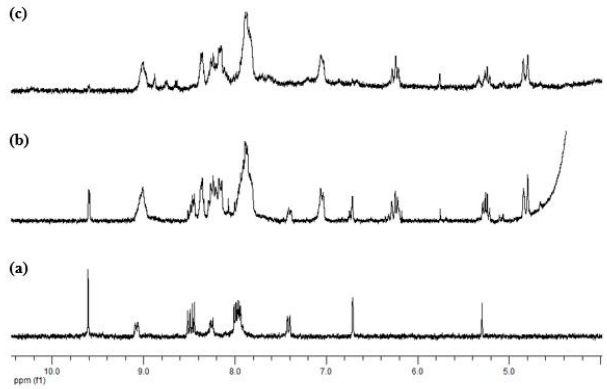

Figure 2-18. Partial ^{1}H NMR spectra of 1 (a), 1 + Hcy (10 eq) (b), and 1 + Hcy (50 eq) (c) in DMSO-d_6.

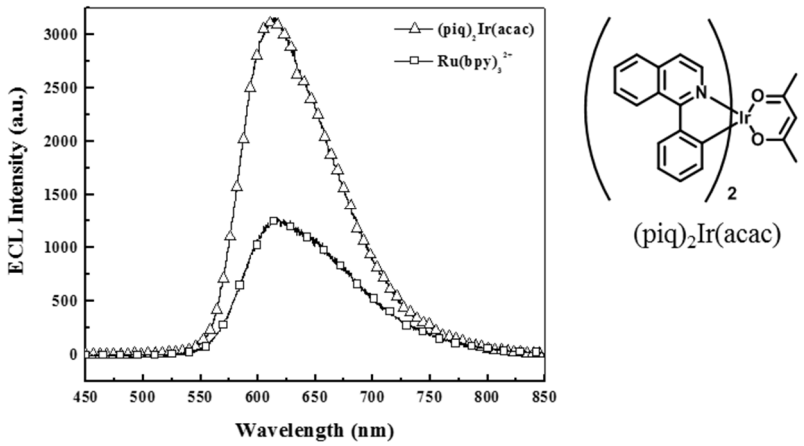

Figure 2-19. ECL spectra of $(piq)_2Ir(acac)$ and $Ru(bpy)_3^{2+}$ (10 μM, each) in MeCN solution. (10 mM TPrA as a coreactant and 0.1M $NaClO_4$ as supporting electrolyte)

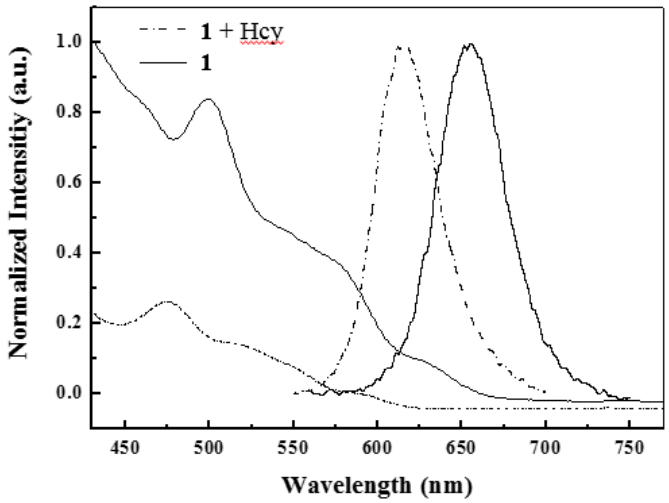

Figure 2-20. Normalized absorption and emission spectra of probe **1** (10 μM) in the absence (solid line) and presence (dotted line) of Hcy (1 mM).

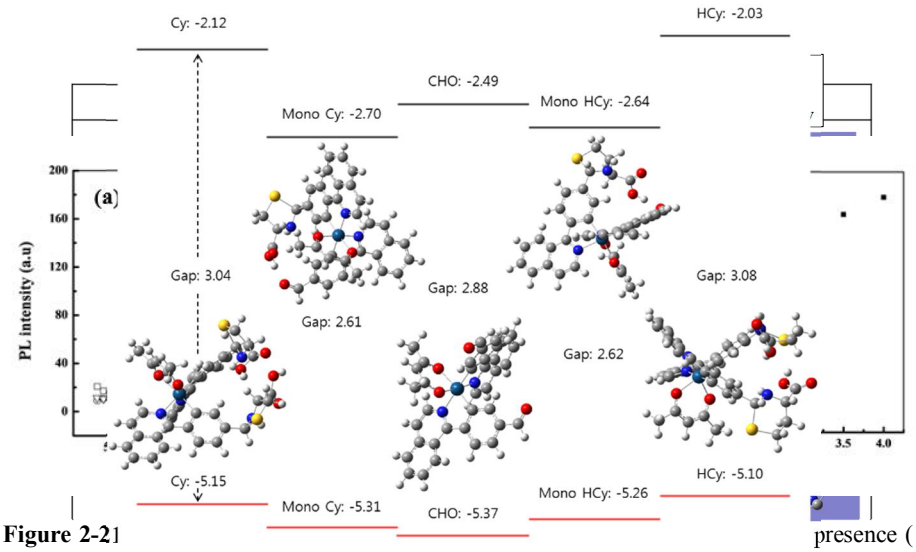

Figure 2-21 presence (1

Figure 2-22. DFT calculation of energetic changes in the complex **1** upon the addition of Hcy (or Cys).

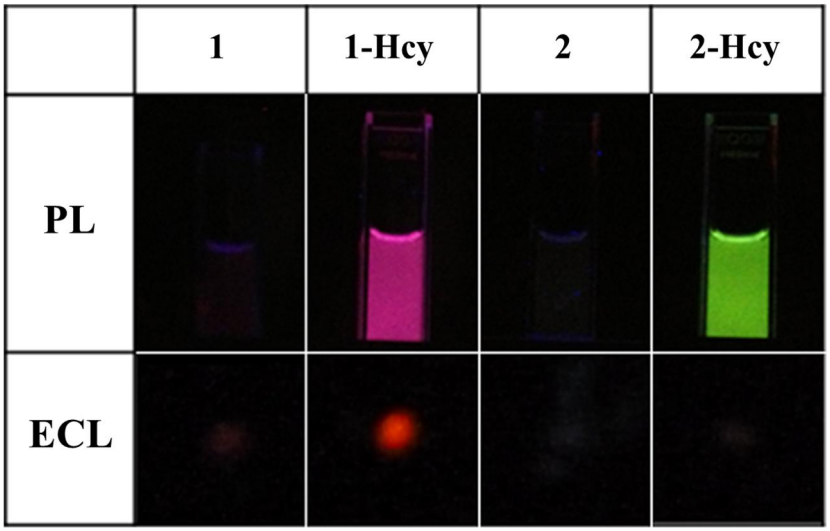

Figure 2-26. PL & ECL images of probe **1** & **2** (10 μM each) in the absence and presence of Hcy (1 mM) (HEPES buffer/MeCN, 1:1 v/v, pH 7.4)

Section 2

The Development of Highly Sensitive ECL Probe for Homocysteine Based Cyclometalated Ir(III) Complex with Enhanced Reactivity by Controlling HOMO Level

1.1. Introduction

In previous study (section 1), we reported the Ir(III)-based probe **1** for Hcy, which has two formyl groups in phenylisoquionline (piq) main ligands. Probe **1** showed the weak PL and ECL signals itself, however, the PL and ECL emission were drastically increased upon the addition of Hcy in blue-shifted region. Although probe **1** has good properties as an ECL probe for Hcy, it still has problems for improvement including low sensitivity, slow reaction rate, and relative low turn-on ratio.

To improve the reactivity between formyl group and Hcy while keeping the good properties of probe **1**, we tried to make the formyl groups more electron-deficiently by introducing other substituents to phenyl rings. Especially, the introduction of electron-donating groups is known to induce the elevation of HOMO level located on phenyl rings and Ir(III) center.[123] This change of electronic distributions induce destabilized electron-deficient formyl group with higher reactivity in the nucleophilic attack process by Hcy.

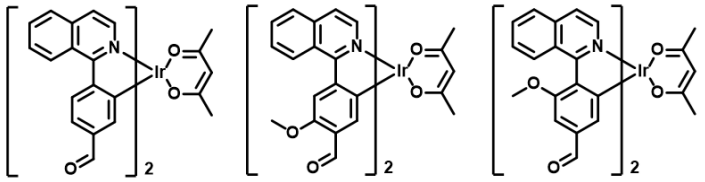

1 2 3

Scheme 2-5. Molecular structures or Ir(III) complexes **1-3.**

In this study, we introduced the additional methoxy group as an electron-donating group to original probe **1**. Two iridium complexes **2** and **3** were synthesized with methoxy group at different position of phenyl rings (Scheme 2-5). The position of electron-donating group with respect to the coordinated carbon of main ligand will strongly influence of ligand field stabilization energy (LFSE) of the Ir(III) complex.[123] For example, Ir(III) complexes bearing methoxy groups *para* to Ir(III) metal exhibited red-shifted emission and elevated HOMO level. [124] On the other hands, those bearing methoxy groups meta to Ir(III) showed nearly similar property with that without methoxy groups.[125]

Based on these backgrounds for modulating HOMO and LUMO energy levels, we expected that probe **2** which has the methoxy groups at *para* position has stronger influence on the HOMO level that probe **3**. Experimental results and antecedent density functional theory (DFT) calculation were also in agreement with this expectation. Probe **2** showed the faster reaction rate and lower detection limit than probe **1**, whereas probe **3** showed the similar properties with **1**. This result provides a new proof-of-concept for rational design of Ir(III)-based probe through the modulation of HOMO and LUMO energy levels by introducing electron-donating substituents to specific site in main ligands.

1.2. Result

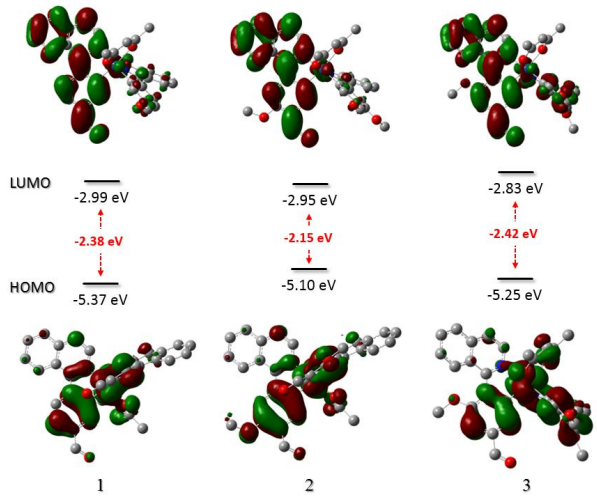

Figure 2-27. Calculated HOMO/LUMO energy levels and electronic distributions of **1**, **2**, and **3**.

Firstly, we performed the density functional theory (DFT) calculations to predict the HOMO and LUMO energy levels of Ir(III) complexes **1**-**3** (Figure 2-27). The HOMO level of Ir(III) complexes **2** was calculated higher than that of **1**, while the LUMO level shows almost no changes. This tendency can be also confirmed by electronic distributions of the HOMO and LUMO. The oxygen atom of methoxy group located *para* to Ir(III) metal in probe **2** contributes the HOMO electronic distribution but does not involved in LUMO electronic distribution. The HOMO-LUMO energy gap of **2** decreased drastically compared to that of **1**, which induced the weaker PL and ECL emission in red-shifted region. Probe **3** shows the slightly different results, in other words, the methoxy group located *meta* to Ir(III) metal in probe **3** has a weak destabilization effect to both HOMO and LUMO levels. The calculated HOMO and LUMO energy levels by CV experiment are described in table 1, which shows the similar tendency with the DFT calculation.

Table 2-2. Electrochemical properties of **1**, **2**, and **3**.

Compound	[a] $E_{ox}^{0'}$ (V vs SCE)	HOMO	LUMO	[b] ΔE (HOMO-LUMO)
1	0.78	-5.57	-3.39	2.18
2	0.54	-5.33	-3.42	1.91
3	0.70	-5.50	-3.34	2.16

[a]The oxidation potentials were measured using cyclic voltammetry at the scan rate of 0.1 V/s in acetonitrile (CH_3CN) solutions with 0.1M tetra-*n*-butylammonium perchlorate as the supporting electrolyte and then the values were calibrated against the oxidation of 1 mM ferrocene (Fc/Fc^+) as a standard and then referenced to SCE. [b]Energy gap (ΔE) was calculated from the cross section wavelength between absorption and emission spectra. (In the case of probe **2**, energy gap was calculated from the absorption edge.)

Figure 2-28 shows the phosphorescent emission spectra of probe **1**-**3**. As expected, probe **2** had no phosphorescence in the absence of Hcy, whereas probe **1** showed the weak emission at 670 nm. However, the fully-quenched emission of **2** was drastically increased upon the addition of Hcy. It showed the improved phosphorescence turn-on ratio for Hcy from 9.12 to 66.3 by introducing additional electron-donating methoxy groups. On the other hands, probe **3** showed the similar result with **1** due to their similar HOMO-LUMO energy gaps.

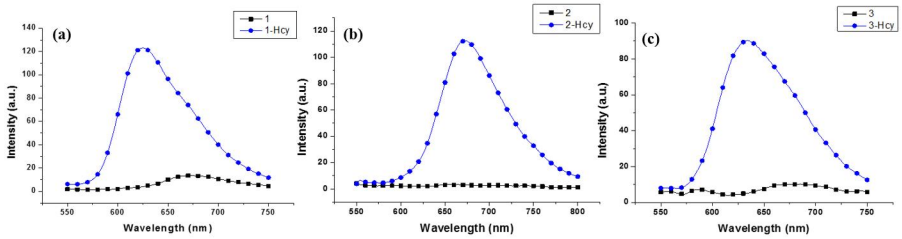

Figure 2-28. Phosphorescent emission spectra of (a) **1**, (b) **2**, and (c) **3** (10 μM each) in the absence (black line) and in the presence of Hcy (5 mM) in H_2O/MeCN (1:1 v/v, pH 7.4, 10 mM HEPES) (λ_{ex}= 500 nm).

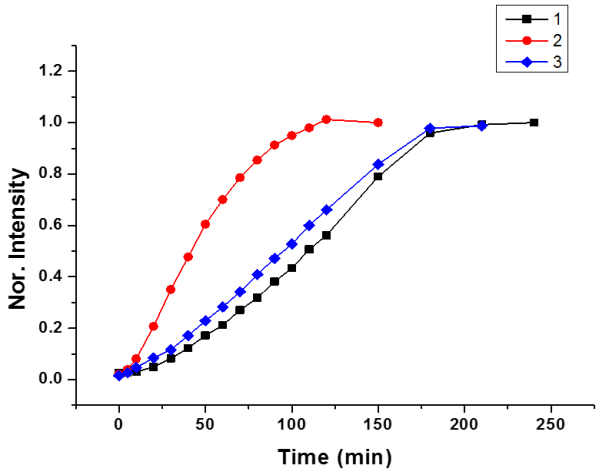

Figure 2-29. Time-course measurements of probe **1-3** (10 μM) in the presence of Hcy (5 mM) in in H_2O/MeCN (1:1 v/v, pH 7.4, 10 mM HEPES) (λ_{ex}= 500 nm).

Next, we measured the reaction rate of **1-3** with the addition of 5 mM of Hcy to 10 μM of each probe (Figure 2-29). It took about 170 min for probe **1** to reach the 90% levels of maximum phosphorescence intensity. However, probe **2** reached the 90% levels of maximum intensity within 85 min, about 2-time faster than probe **1**. Probe **3** also showed the slightly faster response than **1**, but much slower than **2**. These results indicate the relationship between the destabilization of HOMO levels and reactivity.

Then, we measured the ECL intensity of probe **2**. Figure 4a shows the ECL emission profiles during the oxidative cyclic voltammetry (CV) experiment. In the range of 0 to 1.4 V, probe **2** (10 μM) showed no ECL intensity at all in aqueous media (pH 7.4, HEPES buffer/MeCN = 1:1 v/v). However, in the presence of Hcy (5 mM), the intense ECL intensity was observed around 1.2V. A binding titration curve was obtained from a plot of the ECL intensity of **2** against various concentrations of Hcy (Figure 2-30b). Especially, the ECL emission of probe **2** (10 μM) increased linearly with Hcy addition in the range of 0-5 mM (Figure 4c). The limit of detection (LOD)

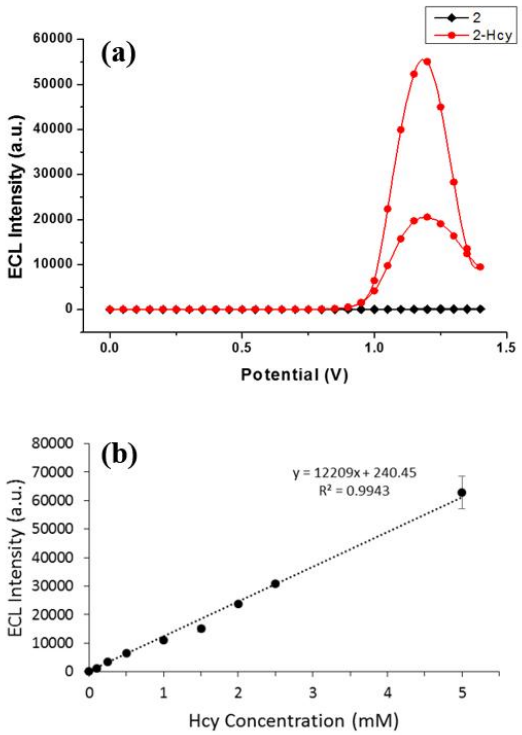

Figure 2-30. (a) ECL intensity of 10 μM **2** upon the addition of Hcy (5 mM) in H_2O/MeCN (1:1 v/v, pH 7.4, 10 mM TPA, 10 mM HEPES, and 0.1 M TBAP as supporting electrolyte). (b) Isothermal binding curve obtained for ECL titration upon the addition of Hcy in H_2O/MeCN (1:1 v/v, pH 7.4, 10 mM TPA, 10 mM HEPES, and 0.1 M $NaClO_4$ as supporting electrolyte).

was calculated to 0.44 μM, much lower than **1** (41 μM) in the same condition (signal-to-noise (S/N) ratio = 3, n = 5).

One considering point to modulate the HOMO level of ECL emitter is that the HOMO level has to be lower than that of TPA for efficient ECL emitting route. Equation (1)-(4) describes the oxidative reduction ECL process.

$$\mathrm{M} - e^- \rightarrow M^{+\cdot} \quad (1)$$

$$\mathrm{TPA} - e^- \rightarrow TPA^{+\cdot} \quad (2)$$

$$M^{+\cdot} + TPA \rightarrow M + TPA^{+\cdot} \quad (2')$$

$$TPA^{+\cdot} \rightarrow TPA^{\cdot} + H^{+} \quad (3)$$

$$M^{+\cdot} + TPA^{\cdot} \rightarrow M^{*} + TPA' \quad (4)$$

Because the oxidation of TPA (equation 2) is relatively slow, it is important that the additional route to produce TPA^{+} by the electron transfer from the TPA to the HOMO of ECL emitter (equation 2'). Therefore, the lower HOMO level is generally favorable in ECL process. Back to the case of probe **2**, the HOMO level calculated by CV experiment is higher than that of probe **1** by the influence of the electron-donating methoxy group, however still lower than that of TPA, known to around -5.1 eV. Consequently, probe **2** can operated as a good ECL emitter with improved properties.

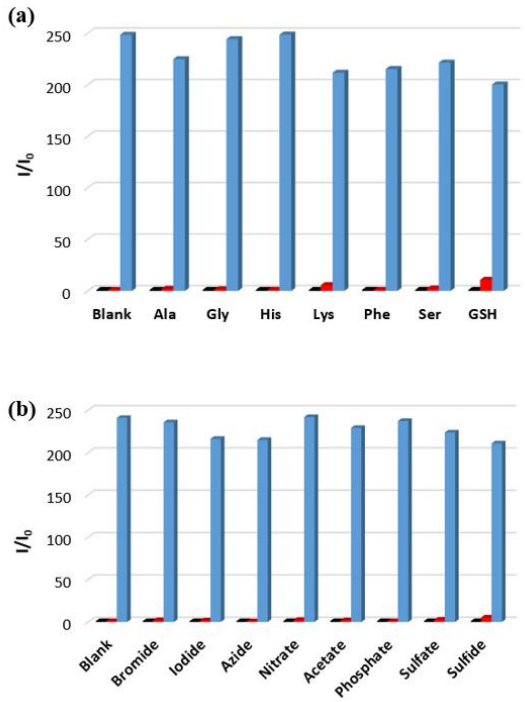

Figure 2-31. Competitive ECL binding assays performed by the addition of Hcy (1 mM) to probe **2** (10 μM) in the presence of (a) other amino acids and (b) various anions (5 mM each).

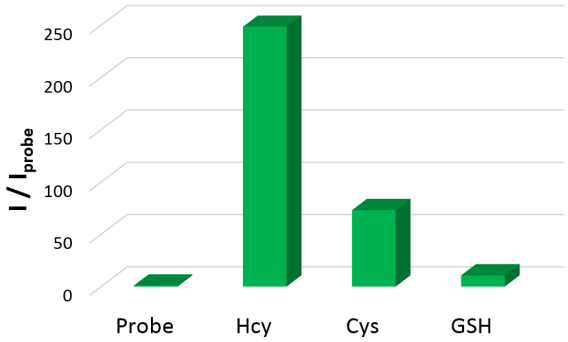

Figure 2-32. comparison of ECL intensity after addition of 5 mM Hcy and 5 mM Cys to 10 μM probe **2** in H_2O/MeCN (1:1 v/v, pH 7.4, 10 mM TPA, 10 mM HEPES, and 0.1 M $NaClO_4$).

The competitive assay was carried out to prove the selectivity of **2** for Hcy versus other amino acids. Probe **2** (10 μM) showed almost no changes in the presence of other amino acids except cysteine, GSH, and sulfide (10 mM each). However, a remarkable change was observed upon the addition of Hcy (5 mM) to a solution of **2** and other analytes. The selectivity test was also performed for other small anions, such as Br^-, I^-, OAc^-, N_3^-, NO_3^{2-}, PO_4^{3-}, and SO_3^{2-}, which also showed no ECL signal change and only increased with Hcy.

Only cysteine (Cys) caused the strong interference signal due to the structural similarity with Hcy. In the ECL study, the signal of **2** was also increased when adding 5 mM of Cys. The reaction rate estimated by PL study also similar to that of Hcy. However, the ECL intensity when adding Hcy was 3.6-times stronger than adding Cys, which correlated with our previous report with probe **1**.

1.3. Conclusion

We developed the new Ir(III) complex based ECL probes **2** and **3** for Hcy with formyl group as a reaction site and methoxy group as a modulation unit

for HOMO energy level. Probe **2** showed the improved properties compared to previous reported probe **1**, including faster reaction time, higher sensitivity, and higher turn-on ratio. The introduction of methoxy group to phenyl rings of main ligands made the HOMO energy level unstable, which caused enhancement of the reactivity of formyl groups. Through this strategy, probe **2** showed 15-times lower detection limit and 2.0-times faster reaction time than **1**. We anticipate that this study provides the new strategy to design Ir(III) complex based molecular probe with high sensitivity and reactivity by the modulation of HOMO and LUMO energy levels with additional electron-donating of withdrawing groups.

1.4. Experimental Section

1.4.1. Instrumentation

^{1}H and ^{13}C NMR spectra were recorded using a Bruker Advance DPX-300. Chemical shifts are given in parts per million using as internal reference the residual resonances of deuterated solvents. ESI-MS data were obtained using a QUATTRO LC Triple Quadrupole Tandem Mass Spectrometer and are reported in units of mass to charge (m/z). High-resolution mass spectroscopy (MALDI-TOF) was performed on a Voyager-DE STR Biospectrometry Workstation. Analytical thin layer chromatography was performed using Kieselgel 60F-254 plates from Merck. Column chromatography was carried out on Merck silica gel 60 (70-230 MESH) and Merck Aluminium oxide 60 (70-230 MESH ASTM).

1.4.2. Materials

All reagents were purchased from either Sigma-Aldrich (Sigma-Aldrich Corp., MO, USA) or TCI (Tokyo Chemical Industry, Tokyo, Japan) and used without any further purification. Deuterated solvents were acquired from CIL (Cambridge Isotopic Laboratories, MA, USA). All amino acids were purchased from Sigma-Aldrich or TCI.

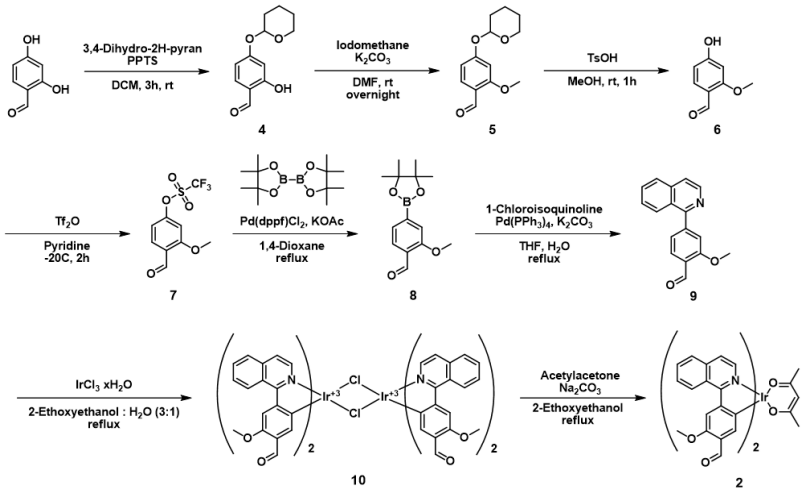

Scheme 2-6. Synthesis of iridium(III) complex **2**

1.4.3. Synthesis of Ir(III) complex

Synthesis of 2-hydroxy-4-(tetrahydro-2H-pyran-2-yloxy)benzaldehyde (4)

A mixture of 2,4-dihydroxybenzaldehyde (4.14 g, 30 mmol) and pyridinium p-toluenesulfonate (PPTS, 0.75 g, 3 mmol) in DCM (100 mL) was stirred at room temperature for 30 min. Then 3,4-dihydro-2H-pyran (54 mg, 0.202 mmol) in DCM was added slowly. The reaction mixture was stirred 3h, after then the solvent was removed under reduced pressure and extracted with DCM, and the organic phase was washed with water, and dried over Na_2SO_4.

The solvent was evaporated to give a colorless liquid product (5.64 g, 84.6% yield). 300 MHz ^{1}H NMR (chloroform-d): δ 11.38 (s, 1H); 9.74 (s, 1H); 7.46 (d, 1H, *J* = 8.49 Hz); 6.64-6.69 (m, 2H); 5.53 (d, 1H, *J* = 2.76 Hz); 3.63-3.89 (m, 2H); 1.62~1.91 (m, 6H).

Synthesis of 2-methoxy-4-(tetrahydro-2H-pyran-2-yloxy)benzaldehyde (5)

A mixture of **4** (2.66 g, 12 mmol) and potassium carbonate (3.29 g, 24 mmol) in dry DMF (50 mL) was stirred at room temperature for 30 min. Then iodomethane (0.745 ml, 18 mmol) in DMF was added slowly. The reaction mixture was stirred 6h, after then the solvent was removed under reduced pressure and extracted with DCM, and the organic phase was washed with water, and dried over Na_2SO_4. The solvent was evaporated to give a colorless liquid product (2.41 g, 85.3% yield), which was purified by silica gel chromatography (Hex/EA: 5:1). 300 MHz ^{1}H NMR (chloroform-d): δ 10.32 (s, 1H); 7.82 (d, 1H, *J* = 8.64 Hz); 6.74 (d, 1H, *J* = 10.41 Hz); 6.65 (s, 1H); 5.55 (t, 1H, *J* = 2.88 Hz, 2.52 Hz); 3.92 (s, 3H); 3.64-3.87 (m, 2H); 1.64~1.92 (m, 6H).

Synthesis of 4-hydroxy-2-methoxybenzaldehyde (6)

5 (2.36 g, 10 mmol) was dissolved in MeOH (100 ml) with catalytic amount of p-toluenesulfonic acid (TsOH, 1 mmol). The reaction mixture was stirred 6h, after then the solvent was removed under reduced pressure and extracted with EA, and the organic phase was washed with water, and dried over Na_2SO_4. The solvent was evaporated to give a colorless liquid product (1.40 g, 92.1% yield). 300 MHz ^{1}H NMR (chloroform-d): δ 10.29 (s, 1H); 7.80 (d, 1H, *J* = 8.16 Hz); 6.51 (d, 1H); 6.47 (s, 1H); 3.92 (s, 3H).

Synthesis of 4-formyl-3-methoxyphenyl trifluoromethanesulfonate (7)

6 (760 mg, 5 mmol) was added in anhydride pyridine (10 ml) and the solution was cooled to -20℃. Trifluoromethanesufonic anhydride (1.346 ml, 10 mmol) was added dropwise and stirred 3h. The mixture was diluted with water for quenching, after then washed with sat. $NaHCO_3$ and water. The solvent was removed under reduced pressure and the residue was purified by silica gel column chromatography (DCM) to give **7** (1.23 g, 87.0% yield) as a colorless liquid. 300 MHz ^{1}H NMR (chloroform-d): δ 10.45 (s, 1H); 7.97 (d, 1H, J = 8.52 Hz); 6.99 (d, 1H, J = 8.58 Hz); 6.92 (s, 1H); 4.00 (s, 3H).

Synthesis of 2-methoxy-4-(4,4,5,5-tetramethyl-1,3,2-dioxaborolan-2-yl)benzaldehyde (8)

The aryl triflate **6** (1.23g, 4.34 mmol), bis(pinacolato)diboron (1.65g, 6.51 mmol), potassium acetate (852 mg, 8.68 mmol), and Pd(dppf)Cl_2 (177mg, 0.217 mmol) were dissolved anhydride 1,4-dioxane (20 mL) and stirred 3h at reflux condition. Then the solvent was removed under reduced pressure and filtered through celite with DCM, and the organic phase was washed with water, and dried over Na_2SO_4. The residue was purified by silica gel column chromatography (DCM) to give **8** (1.23 g, 87.0% yield) as a colorless liquid. 300 MHz ^{1}H NMR (chloroform-d): δ 10.52 (s, 1H); 7.83 (d, 1H, J = 6.42 Hz); 7.41-7.47 (m, 2H); 3.99 (s, 3H); 1.37 (s, 12H).

Synthesis of 4-(isoquinolin-1-yl)-2-methoxybenzaldehyde (9)

A mixture of **8** (745 mg, 2.85 mmol), 1-chloroisoquinoline (473 mg, 2.59 mmol), $Pd(PPh_3)_4$ (60 mg, 0.052 mmol) and potassium carbonate (1.08 g, 7.28 mmol) in THF (20 mL) and H_2O (20 mL) was refluxed for 24 h. After cooling to room temperature, the reaction mixture was extracted with dichloromethane (DCM), and the organic phase was washed with water, and dried over Na_2SO_4. The solvent was evaporated to give a white solid product (570 mg, 83.6% yield), which was purified by silica gel column chromatography (DCM/MeOH: 100/1). 300 MHz ^{1}H NMR (chloroform-d): δ 10.60 (s, 1H); 8.67 (d, 1H, *J* = 5.7 Hz); 8.10 (d, 1H, *J* = 8.49 Hz); 8.02 (d, 1H, *J* = 7.8 Hz); 7.96 (d, 1H, *J* = 8.22 Hz); 7.73-7.78 (m, 2H); 7.63 (t, 1H, *J* = 8.13, 8.22 Hz); 7.38 (s, 2H); 7.37 (d, 1H, *J* = 8.22 Hz); 4.04 (s, 3H)

Synthesis of 10

A mixture of **9** (570, 2.17 mmol) and iridium chloride hydrate (291 mg, 0.97 mmol) in 2-ethoxyethanol (21 mL) and H_2O (7 mL) was refluxed for 12h. After cooling to room temperature, pouring cold water (~100 mL) to reaction mixture. Then a black precipitate was filtered to crude cyclometalated Ir(III) chloro-bridged dimer.

Synthesis of 2

A mixture of crude cyclometalated Ir(III) dimer (**10,** 100 mg, 0.066 mmol), sodium carbonate (21 mg, 0.199 mmol) and acetylacetone (0.020 mL, 0.199 mmol) in 2-ethoxyethanol (10 mL) was refluxed 1h. After cooling to room temperature, the reaction mixture was extracted with dichloromethane (DCM), and the organic phase was washed with water, and dried over Na_2SO_4. The solvent was evaporated to give a black solid product (34 mg, 31.6% yield), which was purified by silica gel column chromatography (EA/Hex: 1/1). 300

MHz ^{1}H NMR (chloroform-d): δ 10.21(s, 2H); 8.94-8.97 (m, 2H); 8.50 (d, 2H *J* = 6.3 Hz); 7.99-8.02 (m, 2H); 7.92 (s, 2H); 7.78-7.81 (m, 4H); 7.61 (d, 2H, *J* = 6.39 Hz); 6.80 (m, 2H); 5.19 (s, 1H); 3.95 (s, 6H), 1.76 (s, 6H).

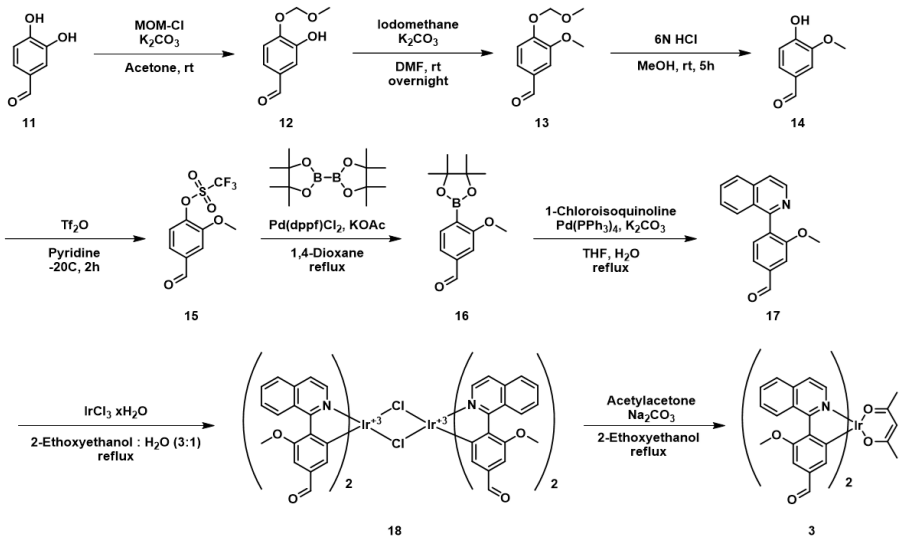

Scheme 2-7. Synthesis of iridium(III) complex **3**

Synthesis of 3-hydroxy-4-(methoxymethoxy)benzaldehyde (12)

A mixture of 3,4-dihydroxybenzaldehyde (4.14 g, 30 mmol) and potassium carbonate (12.44 g, 90 mmol) in acetone (100 mL) was stirred at room temperature for 30 min. Then Chloromethyl methyl ether (2.28 ml, 30 mmol) in acetone was added slowly. The reaction mixture was stirred 3h, after then the solvent was removed under reduced pressure and extracted with DCM, and the organic phase was washed with water, and dried over Na_2SO_4. The solvent was evaporated to give a white solid product, which was purified by silica gel chromatography (Hex/EA: 5:1). (3.44 g, 70.7% yield).

Synthesis of 3-methoxy-4-(methoxymethoxy)benzaldehyde (13)

A mixture of **12** (0.95 g, 5.21 mmol) and potassium carbonate (1.44 g, 10.42 mmol) in dry DMF (50 mL) was stirred at room temperature for 30 min. Then iodomethane (0.666 ml, 7.82 mmol) in DMF was added slowly. The reaction mixture was stirred 12h, after then the solvent was removed under reduced pressure and extracted with DCM, and the organic phase was washed with water, and dried over Na_2SO_4. The solvent was evaporated to give a white solid product (0.86 g, 84.2% yield), which was purified by silica gel chromatography (Hex/EA: 5:1). 300 MHz ^{1}H NMR (chloroform-d): δ 9.89 (s, 1H); 7.46 (s, 1H); 7.45 (d, 1H, J = 6.71 Hz); 7.30 (d, 1H, J = 8.61 Hz); 5.34 (s, 2H); 3.97 (s, 3H); 3.54 (s, 3H).

Synthesis of 4-hydroxy-3-methoxybenzaldehyde (14)

13 (0.589 g, 3 mmol) was dissolved in MeOH (25 mL) and 6N HCl solution (15 mL) was added. The reaction mixture was stirred 6h, after then the solvent was removed under reduced pressure and extracted with EA, and the organic phase was washed with sat. $NaHCO_3$, and dried over Na_2SO_4. The solvent was evaporated to give a white solid product (1.40 g, 92.1% yield). 300 MHz ^{1}H NMR (chloroform-d): δ 9.85 (s, 1H); 7.44-7.46 (m, 2H); 7.07 (d, 1H, J = 8.45 Hz); 6.26 (s, 1H); 3.99 (s, 3H).

Synthesis of 4-formyl-2-methoxyphenyl trifluoromethanesulfonate (15)

14 (760 mg, 5 mmol) was added in anhydride pyridine (10 ml) and the solution was cooled to -20℃. Trifluoromethanesufonic anhydride (1.346 ml, 10 mmol) was added dropwise and stirred 3h. The mixture was diluted with

water for quenching, after then washed with sat. $NaHCO_3$ and water. The solvent was removed under reduced pressure and the residue was purified by silica gel column chromatography (DCM) to give **15** (1.12 g, 79.5% yield) as a colorless liquid. 300 MHz ^{1}H NMR (chloroform-d): δ 10.01 (s, 1H); 7.59 (s, 1H); 7.55 (d, 1H, J = 8.16 Hz); 7.45 (d, 1H, J = 8.13 Hz); 4.02 (s, 3H).

Synthesis of 3-methoxy-4-(4,4,5,5-tetramethyl-1,3,2-dioxaborolan-2-yl)benzaldehyde (16)

The aryl triflate **15** (1.12g, 3.92 mmol), bis(pinacolato)diboron (1.49 g, 5.87 mmol), potassium acetate (852 mg, 8.68 mmol), and $Pd(dppf)Cl_2$ (64 mg, 0.078 mmol) were dissolved anhydride 1,4-dioxane (15 mL) and stirred 3h at reflux condition. Then the solvent was removed under reduced pressure and filtered through celite with DCM, and the organic phase was washed with water, and dried over Na_2SO_4. The residue was purified by silica gel column chromatography (DCM) to give **8** (1.18 g, 81.8% yield) as a colorless liquid.

Synthesis of 4-(isoquinolin-1-yl)-3-methoxybenzaldehyde (17)

A mixture of **16** (290 mg, 1.11 mmol), 1-chloroisoquinoline (163 mg, 1.00 mmol), $Pd(PPh_3)_4$ (64 mg, 0.056 mmol) and potassium carbonate (308 g, 2.23 mmol) in THF (10 mL) and H_2O (10 mL) was refluxed for 12 h. After cooling to room temperature, the reaction mixture was extracted with dichloromethane (DCM), and the organic phase was washed with water, and dried over Na_2SO_4. The solvent was evaporated to give a white solid product (179 mg, 61.6% yield), which was purified by silica gel column chromatography (DCM/MeOH: 100/1). 300 MHz ^{1}H NMR (chloroform-d): δ

10.11 (s, 1H); 8.66 (d, 1H, *J* = 5.67 Hz); 8.10 (d, 1H, *J* = 8.49 Hz); 7.92 (d, 1H, *J* = 8.25 Hz); 7.73 (d, 1H, *J* = 5.67 Hz); 7.60-7.67 (m, 4H); 7.54 (d, 1H, *J* = 7.53 Hz); 3.79 (s, 3H).

Synthesis of 18

A mixture of **17** (114 mg, 0.43 mmol) and Iridium chloride hydrate (58 mg, 0.20 mmol) in 2-ethoxyethanol (10 mL) and H_2O (3 mL) was refluxed for 12h. After cooling to room temperature, pouring cold water (~50 mL) to reaction mixture. Then a black precipitate was filtered to crude cyclometalated Ir(III) chloro-bridged dimer.

Synthesis of 3

A mixture of crude cyclometalated Ir(III) dimer (**18,** 100 mg, 0.066 mmol), sodium carbonate (21 mg, 0.199 mmol) and acetylacetone (0.020 mL, 0.199 mmol) in 2-ethoxyethanol (10 mL) was refluxed 1h. After cooling to room temperature, the reaction mixture was extracted with dichloromethane (DCM), and the organic phase was washed with water, and dried over Na_2SO_4. The solvent was evaporated to give a black solid product (24 mg, 22.7% yield), which was purified by silica gel column chromatography (EA/Hex: 1/1). 300 MHz ^{1}H NMR (chloroform-d): δ 9.46 (s, 2H); 8.44 (d, 2H *J* = 6.23 Hz); 8.34 (d, 2H *J* = 8.24 Hz); 7.94 (t, 2H, *J* = 7.97 Hz, 7.78 Hz); 7.60-7.65 (m, 4H); 6.96 (s, 2H); 6.27 (s, 2H); 5.23 (s, 1H); 3.85 (s, 6H), 1.75 (s, 6H).

Section 3

Highly Sensitive and Selective Electrochemiluminescent Probe for Cyanide via Chemodosimetric Approach Based on Cyclometalated Iridium(III) Complex

1.1. Introduction

Cyanide anion (CN^-) is a well-known hazardous chemical that can lead to death of mammals upon binding to a heme unit of the binding site of cytochrome-c.[126] The strong interactions between the cyanide anion and cytochrome-c is known to interrupt the mitochondrial electron transfer cycle, which leads to inhibition of the process of the oxidation metabolism and cellular respiration.[127-129] For these reasons, World Health Organization (WHO) regulate the maximum permissive level of cyanide in drinking water as 1.9 μM.[130] Because a large amount of cyanide anions are widely used in many industries such as gold mining, electroplating, and metallurgy, about 1.5 million tons per year, it can be accumulated at certain foods and plants through the inflow from polluted environments.[131, 132] As a result, there is a great interest in the development of sensitive and selective detection of cyanide anion.

So far, various cyanide sensors are developed, including electrochemical [133, 134], colorimetric [135-139], fluorescent [140-151], and phosphorescent assays [152, 153]. Among them, fluorescent chemosensors have many advantages such as high sensitivity, good selectivity, and suitability as a diagnostic tool for biological concern. In recent years, chemodosimetric approaches based on strong nucleophilicity of cyanide anion have been reported [140-149], which showed good sensing properties in almost 100% aqueous condition. [147-149] However, fluorescent assays are constrained to apply a tool of point-of-care (POC) detection due to a necessity of an extra optical source.

To overcome this drawback, electrogenerated chemiluminescence (ECL), a light emission process through the electron transfer reactions between electrochemically generated radicals in a working electrode, [154] has attracted increasing interests. In comparison to conventional fluorescent techniques, the ECL assay has a lot of advantages including high sensitivity, wide linear response range, and good reproducibility. Especially, ECL is a useful tool for developing portable instruments because no bulky equipment like external optical sources or additional reagents are required.

Due to these merits, ECL has been widely studied in bioanalysis, and some of them already have been commercialized and used in immunoassays. However, ECL sensing of small molecules is still a great challenge because most of ECL detection methods have been developed *via* specific biomacromolecular recognition such as antibody-antigen [155-157] and DNA hybridization. [116c, 158] For this reason, only a few ECL-based small molecule probes for anions have been published until now. [102, 103, 105, 116c, 117a, 160]

Herein, we introduce a new ECL chemodosimetric sensing strategy for cyanide anion based on the organometallic iridium(III)-based probe (***1***) (Scheme 2-8). Some iridium(III) complexes are known as good ECL luminophore which enable to emit bright light at various wavelength by

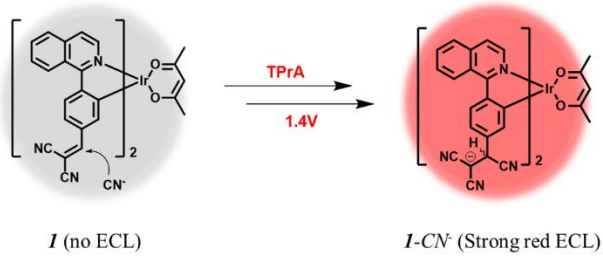

Scheme 2-8. Electrochemiluminescent sensing of cyanide via chemodosimetric approach in aqueous condition

modulating main ligand. Among them, $(piq)_2Ir(acac)$ (piq : phenylisoquinoline, acac : acetylacetone) especially exhibits efficient orange-red ECL around 615 nm with TPrA in air-saturated condition. According to our previous report, the relative intensity of ECL emission is estimated to be 2-time higher than that of $Ru(bpy)_3^{2+}$, the representative ECL luminophore. Thus, we designed the ECL turn-on sensor based on $(piq)_2Ir(acac)$ complex by introducing dycyanovinyl group, as a specific reaction site for cyanide, to piq main ligand.

1.2. Results

Figure 2-32 shows the absorption and emission spectra of probe ***1*** (10 μM) measured in 5:5 HEPES buffer/DMSO condition (pH 7.4). Probe ***1*** displayed the intense absorption at 375 nm, which correspond to spin-allowed ligand-centered (^{1}LC) transition states. In addition, broad absorption around 500-650 nm was observed, the typical shape of metal-to-ligand charge-transfer (^{1}MLCT and ^{3}MLCT) transitions. When adding cyanide anion (1 mM, 100 equiv.) the absorption spectrum around 375 nm decreased gradually (Fig 2-32a). This phenomenon could be also observed naked-eye detection. (Figure 2-32 inset).

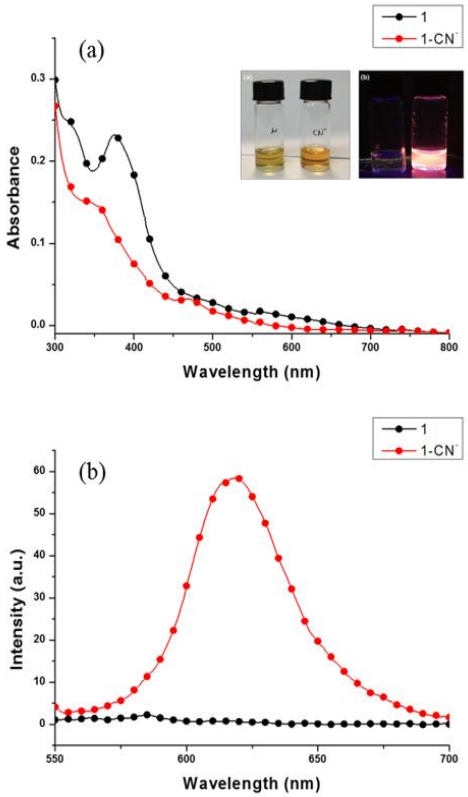

Figure 2-32. (a) Absorbance and (b) phosphorescent emission spectra of ***1*** (10 μM) upon addition of cyanide (1 mM) in H_2O/MeCN (1:1 v/v, pH 7.4, 10 mM HEPES) (λ_{ex}= 500 nm). (inset) (a) Naked-eye and (b) phosphorescent image of ***1*** & ***1***-CN^- (probe: (a) 50 μM, (b) 10 μM, cyanide anion: (a) 5 mM, (b) 1 mM)

Probe ***1*** has two dicyanovinyl functional groups, known to have a strong electron withdrawing ability. In our previous report, $(piq\text{-}CHO)_2Ir(acac)$ complex showed negligible emission in highly red-shifted region due to strong electron withdrawing ability of aldehyde group. The emission of probe ***1*** was even lower than $(piq\text{-}CHO)_2Ir(acac)$, which was caused by higher electron withdrawing ability of dicyano-vinyl group than that of aldehyde. However, in the presence of cyanide anion, it could attack the α-position of dicyano-vinyl group to form the stabilized anionic species (Scheme 2-8). As a result, quenched PL emission of probe ***1*** was fully recovered in blue-shifted

region (λ_{max}: 619 nm), which is almost identical to that of $(piq)_2Ir(acac)$. (Fig 2-32b)

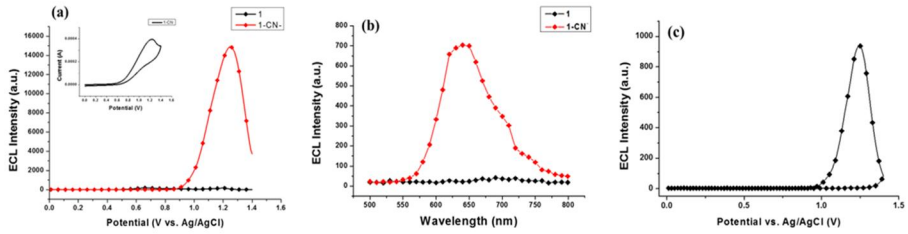

Figure 2-33. (a) ECL intensity of ***1*** (10 μM) upon the addition of cyanide (1 mM) in H_2O/MeCN (1:1 v/v, pH 7.4, 10 mM TPA, 10 mM HEPES, and 0.1 M $NaClO_4$ as supporting electrolyte) while the potential is swept at a Pt disk electrode (diameter: 2 mm) in the range 0–1.4 V vs Ag/AgCl (scan rate: 0.1 V/s) (Inset: Cyclic voltammogram (CV) of a solution of 10 μM ***1*** in the presence of 500 μM cyanide) (b) ECL spectrum of ***1*** (10 μM) upon the addition of cyanide (1 mM) in MeCN (10 mM TPA, 0.1 M tetrabutylammonium perchlorate (TBAP) as supporting electrolyte) (c) ECL intensity of ***1*** (10 μM) upon the addition of cyanide in H_2O/DMSO (99.99:0.01 v/v, pH 7.4, 10 mM TPA, 10 mM HEPES, and 0.1 M $NaClO_4$)

A similar tendency to the fluorescence upon the addition of cyanide was observed in ECL. Figure 2-33a shows the ECL emission profile during cyclic voltammetry. In the range from 0 to 1.4V, probe ***1*** alone (10 μM) produced almost no ECL signal in aqueous media (pH 7.4, HEPES buffer/MeCN = 1:1 v/v). However, in the presence of cyanide (500 μM, 50 equiv.), a strong ECL signal was observed around 1.2V. This strong ECL signal is also very stable during over 10-cycles potential scanning. The maximum emission wavelength of ECL spectra was measured to be about 631nm, slightly red-shifted region compared to PL spectra (Figure 2-33b). This “turn-on” phenomenon was also observed in nearly 100% aqueous media containing 0.01% DMSO solution (Figure 2-33c).

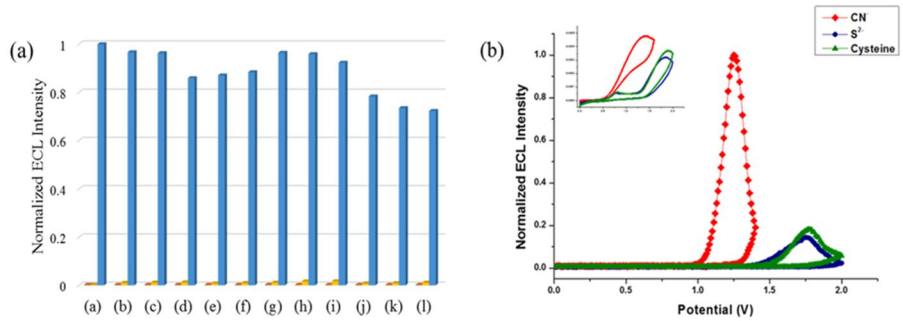

Figure 2-34. (a) Competitive ECL binding assays performed by the addition of cyanide (1 mM) to probe ***1*** (10 μM) in the presence of various anions (5 mM each, (a) blank; (b) Br^-; (c) $C_6H_5O_7^{3-}$; (d) Cl^-; (e) F^-; (f) N_3^-; (g) NO_3^{2-}; (h) OAc^-; (i) SO_4^{2-}; (j) S^{2-}; (k) cysteine; (l) homocysteine). (b) ECL intensities of 10 μM ***1*** upon the addition of CN^-, S^{2-}, and cysteine respectively (1 mM for CN^-, 10 mM for S^{2-} and cysteine) in H_2O/MeCN (1:1 v/v, pH 7.4, 10 mM TPA, 10 mM HEPES, and 0.1 M TBAP as supporting electrolyte) in the potential range 0–2.0 V vs Ag/AgCl (scan rate: 0.1 V/s). (Inset: Cyclic voltammogram (CV) of a solution of 10 μM ***1*** in the presence of CN^-, S^{2-}, and cysteine respectively).

The selectivity of probe ***1*** was evaluated by competition assay, which was performed by adding 500 μM of cyanide anion to 10 μM probe ***1*** in the presence of 1 mM of other anions (Figure 2-34a). The ECL intensity of probe ***1*** showed no significant changes when adding excess amounts of other anions, such as F^-, Br^-, Cl^-, N_3^-, $C_6H_5O_7^-$, OAc^-, NO_3^{2-}, PO_4^{3-}. However, significant increasing of ECL signal (~ 160 fold) was observed after adding 500 μM (50 equiv.) of cyanide to the solution.

Sulfide and biothiols need to be considered in the development of cyanide-selective chemodosimeters due to their similar properties. In PL studies, we observed a little enhancement upon addition of sulfide anion and biothiols such as cysteine and homocysteine. Although their PL turn-on ability was only 4~15% levels compared to that of cyanide, the presence of such analytes could interfere the accurate quantitative detection of cyanide.

When the selectivity test was performed by ECL, it showed slightly different results compared to PL experiment. In the range of 0 to 1.4V, the mixture of probe ***1*** and 1 mM of sulfide anion (***1***-S^{2-}) caused no ECL signal changes in aqueous condition. However, the weak ECL signal (~20% levels of ***1***-CN^-) was observed around 1.7 V while the signal of ***1***-CN^- was observed around 1.2V. Although DFT calculation proved that the HOMO energy level of ***1***-S^{2-} is higher than that of ***1***-CN^-, CV experiment (Figure 2-31b inset) also showed that ***1***-CN^- has more positive oxidation potential than ***1***-S^{2-}. This phenomenon could be explained that thiol groups of ***1***-S^{2-} passivate the Pt working electrode through Pt-SH binding. Because the adsorption of ***1***-S^{2-} and remaining excess sulfide anions to Pt working electrode disturbs the oxidation of ***1***-S^{2-}, the higher potential is needed to oxidized ***1***-S^{2-} than ***1***-CN^-.

To investigate this phenomenon in more detail, we introduced the glassy carbon (GC) working electrode instead of platinum (Pt) to exclude the passivation effect. In this condition, the ECL signal started to increase around 0.8V and reached to maximum intensity at 1.6V in the presence of Na_2S. We also measured the ECL intensity of ***1***-CN^- using GC electrode under an identical condition, ECL turn-on voltage was still delayed over 1.2V.

$$\mathrm{M} - e^- \rightarrow M^{+\cdot} \quad (1)$$

$$\mathrm{TPA} - e^- \rightarrow TPA^{+\cdot} \quad (2)$$

$$M^{+\cdot} + TPA \rightarrow M + TPA^{+\cdot} \quad (2')$$

$$TPA^{+\cdot} \rightarrow TPA^{\cdot} + H^+ \quad (3)$$

$$M^{+\cdot} + TPA^{\cdot} \rightarrow M^* + TPA' \quad (4)$$

The calculated HOMO energy level by DFT calculation and the experimental value of the oxidation potential for ***1***-S^{2-} provide the evidence for these results. In oxidative reduction ECL process, the TPA oxidation process is relatively slow (equation 2). Therefore, the additional catalytic reaction that produces TPA cation by electron transfer from iridium oxidation species to TPA has a large contribution to ECL emitting (equation 2'). However, ***1***-S^{2-} has too high HOMO level that almost similar to the energy level of TPA. This makes the electron transfer process into trouble, which induces the delayed time to reach the maximum ECL intensity.

Then we applied the probe ***1*** to quantitatively determine the concentration of cyanide anion. As shown in Figure 2-35a, the ECL signal was dependent on the concentration of cyanide. Especially, the ECL intensity linearly increased with the cyanide addition in the range of 0–0.25 mM (Figure 2-35, R^2=0.9987). The limit of detection (LOD) was estimated to be 0.298 μM, much lower than WHO permissive level.

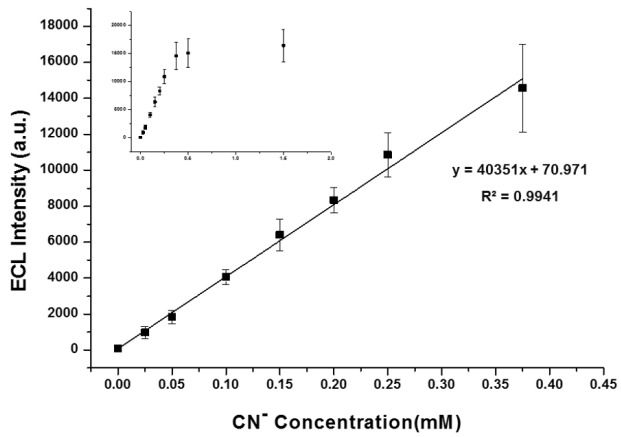

Figure 2-35. Isothermal binding curve obtained for ECL titration upon the addition of cyanide in H_2O/MeCN (1:1 v/v, pH 7.4, 10 mM TPA, 10 mM HEPES, and 0.1 M $NaClO_4$ as supporting electrolyte).

Table 2-3. Quantification test for cyanide in tab water

CN^- Concentration	Intensity (n=5)	Standard deviation	Δ Intensity (exp.)	Δ Intensity (cal.)	Recovery (%)	
[a]Reference	89.837	1.586	-	-	-	
0 μM	100.035	4.943	-	-	-	
1 μM	141.475	0.808	41.440	40.531	102.24 ± 1.99 %	
10 μM	500.703	5.497	400.668	405.31	98.85 ± 1.36 %	
250 μM	9815.997	79.976	9715.962	10132.75	95.89 ± 0.89 %	

All ECL intensities were measured using cyclic voltammetry at the scan rate of 0.1 V/s in the potential range 0-1.4V with 0.01M TPA as the coreactant and 0.1M TBAP as the supporting electrolyte. [a]Reference experiment was performed with 10 μM probe ***1*** in HEPES (pH 7.4, 10 mM) /MeCN (1:1 v/v)

To confirm the reliability of ECL sensing system in real sample, we examined the quantification of the cyanide in the tap water, diluted with the same amount of acetonitrile, by standard addition method. Firstly, we measured the ECL emission of probe ***1*** (10 μM) in tap water (tap water/MeCN = 1:1 v/v). As shown table 1, when using tap water instead of HEPES buffer, we observed that almost no ECL signal appears. This result means the amount of cyanide in tap water is negligible, which is in agreement with the known results. In sequence, different concentrations of cyanide were added to the tap water, and the recovery was determined. The recoveries of cyanide range were from 95 to 102%, suggesting that our sensing system is highly reliable. Especially, we succeed to detect the very low concentration of cyanide (1 μM, 0.1 eq), which shows that our ECL analytical system can be utilized to detect the small amount of cyanide in real environmental samples.

Lastly, we performed the theoretical DFT calculations to confirm the HOMO/LUMO energy level and electronic distribution of ***1***, ***1***-CN^- and $(piq)_2Ir(acac)$ as a control group. (Figure 2-36) For $(piq)_2Ir(acac)$, which have no other substituents, the HOMO electronic distribution is centered on the Ir(III) metal and the phenyl part of the phenylisoquionline (piq) main ligands, and the LUMOs is mainly localized on the isoquinoline part of the piq main ligands. The strong electron withdrawing ability of isoquinoline contributes to

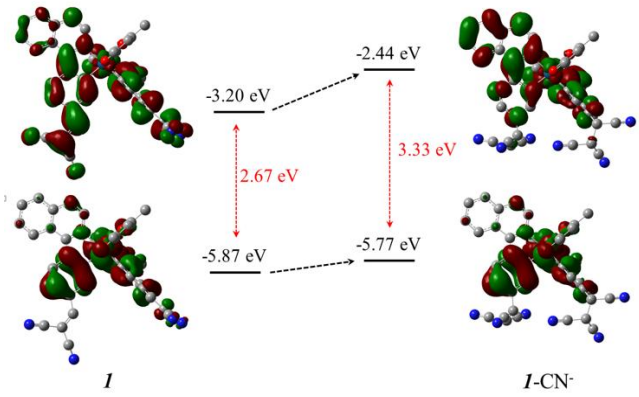

Figure 2-36. Calculated HOMO/LUMO energy levels and electronic distributions of ***1*** and ***1***-CN^-.

lower the LUMO energy level which enables the smooth electron transfer from the TPA radical.

The HOMOs of ***1*** & ***1***-CN^- showed similar electronic distribution with $(piq)_2Ir(acac)$, however, the LUMOs showed some differences. The introduction of dicyanovinyl groups to phenyl part of piq main ligands, at the opposite site of isoquinolines, caused the additional stabilization effect of the LUMO level of probe ***1***. In other words, the LUMO electronic distribution of ***1*** delocalized on piq main ligand entirely, and especially dicynovinyl group (and benzene) had a higher density even than isoquinolines. After reaction with cyanide, ***1***-CN^- recovered similar electronic distribution with $(piq)_2Ir(acac)$. The breakdown of strong electron withdrawing groups caused the destabilization of LUMO energy and the localization of the electronic distribution on two isoquionlines. Because of the strong LUMO stabilization effect of isoquinolines, the elevation of LUMO energy level did not affect the electron transfer from the TPA radical to Ir(III) complex for ECL process.

1.3. Conclusion

In conclusion, we developed the cyclometalated Ir(III) complex ***1*** as a selective probe for cyanide. Probe ***1*** shows drastic ECL enhancing and blue-shifted emission after the reaction with cyanide in aqueous solution. Sulfide and biothiols such as cysteine and homocysteine also react with probe ***1*** a little, however, the perturbation effect enables to distinguish cyanide from biothiols based on ECL analysis by modulating turn-on voltage. We also carry out the quantification test successfully both in buffer solution and tap water. We expect that our ECL chemodosimetric sensing system based on Ir(III) complex suggests the general ECL sensing analysis tools for small biomolecules.

1.4. Experimental Section

1.4.1. Synthesis and characterization

Instrumentation

^{1}H and ^{13}C NMR spectra were recorded using a Bruker Advance DPX-300. Chemical shifts are given in parts per million using as internal reference the residual resonances of deuterated solvents. ESI-MS data were obtained using a QUATTRO LC Triple Quadrupole Tandem Mass Spectrometer and are reported in units of mass to charge (m/z). High-resolution mass spectroscopy (MALDI-TOF) was performed on a Voyager-DE STR Biospectrometry Workstation. Analytical thin layer chromatography was performed using Kieselgel 60F-254 plates from Merck. Column chromatography was carried out on Merck silica gel 60 (70-230 MESH) and Merck Aluminium oxide 60 (70-230 MESH ASTM).

Materials

All reagents were purchased from either Sigma-Aldrich (Sigma-Aldrich Corp., MO, USA) or TCI (Tokyo Chemical Industry, Tokyo, Japan) and used without any further purification. Deuterated solvents were acquired from CIL (Cambridge Isotopic Laboratories, MA, USA). All amino acids were purchased from Sigma-Aldrich or TCI.

Synthesis of Ir(III) complex

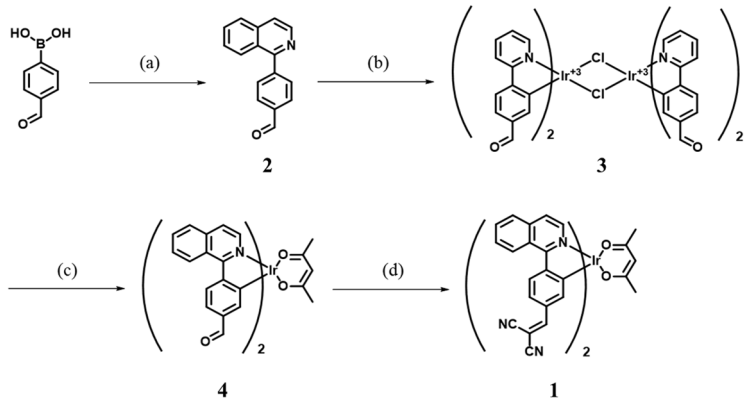

Scheme 2-9. Synthesis of Iridium(III) complex **1**. (a) 1-chloroisoquinoline, $Pd(PPh_3)_4$, K_2CO_3, THF, H_2O, reflux; (b) Iridium chloride hydrate, 2-ethoxyethanol, H_2O, reflux; (c) acetylacetone, Na_2CO_3, 2-ethoxyethanol, reflux; (d) malononitrile, TEA, EtOH, reflux.

Synthesis of 4-(isoquinolin-1-yl)benzaldehyde (2)

A mixture of 4-formylphenylboronic acid (1145 mg, 7 mmol), 1-chloroisoquinoline (1049 mg, 7 mmol), $Pd(PPh_3)_4$ (404 mg, 0.35 mmol) and potassium carbonate (1934mg, 14 mmol) in THF (40 mL) and H_2O (40 mL) was refluxed for 24 h. After cooling to room temperature, the reaction mixture was extracted with dichloromethane (MC), and the organic phase was washed with water, and dried over Na_2SO_4. The solvent was evaporated to give an

white solid product (1372 mg, 84% yield), which was purified by silica gel column chromatography (eluent; EA/Hexane (Hex)=1:5).

300 MHz ^{1}H NMR (chloroform-d): δ 10.15 (s, 1H); 8.65 (d, 1H, *J* = 6.3 Hz); 8.02~8.08 (m, 3H); 7.93 (d, 1H, *J* = 10.1 Hz); 7.89 (d, 2H, *J* = 10.1 Hz); 7.73 (t, 1H, *J* = 7.8 Hz); 7.72 (d, 2H, *J* = 7.1 Hz); 7.58 (t, 1H, *J* = 8.0 Hz).

Synthesis of 3

A mixture of **5** (1g, 4.29 mmol) and Iridium chloride hydrate (576 mg, 1.93 mmol) in 2-ethoxyethanol (30 mL) and H_2O (10 mL) was refluxed for 12h. After cooling to room temperature, pouring cold water (~50 mL) to reaction mixture. Then a dark brown precipitate was filtered to crude cyclometalated Ir(III) chloro-bridged dimer.

Synthesis of 4

A mixture of crude cyclometalated Ir(III) dimer (**6,** 330 mg, 0.245 mmol), sodium carbonate (260 mg, 2.45 mmol) and acetylacetone (0.252 mL, 2.45 mmol) in 2-ethoxyethanol (10 mL) was refluxed for 8h. After cooling to room temperature, the reaction mixture was extracted with dichloromethane (MC), and the organic phase was washed with water, and dried over Na_2SO_4. The solvent was evaporated to give a black solid product (229 mg, 61% yield), which was purified by silica gel column chromatography (eluent; MC/methanol = 100:1).

300 MHz ^{1}H NMR (DMSO-d_6): δ 9.59 (s, 2H); 9.06 (d, 2H *J* = 8.85 Hz); 8.46 (m, 4H); 8.24 (d, 2H, *J* = 7.11 Hz); 7.98 (m, 6H); 7.40 (d, 2H, *J* = 8.25 Hz); 6.70 (s, 2H); 5.28 (s, 1H); 1.70 (s, 6H). 75 MHz ^{13}C ($CDCl_3$-d): δ

193.268, 185.179, 152.895, 151.009, 140.470, 137.315, 135.466, 134.930, 131.164, 129.581, 128.464, 127.605, 126.898, 126.500, 121.723, 121.592, 28.690. HRMS (FAB^+, *m*-NBA): *m/z* observed 756.1602 (calculated for $C_{37}H_{27}N_2IrO_4$ $[M]^+$ 756.1600).

Synthesis of 1

A mixture of **4** (151 mg, 0.2 mmol), malononitrile (39 μM, 0.6 mmol), and triethylamine (60 μL, 0.6 mmol) in anhydrous ethanol (10 mL) was refluxed overnight. The solvents was dried in vacuo and extracted with dichloromethane (MC), and the organic phase was washed with water, and dried over Na_2SO_4. The solvent was evaporated to give a black solid product (70 mg, 41% yield), which was purified by silica gel column chromatography (eluent; MC/methanol = 100:1).

400 MHz ^{1}H NMR (DMSO-d_6): δ 9.04 (d, 2H, *J* = 8.8 Hz); 8.47 (d, 2H, *J* = 8.4 Hz); 8.36 (d, 2H, *J* = 6.4 Hz); 8.17 (m, 4H); 7.98 (m, 6H); 7.44 (d, 2H, *J* = 6.8 Hz); 6.96 (s, 2H); 5.23 (s, 1H); 1.66 (s, 6H).

1.4.2. Electrochemical and electrogenerated chemiluminescent (ECL) measurements

Electrochemical study was performed with a CH Instruments 660 Electrochemical Analyzer (CH Instruments, Inc., TX, USA). In the electrochemical study, cyclic voltammetry (CV) and differential pulse voltammetry (DPV) was applied to the individual solutions in order to investigate electrochemical oxidative and reductive behaviors. Particularly, a CH Instruments 650B Electrochemical Analyzer was used in the ECL experiments to apply potential sweeps. ECL spectra was gained using a

charge-coupled device (CCD) camera (LN/CCD 1752-PB/VSAR, Princeton Instruments, NJ, USA) cooled to below −120 ^{o}C using liquid N_2. The ECL intensity profile was obtained using a low-voltage photomultiplier tube module (H-6780, Hamamatsu photonics K. K., Tokyo, Japan) operated at 1.0 V. A 10 mL-sized ECL cell was directly mounted CCD or PMT module with home-made mounting support during the experiments. All the ECL data were collected upon the simultaneous cyclic voltammetry on the solution. The ECL solutions commonly contained 10 μM 1-2Zn, 10 mM TPrA (Sigma-Aldrich, MO, USA) coreactant, and 0.1 M tetrabutylammonium hexafluorophosphate (TBAPF6, Sigma-Aldrich) supporting electrolyte in acetonitrile (MeCN, HPLC grade, Sigma-Aldrich) solution. Especially, TPrA was selected and used as an ECL coreactant as it has been widely studied and known on its electrochemical properties. The ECL solutions were prepared in a dry-box incorporating a N_2 atmosphere or were prepared in air, purged with N2, and then sealed in an air-tight cell. All the electrochemical and ECL experiments were referenced with respect to an Ag/Ag+ reference electrode. All potential values were calibrated against the saturated calomel electrode (SCE) by measuring the oxidation potential of 1 mM ferrocene (vs Ag/Ag+) as a standard (Eo(Fc+/Fc) = 0.424 V vs SCE). Cyclic voltammetry for ECL experiments was applied to Pt disk electrode (2 mm dia.) ranged between 0.3 ~ 1.3 V at the scan rate of 0.1 V/s. The electrochemical and ECL solutions were freshly prepared in each experiment, and Pt working electrode was polished with 0.05 M alumina (Buehler, IL, USA) on a felt pad following sonication in the 1:1 mixed solution of deionized water and absolute ethanol for 5 min. Then the electrode was blown by ultra pure N_2 gas for 1 min. A single solution was only used for one experimental try, and discarded after collecting data. The reported ECL values were obtained by averaging the values from at least five tries with a good reliability in the MeCN solution.

Table 2-4. Electrochemical properties of ***1***, ***1***-CN^-, and S^{2-}.

Compound	[a] $E_{ox}^{0'}$ (V vs SCE)	HOMO	LUMO	[b] ΔE (HOMO-LUMO)
1	0.95	-5.75	-3.72	2.03
1-CN^-	0.68	-5.48	-3.14	2.34
1-S^{2-}	1.19[c] 0.51[d]	-5.31[d]	-2.99[d]	2.32

[a]The oxidation potentials were measured using cyclic voltammetry at the scan rate of 0.1 V/s in acetonitrile (CH_3CN) solutions with 0.1M tetra-*n*-butylammonium perchlorate as the supporting electrolyte and then the values were calibrated against the oxidation of 1 mM ferrocene (Fc/Fc^+) as a standard and then referenced to SCE. [b]Energy gap (ΔE) was calculated from the cross section wavelength between absorption and emission spectra. [c]Pt working electrode. dGlassy carbon (GC) working electrode

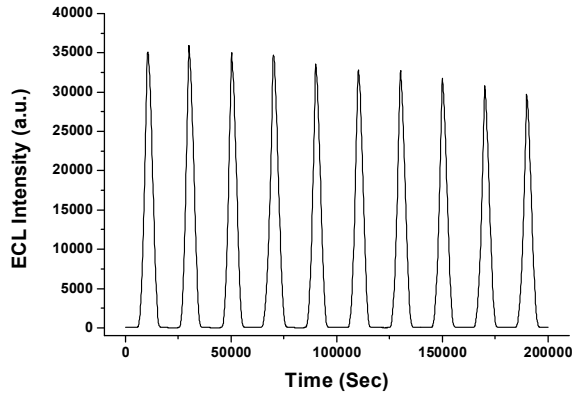

Figure 2-37. Continuous cyclic ECL scans of **1** (10 μM) in the presence of cyanide (500 μM) in H_2O/MeCN (1:1 v/v, pH 7.4, 10 mM TPA, 10 mM HEPES, and 0.1 M $NaClO_4$ as supporting electrolyte) while the potential is swept at a Pt disk electrode in the range 0–1.5 V vs Ag/AgCl (scan rate: 0.15 V/s).

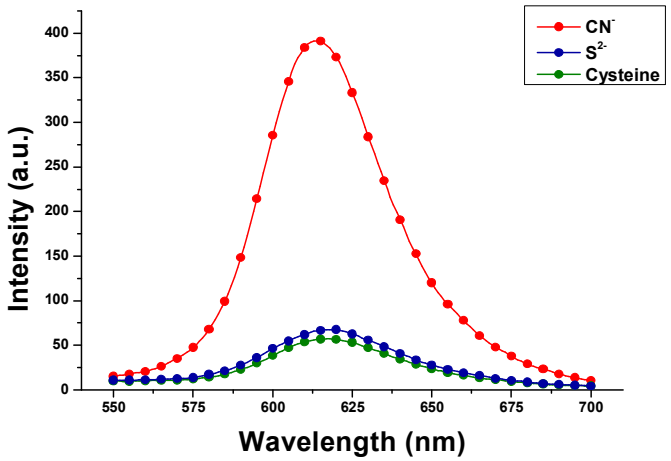

Figure 2-38. PL emission spectra of **1** (10 μM) in the presence of cyanide (500 μM), S^{2-}(1 mM), and cysteine (1 mM) in H_2O/MeCN (1:1 v/v, pH 7.4, 10 mM HEPES, λ_{ex} : 500 nm).

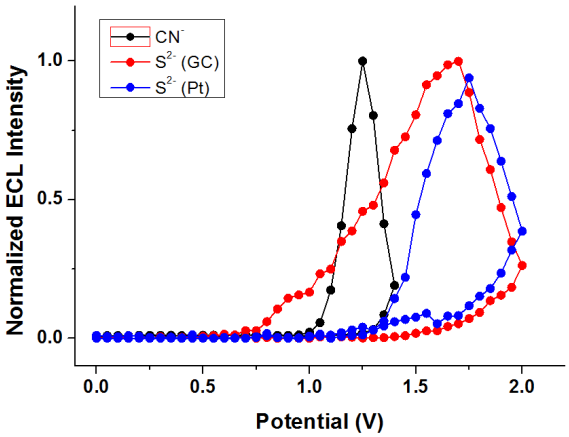

Figure 2-39. ECL intensities of 10 μM ***1*** upon the addition of CN^-, S^{2-} respectively (1 mM for CN^-, 10 mM for S^{2-}) in H_2O/MeCN (1:1 v/v, pH 7.4, 10 mM TPA, mM HEPES, and 0.1 M TBAP as supporting electrolyte) in the potential range 0–1.4 V vs Ag/AgCl (scan rate: 0.1 V/s).

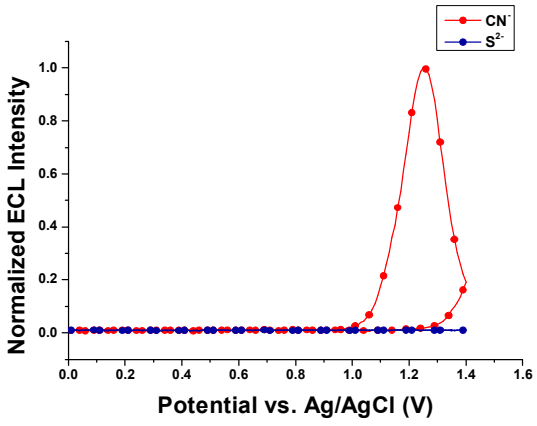

Figure 2-40. Normalized ECL intensities of 10 μM ***1*** upon the addition of CN^-, S^{2-} (using GC and Pt working electrode respectively,1 mM for CN^-, 10 mM for S^{2-}) in H_2O/MeCN (1:1 v/v, pH 7.4, 10 mM TPA, 10 mM HEPES, and 0.1 M TBAP as supporting electrolyte) in the potential range 0–2.0 V vs Ag/AgCl (scan rate: 0.1 V/s).

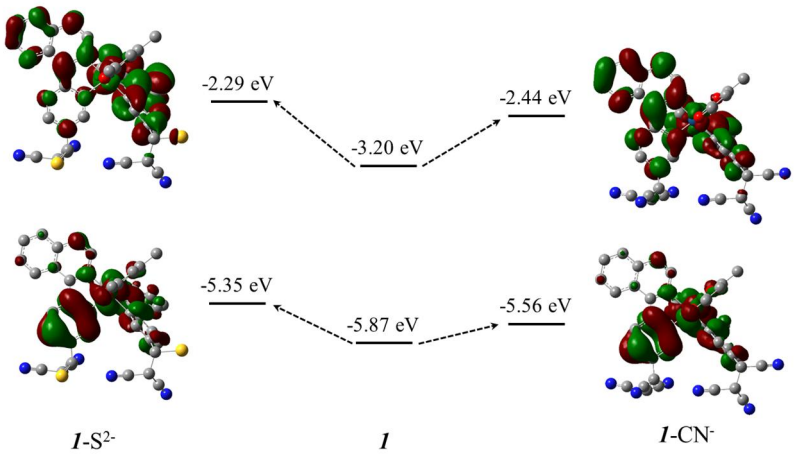

Figure 2-41. Calculated HOMO/LUMO energy levels and electronic distributions of ***1***, ***1***-CN^-, and ***1***-S^{2-}

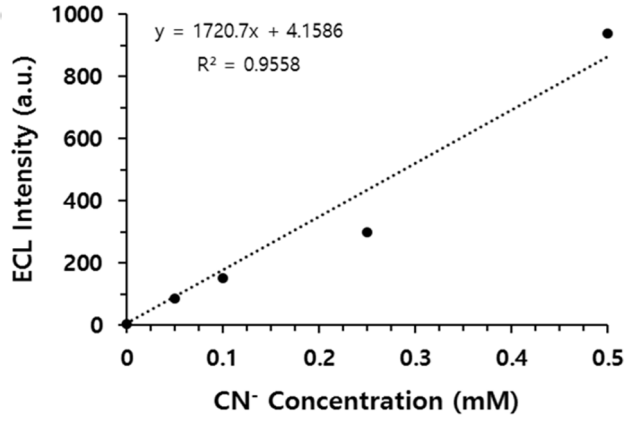

Figure 2-42. Isothermal binding curve obtained for ECL titration upon the addition of cyanide in H_2O/DMSO (99.99:0.01 v/v, pH 7.4, 10 mM TPA, 10 mM HEPES, and 0.1 M NaClO4 as supporting electrolyte).

Section 4

Electrogenerated Chemiluminescence Detection of sulfide with High selectivity based on Double-quenched Cyclometalated Ir(III) Complexes

1.1. Introduction

Hydrogen sulfide (H_2S), which is best known for its rotten egg smell, has been regarded as toxic gas. However, H_2S is also produced in our body endogenously from cysteine by enzymatic catalyzed reactions including cystathionin β-synthase (CBS), [161] cystathionine γ-lyase (CSE), [162] and 3-mercaptopyruvate sulfurtransferase (3MST). [163] Endogenously produced H_2S in human body has an important role as a cell signaling molecule in diverse physiological process, such as neuromodulation in the brain, smooth muscle relaxation in vascular system, and modulation of blood pressure. [164] H_2S is also involved in the therapeutic pathways including inflammation, insulin release, angiogenesis, and reduction of ischemia reperfusion injury. [165] Changing levels of endogenous H_2S can be a sign of various diseases, such as Down syndrome and Alzheimer's diseases. [166] Therefore, there have been

studied that selective and accurate determination for H_2S in steady increasing interests in recent years.

In addition to traditional H_2S detection methods based on gas chromatography, [167] sulfide precipitation, [168] colorimetric assays, [169] fluorescence based assays [116c, 170-172] have been studied actively in recent years due to high sensitivity and relatively facile analysis process. Most of the H_2S fluorescent probe were developed based on the unique characteristics of sulfide anion including reducing or nucleophilic properties. One strategy to design the H_2S probe is to introduce the Michael acceptor-type α,β-unsaturated carbonyl unit [171] or dinitrobenzene ether (DNB) group [172] as a nucleophilic attack site for sulfide anion. However, fluorescence based probes have a fundamental limitation to apply the portable point-of-care (POC) system because it requires the additional bulky equipment during the analysis process.

Electrogenerated chemiluminescence (ECL) is the light emitting process that chemical species undergo the homogeneous electron transfer reactions at the surface of the working electrode in solution. ECL based chemosensors are powerful candidates for point-of-care testing (POCT) due to their simple sensing process and easy handling. So far, most of ECL sensing systems have been developed based on the efficient ECL emission through oxidative reduction process between ruthenium trisbipyridine complex ($(Ru(bpy)_3^{2+}$), well-known ECL luminophore, and Tripropylamine (TPA) as a coreactant. Various types of $Ru(bpy)_3$ based biosensor and immunoassays have been developed, [116c, 173] Some of which are commercially available. However, many attempts still have been carried out to overcome the limitation of Ru^{II} species such as narrow emission range and relatively low ECL efficiency.

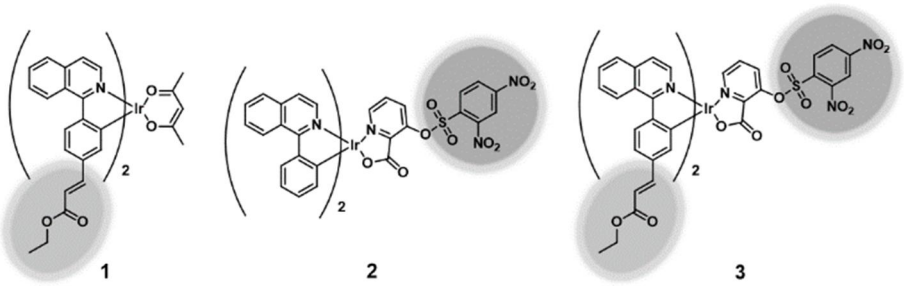

Scheme 2-10. The molecular structures of iridium complex based probes **1**-**3**.

Cyclometalated Ir^{III} complexes are currently of great interest for the development of high-efficient ECL lumionphores.[97, 174] Iridium complexes have a number of advantages compared to ruthenium derivatives including higher PL efficiency, easy control of wide emission range by modification of main ligands or ancillary ligand, and suitability for multiplexing detection.

In this study, we designed three kinds of Ir^{III} complex based probes introducing the specific reaction site that could induce the ECL signal change in the presence of H_2S. (Scheme 2-10) Probe **1** has α,β-unsaturated carbonyl groups as a Michael acceptor in phenylisoquionline (PIQ) main ligands. The reaction between unsaturated acrylate and sulfide resulted in a change in the electronic distribution of **1**, which induced the PL and ECL change. Next, we introduced dinitrobenzene sulfonyl (DNBS) group to ancillary ligand of probe **2**. DNBS group was a well-known strong electron acceptor that could operate as a high efficient photo-induced electron transfer (PET) quencher.[175] After the reaction with sulfide, the cleavage of DNBS group through nucleophilic aromatic substitution restored the strong red emission of **2** in both PL and ECL. Finally, we designed the probe **3** combining the concepts of probe **1** and **2**, introducing α,β-unsaturated carbonyl groups to main ligands and DNBS group to ancillary ligand. Probe **3** showed advanced properties that hybridize the good selectivity of **1** and the excellent turn-on ratio of **2**.

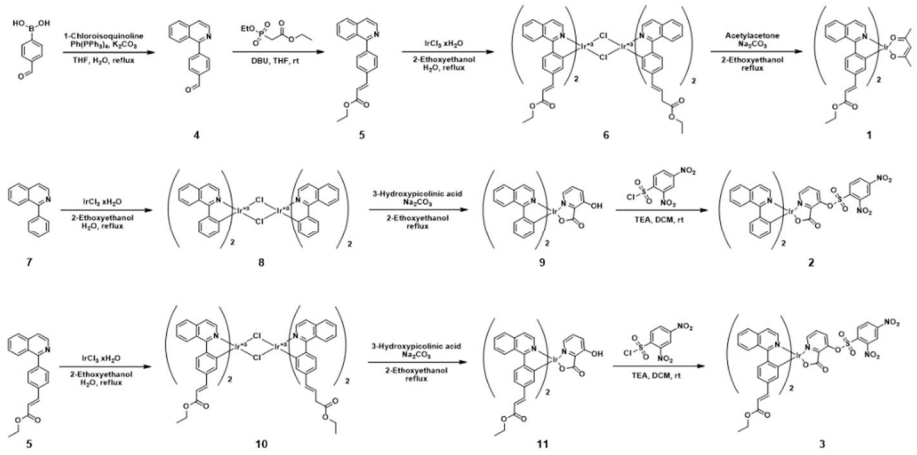

Scheme 2-11. Synthetic schemes of iridium complexes **1-3**.

1.2. Results

Synthesis

The synthetic route of iridium probes **1-3** was described in scheme 2-11. Firstly, 4-formylphenylisoquinoline was synthesized by Suzuki coupling between 1-chloroisoquinoline and 4-formylphenylboronic acid. After then, Horner-Wardsworth-Emmons (HWE) reaction was carried out for introducing the α,β-unsaturated ethyl ester to phenylisoquinoline. The chloro-bridged dinuclear cyclometalated Ir^{III} species was synthesized following the general synthetic method. Finally, probe **1** was obtained through the subsequent complexation with acetylacetone as an ancillary ligand. In the case of probe **2**, phenylisoquinoline was synthesized by Suzuki coupling and formed chloro-bridged Ir^{III} dimer as a same way to probe **1**. After complexation with 3-hydroxypicolinic acid, probe **2** was obtained through the reaction between Ir^{III} complex **9** and 2,4-dinitrobenzenesulfornyl chloride. Finally, We synthesized probe **3** through the complexation between Ir^{III} dimer 6 and 3-

hydroxypicolinic acid, and subsequent reaction with 2,4-dinitrobenzenesulfornyl chloride.

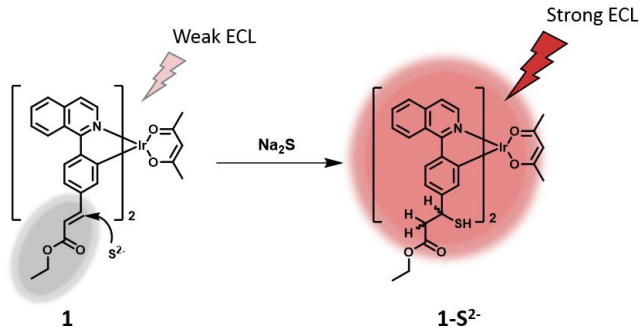

Scheme 2-12. Proposed mechanism of probe **1**

Properties of probe 1

Probe **1** shows the weak PL emission at 673 nm DMSO/HEPES (pH 7.4, 10 mM) (1:1 v/v), 58 nm red-shifted region compared to $(piq)_2Ir(acac)$. This phenomenon is due to the electron withdrawing character of α,β-unsaturated carbonyl group, which induces the change of the electronic distribution and stabilizes of the LUMO energy level. However, PL emission was drastically increased after reation with sulfide due to the disappearance of the eletron-withdrawing character. The 16-fold increase and blue-shifted emission change were observed when adding of Na_2S as a sulfide donor to probe **1**. Figure 2-43a shows the change of phosphorescent intensity when adding varying concentrations of sulfide. Phosphorescent intensity increased significantly with the gradual addition of sulfide. Next, we evaluated the selectivity of probe **1** by measuring its response toward other analytes, especially biothiols and cyanide. As shown Figure 2-43b, any phosphorescent change did not occurred in the presence of excess amount of other analytes except for sulfide.

We also performed the ECL experiment for probe **1**. Firstly, we changed the organic solvent to acetonitrile because DMSO is known to electrochemically unstable during electrochemical oxidation process. However, when replacing DMSO to acetonitrile, two unexpected problems were occurred; (i) reaction rate was too slow, (ii) the initial intensity of probe **1** was increased due to the declining of quenching ability of unsaturated

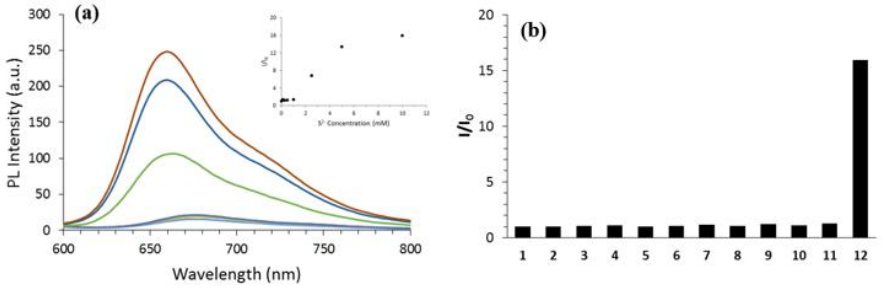

Figure 2-43. (a) Fluorescent emission spectra of **1** (10 μM) in the presence of 0-10 mM of sulfide in aqueous solution (DMSO/HEPES = 1:1) (inset) Turn-on ratio plotting data of probe **1** in the presence of 0-10 mM of sulfide in aqueous solution (DMSO/HEPES = 1:1) (c) Fluorescent responses of **1** (10 μM) in the presence of various analytes (10 mM) in aqueous solution (DMSO/HEPES = 1:1). (1) Probe **1** only (2) Br^- (3) I^- (4) NO_3^- (5) SO_3^- (6) N_3^- (7) CO_3^{2-} (8) SO_4^{2-} (9) CN^- (10) Cys (11) Hcy (12) S^{2-}

acrylate unit in acetonitrile. For example, only 1.6-fold increasing phosphorescence was observed in HEPES buffer/MeCN (1:1 v/v) condition upon the addition of sulfide. Considering all things including the reaction time, turn-on ratio, and the electrochemical stability, we optimized the solvent condition in ECL study as DMSO/MeCN/HEPES buffer (10:40:50 v/v %) containing 0.1M tetrabutylammonium perchlorate (TBAP) as an electrolyte

and 0.01M tripropylamine (TPA). In the ECL channel, initial intensity of probe **1** was observed around 1.4V during CV experiment. However, when adding sulfide, probe **1** showed a strong ECL enhancement, as expected. (Figure 2-44a) The addition of 10 mM of sulfide leaded to 2.3-fold signal enhancement at a similar potential and maintained the ECL signal more than 20-sweep CV cycles. A linear relationship between sulfide concentration and ECL intensity was observed in the range of 0.5 to 5 mM. The estimated limit of detection (LOD) was calculated to 12.1 μM. This relatively high LOD is caused by low reactivity and initial ECL intensity of free probe **1**.

DFT theoretical calculation was applied to probe **1** to identify the HOMO/LUMO electronic distributions (Scheme 2-13). The HOMO of probe **1** is locate on phenyl group but LUMO are delocalized on whole main ligand. This delocalized electronic distribution is due to the additional electron withdrawing character of unsaturated acrylate ester. The HOMO of the **1**-S^{2-} is similar to that of HOMO of probe **1**, which is mainly localized on benzene rings of main ligands. However, the LUMO distribution of **1**-S^{2-} is much

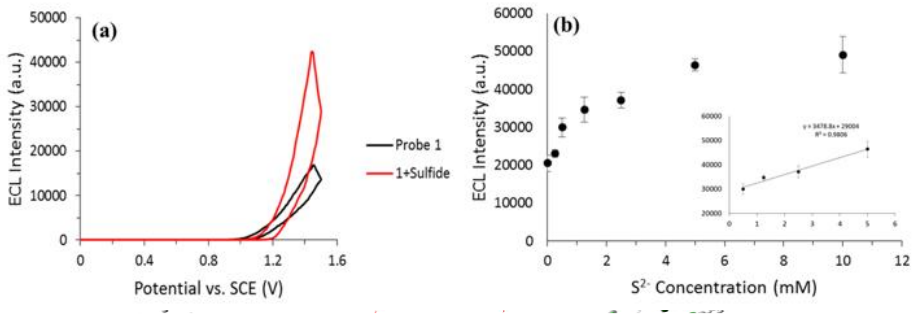

Figure 2-44. (a) ECL intensity of **1** (10 μM) upon the addition of sulfide (10 mM) in H_2O/MeCN/DMSO (5:4:1 v/v/v, pH 7.4, 10 mM TPA, 10 mM HEPES, and 0.1 M $NaClO_4$ as supporting electrolyte) while the potential is swept at a Pt disk electrode (diameter: 2 mm) in the range 0–1.5 V (scan rate: 0.1 V/s) (b) Isothermal binding curve obtained for ECL titration upon the addition of sulfide (10 mM) in H_2O/MeCN/DMSO (5:4:1 v/v/v, pH 7.4, 10 mM TPA, 10 mM HEPES, and 0.1 M $NaClO_4$ as supporting electrolyte).

different from that of **1**. In other words, the LUMO of **1**-S^{2-} localized on whole ligand but specially located on isoquinoline, similar to general C^N chelating cyclometalated Ir(III) complexes. This result proves that the introduction of electron withdrawing group to C-ring of C^N main ligands comes to stabilization of LUMO but has lower influence to HOMO. In ECL process, similar HOMO levels of two compounds relate to invariant ECL turn-on voltage around 1.4V. On the other hands, the destabilization of LUMO affects the light emission region and intensity through the change of HOMO-LUMO energy gap. Elevated LUMO level sometimes makes a trouble that blocks the electron transfer process from TPA radical to iridium complex. However, the LUMO of probe **1** is low enough in this case under the influence of electron-rich isoquinoline.

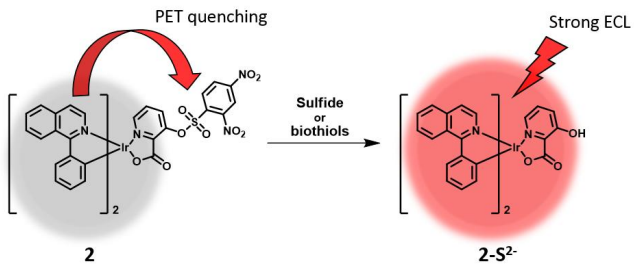

Scheme 2-14. Proposed mechanism of probe **2**

Properties of probe 2

Probe **2** shows the dynamic color change from colorless to yellow upon the addition of sulfide. At first, probe **2** displayed the intense absorption at 280 nm and 340 nm, which correspond to spin-allowed ligand-centered (^{1}LC) transition states. In addition, broad absorption at 430-550 nm is the typical shape of metal-t o-ligand charge-transfer (^{1}MLCT and ^{3}MLCT) transitions.

Upon the addition of sulfide, however, the intense absorption band appeared around 450 nm, which indicated the cleavage of 2,4-dinitrophenyl moiety by the reaction with sulfide. This distinct color change was also visible to naked-

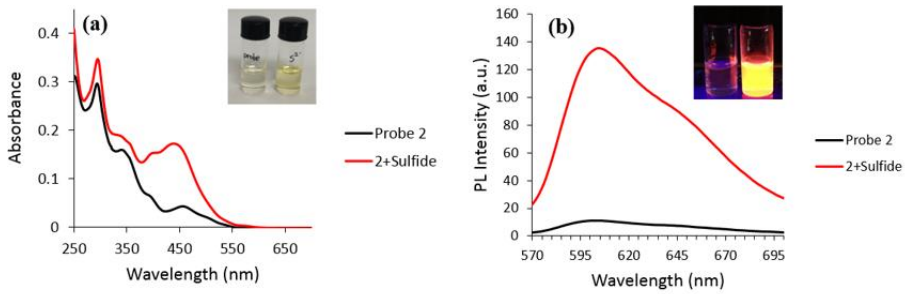

Figure 2-45. (a) UV-vis absorption of probe **2** (10 μM) before and after addition of sulfide (20 μM) in aqueous solution (MeCN/HEPES = 1:1) (b) Phosphorescence emission spectra (λ_{ex}=500 nm) of probe **2** before and after addition of sulfide (20 μM) in aqueous solution (MeCN/HEPES = 1:1)

eye (Figure 2-45a).

Free probe **2** had no phosphorescence when excited at 500 nm. However, upon the addition of sulfide, a large phosphorescent enhancement at 606 nm was observed (Figure 2-45b). Compared to probe **1**, probe **2** showed high sensitivity and fast response. As shown Figure 4a, the phosphorescence intensity of **2** increased gradually toward various concentrations of sulfide. Furthermore, it turned out that the enhancement of the phosphorescent intensity is linear with the concentration of sulfide in the range of 0-20 μM. The detection limit measured by PL was calculated at 1.28 μM. Next, we measure the response time towards sulfide. After addition of 20 μM sulfide in MeCN/HEPES (1:1 v/v), the reaction was complete within 60 min. (Figure 2-46b)

The selectivity test was carried out by adding other anions or biothiols to the solution of probe **2**. As shown Figure 2-46c, no PL enhancement was

observed in the excess amount of other anions. However, we failed to discriminate sulfide to other biothiols such as cysteine (Cys), homocysteine (Hcy), and glutathione (GSH), although the adding of excess GSH induced the weaker response than Cys or Hcy to probe **2** because of its bulkiness. Therefore, it needs to develop the probe which has an improved performance

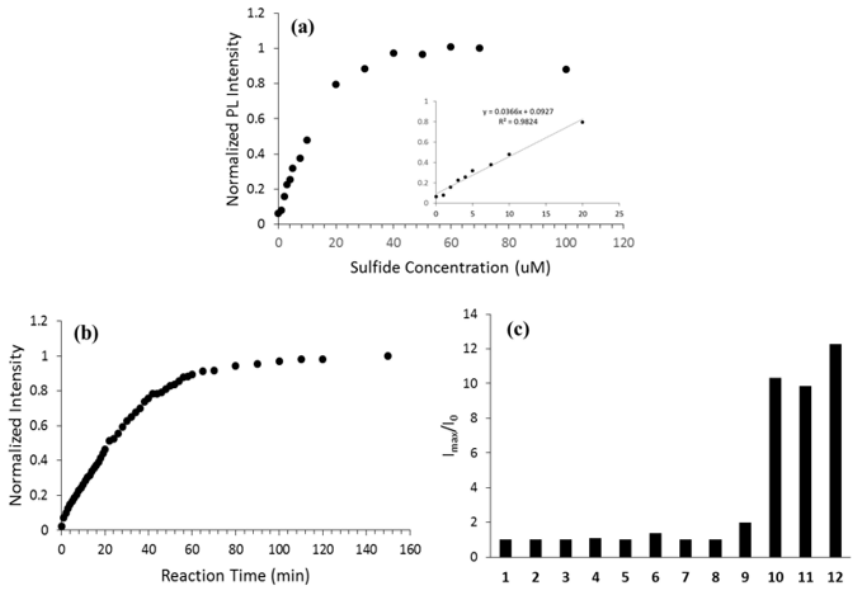

Figure 2-46. (a) Changes in phosphorescent intensity of **2** (10 μM) at 605 nm upon the addition of sulfide (0-100 μM) in aqueous solution (MeCN/HEPES 1:1) (b) Time-dependent phosphorescence profiles of **2** (10 μM) at 605 nm with 20 μM sulfide in aqueous solution (MeCN/HEPES 1:1) (b) (c) Fluorescent responses of of **2** (10 μM) in the presence of various analytes (50 μM) in aqueous solution (MeCN/HEPES 1:1). (1) Probe **2** only (2) Br^- (3) I^- (4) NO_3^- (5) SO_3^- (6) N_3^- (7) CO_3^{2-} (8) SO_4^{2-} (9) CN^- (10) Cys (11) Hcy (12) S^{2-}

that overcomes the selectivity problems.

Figure 2-47a shows the ECL spectrum of probe **2** while the potential is swept at a Pt electrode in the range of 0-1.6V. A similar tendency to the phosphorescence study was observed in ECL. In other words, in the absence of sulfide free probe **2** had no ECL during the potential sweep. This data

proves that PET-driven quenching mechanism by DNBS group was still working in ECL process with the additional heterogeneous electron transfer process from the working electrode during oxidation scanning. Upon increasing the sulfide concentration, the ECL intensity gradually increased and saturated when the concentration reaches 4 equivalent. Especially, the ECL intensity showed a linear correlation from 0 to 2 equiv. of sulfide. The

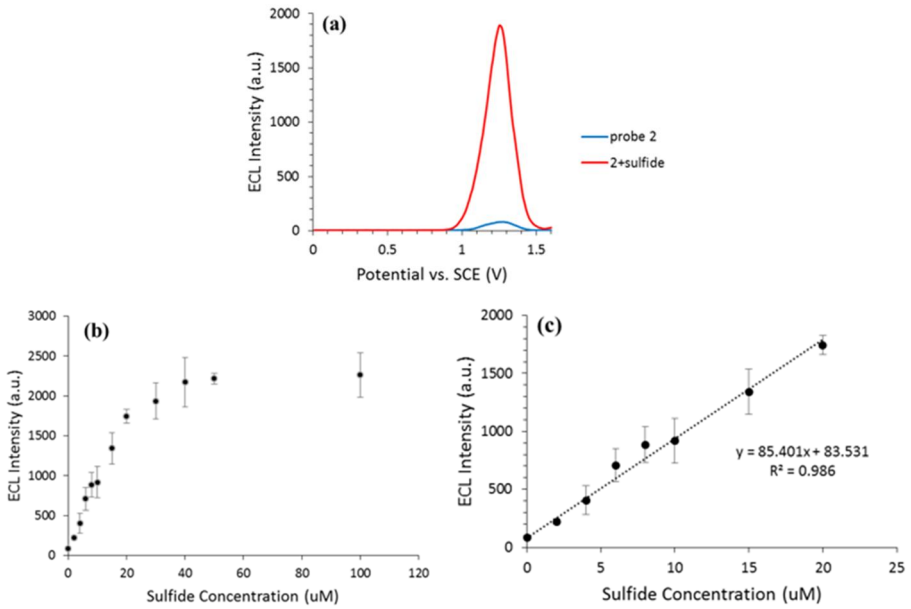

Figure 2-47. (a) ECL intensity of 2 (10 μM) upon the addition of sulfide (20 μM) in aqueous solution (MeCN/HEPES 1:1, pH 7.4, 10 mM TPA, 10 mM HEPES, and 0.1 M TBAP as supporting electrolyte) while the potential is swept at a Pt disk electrode (diameter: 2 mm) in the range 0–1.6 V (scan rate: 0.1 V/s) (b) Isothermal binding curve obtained for ECL titration upon the addition of sulfide (10 mM) in aqueous solution (MeCN/HEPES 1:1, pH 7.4, 10 mM TPA, 10 mM HEPES, and 0.1 M TBAP as supporting electrolyte) (c) Linear plot of the ECL intensity at 1.4V upon the addition of varying concentrations of sulfide

detection limit was calculated at 142 nm, much lower than PL value.

DFT calculation explains the turn-on mechanism of probe **2** upon the addition of sulfide. The HOMO is located whole C^N main ligand, and the

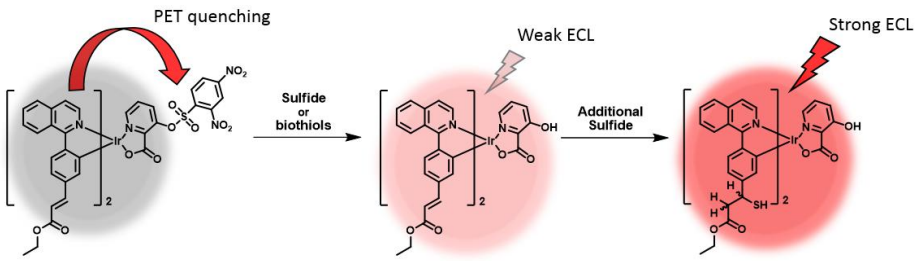

Scheme 2-15. Proposed mechanism of probe **3**

LUMO localizes at DNBS group, not main ligands. This separated HOMO/LUMO distribution induces the electron transfer process from Ir(III) complex to DNBS group, which results in non-luminescent excited states. After cleavage of DNBS group by reaction with sulfide, the LUMO moved to isoquinoline and whole main ligand broadly, as a result, red phosphorescence and ECL were recovered.

Properties of probe 3

Finally, we designed the probe **3** by introducing the main ligands of probe **1** and the ancillary ligand of probe **2**. The purpose of this strategy is as follows; (i) the DNBS group in ancillary ligand has two roles, which is the almost complete quenching of the phosphorescence and ECL of iridium complex and give a primary selectivity for sulfide and biothiols against other anions; (ii) unsaturated acrylate in main ligand contributes to unique selectivity for sulfide and removes the remaining phosphorescence and ECL entirely. Based on this principle, we developed more advanced type of probe **3** for sulfide, which has an excellent turn-on ratio and complemented good selectivity that overcomes the weak point of probe **2**.

We measured the PL and ECL properties of probe **3**. Figure 2-48 shows the enhancement of ECL intensity of probe **3** upon the addition of sulfide. The

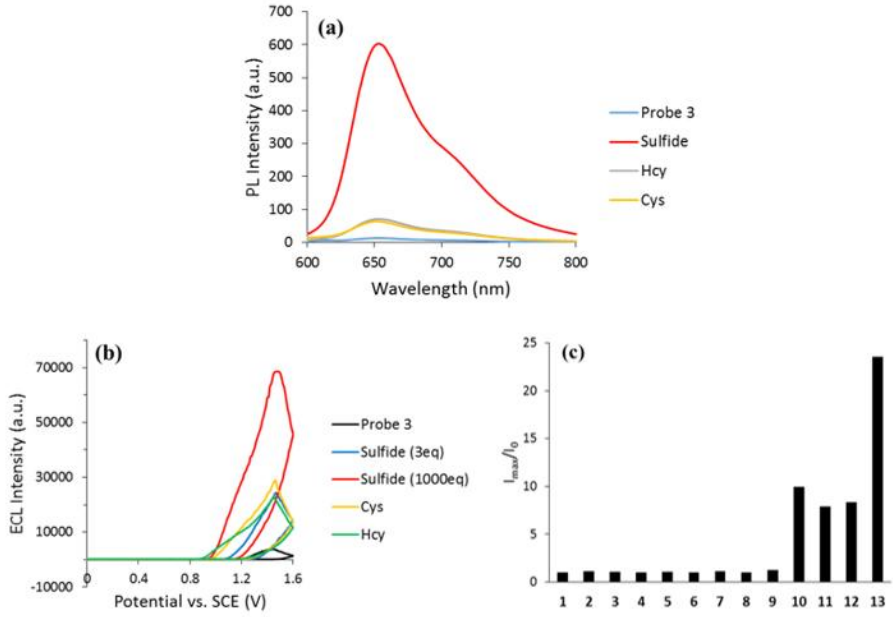

Figure 2-48. (a) PL intensity of **3** (10 μM) in the presence of sulphide, cysteine, and homocysteine in aqueous solution (DMSO/HEPES 1:1, pH 7.4). (b) ECL intensity of **3** (10 μM) in the presence of sulphide (3 equiv. and 1000 equiv. each), cysteine, and homocysteine in aqueous solution (DMSO/MeCN/HEPES 5:4:1, pH 7.4, 10 mM TPA, 10 mM HEPES, and 0.1 M TBAP as supporting electrolyte). (c) ECL responses of of **3** (10 μM) in the presence of various analytes (10 mM) in aqueous solution (MeCN/HEPES 1:1). (1) Probe **3** only (2) Br^- (3) I^- (4) NO_3^- (5) SO_3^- (6) N_3^- (7) CO_3^{2-} (8) SO_4^{2-} (9) CN^- (10) Cys (11) Hcy (12) S^{2-} (3 equiv.) (13) S^{2-} (1000 equiv.)

ECL emission of probe **3** increased through two reaction events in the presence of sulfide. Firstly, the cleavage of DNBS group made the ECL enhancement upon the addition of 0-3 equiv sulfide, whose intensity in this condition was almost similar to that of free probe **1**. (Figure 2-48b) Because both acetylacetone and picolinic acid hardly contributed the emission mechanism of iridium complex, the effect of ancillary ligand variation was negligible in this case. Next, it occurred the second reaction between unsaturated acrylate and sulfide in the presence of over 100eq sulfide. Through this Michael-type reaction, probe **3** recovered the ECL signal

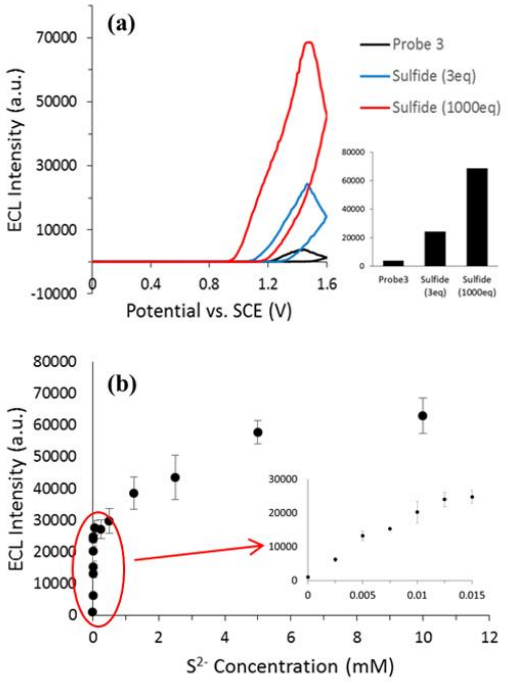

Figure 2-49. (a) ECL intensity of **3** (10 μM) upon the addition of sulfide (30 μM and 10 mM each) in aqueous solution (DMSO/MeCN/HEPES 5:4:1, pH 7.4, 10 mM TPA, 10 mM HEPES, and 0.1 M TBAP as supporting electrolyte) while the potential is swept at a Pt disk electrode (diameter: 2 mm) in the range 0–1.6 V (scan rate: 0.1 V/s) (b) Isothermal binding curve obtained for ECL titration upon the addition of sulfide (0-10 mM) in aqueous solution (inset) Linear plot of the ECL intensity at 1.4V upon the addition of varying concentrations of sulfide (0-15 μM)

entirely, similar to that of **1**-S^{2-}. Especially, the second reaction event occurs only by sulfide, which succeeds to overcome the selectivity problem against biothiols of probe **2**.

To prove this result more specifically, the selectivity of probe **3** toward sulfide and biothiols was investigated. We observed a slight enhancement of PL intensity in DMSO/HEPES (1:1 v/v) upon the addition of biothiols such as Cys and Hcy, which is 10% level of **3**-S^{2-} (Figure 2-49a). In the ECL channel, the intensity of **3** in the presence of biothiols showed relatively large enhancement by the influence of solvent condition (DMSO/MeCN/HEPES

1:4:5), which was ~30% levels of **3**-S^{2-} (Figure 2-49b). Especially, we also measured the the ECL of **3** with small amount of sulfide (30 μM), which was almost identical to that with biothiols. Other anions except sulfide and biothiols showed no ECL signal change. (Figure 2-49c) Through this experiment, we confirmed that the addition of biothiols can block the PET quenching from DNBS group by first reaction event, however, it still remained the quenching effect by unsaturated acrylate unit.

1.3. Conclusion

We developed the iridium based chemodosimeters for sulfide using ECL method. Sulfide selectively reacted with unsaturated acrylate followed by light enhancing through electrochemical process. Furthermore, dinitrobenzenesulfornyl (DNBS) group operated as a PET quencher, which was cleaved by sulfide or biothiols. Combining two reaction sites, we finally synthesized probe **3** with good selectivity and high turn-on ratio. DFT calculation assists the turn-on mechanism in sensing process. We expect that this rational design and application to ECL analysis can be promising point-of-care (POC) detecting tools for early diagnosis.

1.4. Supporting Information

Instrumentation: ^{1}H and ^{13}C NMR spectra were recorded using a Bruker Advance DPX-300. Chemical shifts are given in parts per million using as internal reference the residual resonances of deuterated solvents. ESI-MS data were obtained using a QUATTRO LC Triple Quadrupole Tandem Mass Spectrometer and are reported in units of mass to charge (m/z). High-resolution mass spectroscopy (MALDI-TOF) was performed on a Voyager-DE STR Biospectrometry Workstation. Analytical thin layer chromatography

was performed using Kieselgel 60F-254 plates from Merck. Column chromatography was carried out on Merck silica gel 60 (70-230 MESH) and Merck Aluminium oxide 60 (70-230 MESH ASTM).

Materials: All reagents were purchased from either Sigma-Aldrich (Sigma-Aldrich Corp., MO, USA) or TCI (Tokyo Chemical Industry, Tokyo, Japan) and used without any further purification. Deuterated solvents were acquired from CIL (Cambridge Isotopic Laboratories, MA, USA). All amino acids were purchased from Sigma-Aldrich or TCI.

Synthesis: Synthesis of **4**: A mixture of 4-formylphenylboronic acid (1.15 g, 7 mmol), 1-chloroisoquinoline (1.05 g, 7 mmol), $Pd(PPh_3)_4$ (404 mg, 0.35 mmol) and potassium carbonate (1.93 g, 14 mmol) in THF (40 mL) and H_2O (40 mL) was refluxed for 24 h. After cooling to room temperature, the reaction mixture was extracted with dichloromethane (DCM), and the organic phase was washed with water, and dried over Na_2SO_4. The solvent was evaporated to give an white solid product (1372 mg, 84% yield), which was purified by silica gel column with gradient elution (DCM:MeOH from 100:1 to 20:1).

300 MHz ^{1}H NMR (chloroform-d): δ 10.15 (s, 1H); 8.65 (d, 1H, J = 6.3 Hz); 8.02~8.08 (m, 3H); 7.93 (d, 1H, J = 10.1 Hz); 7.89 (d, 2H, J = 10.1 Hz); 7.73 (t, 1H, J = 7.8 Hz); 7.72 (d, 2H, J = 7.1 Hz); 7.58 (t, 1H, J = 8.0 Hz).

Synthesis of **5**: A mixture of 4 (700 mg, 3 mmol), triethyl phosphonoacetate (0.90 ml, 4.5 mmol) and 1,8-diazabicyclo[5,4,0]undec-7ene (DBU, 0.90 ml, 6 mmol) in THF (15 mL) was stirred for 5h at room temperature in N_2 condition. After checking TLC, the reaction mixture was extracted with dichloromethane (DCM), and the organic phase was washed with water, and dried over Na_2SO_4.

The solvent was evaporated to give an white solid product (783 mg, 86% yield), which was purified by silica gel column chromatography (eluent; EA/Hexane =1:5).

300 MHz ^{1}H NMR (chloroform-d): δ 8.65 (d, 1H, J = 5.7 Hz); 8.13 (d, 1H, J = 8.5 Hz); 7.93 (d, 1H, J = 8.1 Hz); 7.83~7.68 (m, 7H); 7.61 (t, 1H, J = 7.1 Hz); 6.59 (d, 1H, J = 16.1 Hz); 7.73 (t, 1H, J = 7.8 Hz); 4.35 (q, 1H, J = 7.1 Hz); 1.41 (t, 3H, J = 7.1 Hz).

Synthesis of **6** (crude form): A mixture of **5** (400 mg, 1.32 mmol) and Iridium chloride hydrate (176 mg, 0.60 mmol) in 2-ethoxyethanol (20 mL) and H_2O (7 mL) was refluxed for 18h. After cooling to room temperature, pouring cold water (~50 mL) to reaction mixture. Then a dark brown precipitate was filtered to crude cyclometalated Ir(III) chloro-bridged dimer.

Synthesis of **1**: A mixture of crude cyclometalated Ir(III) dimer (**6**, 300 mg, 0.180 mmol), sodium carbonate (192 mg, 1.80 mmol) and acetylacetone (0.185 mL, 1.80 mmol) in 2-ethoxyethanol (10 mL) was refluxed 3h. After cooling to room temperature, the reaction mixture was extracted with dichloromethane (DCM), and the organic phase was washed with water, and dried over Na_2SO_4. The solvent was evaporated to give a dark brown solid product (229mg, 61% yield), which was purified by silica gel column chromatography (eluent; EA/Hex= 1:1).

300 MHz ^{1}H NMR (chloroform-d): δ 8.98 (q, 2H, J = 3.38 Hz); 8.47 (d, 2H, J = 6.36 Hz); 8.25 (d, 2H J = 8.40 Hz); 8.02 (q, 2H, J = 4.17 Hz); 7.79 (q, 4H J = 2.37 Hz); 7.57 (d, 2H, J = 6.38 Hz); 7.33 (d, 2H, J = 16.3 Hz); 7.14 (d, 2H, J = 7.7 Hz); 6.50 (s, 2H); 6.08 (d, 2H, J = 16.0 Hz); 4.19 (m, 4H); 1.78 (s, 6H); 1.28 (m, 6H).

^{13}C NMR (75 MHz, chloroform-d): δ 14.280, 28.706, 60.224, 100.649, 118.062, 120.061, 120.540, 126.579, 127.488, 128.047, 129.596, 130.881, 134.021, 134.146, 137.228, 140.440, 145.316, 148.956, 151.400, 167.118, 168.144, 184.981.

Synthesis of **7**: This compound was synthesized according to the literature procedure.

Synthesis of **8**: This compound was synthesized according to the literature procedure.

Synthesis of **9**: A mixture of crude cyclometalated Ir(III) dimer (**8**, 500mg, 0.393 mmol), sodium carbonate (209 mg, 1.96 mmol) and 3-hydroxypicolinic acid (164 mg, 1.18 mmol) in 2-ethoxyethanol (10 mL) was refluxed 3h. After cooling to room temperature, the reaction mixture was extracted with dichloromethane (DCM), and the organic phase was washed with water, and dried over Na_2SO_4. The solvent was evaporated to give a red solid product (160 mg, 55% yield), which was purified by silica gel column chromatography (eluent; EA/Hex= 1:1).

300 MHz ^{1}H NMR (chloroform-d): δ 13.84 (s, 1H); 8.98 (m, 2H); 8.67 (d, 1H, J = 6.4 Hz); 8.27 (d, 1H, J = 7.9 Hz); 8.21 (d, 1H, J = 7.9 Hz); 7.85 (m, 1H); 7.72 (m, 4H); 7.52 (d, 1H, J = 6.4 Hz); 7.47 (d, 1H, J = 6.4 Hz); 7.37 (m, 2H); 7.14 (m, 2H); 7.11 (t, 1H, J = 6.9 Hz); 7.01 (t, 1H, J = 6.8 Hz); 6.79 (t, 1H, J = 6.9 Hz); 6.73 (t, 1H, J = 6.9 Hz); 6.51 (d, 1H, J = 7.6 Hz); 6.25 (d, 1H, J = 7.5 Hz).

Synthesis of **2**: A mixture of **9** (100 mg, 0.135 mmol) and trimethylamine (25 μM, 0.270 mmol) in DCM was stirred at room temperature for 30 min. Then 2,4-dinitrobenzenesulfonyl chloride (54 mg, 0.202 mmol) in DCM was added

slowly. The reaction mixture was stirred 6h, after then the solvent was removed under reduced pressure and extracted with DCM, and the organic phase was washed with water, and dried over Na_2SO_4. The solvent was evaporated to give a red solid product (69 mg, 53% yield), which was purified by silica gel column chromatography (eluent; MC/MeOH= 100:1 – 20:1).

300 MHz ^{1}H NMR (chloroform-d): δ 8.96 (m, 2H); 8.65 (d, 1H, J = 8.7 Hz); 8.57 (d, 1H, J = 6.4 Hz); 8.52 (m, 2H); 8.29 (d, 1H, J = 7.9 Hz); 8.15 (d, 1H, J = 7.9 Hz); 7.92 (m, 3H); 7.77 (m, 4H); 7.67 (d, 1H, J = 4.4 Hz); 7.49 (d, 1H, J = 6.4 Hz); 7.40 (m, 2H); 7.03 (t, 1H, J = 6.9 Hz); 6.90 (t, 1H, J = 6.8 Hz); 6.82 (t, 1H, J = 6.9 Hz); 6.67 (t, 1H, J = 6.9 Hz); 6.49 (t, 1H, J = 7.4 Hz); 6.14 (d, 1H, J = 7.5 Hz).

Synthesis of **11**: The synthetic process is similar to **9**. A mixture of crude cyclometalated Ir(III) dimer (6, 655 mg, 0.393 mmol), sodium carbonate (209 mg, 1.96 mmol) and 3-hydroxypicolinic acid (164 mg, 1.18 mmol) in 2-ethoxyethanol (10 mL) was refluxed 3h. After cooling to room temperature, the reaction mixture was extracted with dichloromethane (DCM), and the organic phase was washed with water, and dried over Na_2SO_4. The solvent was evaporated to give a dark brown solid product (121 mg, 33% yield), which was purified by silica gel column chromatography (eluent; EA/Hex= 1:1).

300 MHz ^{1}H NMR (chloroform-d): δ 13.75 (s, 1H); 8.98 (m, 2H); 8.67 (d, 1H, J = 6.4 Hz); 8.31 (d, 1H, J = 8.4 Hz); 8.24 (d, 1H, J = 8.3 Hz); 7.99 (m, 2H); 7.80 (m, 4H); 7.61 (d, 1H, J = 6.4 Hz); 7.47 (d, 1H, J = 6.4 Hz); 7.39 (m, 2H); 7.14 (m, 2H); 7.32-7.17 (m, 3H, J = 6.9 Hz); 6.61 (s, 1H); 6.31 (s, 1H); 6.05 (d, 1H, J = 18.2 Hz); 5.99 (d, 1H, J = 11.4 Hz); 4.16 (m, 4H); 1.27 (m, 6H).

Synthesis of **3**: The synthetic process is similar to **2**. A mixture of **11** (100 mg, 0.107 mmol) and trimethylamine (20 μM, 0.214 mmol) in DCM was stirred at room temperature for 30 min. Then 2,4-dinitrobnzenesulfonyl chloride (43 mg, 0.161 mmol) in DCM was added slowly. The reaction mixture was stirred 6h, after then the solvent was removed under reduced pressure and extracted with DCM, and the organic phase was washed with water, and dried over Na2SO4. The solvent was evaporated to give a red solid product (49 mg, 39% yield), which was purified by silica gel column chromatography (eluent; MC/MeOH= 100:1 – 20:1).

300 MHz ^{1}H NMR (chloroform-d): δ 8.94 (m, 2H); 8.65 (d, 1H, J = 8.6 Hz); 8.58 (d, 1H, J = 6.4 Hz); 8.51-8.33 (m, 2H); 8.33 (d, 1H, J = 8.4 Hz); 8.19 (d, 1H, J = 8.4 Hz); 7.99-7.91 (m, 3H); 7.83-7.80 (m, 4H); 7.73 (d, 1H, J = 5.0 Hz); 7.56 (d, 1H, J = 6.4 Hz); 7.50-7.19 (m, 7H); 7.14 (d, 1H, J = 6.6 Hz); 6.59 (s, 1H); 6.21 (s, 1H); 6.11 (d, 1H, J = 16.0 Hz); 5.96 (d, 1H, J = 16.0 Hz); 4.22-4.10 (m, 4H); 1.30-1.23 (m, 6H).

13C NMR (75 MHz, chloroform-d): δ 14.275, 60.287, 60.460, 76.598, 118.353, 119.102, 119.911, 120.431, 120.822, 121.328, 121.640, 126.089, 127.022, 127.350, 127.922, 128.651, 128.786, 129.131, 130.031, 130.216, 131.545, 131.601, 133.114, 133.369, 134.621, 134.693, 134.773, 135.383, 135.498, 137.076, 137.207, 140.256, 140.48, 144.277, 144.346, 144.872, 148.169, 148.268, 149.013, 150.520, 151.082, 166.819, 166.996, 167.174, 168.749, 168.988.

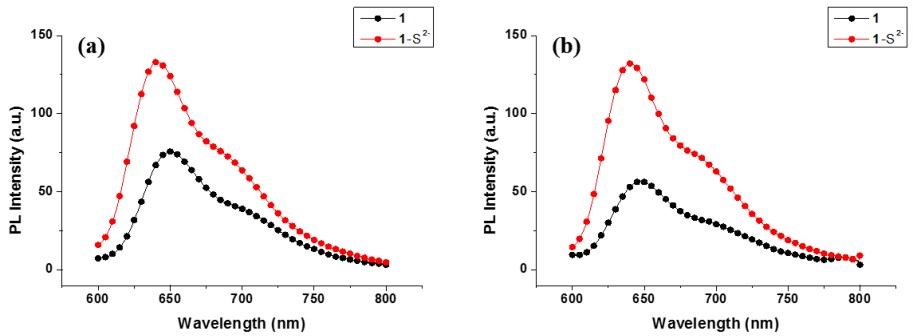

Figure 2-50. Fluorescent emission spectra of **1** (10 μM) in the presence of 10 mM of sulfide in (a) MeCN/DMSO (9:1 v/v) and (b) MeCN/HEPES/DMSO (4:5:1 v/v/v).

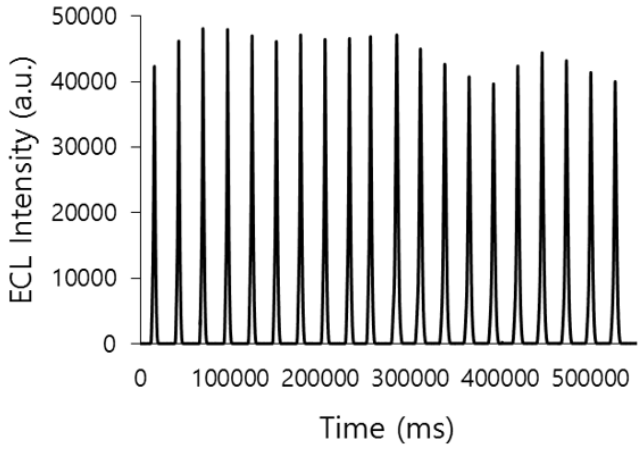

Figure 2-51. Continuous cyclic ECL scans of **1** (10 μM) in the presence of sulfide (5 mM) in MeCN/HEPES /DMSO (4:5:1 v/v/v, pH 7.4, 10 mM TPA, 10 mM HEPES, and 0.1 M TBAP as supporting electrolyte) while the potential is swept at a Pt disk electrode in the range 0–1.5 V (scan rate: 0.15 V/s).

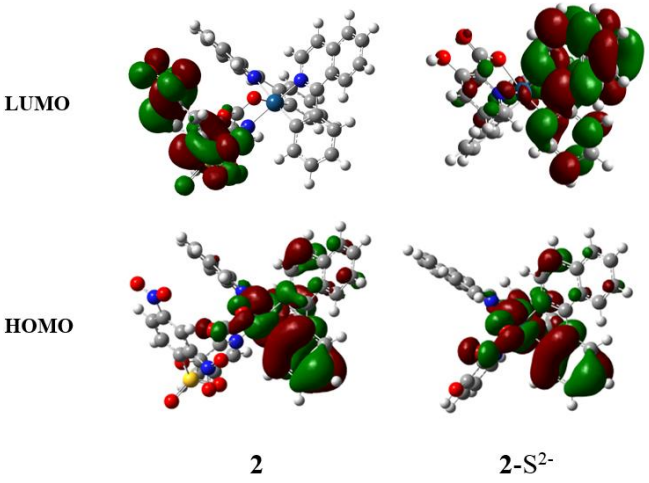

Figure 2-52. The HOMO/LUMO electron distributions of probe **2** and **2**-S^{2-}.

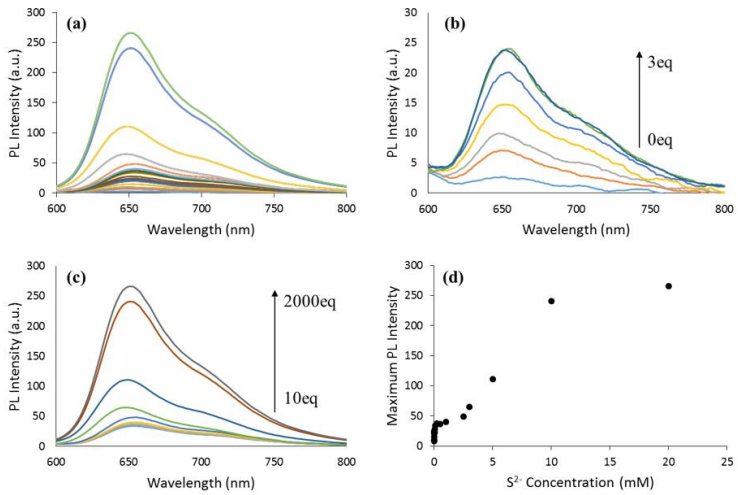

Figure 2-53. (a) Fluorescent emission spectra of **3** (10 μM) in the presence of (a) 0-2 mM of sulfide in aqueous solution (DMSO/HEPES = 1:1) (b) The first phosphorescence increase in the presence of 0-30 μM of sulfide (c) The second phosphorescence increase in the presence of 0.1-2 mM of sulfide (d) Changes in phosphorescent intensity of **3** (10 μM) at 650 nm upon the addition of sulfide (0-2 mM) in aqueous solution (DMSO/HEPES 1:1)

Part III

The Rational Design and Mechanistic Study of Ir(III)-based ECL Probes by Tuning LUMO Energy Level

Background

1. Tuning the HOMO and LUMO Energy Levels of Cyclometalated Iridium(III) Complex

Cyclometalated Ir(III) complexes have a great merit for tuning emission color from blue to red by modifying chelating ligands. This characteristic comes from the unique construction of excite states, which has the limited access to the high-lying metal-centered ligand-field state (MC) involved in phosphorescence quenching. Therefore, it enables to control the orbital energy levels by modifying the chelating ligands without taking into account MC states. This tunability contrasts sharply with the limited photophysical controllability of other metal complexes such as Ru(II) polyamine complexes with low-lying MC states. [176]

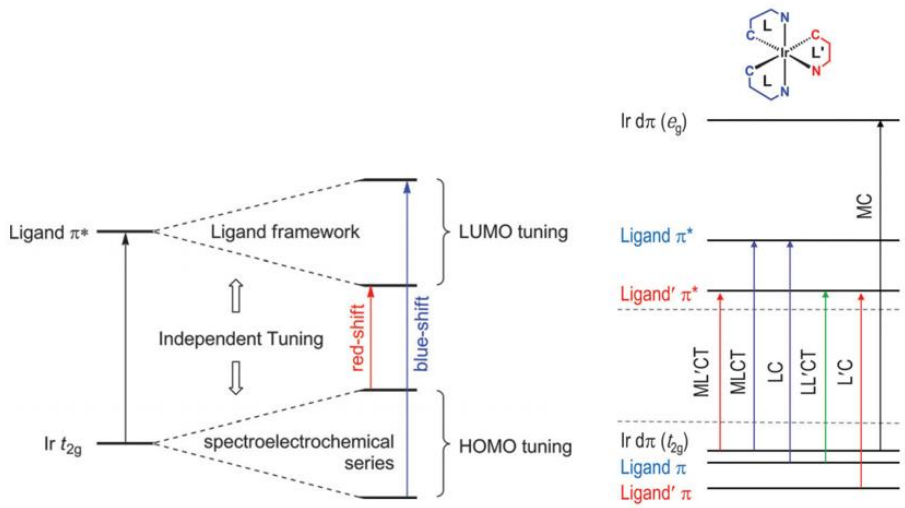

Figure 3-1. (Left) MLCT state energy tuning via frontier molecular orbital control. (Right) the construction of excited states via molecular orbital interactions.

Heteroleptic Ir(III) complexes exhibit complicate photophysics as following in Figure 3-1. In addition to MLCT (metal-to-ligand charge-transfer), LC (ligand-centered transitions), and MC states, the ancillary ligand (L') enables additional L'C, ML'CT, and LL'CT transitions. However, the heteroleptic structure permits facile phosphorescence color change, because the phosphorescent transition energy is determined by a global LUMO energy level among the three ligands.

To control HOMO and LUMO energy levels with a modulation of main ligands excluding the influence of ancillary ligand, some kinds of ancillary ligands which cannot contribute the emission process are often used. For example, acetylacetone (acac) and picolinic acid (pic) are most used ancillary ligand when controlling energy levels by modifying main ligands. Park. S. Y. et al. studied the influence of ancillary ligand to emission change in the Ir(III) complexes in 2005. [177] The inter-ligand energy transfer (ILET) to ancillary ligand was only available when the ^{3}LX energy level was lower than ^{3}MLCT level, which induces the red-shifted emission or emission quenching. In other words, if the ^{3}LX state is higher than that of ^{3}MLCT such as the case of FIrpic (Figure 3-2), the ancillary ligand has no influence on emission of Ir(III) complexes.

There are two strategies to control the HOMO and LUMO energy levels by deliberately adjusting the energy of metal and ligand orbitals, which can be achieved through substituent effects or by changing the ligand parent structure entirely. [178] To develop the Ir(III) complex based ECL probe based on chemodosimetric approach, it is important to understand the principle of controlling orbital energy levels by introducing specific reaction site that has electron-withdrawing or electron-donating ability.

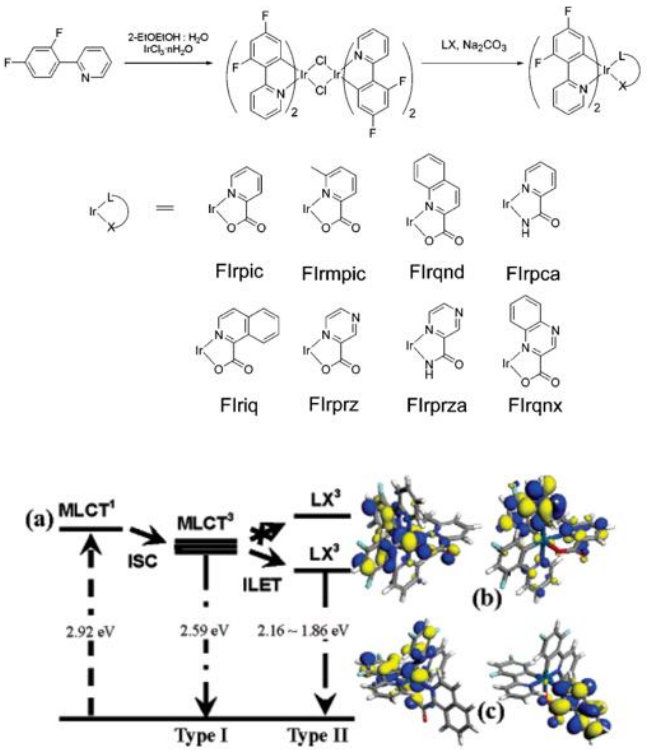

Figure 3-2. (a) A suggested mechanism of color tuning invoked by the ILET to ancillary ligand, and HOMO and LUMO of (b) FIrmpic and (c) FIriq.

Because phosphorescent dyes such as Ir(III) complexes have increased research interest in organic light-emitting diodes (OLEDs), many studies related to control the orbital energy levels have been reported so far. In general, electronic effects have been considered due to their profound influence on orbital energies as well as the relative ease with which electron-withdrawing and electron-donating groups can be incorporated into the ligand structure.[179] For example, electron-withdrawing substituents on pyridine tend to stabilize the HOMO by removing electron density from the metal, whereas donating groups have an inverse effect. This relationship is convoluted by the fact that withdrawing groups may also lower the energy of the LUMO (i.e., increasing the electron affinity of the parent ligand). Fortunately, the cyclometalating and ancillary ligands can be separately substituted with

electron-withdrawing and –donating groups in heteroleptic complexes, which enables deliberate control over the excited state. [180]

The position of these substituents with respect to the coordinating carbon of a cyclometalating ligand will strongly influence the ligand field stabilization energy (LFSE) of the resulting complex. For example, electron-withdrawing groups *meta* to the site of coordination (and donating groups *ortho* or *para* to this position) increase the field strength of the ligand and concomitantly enhance d-orbital splitting. Interestingly, opposing spectroscopic trends have been observed for fluoro (-F) and trifluoromethyl (-CF_3) substituents at the same position of a cyclometalating ring despite their similar electronic effects.[179]

Tsuzuki, T. et al. reported the color tunable OLED materials using pentafluorophenyl-substituted iridium complexes.[180] By introducing the pentafluorophenyl substituent into the phenylpyridine main ligands of $(ppy)_2Ir(acac)$ and by changing the position of the substitution, dynamic PL emission change was observed due to their orbital energy level change.

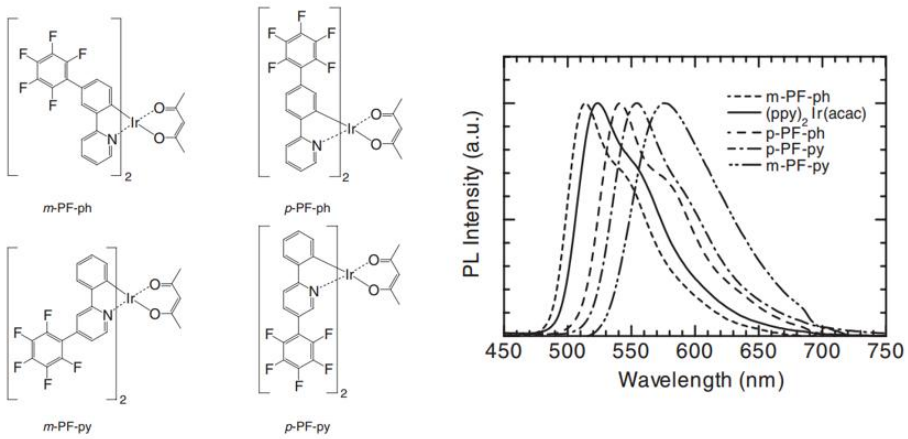

Figure 3-3. Chemical structures of iridium complexes and their PL spectra.

Malliaras and Bernhard studied the color-tuning of phenylpyridine (ppy) based Ir(III) complex using electrochemical experiments and DFT calculations.[181] Four different ppy-based main ligands were used, which were introduced various substituents to pyridine or benzene. The introduction of electron-withdrawing fluoro groups to benzene *meta* to the site of coordination caused to more positive oxidation potentials, by contrast reduction potential showed almost no changes. On the other hand, the dynamic change of reduction potential was observed when introducing trifluoromethyl group to pyridine, which showed -0.29 V negative shift of reduction potential compared to that of methylpyridine. These results proved that the introduction of electron-withdrawing groups to phenylpyridine induces the changes of orbital energy level. Especially the HOMO is affected by phenyl modification and the LUMO is influenced by pyridine modification.

It is clear that the HOMO of Ir(III) complexes consist principally of a mixture of phenyl π and Ir- d-orbitals, whereas the LUMO is localized largely on ppy, with the predominant contribution derived from the pyridyl π-orbitals. Therefore, that would be one major strategy to control HOMO and LUMO level selectively by introducing electron-withdrawing or –donating substituent to pyridine or benzene. However, the modulation of HOMO (or LUMO) level with fixed LUMO (or HOMO) is difficult because the introduction of substituents have an influence on the electronic distributions of whole ppy ligand. According to the literature, for example, the pyridyl ring π-orbitals contribute 60-70 % to the LUMOs of typical of Ir(III) complexes and the rest is depends on the benzene rings and other components of Ir(III) complexes.[182] As a result, HOMO and LUMO energy level tend to move together when introducing the electron-withdrawing or –donating substituents, and which energy level is more affected is determined by the location of substituents.

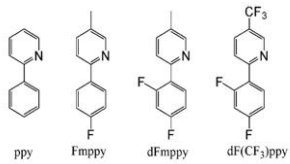

complex	emission max (eV)	$E^{0'}$ $^*IrL_3^{3+}/IrL_3^{4+}$ (V vs SCE)	$E^{0'}$ $^*IrL_3^{3+}/IrL_3^{2+}$ (V vs SCE)
$[Ir(ppy)_2(dtbbpy)]^+$	2.17	−0.96	+0.66
$[Ir(Fmppy)_2(dtbbpy)]^+$	2.27	−0.94	+0.77
$[Ir(dFmppy)_2(dtbbpy)]^+$	2.41	−0.92	+0.97
$[Ir(dF(CF_3)ppy)_2(dtbbpy)]^+$	2.58	−1.21	+0.89

Figure 3-4. Four ppy-based main ligands and excited state redox properties of iridium complexes.

In 2008, Zhou, G.-J. et al. studied the color tuning of Iridium

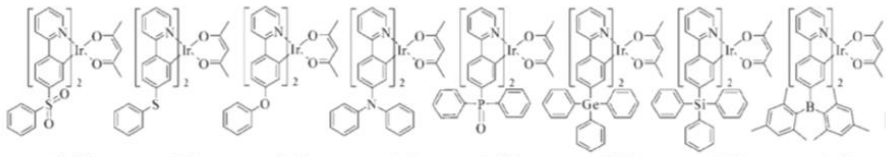

Ir-SO_2 Ir-S Ir-O Ir-N Ir-PO Ir-Ge Ir-Si Ir-B

Compound	Absorption (293 K) λ_{abs} [nm][a]	Emission λ_{em} [nm] 293 K/77 K	Φ_p [b]	τ_p [μs] [c]	τ_r [μs] [d]	$\Delta T_{5\%}/T_g$ [°C][e]	HOMO/LUMO [eV]	$E^{ox}_{1/2}$ [V]	$E^{red}_{1/2}$ [V]
Ir-B	289 (4.54), 334 (4.67), 419 (3.54), 513 (3.40), 576sh (2.71)	605/603	0.18	2.67	14.83	360/162	−5.16/−2.39	0.36	−2.41, −2.63, −2.88
Ir-Si	264 (4.60), 272 (4.59), 281 (4.60), 349 (3.74), 414 (3.43), 473 (3.30) 508 (2.45)	535/529	0.39	2.44	6.26	379/164	−5.18/−2.11	0.38	−2.69
Ir-Ge	263 (4.69), 279 (4.69), 347 (3.84), 412 (3.51), 467 (3.36), 505 (2.40)	530/521	0.40	2.17	5.43	360/165	−5.22/−2.08	0.42	−2.72
Ir-N	257 (4.57), 301 (4.53), 379 (4.50), 393 (4.51), 450 (3.82)	533/525	0.14	5.00	35.71	366/160	−5.11/−1.98	0.31	−2.82 [f]
Ir-PO	261 (4.56), 274 (4.55), 280 (4.56), 353 (3.67), 393 (3.52), 420 (3.42) 476 (3.31), 510 (2.67)	541/537	0.19	2.56	13.47	366/158	−5.38/−2.40	0.58	−2.40, −2.64
Ir-O	282 (4.55), 403 (3.58), 430 (3.45), 481 (2.54)	505/499	0.40	1.66	4.15	351/155	−5.22/−2.00	0.42	−2.80
Ir-S	255 (4.53), 291 (4.48), 322 (4.53), 414 (3.57), 445 (3.47), 502 (2.40)	527/524	0.52	2.53	4.87	350/150	−5.21/−2.08	0.41	−2.72
Ir-SO_2	263 (4.63), 280 (4.68), 356 (3.71), 395 (3.56), 422 (3.51), 478 (3.29) 513 (2.32)	550/548	0.86	2.69	3.13	377/159	−5.46/−2.54	0.66, 0.83	−2.26, −2.48

[a] Measured in CH_2Cl_2 at a concentration of 10^{-5} M and logε values are shown in parentheses. sh = shoulder. [b] In degassed toluene relative to *fac*-[Ir(ppy)$_3$] ($\Phi_p = 0.40$), $\lambda_{ex} = 360$ nm. [c] Measured in freeze-pump-thaw degassed toluene solutions at a sample concentration of ca. 10^{-5} M and the excitation wavelength was set at 355 nm for all the samples at 293 K. [d] The triplet radiative lifetimes were deduced from $\tau_r = \tau_p/\Phi_p$. [e] $\Delta T_{5\%}$ is the 5% weight-reduction temperature and T_g is the glass transition temperature. [f] Irreversible.

Figure 3-5. The chemical structures of [Ir(ppy-X)$_2$(acac)] iridium complexes and their photophysical, thermal and electrochemical properties.

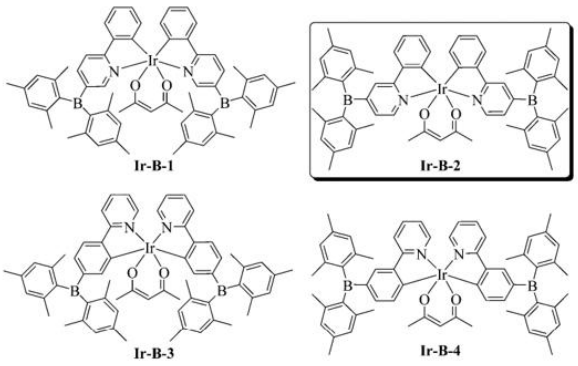

Complex	$E_{1/2}^{ox}$ (V)	$E_{1/2}^{red}$ (V)	HOMO (eV)	LUMO (eV)
Ir-B-1	0.42	−2.20, −2.30	−5.22	−2.60
Ir-B-3[a]	0.36	−2.41, −2.63, −2.88	−5.16	−2.39
Ir-B-4	0.43	−2.70	−5.23	−2.10

Figure 3-6. The molecular structure and electrochemical properties of Ir(III) ppy-type complexes bearing dimesitylboron unit.

electrophosphors by simple tailoring of the phenyl ring of ppy with various main group moieties.[183] The complexes with weak electron-donating and –withdrawing main group moieties (Ir-Si, Ir-Ge, Ir-O, and Ir-S) show a similar oxidation potential $E_{1/2}^{ox}$, while those possessing strongly electron-withdrawing moieties (Ir-PO and Ir-SO_2) show much higher $E_{1/2}^{ox}$ values. Ir-Si, Ir-Ge, Ir-N, Ir-O, and Ir-S have similar reduction potentials $E_{1/2}^{red}$, while Ir-B, Ir-PO, and Ir-SO_2 show much less negative $E_{1/2}^{ox}$ values, which indicates their lower LUMO energy levels. Time-dependent density functional theory (TD-DFT) calculations show the contributions of Ir(III) complexes in HOMO and LUMO level. It shows similar HOMO characters with the major contribution coming from the π-orbitals of the phenyl ring in each case. On the contrary, the LUMOs show large differences among the complexes, providing significant LUMO level modulation for Ir-B, Ir-PO, and Ir-SO_2. While the pyridyl ring π-orbitals contribute 63-71% to the LUMOs of Ir-Si, Ir-Ge, Ir-N, Ir-O, Ir-S, and Ir-PO, the corresponding contributions are only 35%

and 44% for Ir-B and Ir-SO_2, respectively. These results indicate us that the introduction of strong electron-withdrawing group to phenyl rings have a strong influence on not only HOMO level but LUMO level or Ir(III) complexes.

In 2013, the study of ppy-type complexes bearing dimesitylboron ($B(Mes)_2$) units have been reported.[184] In that case, a series of Ir(III) complexes showed the different electronic characters by changing the substitution position. The changes of HOMO and LUMO energy level were measured by CV experiment. Ir-B-4 showed almost unchanged energy levels compared to original $(ppy)_2Ir(acac)$ complex. On the other hands, the HOMO and LUMO levels of Ir-B-3 were slightly stabilized due to the substitution position. Ir-B-1 exhibited the greatest influence on LUMO energy level. The substitution to pyridyl rings had an effect on greater LUMO stabilization than the substitution to phenyl rings. The introduction of electron-withdrawing group to main ligand affects the LUMO level largely because the LUMO mainly locates on pyridyl rings in most ppy-type Ir(III) complexes. In the case of introduction of electron-withdrawing group to phenyl ring, the substitution position is very important. As described previously, the substitution at *meta* position to coordinated Ir(III) meal largely influences to HOMO and LUMO level. On the other hands, in the case of electron-donating group, the *meta*-substitution has little effect on energy levels but *ortho*- or *para*- substitution makes the HOMO level unstable.

These studies suggest the general tendencies for the change of HOMO and LUMO energy levels when introducing the electron-withdrawing group (EWG) or electron-donating group (EDG) to C^N main ligands of Ir(III) complex.

I. In general, the introduction of EWG induces the stabilization of HOMO and LUMO energy levels, whereas the introduction of EDG induces the destabilization of those levels.

II. The modification of N-heterorings in C^N main ligand such as pyridine has a majoric effect to LUMO level.

III. The modification of phenyl rings affects both the HOMO and LUMO energy levels.

IV. The substitution of *meta* position to Ir(III) metal induces the change of HOMO and LUMO energy levels. Especially, the introduction of strong EWG influences the stabilization of LUMO level by changing the electronic distribution of LUMO state which localizes on pyridyl rings in general cases.

V. The substitution of *ortho* or *para* position to Ir(II) metal has a majoric influence on HOMO level. The introduction of EWG stabilizes the HOMO and LUMO levels, however, the stabilization effect are lower than that of *meta* substitution. On the other hands, the introduction of EDG induces the destabilization of HOMO level, keeping the LUMO level similarly.

VI. The substitution of phenyl rings sometimes do not follow these tendencies, which induces the unexpected change of HOMO level.

Section 1

The Rational Design of ECL Probes for Cyanide based Cyclometalated Ir(III) Complexes by Controlling LUMO Energy Levels

1.1. Introduction

Electrogenerated chemiluminescence (ECL) involves a light emission process through the electron transfer reaction between electrochemically generated radicals at working electrode.[185] Especially, co-reactant ECL has been studied specially in the bioanalysis field due to its high sensitivity. Most studies have been developed based on tris(2,2'-bipyridine)ruthenium(II), known as $[Ru(bpy)_3]^{2+}$, and other Ru(II) species with orange-red ECL emission.[186]

However, Ru(II)-based ECL assays have several limitations including narrow emission range and low PL quantum yield. Because Ru(II) complexes have the limited photophysical controllability with low-lying MC state, the modification of ligands almost has no influence on emission wavelength. These disadvantages make it hard to develop ratiometric or turn-on probes for specific targets based on chemodosimetric approach based on Ru(II) complexes.[181]

Cyclometalated Ir(III) complexes are spotlighted currently with great interest in the ECL study due to their wide emission range and extraordinary ECL efficiencies.[187-192] Contrary to Ru(II) derivatives, Ir(III) complexes have a great merit for tuning emission color from blue to red by modifying chelating ligands. This characteristic comes from the high contributions of MLCT and LC characters in excited state construction and phosphorescence emission process. Therefore, the introduction of electron-donating or –withdrawing groups to chelating ligands strongly affect the HOMO and LUMO energy levels and emission color. As a result, it is easier to develop the chemodosimeter based on Ir(III) complex by introducing the specific reaction sites to chelating ligand.[181]

The LUMO level of Ir(III) complex is of particular importance in the ECL emitting process. In oxidative reduction ECL process, the excited states are formed by the electron transfer from the TPA radical to the LUMO level of ECL emitter, therefore, the LUMO level should be higher than the energy level of TPA radical.[183, 187] In this study, we synthesized a series of Ir(III) complexes by introducing the formyl group as a reactive site for cyanide to pyridine of main ligand. The Ir(III) complexes bearing phenylpyridine (ppy) as a main ligand have been studied steadily, especially in OLED.[194-197] However, the LUMOs of ppy-based Ir(III) complex such as $(ppy)_2Ir(acac)$ or $Ir(ppy)_3$ is known to similar or slightly higher than that of TPA radical, which induces the poor ECL efficiencies. As a result, it needs to lower the LUMO level of ppy-based Ir(III) complexes to enhance the ECL efficiency.

Generally, the LUMOs of Ir(III) complex mainly locate on pyridine, whereas the HOMOs are delocalized on phenyl ring and Ir(III) metal center. Therefore, the most effective strategy to control LUMO level is modifying the pyridine unit to more electron-withdrawing N-hetero rings such as

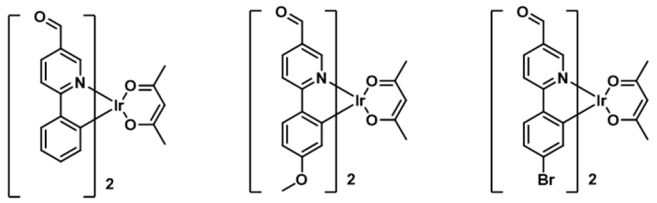

Scheme 3-1. The molecular structures of Ir(III) based probes.

phenylquionline (pq) or phenylisoquionline (piq). The introduction of electron withdrawing group is also known to stabilize the LUMO level. On the other hands, the modification of phenyl part has a large influence to HOMO level. However, the introduction of substituents to specific location, e.g. *meta* position to Ir(III), has the minor influence on LUMO level.[178]

In this study, we developed three iridium complexes possessing the formyl groups in pyridine ring of ppy main ligands. The formyl group functions as a specific reaction site for cyanide,[194-196] and has another role to stabilize LUMO level as a strong electron-withdrawing group. In the presence of formyl groups, the Ir(III) complexes showed the weak emission in red-shifted region due to the narrowing of the HOMO-LUMO energy gap. However, after reaction with cyanide, the disappearance of formyl groups caused the recovery of the LUMO level similar to $(ppy)_2Ir(acac)$ complex with green phosphorescence. Additionally, we introduced the electron-withdrawing and –donating groups *meta* position to phenyl parts of Ir(III) complexes as an additional control unit of LUMO energy level.

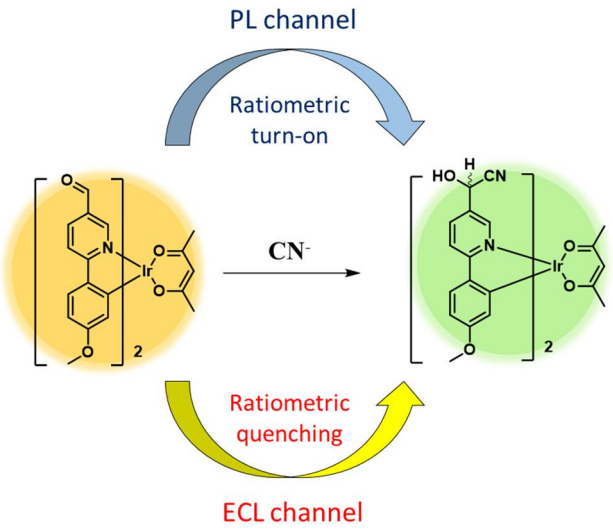

Scheme 3-2. The sensing strategy of **OMe_acac** for cyanide.

We designed three iridium-based probes introducing the methoxy group and bromo group respectively, using **H-acac** as a standard. Through the introduction of various substituents, different ECL signal changes were observed that depended on their LUMO energy levels. Especially, **OMe_acac** showed drastic ECL quenching in the presence of cyanide. This result provides the rational design of ECL probe based on ECL quenching or enhancing route by controlling LUMO level.

1.2. Results

Firstly, we predicted the HOMO and LUMO energy levels of three Ir(III) probes by DFT calculation. Three Ir(III) complexes showed the similar tendency in the way that the elevation of LUMO level and an increase of HOMO-LUMO energy gap in the presence of cyanide. However, the absolute values of LUMO level showed the clear differences. As shown Figure 1a, the LUMO level of **OMe_acac** was calculated as -3.03 eV, much lower than the

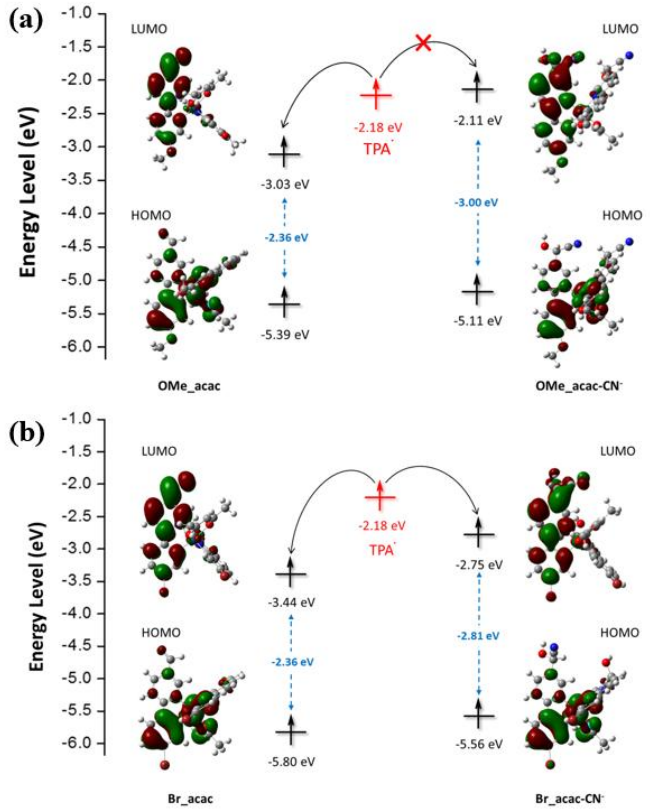

Figure 3-8. The estimated HOMO and LUMO energy level and electronic distributions of (a) **Ome_acac** and (b) **Br_acac** by DFT calculation.

calculated energy level of TPA radical. After the reaction with cyanide, the LUMO level was drastically increased, even higher than that of TPA raidcal. This elevated LUMO level was expected to block the electron transfer process from TPA radical to the LUMO level of Ir(III) complex, which results in the degradation of ECL efficiency.

On the other hands, the HOMO and LUMO energy levels of **Br_acac** was stabilized due to the introduction of electron-withdrawing groups (Figure 3-8b). After the reaction with cyanide, the LUMO level of **Br_acac** was also increased, however, still lower than the energy level of TPA radical in this case. As a result, **OMe_acac** and **Br_acac** would show the different ECL

change pattern in the presence of cyanide, although it was expected that two iridium complexes shows the similar phosphorescence changes.

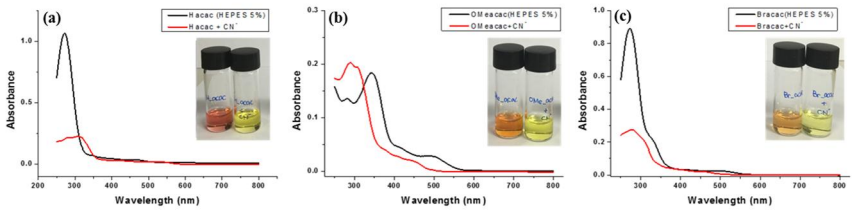

Figure 3-9. UV-vis spectra of (a) **H_acac**, (b) **OMe_acac**, and (c) **Br_acac** (10 μM each) upon addition of cyanide (1 mM) in H_2O/MeCN (0.5:9.5 v/v, pH 7.4, 10 mM HEPES).

Figure 3-9 shows the color change of three iridium complexes in the absence and presence of cyanide, respectively. Three probes showed the similar patterns. For example, OMe_acac displayed the intense absorbance around 350 nm, which corresponded to spin-allowed ligand-centered (^{1}LC) transition state. The broad absorption around 500-600 nm was the typical shape of MLCT transitions. In the presence of cyanide, the absorption of LC transitions were changed and that of MLCT transitions were decreased. This absorbance change also could be observed by naked-eye detection.

Next, we measured the phosphorescence emission of three probes. The electron-withdrawing formyl group induced the phosphorescence in red-shifted region with weaker PL intensity. However, when adding cyanide, it could attack the formyl groups to form the stabilized species. The disappearance of electron-withdrawing group caused the recovery of green PL emission, which showed the dynamic ratiometric change. Furthermore, the emission of three Ir(III) complexes were decreased in water-containing solvent, which corresponds to previous report. As a result, the turn-on ratiometric properties were observed in aqueous solution.

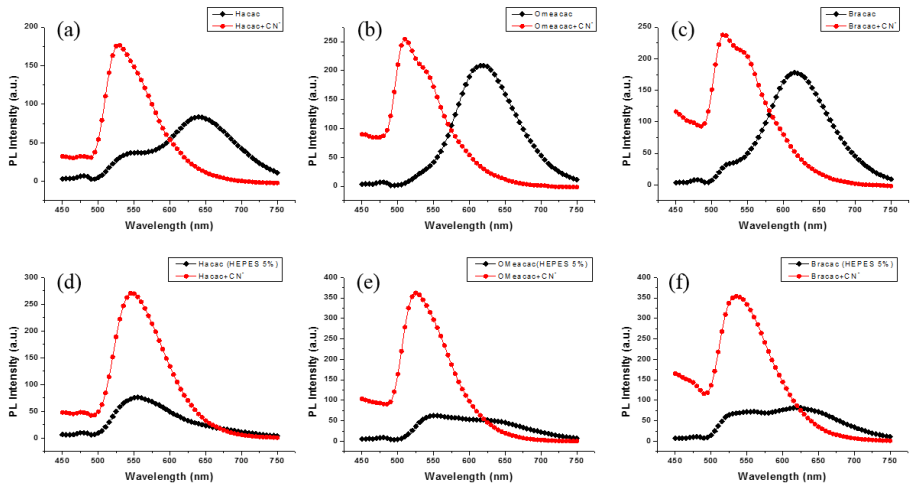

Figure 3-10. Phosphoresce spectra of **H_acac**, **OMe_acac**, and **Br_acac** (10 μM each) upon addition of cyanide (1 mM). (a)-(c) were measured in MeCN and (d)-(f) in H_2O/MeCN (0.5:9.5 v/v, pH 7.4, 10 mM HEPES).

Then we tried to applicate probes to ECL analysis. Interestingly, **Br_acac** and **OMe_acac** showed the conflicting result. In the case of **Br_acac**, the

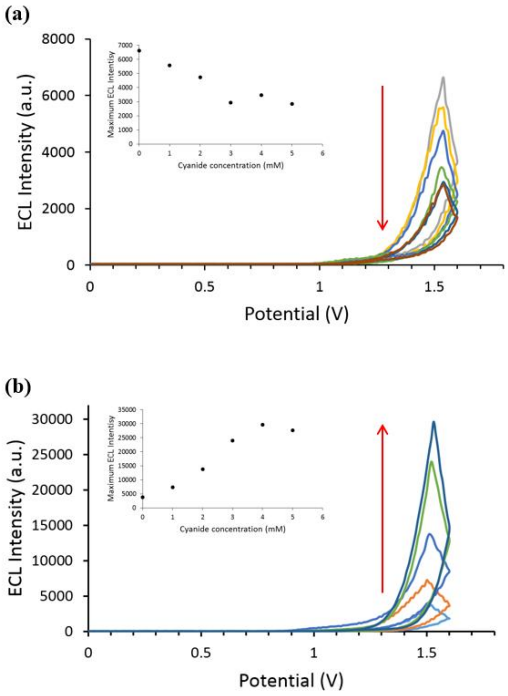

Figure 3-11. ECL emission spectra of (a) Ome_acac and (b) Br_acac (10 μM each) in the presence of 0-5 mM of cyanide in MeCN containing 5% water (pH 7.4, 10 mM HEPES).

ECL intensity was gradually increased upon the addition of cyanide in MeCN containing 5% water (pH 7.4, 10 mM HEPES), which was the similar tendency to PL study. However, **OMe_acac** had an opposite result to PL study.

In other words, the ECL intensity was rather decreased in the presence of cyanide (Figure 3-11). Figure 3-12 shows the relative PL and ECL change upon the addition of cyanide. In the case of **Br_acac**, it showed the similar

Table 3-1. Electrochemical properties of Br-acac and OMe-acac.

Compound	[a] $E_{ox}^{0'}$ (V vs SCE)	[b] $E_{red}^{0'}$* (V vs SCE)	E_{0-0}* (eV)
Br-acac	1.34	-0.97	2.31
Br-acac-CN$^-$	1.17	-1.38	2.55
OMe-acac	1.03	-1.31	2.34
OMe-acac-CN$^-$	0.82	-1.86	2.68

[a]The oxidation potentials were measured using cyclic voltammetry at the scan rate of 0.1 V/s in acetonitrile (CH_3CN) solutions with 0.1M tetra-*n*-butylammonium perchlorate as the supporting electrolyte and then the values were calibrated against the oxidation of 1 mM ferrocene (Fc/Fc^+) as a standard and then referenced to SCE. [b]The values of the reduction potential were calculated from the excitation energies (E_{0-0}) and the oxidation potentials ($E_{ox}^{0'}$).

tendency by 4.30-fold increase in PL and 4.59-fold increase in ECL. The PL and ECL intensity of **H_acac** also increased 3.67-fold and 2.25-fold

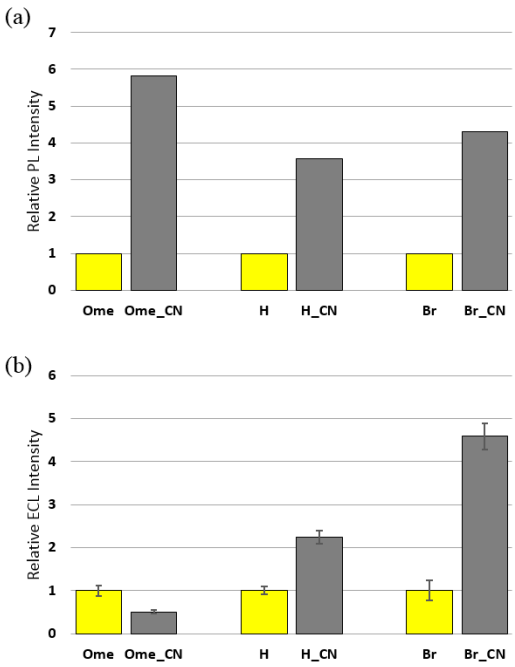

Figure 3-12. Relative PL and ECL intensity of Ome_acac, **H_acac** and **Br_acac** (10 μM each) in the presence of 5 mM of cyanide in MeCN containing 5% water (pH 7.4, 10 mM HEPES).

respectively. On the other hands, **OMe_acac** showed the 5.82-fold increase in PL but ECL signal rather decreased about by half. These results correlate to the prediction by DFT calculation when designing molecules. To evaluate these result more precisely, we measured the electrochemical properties of Br-acac and OMe-acac. As shown table 1, the reduction potential of **Br_acac** was -0.97 V (vs. SCE) and negatively shifted to -1.38 V after reaction with cyanide. Because the reduction potential of TPA was estimated as -1.7 V, the efficient production of excited states and ECL emission were expected. OMe-acac also had a relatively mild reduction potential ($E^{o'}_{red} = -1.34$ V (vs SCE)), which was less negative than the reduction potential of the TPA radical. However, after the reaction with CN^-, the product after the reaction with cyanide had a more negative reduction potential at -1.86V, more negative than that of TPA radical.

1.3. Conclusion

We developed a series of Ir(III) complexes with formyl group and other substituents to phenylpyridine (ppy) main ligands. The formyl groups in pyridyl rings strongly stabilized the LUMO level in addition to operate as a reaction site for cyanide. Furthermore, the additional substitution of electron-withdrawing or –donating group to phenyl rings has a role to modulate the HOMO and LUMO levels, while keeping the HOMO-LUMO energy gap of each iridium complex. The HOMO and LUMO levels were destabilized when introducing the electron-donating methoxy groups, whereas electron-withdrawing bromo groups made the energy level stable. The change of LUMO level resulted in the different ECL properties due to their suitability to excited states formation. Especially, **OMe_acac** showed the different signal changes in PL and ECL upon the addition of cyanide. The obvious ratiometric

change was observed in PL study, while ECL signal was rather decreased. This study provides the new sensing strategy by blocking the electron transfer process in ECL with LUMO level control of ECL-active probe.

1.4. Experimental Section

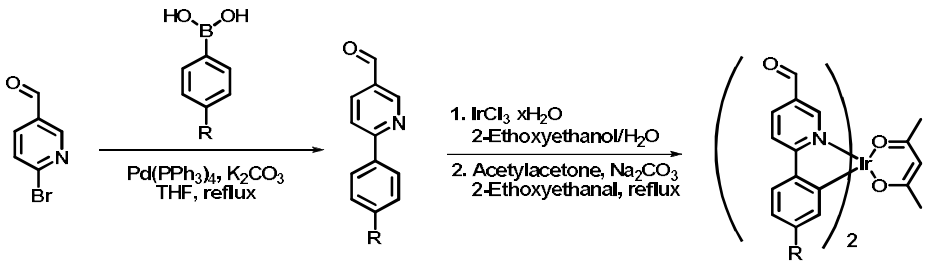

Preparation of phenylpyridine derivatives

A mixture of 4-formylpyridine (491 mg, 3 mmol), $Pd(PPh_3)_4$ (173mg, 0.15 mmol), potassium carbonate (829 mg, 6 mmol) and phenylboronic acid derivatives (3.3 mmol) in THF (20 mL) and H_2O (20 mL) was refluxed for 24 h. After cooling to room temperature, the reaction mixture was extracted with dichloromethane (DCM), and the organic phase was washed with water, and dried over Na_2SO_4. The solvent was evaporated to give an white solid product with 74-83% yields, which was purified by silica gel column chromatography (DCM / MeOH).

Preparation of chloro-bridged iridium dimers

A mixture of ppy derivatives (2 mmol) and Iridium chloride hydrate (269 mg, 0.9 mmol) in 2-ethoxyethanol (15 mL) and H_2O (5 mL) was refluxed for 12h. After cooling to room temperature, pouring cold water (~50 mL) to

reaction mixture. Then a red-orange precipitate was filtered to crude cyclometalated Ir(III) chloro-bridged dimer.

Preperation of Ir(III) complexes

A mixture of crude cyclometalated Ir(III) dimer (1 mmol), sodium carbonate (531 mg, 5 mmol) and acetylacetone (0.514 mL, 5 mmol) in 2-ethoxyethanol (10 mL) was refluxed 1h. After cooling to room temperature, the reaction mixture was extracted with dichloromethane (DCM), and the organic phase was washed with water, and dried over Na_2SO_4. The solvent was evaporated to give a red-orange solid product with 24-43% yield, which was purified by silica gel column chromatography (EA/Hex: 1/1).

H-acac: 300 MHz ^{1}H NMR (Chloroform-d): δ 10.04 (s, 2H); 8.96 (s, 2H); 8.23 (d, 2H, *J* = 8.46 Hz); 8.03 (d, 2H, *J* = 8.52 Hz); 7.70 (d, 2H, *J* = 7.56 Hz); 6.90 (t, 2H, *J* = 7.14 Hz, 7.62 Hz); 6.79 (t, 2H, *J* = 7.41 Hz, 7.17 Hz); 6.33 (d, 2H, *J* = 7.44 Hz); 5.28 (s, 1H); 1.86 (s, 6H).

OMe-acac: 300 MHz ^{1}H NMR (Chloroform-d): δ 9.98 (s, 2H); 8.86 (s, 2H); 8.15 (d, 2H, *J* = 8.53 Hz); 7.87 (d, 2H, *J* = 8.57 Hz); 7.64 (d, 2H, *J* = 8.66 Hz); 6.52 (d, 2H, *J* = 8.62 Hz); 5.80 (d, 2H, *J* = 2.36 Hz); 5.29 (s, 1H); 3.59 (s, 6H); 1.86 (s, 6H).

Br-acac: 300 MHz ^{1}H NMR (Chloroform-d): δ 10.06 (s, 2H); 8.87 (s, 2H); 8.27 (d, 2H, *J* = 8.43 Hz); 8.03 (d, 2H, *J* = 8.31 Hz); 7.57 (d, 2H, *J* = 8.16 Hz); 7.12 (d, 2H, *J* = 8.19 Hz); 6.36 (d, 2H, *J* = 1.74 Hz); 5.31 (s, 1H); 1.88 (s, 6H).

Section 2

PL and ECL Dual-channel Sensing of H_2O_2 with Mechanistic Study Based on Borylated Ir(III) Complexes

1.1. Introduction

Reactive oxygen species (ROS) play fundamental roles in physiology, aging and diseases in living organism but are difficult to study because of their reactive and transient nature. Hydrogen peroxide is the major ROS in living system, which acts a second messenger in normal cellular signal transduction. H_2O_2 is involved in therapeutic processes including wound healing, anti-bacterial defense, and stem cell proliferation. [197-202] However, the overproduction of H_2O_2 will lead to accumulation of oxidative damage, which is connected to aging and diseases such as cancer, cardiovascular disorders, and Alzheimer's diseases.[203-210]

The most well-known method for detecting H_2O_2 is based on boronate chemistry. [211-216] In the presence of H_2O_2 the alkylboronates convert to phenol groups, which induces the fluorescent change. A lot of H_2O_2 probe have been reported based on this strategy so far by introducing boronate to various fluorophores.

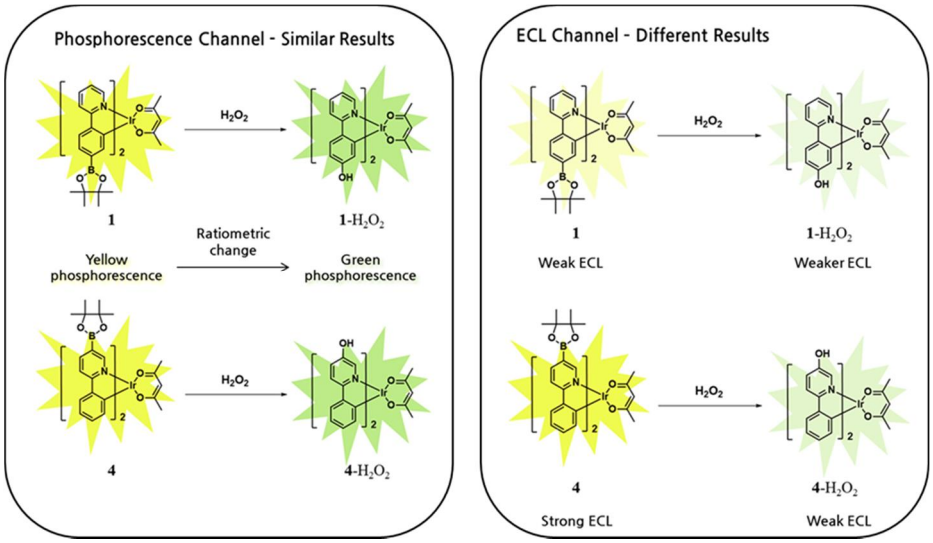

Scheme 3-3. Phosphorescence and ECL changes of **1** and **4** upon the addition of H_2O_2.

In this study, we developed a series of Ir(III) complexes introducing boronate to main ligands as a reaction site for H_2O_2 and to contribute electron-withdrawing character. The phenol group produced by the reaction with H_2O_2 has electron-donating ability compared to boronate. Therefore, the conversion from electron-withdrawing group to electron-donating group has the strong influence on the electronic distributions of ligands, which induces the change of energy levels and emission color. To observe the dynamic emission change, we designed the H_2O_2 probes using $(ppy)_2Ir(acac)$ (ppy: phenylpyridine, acac: acetylacetonate) as a basic backbone molecule, representative green-emitting Ir(III) complex that shows the drastic color change only small blue-shifts or red-shifts.

Another expectation by using ppy ligand is that it can induce the additional ECL quenching. In ECL emitting process, the excited species are formed by the electron transfer reaction from TPA radical to the LUMO level of luminophore. For example, if the change of substituents from boronate to phenol causes the stabilization of destabilization of LUMO level, it can affect the ECL efficiency strongly.

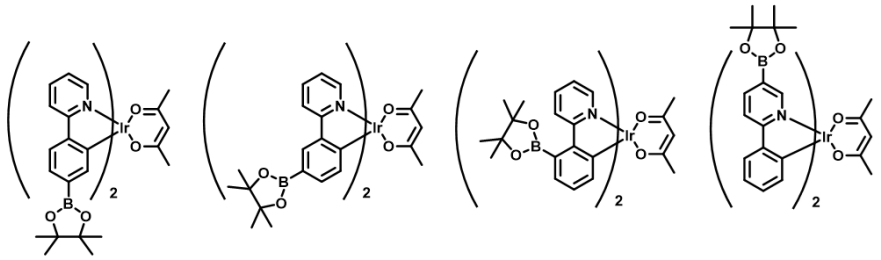

Scheme 3-4. The molecular structures of Ir(III) complexes **1**-**4**.

Wong, W.-Y. et al. reported the study of borylated iridium (III) complexes based $(ppy)_2Ir(acac)$ in 2013.[217] In that paper, the *meta*-substituted Ir(III) complexes showed the yellow emission, whereas he para-substituted Ir(III) complexes showed the green emission, almost identical to $(ppy)_2Ir(acac)$. Herein, we synthesized Ir(III) complexes **1**-**4** by introducing boronate moiety to various sites of ppy main ligand. The emission spectrum of **1**-**4** showed the similar tendency to previous report. Among them, probe **1** showed the good ratiometric phosphorescence change in the presence of H_2O_2 due to the change of energy levels. Probe **4** also showed similar ratiometric change in PL, however, in the ECL channel two probes had some different properties. The drastic decrease of ECL was observed for **4** after the reaction with H_2O_2, whereas the ECL intensity of probe **1** showed smaller decrease than that of **4**. In this paper, we suggest the mechanistic explanations for these phenomenon, and provide the general strategy for rational designing of Ir(III) complex based ECL probes.

1.2. Results

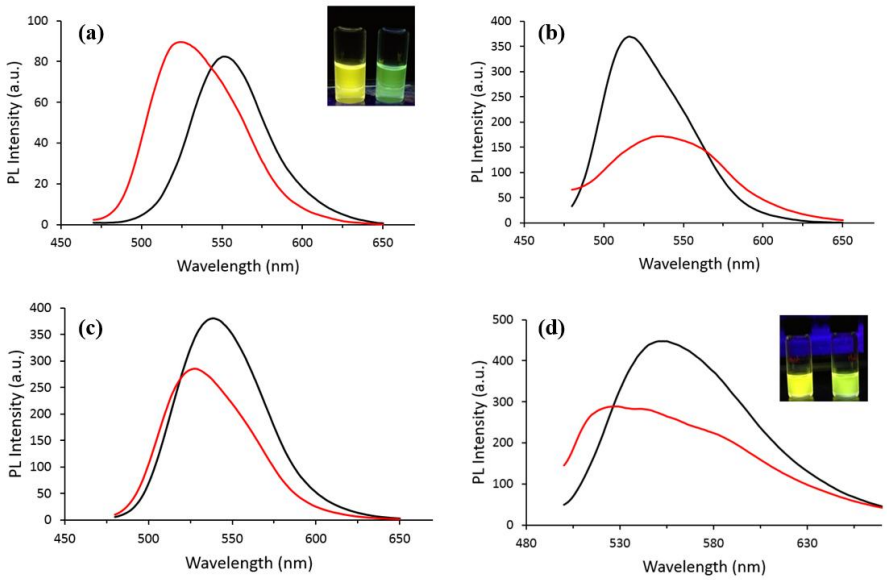

Figure 3-13. Phosphorescent emission spectra of **1** (a), **2** (b), **3** (c), and **4** (d) (10 μM each) in the absence (black line) and presence (red line) of hydrogen peroxide (5 mM) in H_2O/DMSO (1:1 v/v, pH 7.4, 10 mM HEPES) (λ_{ex}= 400 nm).

Figure 3-13 shows the phosphorescence emission of four iridium(III) complexes. Probe **1**, introduced boronate meta to coordinated Ir(III), showed the yellow emission at 551 nm, ~ 30 nm red-shifted region compared to original $(ppy)_2Ir(acac)$. This red-shifted emission is caused by the electron-withdrawing boronate, which makes the HOMO energy level unstable. After the reaction with H_2O_2, the green phosphorescence at 523 nm was recovered due to the conversion of boronate to phenol. Probe **3** also shows similar blue-shifted ratiometric change in the presence of H_2O_2, but less effective than **1**. The 12-nm blue-shifted emission was observed, about a half value of **1** (28-nm blue shift).

Interestingly, probe **2** shows the opposite appearance to **1** and **3**. The boronate group para to iridium(II) has little effect to HOMO and LUMO energy levels of Ir(II) complex, which has a green phosphorescence originally. However, the conversion to electron-donating phenol group causes the

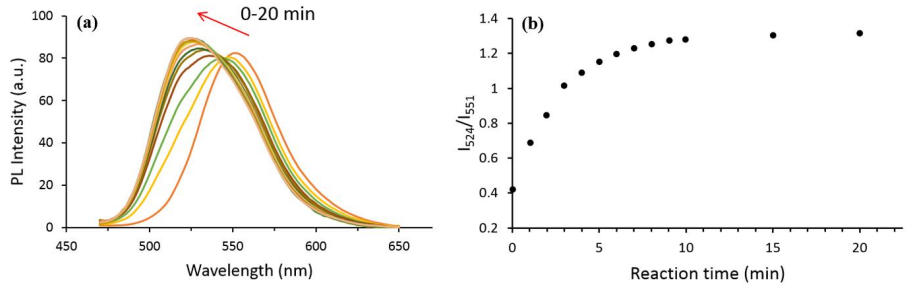

Figure 3-14. Time-course kinetic measurement of the phosphorescence response of **1** (10 μM) to H_2O_2 (5 mM).

dynamic emission change to yellow. The electron-withdrawing groups *meta* to the site of coordination make the HOMO and LUMO level stable, whereas the donating groups *ortho* or *para* to the site induces the HOMO level unstable. On the other hands, the electron-withdrawing groups *ortho* or *para* to the site or the electron- donating groups *meta* to the site has little effect to HOMO and LUMO levels. For this reason, probe **1** and **3** were affected by electron-withdrawing boronate groups, while probe **2** was strongly influenced by electron-donating hydroxyl groups.

Contrary to probe **1-3**, probe **4** has boronate groups in pyridine ring of main ligand. According to the literature, in $(ppy)_2Ir(acac)$ complex, the pyridyl ring π-orbitals contribute 60-70 % to the LUMOs and the rest is depends on the benzene rings and other components of Ir(III) complexes. The introduction of boronate to pyridyl ring induces the stabilization of LUMO level, which results in the red-shifted emission. As a result, probe **4** also shows the yellow emission at 553nm and shifts to green upon the addition of H_2O_2.

Next, we performed the detailed study with probe **1** which showed best properties in PL experiment. The phosphorescence of **1** (10 μM) saturated within 10 minute in the presence of 5 mM H_2O_2. Figure 2b describes the change of I_{524}/I_{551} value, which shows the typical shape of pseudo-first

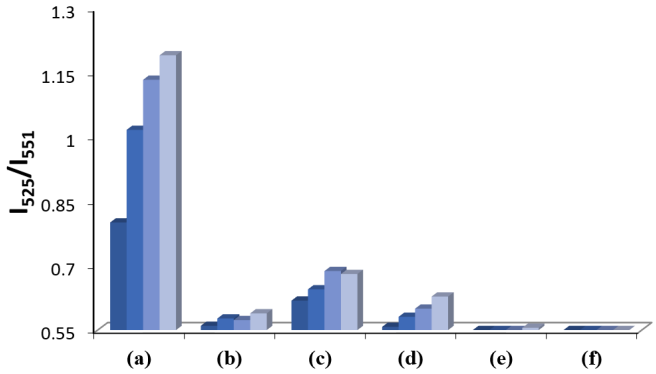

Figure 3-15. Phosphorescence responses of **1** (10μM) to various reactive oxygen species (5 mM). Bars represent intensity ratio at 1, 5, 10 and 20 min after addition of each ROS: (a) H_2O_2; (b) ClO^-; (c) $NO^{\bullet}$; (d) TBHP; (e) $^{\bullet}OH$; (f) $O_2^{\bullet-}$.

reaction curve. Figure 3 compares the relative reactivity of probe **1** toward other ROS. Probe 1 exhibits the extraordinary selectivity for H_2O_2, >5-fold more selective than nitric oxide (NO), >7-fold than *tert*-butyl hydroperoxide (TBHP), and >15-fold than hypochlorite (^-OCl). Especially, the phosphorescence emission is fully quenched upon the addition of superoxide due to the quenching effect of produced oxygen.

To investigate the change of energy levels and electronic distributions, we performed DFT calculation of probe **1** and **4**. As expected, probe **1** shows the stabilization of HOMO level in the presence of H_2O_2, while probe 4 shows different tendency. In the case of probe **4**, the initial LUMO level is lower than that of **1**, but has similar HOMO level. After the reaction with H_2O_2, the LUMO level is elevated the similar level with **1** and **1**-H_2O_2, which causes the broader HOMO-LUMO energy gap.

Although two probes have in common with increasing energy gaps and blue-shifted emission change upon the addition of H_2O_2, the different LUMO level might induce the different ECL efficiencies. Probe **1** has much higher LUMO level than the HOMO level of TPA radical and maintains the LUMO

level still unchanged after the reaction with H_2O_2. This destabilized LUMO level disturbs the formation of excite states in ECL process. Compared to **1** and **1**-H_2O_2, the LUMO level of **4** is stabilized, similar to the HOMO of TPA radical. The relatively stabilized LUMO level offers more chances to form excited species by electron transfer process, although still high-lying LUMO level ,compared to ideal ECL process, lowers the ECL efficiency. However,

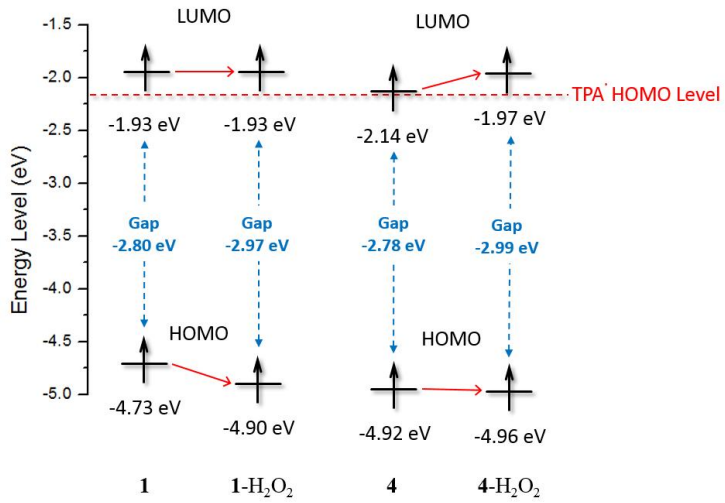

Scheme 3-5. The calculated HOMO and LUMO energy level of **1** and **4** in the absence and presence of H_2O_2.

the addition of H_2O_2 to probe **4** destabilize the LUMO level similar levels to **1** and **1**-H_2O_2, which causes the degradation of ECL efficiency. Consequently, probe **4** showed the notable ECL quenching ability in the presence of H_2O_2 compared to **1**.

Lastly, we investigated the reasons for decreased of ECL signal of **1**, although the LUMO level did not change and PL intensity was rather 1.27-fold increased. One possibility is the influence of reaming H_2O_2, wich disturbs the ECL emitting through the oxidation and generation of O_2 bubble at the

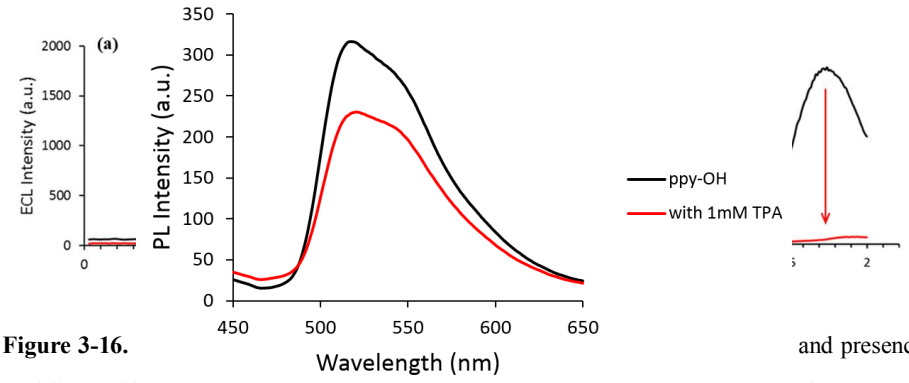

Figure 3-16. and presence (red line) of

Figure 3-18. Phosphorescent emission spectra of $(ppy\text{-}OH)_2Ir(acac)$ (10 μM each) in the absence (black line) and presence (red line) of hydrogen peroxide (5 mM) in H_2O/DMSO (1:1 v/v, pH 7.4, 10 mM HEPES) (λ_{ex}= 400 nm).

surface of Pt working electrode. Although we treated the sodium thiosulfate to remove excess amounts of H_2O_2, ECL emission still might be lowerd by remaining H_2O_2. To confirm this assumption we synthesized the (ppy-OH)$_2$Ir(acac), as the product of **1** with H_2O_2. As shown Figure 3-17, the ECL of **1**-H_2O_2 is the only ~70% levels of (ppy-OH)$_2$Ir(acac) at the same condition.

Furthermore, the general experimental condition in oxidative reduction ECL is quite basic due to the coreactant TPA. Becuase (ppy-OH)$_2$Ir(acac) exists the phenolate form in basic condition, this anionic species might lowered the PL efficiency. We tested the PL property of (ppy-OH)$_2$Ir(acac) at neutral condition and baic condition with 1mM TPA repectively. The phosphorescence was slightly decreased in basic pH, which showed about 75% levels of that in neutral condition. Consequently, we conclude the decrease of ECL signal for **1**-H_2O_2 is a combination of these factors.

1.3. Conclusion

We introduced the electron-withdrawing boronate groups to Ir(III) complexes as a reaction site for H_2O_2. The change of HOMO and LUMO levels depends on the location of substitution and their electronic properties. Probe **1** and **3** showed the yellow phophorescence emission due to the destabilization of HOMO level, whereas probe **2** bearing boronate group *para* to Ir(III) metal had an MLCT state with a similar energy level to that in (ppy)$_2$Ir(acac) and showed green phosphorescence. The boronate group converted to the electron-donating hydoxyl group after the reaction with H_2O_2, which worked against boronate group. In other words, the phosphorescence of probe **2** bearing hydroxyl group *para* to Ir(III) metal shifted green to yellow, due to the destabilization of HOMO level. On the other hands, the

disappearnce of electron-withdrawing group in *meta*-position in Probe **1** and **3** restored green phosphorescence. Especially, the addition of H_2O_2 to probe **4** posseing boronate in pyridyl rings induced the dynamic change of LUMO energy level, which induces the ratiometric emission change from yellow to green. Furthermore, the destabilization of LUMO level of probe **4** caused the degradation of ECL efficiency by blocking the ECL electron transfer process. The ECL intensity of **4** drastically decreased upon the addition of H_2O_2, compared to other probes which showed similar properties with PL study. This work provides the rational design of ECL probe based on ECL quenching route *via* the control of LUMO level, which is differentiated strategy to develop general PL-based probes.

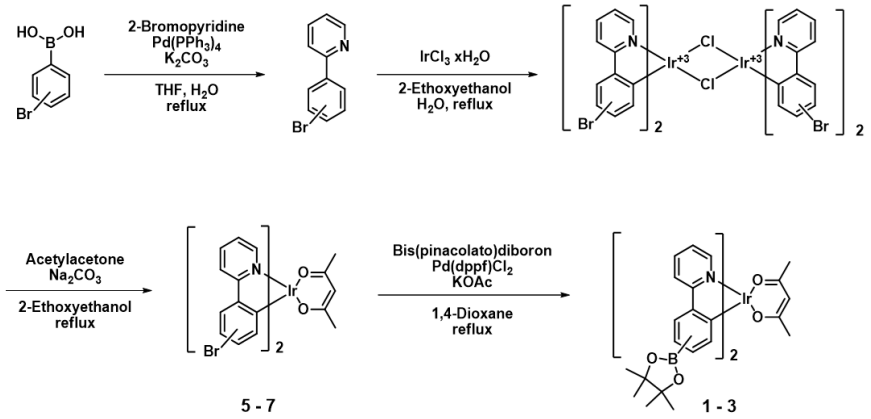

Scheme 3-6. Synthetic scheme of Ir(III) complexes **1-3**.

1.4. Experimental Section

Preparation of bromophenylpyridines

A mixture of bromophenylboronic acid (662 mg, 3.3 mmol), $Pd(PPh_3)_4$ (173 mg, 0.15 mmol), potassium carbonate (829 mg, 6 mmol) and 2-bromopyridine (0.286 mL, 3 mmol) in THF (20 mL) and H_2O (20 mL) was refluxed for 12 h. After cooling to room temperature, the reaction mixture was extracted with dichloromethane (DCM), and the organic phase was washed with water, and dried over Na_2SO_4. The solvent was evaporated to give a white solid product with 73-88% yields, which was purified by silica gel column chromatography (DCM / MeOH).

Preparation of chloro-bridged iridium dimers

A mixture of ppy derivatives (2 mmol) and Iridium chloride hydrate (269 mg, 0.9 mmol) in 2-ethoxyethanol (15 mL) and H_2O (5 mL) was refluxed for 12h. After cooling to room temperature, pouring cold water (~50 mL) to reaction mixture. Then a red-orange precipitate was filtered to crude cyclometalated Ir(III) chloro-bridged dimer.

Preperation of Ir(III) complexes 5-7

A mixture of crude cyclometalated Ir(III) dimer (1 mmol), sodium carbonate (531 mg, 5 mmol) and acetylacetone (0.514 mL, 5 mmol) in 2-ethoxyethanol (10 mL) was refluxed 1h. After cooling to room temperature, the reaction mixture was extracted with dichloromethane (DCM), and the organic phase was washed with water, and dried over Na_2SO_4. The solvent was evaporated to give a red-orange solid product with 44-60% yield, which was purified by silica gel column chromatography (EA/Hex: 1/1).

5: 300 MHz ^{1}H NMR (DMSO-d_6): δ 8.41 (d, 2H, *J* = 4.23 Hz); 8.24 (d, 2H *J* = 8.97 Hz); 8.04 (t, 2H, *J* = 7.87 Hz, 7.76 Hz); 7.73 (d, 2H, *J* = 8.22 Hz); 7.52 (t, 2H, *J* = 7.27 Hz, 7.14Hz); 7.04 (d, 2H, *J* = 8.20 Hz); 6.07 (s, 2H); 5.29 (s, 1H); 1.75 (s, 6H).

6: 300 MHz ^{1}H NMR (DMSO-d_6): δ 8.41 (d, 2H, *J* = 5.50 Hz); 8.28 (d, 2H *J* = 7.99 Hz); 8.00 (t, 2H, *J* = 7.60 Hz, 7.97 Hz); 7.92 (s, 2H); 7.47 (t, 2H, *J* = 6.54 Hz, 6.44 Hz); 6.80 (d, 2H, *J* = 8.09 Hz); 5.98 (d, 2H, *J* = 8.15 Hz); 5.28 (s, 1H); 1.73 (s, 6H).

Preperation of Ir(III) complexes 1-3

A mixture of Ir(III) complexes **1-3** (151 mg, 0.2 mmol), bis(pinacolato)diboron (152 mg, 0.6 mmol), [1,1′-Bis(diphenylphosphino)ferrocene]dichloropalladium(II) (16 mg, 0.02 mmol), and potassium acetate (118 mg, 1.2 mmol) in 1,4-dioxane (10 mL) was refluxed 3h. After cooling to room temperature, the solvent was removed under reduced pressure and filtered through celite with DCM, the organic phase was washed with water, and dried over Na_2SO_4. The residue was purified by silica gel column chromatography (DCM) to give a yellow or yellow-orange solid product with 18-34% yield, which was purified by silica gel column chromatography (EA/Hex: 1/1).

1: 300 MHz ^{1}H NMR (DMSO-d_6): δ 8.44 (d, 2H, *J* = 5.19 Hz); 8.22 (d, 2H *J* = 8.11 Hz); 8.00 (t, 2H, *J* = 7.28 Hz, 7.76 Hz); 7.72 (d, 2H, *J* = 7.71 Hz); 7.44 (t, 2H, *J* = 6.16 Hz, 6.25 Hz); 7.11 (d, 2H, *J* = 7.69 Hz); 6.53 (s, 2H); 5.23 (s, 1H); 1.70 (s, 6H), 1.15 (s, 24H).

2: 300 MHz ^{1}H NMR (Chloroform-d): δ 8.50 (d, 2H, *J* = 5.60 Hz); 8.04 (d, 2H); 8.00 (s, 2H); 7.78 (t, 2H, *J* = 7.58 Hz, 7.82 Hz); 7.18 (t, 2H, *J* = 6.22 Hz, 6.93 Hz); 7.10 (d, 2H, *J* = 7.58 Hz); 6.32 (d, 2H, *J* = 7.52 Hz); 5.21 (s, 2H); 1.78 (s, 6H), 1.28 (s, 24H).

3: 300 MHz ^{1}H NMR (DMSO-d_6): δ 8.45 (d, 2H, *J* = 6.10 Hz); 8.13 (d, 2H *J* = 8.23 Hz); 7.96 (t, 2H, *J* = 6.83 Hz, 7.10 Hz); 7.70 (d, 2H, *J* = 7.85 Hz); 7.41 (t, 2H, *J* = 6.36 Hz, 5.95 Hz); 6.57 (t, 2H, *J* = 7.61 Hz, 7.30 Hz); 5.27 (s, 2H); 1.73 (s, 6H), 1.39 (s, 24H).

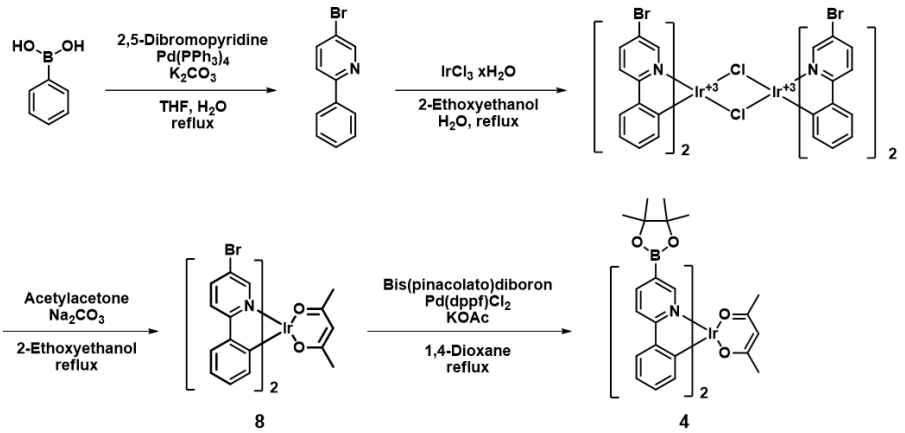

Scheme 3-7. Synthetic scheme of Ir(III) complex **4.**

Preparation of 5-bromo-2-phenylpyridine

A mixture of phenylboronic acid (402 mg, 3.3 mmol), $Pd(PPh_3)_4$ (173 mg, 0.15 mmol), potassium carbonate (829 mg, 6 mmol) and 2,5-dibromopyridine (711 mg, 3 mmol) in THF (20 mL) and H_2O (20 mL) was refluxed for 12 h. After cooling to room temperature, the reaction mixture was extracted with

dichloromethane (DCM), and the organic phase was washed with water, and dried over Na_2SO_4. The solvent was evaporated to give a white solid product (476 mg, 68.4 % yield), which was purified by silica gel column chromatography (DCM / MeOH).

8: 300 MHz ^{1}H NMR (DMSO-d_6): δ 8.40 (d, 2H, *J* = 5.50 Hz); 8.22 (d, 2H *J* = 2.09 Hz); 8.19 (s, 2H); 7.58 (d, 2H, *J* = 7.80 Hz); 6.84 (t, 2H, *J* = 7.41 Hz, 8.56 Hz); 6.71 (t, 2H, *J* = 7.43 Hz, 7.33 Hz); 6.10 (d, 2H, *J* = 7.53 Hz); 5.35 (s, 1H); 1.78 (s, 6H).

4: 300 MHz ^{1}H NMR (Chloroform-d): δ 8.84 (s, 2H); 8.04 (d, 2H *J* = 8.02 Hz); 7.84 (d, 2H *J* = 7.72 Hz); 7.57 (d, 2H, *J* = 9.86 Hz); 6.80 (t, 2H, *J* = 7.48 Hz, 7.85 Hz); 6.69 (t, 2H, *J* = 7.13 Hz, 7.54 Hz); 6.28 (d, 2H, *J* = 7.24 Hz); 5.22 (s, 1H); 1.82 (s, 6H), 1.23 (s, 24H).

9: 300 MHz ^{1}H NMR (DMSO-d_6): δ 9.23 (s, 2H); 8.29 (d, 2H *J* = 5.71 Hz); 7.92 (d, 2H, *J* = 7.96 Hz); 7.85 (t, 2H, *J* = 7.27 Hz, *J* = 7.27 Hz); 7.51 (d, 2H, *J* = 8.35 Hz); 7.24 (t, 2H, *J* = 7.07 Hz, 5.91 Hz); 6.23 (d, 2H, *J* = 8.35 Hz); 5.49 (s, 2H, *J* = 7.53 Hz); 5.22 (s, 1H); 1.70 (s, 6H).

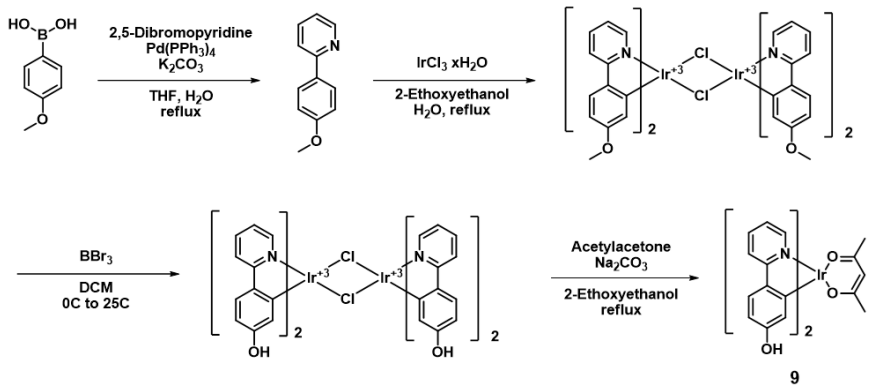

Scheme 3-8. Synthetic scheme of Ir(III) complex **9.**

References and Notes

1. Part I

1. (a) Beer, P. D.; Gale, P. A. *Angew. Chem. Int. Ed. Engl.* **2001**, *40*, 486; (b) Schmi-dtchen, F. P.; Berger, M. *Chem. Rev.* **1997**, *97*, 1609-1646; (c) *Comprehensive Supramolecular Chemistry;* Atwood, J. L.; Davies, J. E. D.; Macnicol, D. D.; Vogtle, F.; Lehn J.-M.; Gokel, G. W., eds.; Elsevier Science: Oxford, 1996, vol. 1; (e) Martinez-Manez, R.; Sancenon, F. *Chem. Rev.* **2003**, *103*, 4419.

2. Lakowicz, J. R., Ed. *Principles of Fluorescence Spectroscopy;* Plenum Publishers Corporation: New York, 1999.

3. Anslyn, E. V. *Curr. Opin. Chem. Biol.* **1999,** *3,* 740.

4. (a) Fabbrizzi, L.; Licchelli, M.; Pallavicini, P.; Parodi, L.; Tagletti, A. *Transition Metals in Suprmolecular Chemistry,* John Wiley & Sons Ltd.: New York, 1999; p 93; (b) de Silva, P.; Gunaratne, H. Q. N.; Gunnlaugsson, T.; Huxley, A. J. M.; McCoy, C. P.; Rademacher, J. T.; Rice, T. E. *Chem Rev.*, **1997**, *97,* 1515.

5. Beer, P. D. *Acc. Chem. Res.* **1998**, *31*, 71.

6. Yuan, L.; Lin, W.; Zheng, K.; Zhu, S. *ACC. Chem. Res.* **2013**, *46*, 1462.

7. Shionoya, M.; Furuta, H.; Lynch, V.; Harriman, A.; Sessler, J. L. *J. Am Chem. Soc.* **1992,** *114,* 5714.

8. (a) Arnaut, L. G.; Formosinho, S. J. *J. Photochem. Photobiol. A: Chem.* **1993,** *75,* 1; (b) Formosinho, S. J.; Arnaut, L. G. *J. Photochem. Photobiol. A: Chem.* **1993,** *75,* 21; (c) Tolbert, L. M.; Solntsev, K. M. *Acc. Chem. Res.* **2002,** *35,* 19; (d) Hynes, J. T.; Trna-Thi, T.-H.; Granucci, G. J. *photochem. Photobiol. A: Chem.* **2002,** *154,* 3; (e) Jarczewskia, A.; Hubbard, C. D. *J. mol. Struct.* **2003,** *649,* 287; (f) Tseng, H.-Y.; Shen, J.-Y.; Kuo, T.-Y.; Tu, T.-S.; Chen, Y.-A.; Demchenko, A. P.; Chou, P.-T. *Chem. Sci.* **2016,** 7, 655.

9. Wiskur, S. L.; Ait-Haddou, H.; Lavigne, J. J.; Anslyn, E. V. *Acc. Chem. Res.* **2001,** *34,* 963.

10. (a) Chae, M.-Y.; Czarnik, A. W. *J. Am. Chem. Soc.* **1992,** *114,* 9704; (b) Dujols, V.; Ford, F.; Czarnik, A. W. *J. Am. Chem. Soc.* **1997,** *119,* 7386.

11. Kim, S. K.; Lee, D. H.; Hong, J.-I.; Yoon, J. *Acc. Chem. Res.* **2009**, *42,* 23.

12. Mathews, C. P.; van Hold, K. E. *Biochemistry;* The Benjamin/Cummings Publishing Company, Inc.: Redwood City, CA, 1990.

13. (a) Nyrén, P. *Anal. Biochem.* **1987**, *167*, 235-238. (b) Ronaghi, M.; Karamohamed, S.; Pettersson, B.; Uhlen, M.; Nyren, P. *Anal. Biochem.* **1996**, *242*, 84-89. (c) Tabary, T.; Ju, L. *J. Immunol. Meth.* **1992**, *156*, 55-60. (d) Stryer, L. *Biochemistry*, 4th ed.; W. H. Freeman and Company: New York, 1998; pp 336, 340.

14. (a) Doherty, M.; Becher, C.; Regan, M.; Jones, A.; Ledingham, J. *Ann.*

Rheum. Dis. **1996**, *66,* 432; (b) Tmees, A. E.; Zhang, Y.; Russell R. G.; Brown, M. A. *Rheumatology,* **2002**, *41*, 725.

15. Vance, D. H.; Czarnik, A. W. *J. Am. Chem. Soc.* **1994**, *116*, 9397.

16. Lee, D. H.; Im, J. H.; Son, S. U.; Chung, Y. K.; Hong, J.-I. *J. Am. Chem. Soc.* **2003**, *125*, 7752.

17. Lee, D. H.; Kim, S. Y.; Hong, J.-I. *Angew. Chem. Int. Ed.* **2004**, *43*, 4777.

18. (a) McDonough, M. J.; Reynolds, A. J.; Lee, W. Y. G.; Jolliffe, K. A. *Chem. Commun.* **2006**, 2971; (b) Cho, H. K.; Lee, D. H.; Hong, J.-I. *Chem. Commun.* **2005**, 1690; (c) Lee, H. N>; Xu, Z.; Kim, S. K.; Swamy, K. M. K.; Kim, Y.; Kim, S.-J.; Yoon, J. *J. Am. Chem. Soc.* **2007**, *129*, 3828.

19. (a) Marrs, T. C. *Pharmacol. Ther.* **1993**, *58*, 51; (b) Sidell, F. R.; Borak, J. *Ann. Emerg. Med.*, **1992**, *21*, 865.

20. Sambrook, M. R.; Notman, S. *Chem. Soc. Rev.* **2013**, *42*, 9251.

21. Van Hooidonk, C.; Breebart-Hansen, J. C. A.E. *Recl. Trav. Chim. Pays-Bas,* **1970**, *90*, 958.

22. Desire, B.; Saint-Andre, S. *Fundam. Appl. Toxicol.* **1986**, *7*, 646.

23. Daly, S. M.; Grassi, M.; Shenoy, D. K.; Ugozzoli, F.; Dalcanale, E. *J. Mater. Chem.* **2007**, *17*, 1809.

24. Dale, T. J.; Rebek, Jr. J. *J. Am. Chem. Soc.* **2006**, *128*, 4500.

25. Dale, T. J.; Rebek, Jr. J. *Angew. Chem. Int. Ed.* **2009**, *48*, 7850.

26. Richer, M. M. *Chemical Reviews*, **2004**, *104*, 3003-3036.

27. Qi, H.; Peng, Y.; Gao, Q.; Zhang, C. *Sensors*, **2009**, *9*, 674.

28. *Electrogenerated Chemiluminescence*; Bard, A. J. Ed.; Dekker: New York, 2004.

29. Hercules, D. M. *Sciences*, **1964**, *145*, 808.

30. Visco, R. E.; Chandross, E. A. *J. Am. Chem. Soc.*, **1964**, *86*, 5350.

31. Santhanam, K. S. V.; Bard, A. J. *J. Am. Chem. Soc.*, **1965**, *87*, 139.

32. Tokel, N.; Bard, A. J. *J. Am. Chem. Soc.,* **1972**, *94*, 2862.

33. Faulkner, L. R.; Bard, A. J. *J. Am. Chem. Soc.,* **1968**, *90*, 6284.

34. Faulkner, L. R.; Bard, A. J. *Electrochemical Chemistry,* Dekker, New York, **1977**, p143.

35. Abruna, H. D.; Bard, A. J. *J. Am. Chem. Soc.,* **1982**, *104*, 2641.

36. Heinze, J. *Angew. Chem. Int. Ed. Engl.,* **1984**, *23*, 831.

37. Carrido, G. A. *J. Chem. Educ.,* **1988,** *65,* 1020.

38. Chang, M.-M.; Saji, T.; Bard, A. J. *J. Am. Chem. Soc.,* **1977**, *99,* 5399.

39. Rubinstein, I.; Bard, A. J. *J. Am. Chem. Soc.,* **1981**, *103,* 512.

40. Kerr, E.; Doeven, E. H.; Wilson, D. J. D.; Hogan, C. F.; Francis, P. S. *Analyst,* **2016**, *141,* 62.

41. Leland, J. K.; Powell, M. J. *J. Electrochem. Soc.,* **1990**, *137,* 3127.

42. Liu, X. Q.; Shi, L. H.; Shi, W. X.; Niu, H.; Li, J.; Xu, G. B. *Angew. Chem., Int. Ed.*, **2007**, *46*, 421.

43. Nagasubramian, G.; Gioda, A. S.; Bard, A. J. *J. Electrochem. Soc.,* **1981**, *128,* 2158.

44. Benzman, R.; Faulkner, L. R. *J. Am. Chem. Soc.,* **1972**, *94,* 6324.

45. Richards, T. C.; Bard, A. J. *Anal. Chem.,* **1995**, *67,* 3140.

46. Omer, K. M.; Ku, S.-Y.; Wong, W.-T.; Bard, A. J. *Angew. Chem. Int. Ed.* **2009**, *48,* 9300.

47. Lee, K.S.; Zu, Y.; Herrmann, A.; Geerts, Y.; Mullen, K.; Bard, A. J. *J. Am. Chem. Soc.,* **1999**, *121,* 3513.

48. Nepomnyashchii, A. B.; Bard, A. *J. Acc. Chem. Res.* **2012**, *45*, 1844.

49. Rubinstein, I.; Bard, A. J. *J. Am. Chem. Soc.,* **1981**, *103,* 512.

50. Miao, W. *Chem. Rev.*, **2008**, *108*, 2506.

51. Kim, J. I.; Shin, I.-S.; Kim. H.; Lee, J.-K. *J. Am. Chem. Soc.,* **2005**, *127,* 1614.

52. Barbanate, G.J.; Doeven, E. H.; Kerr, E.; Connell, T. U.; Donnelly, P. S.; White, J. M. Lopes, T. Laird, S. Wilson, D. J. D.; Barnard, P. J.; Hogan, C. F.; Francis, P. S. *Chem. Eur. J.* **2014**, *20*, 3322.

53. Bolletta, F.; Rossi, A.; Balzani, V. *Inorg. Chim. Acta*, **1981**, *53*, L23.

54. Ding, Z.; Quinn, B. M.; Haram, S. K.; Pell, L. E.; Korgel, B. A.; Bard, A. J. *Science*, **2002**, *296*, 1293.

55. Zheng, L. Y.; Chi, Y. W.; Dong, Y. Q.; Lin, J. P.; Wang, B. B.; *J. Am. Chem. Soc.* **2009**, *131*, 4564.

56. (a) Nyrén, P. *Anal. Biochem.* **1987**, *167*, 235-238. (b) Ronaghi, M.; Karamohamed, S.; Pettersson, B.; Uhlen, M.; Nyren, P. *Anal. Biochem.*

1996, *242*, 84-89. (c) Tabary, T.; Ju, L. *J. Immunol. Meth.* **1992**, *156*, 55-60. (d) Stryer, L. *Biochemistry*, 4th ed.; W. H. Freeman and Company: New York, 1998; pp 336, 340.

57. (a) McCarty, D. J. *Arthritis Rheum.* **1976**, *19*, 275-285. (b) Caswell, A.; Guilland-Cumming, D. F.; Hearn, P. R.; McGuire, M. K.; Russell, R. G. *Ann. Rheum. Dis.* **1983**, *42* (suppl 1), 27-37. (c) Doherty, M. *Ann. Rheum. Dis.* **1983**, *42* (suppl 1), 38-44.

58. (a) Knowles, J. R. *Annu. Re*V. *Biochem.* **1980**, *49*, 877–919.

59. (a) Takeda, E.; Yamamoto, H.; Nashiki, K.; Sato, T.; Arai, H.; Taketani, Y. *J. Cell. Mol. Med.,* **2004**, *8*, 191. (b) Beer, P. D.; Gale, P. A. *Angew. Chem. Int. Ed.* **2001**, *40*, 486; (c) Kornberg, A., *J. Biol. Chem.,* **1988**, *263*, 1–4. (b) Shen, X.; Mizuguchi, G.; Hamiche, A.; Wu, C., *Nature,* **2000**, *406*, 541–544.

60. Alberts, B.; Johnson, A.; Lewis, J.; Raff, M.; Roberts, K.; Walter. P., *Molecular Biology of the Cell; Garland Science: New York*, **2002**.

61. (a) Vance, D. H.; Czarnik, A. W. *J. Am. Chem. Soc.* **1994**, *116*, 9397-9398. (b) Czarnik, A. W. *Acc. Chem. Res.* **1994**, *27*, 302-308. (c) Mizukami, S.; Nagano, T.; Urano, Y.; Odani, A.; Kikuchi, K. *J. Am. Chem. Soc.* **2002**, *124*, 3920-3925. (d) Fabbrizzi, L.; Marcotte, N.; Stomeo, F.; Taglietti, A. *Angew. Chem. Int. Ed.* **2002**, *41*, 3811-3814. (e) Jang, Y. J.; Jun, E. J.; Lee, Y. J.; Kim, Y. S.; Kim, J. S.; Yoon, J. *J. Org. Chem.* **2005**, *70*, 9603-9606. (f) Lee, H. N.; Xu, Z.; Kim, S. K.; Swamy, K. M. K.; Kim, Y.; Kim, S.-J.; Yoon, J. *J. Am. Chem. Soc.* **2007**, *129*, 3828-3829. (g) Lee, H. N.; Swamy, K. M. K.; Kim, S. K.; Kwon, J.-Y.; Kim, Y.; Kim, S.-J.; Yoon, Y. J.; Yoon, J. *Org. Lett.* **2007**, *9*, 243-246. (h) Kim, M. J.; Swamy, M. K. K.; Lee, K. M.; Jagdale, A. R.; Kim, Y.; Kim, S.-J.; Yoo, K. H.; Yoon, J. *Chem.*

Commun. **2009**, 7215-7217.

62. (a) Cho, H. K.; Lee. D. H.; Hong, J.-I. *Chem. Commun.* **2005**, 1690-1692. (b) Lee, J. H.; Park, J.; Lah, M. S.; Chin, J.; Hong J.-I. *Org. Lett.* **2007**, *9*, 3729-3731. (c) Lee, D. H.; Kim, S. Y.; Hong, J-I *Tetrahedron Lett.* **2007**, *48*, 4477-4480. (d) Kim, S. Y.; Hong, J.-I. *Tetrahedron Lett.* **2009**, *50*, 1951–1953. (e) Kim, S. K.; Lee, D. H.; Hong, J.-I.; Yoon, J. Y. *Acc. Chem. Res.* **2009**, *42*, 23-31. (f) Park, C.; Hong, J-I. *Tetrahedron Lett*. **2010**, 51, 1960-1962. (g) Kim, S. Y.; Hong, J.-I. *Bull. Korean Chem. Soc.* **2010**, *31*, 716-719 (h) Kim, H. J.; Lee, J. H.; Hong, J.-I. *Tetrahedron Lett.* **2011**, *52*, 4944-4946. (i) Lee, D. N.; Jo, A.; Park, S. B.; Hong, J.-I. *Tetrahedron Lett.* **2012**, *53*, 5528-5530.

63. ATP sensors: (a) Xu, Z.; Singh, N. J.; Lim, J.; Pan, J., Kim, H. N.; Park, S.; Kim, K. S.; Yoon, J. *J. Am. Chem. Soc.* **2009**, *131*, 15528-15533. (b) Moro, A. J.; Cywinsky, P. J.; Korsten, S.; Mohr, G. J. *Chem. Commun.* **2010**, *46*, 1085-1087. (d) Ghosh, K.; Saha, I. *New. J. Chem.* **2011**, *35*, 1397-1402.

64. GTP sensors: (a) Kwon, J.Y.; Singh, N. J.; Kim, H. N.; Kim, S. K.; Kim, K. S.; Yoon, J.; *J. Am. Chem. Soc.* **2004**, *126*, 8892-8893. (b) Neelakanda, P. P.; Hariharan, M.; Ramaiah, D. *J. Am. Chem. Soc.* **2006**, *128*, 11334-11335.

65. (a) de Silva, A. P.; Gunaratne, H. Q. N.; Gunnlaugsson, T.; Huxley, A. J. M.; McCoy, C. P.; Rademacher, J. T.; Rice, T. E. *Chem. Rev.* **1997**, *97*, 1515. (b) Burdette, S. C.; Frederickson, C. J.; Bu, W.; Lippard, S. J. *J. Am. Chem. Soc.* **2003**, *125*, 1778. (c) Burdette, S. C.; Walkup, G. K.; Spingler, B.; Tsien, R. Y.; Lippard, S. J. *J. Am. Chem. Soc.* **2001**, *123*, 7831. (d) Hirano, T.; Kikuchi, K.; Urano, Y.; Nagano, T. *J. Am. Chem. Soc.* **2002**,

124, 6555. (e) Ojida, A.; Mito-oka, Y.; Sada, K.; Hamachi, I. *J. Am. Chem. Soc.* **2004**, *126*, 2454-2463.

66. Picraus, L. B.; Weldon, B. T.; McCusker, J. K. *Inorg. Chem.* **2003**, *42*, 273-282.

67. Lee, H. N.; Xu, Z.; Kim, S. K.; Swamy, K. M. K.; Kim, Y.; Kim, S.-J.; Yoon, J. *J. Am. Chem. Soc.* **2007**, *129*, 3828-3829.

68. Kim, K.; Tsay, O. G.; Atwood, D. A.; Churchill, D. G. *Chem. Rev.* **2011**, *111*, 5345-5403.

69. Marrs, T. C. *Pharmacol. Ther.* **1993**, *58*, 51-66.

70. Sidell, F. R.; Borak, *J. Ann. Emerg. Med.* **1992**, *21*, 865-871.

71. Tuovinen, K. *Toxicology*, **2004**, *196*, 31-39.

72. Cheng, T.-C.; Rastogi, V. K.; Defrank, J. J.; Sawiris, G. P. *Ann. N.Y. Acad. Sci.* **1998**, *864*, 253-258.

73. Tan, H. Y.; Loke, W. K.; Tan, Y. T.; Nguyen, N.-T. *Lab on a Chip* **2008**, *8*, 885-891.

74. Stein, K.; Schwedt, G. *Anal. Chim. Acta* **1993**, *272*, 73-81.

75. Ristori, C.; Carlo, C. D.; Martini, M.; Barbaro, A.; Ancarni, A. *Anal. Chim. Acta* **1996**, *325*, 151-160.

76. Terrier, F.; Rodriguez-Dafonte, P.; Le Guevel, E.; Moutiers, G. *Org. Biomol. Chem.* **2006**, *4*, 4352-4363.

77. Steiner, W. E.; Klopsch, S. J.; English, W. A.; Clowers, B. H.; Hill, H. *Anal. Chem.* **2005**, *77*, 4792 – 4799.

78. Sohn, H.; Letant, S.; Sailor, M. J.; Trogler, W. C. *J. Am. Chem. Soc.* **2000**,

122, 5399 –5440.

79. Van Houten, K. A.; Heath, D. C.; Pilato, R. S. *J. Am. Chem. Soc.* **1998**, *120*, 12359-12360.

80. Zhan, S.-W.; Swager, T. *J. Am. Chem. Soc.* **2003**, *125*, 3420-3421.

81. Dale, T. J.; Rebek, Jr. J. *J. Am. Chem. Soc.* **2006**, I, 4500-4501.

82. Burnworth, M.; Rowan, S. J.; Weder, C. *Chem. Eur. J.* **2007**, *13*, 7828.

83. Dale, T. J.; Rebek, Jr. J. *Angew. Chem. Int. Ed.* **2009**, *48*, 7850-7852.

84. Costero, A. M.; Parra, M. Gil, S.; Gotor, R.; Mancini, P. M. E.; Martinez-Manez, R.; Sancenon, F.; Royo, S. *Chem. Asian. J.* **2010**, *5*, 1573-1585.

85. Han, S.; Xue, Z.; Wang, Z.; Wen, T. B. *Chem. Commun.* **2010**, *46*, 8413-8415.

86. Wu, Z.; Wu, X.; Han, S. *Chem. Commun.* **2011**, *47*, 11468-11470.

87. Xuan, W.; Cao, Y.; Zhou, J.; Wang W. *Chem. Commun.* **2013**, *49*, 10474-10476.

88. Costero, A. M.; Gil, S.; Parra, M.; Mancini, P. M. E.; Martinez-Manez, R.; Sancenon, F.; Royo, S. *Chem. Commun.* **2013**, *49*, 10474-10476.

89. Wu, W.-H.; Dong, J.-J.; Wang, X.; Li, J.; Sui, S.-H.; Chen, G.-Y.; Liu, J.-W.; Zhang, M. *Analyst* **2012**, *137*, 3224-3226.

90. Maloy, J. T.; Bard, A. J. *J. Am. Chem. Soc.* **1971**, *93*, 5968-5981.

91. Lotnik, S. V.; Kazakov, V. P. Deposited Doc. 1982 No. VINITI 5069-82 USSR; *Chem. Abstr.* **1983**, *99*, 221604w.

92. Lai, R. Y.; Bard, A. J. *J. Phys. Chem. A* **2003**, *107*, 3335-3340.

93. Kim, J. I.; Shin, I.S.; Kim, H.; Lee, J.-K. *J. Am. Chem. Soc.* **2005**, *127*, 1614-1615.

3.2. Part II

94. Gross, E. M.; Anderson, J. D.; Slaterbeck, A. F.; Thayumanavan, S.; Barlow, S.; Zhang, Y.; Marder, S. R.; Hall, H. K.; Nabor, M. F.; Wang, J.-F.; Mash, E. A.; Armstrong, N. R.; Wightman, R. M. J. Am. Chem. Soc. 2000, 122, 4972-4979.

95. Gross, E. M.; Armstrong, N. R.; Wightman, R. M. J. Electrochem. Soc. 2002, 149, E137-E142.

96. Bruce, D.; Richter, M. M. Anal. Chem. 2002, 74, 1340-1342.

97. Kim, J. I.; Shin, I.S.; Kim, H.; Lee, J.-K. J. Am. Chem. Soc. 2005, 127, 1614-1615.

98. Muegge, B. D.; Richter, M. M. Anal. Chem. 2004, 76, 73-77.

99. Lai, R. Y.; Bard, A. J. J. Phys. Chem. A 2003, 107, 3335-3340.

100. Kerr, E.; Doeven, E. H.; Wilson, D. J. D.; Hogan, C. F.; Francis, P. S. Analyst, 2016, 141, 62-69.

101. Lin, H.; Cinar, M. E.; Schmittel, M. Dalton Trans., 2010, 39, 5130-5138.

102. Schmittel, M.; Qinghai, S. Chem. Commun. 2012, 48, 2707-2709.

103. Shu, Q.; Brilenbach, L.; Schmittel, M. Inorg. Chem. 2012, 51, 13123-13127.

104. Chen, K.; Schmittel, M. Analyst 2013, 138, 6742-6745.

105. Chen, K.; Schmittel, M. Chem. Commun. 2014, 50, 5756-5759.

106. Wood, Z. A.; Schröder, E.; Harris, J. R.; Poole, L. B. Trends Biochem. Sci. 2003, 28, 32–40; (b) Carmel, R.; Jacobsen, D. W. Homocysteine in

Health and Disease, Cambridge University Press, Cambridge, U.K., 2001.

107. (a) Malinow, M. R. Clin. Chem. 1995, 41, 173–176; (b) Guba, S. C.; Fink, L. M.; Fonseca, V. Am. J. Clin. Pathol. 1996, 106, 709–722; (c) Medina, M. A.; Amores-Sanchez, M. I. Eur. J. Clin. Invest. 2000, 30, 754–762; (d) Medina, M. A.; Urdiales, J. L.; Amores-Sanchez, M. I. Eur. J. Biochem. 2001, 268, 3871–4111; (e) Wu, L. L.; Wu, J. T. Clin. Chim. Acta 2002, 322, 21–28; (f) Lievers, K. J. A.; Afman, L. A.; Kluijtmans, L. A. J.; Boers, G. H. J.; Verhoef, P.; den Heijer, M.; Trijbels, F. J. M.; Blom, H. J. Clin. Chem. 2002, 48, 1383–1389.

108. (a) Jakubowski, H.; Ambrosius, W. T.; Pratt, J. H. FEBS Lett. 2001, 491, 35–39; (b) Yang, X.; Gao, Y.; Zhou, J. Clin. Chim. Acta 2006, 364, 230–234; (c) Nygård, O.; Nordrehaug, J. E.; Refsum, H.; Ueland, P. M.; Farstad, M.; Vollset, S. E. N. Engl. J. Med. 1997, 337. 230–237.

109. Seshadri, S.; Beiser, A.; Selhub, J.; Jacques, P. F.; Rosenberg, I. H.; D'Agostino, R. B.; Wilson, P. W. F. New Engl. J. Med. 2002, 346, 476–483.

110. van Meurs, J. B. J.; Dhonukshe-Rutten, R. A. M.; Pluijm, S. M. F.; van der Klift, M.; de Jonge, R.; Lindemans, J.; de Groot, L. G. M.; Hofman, A.; Witteman, J. C. C. P. M.; van Leeuwen, J. P. T. M.; Breteler, M. M. B.; Lips, P.; Pols, H. A. P.; Uitterlinden, A. G. New Engl. J. Med. 2004, 20, 2033–2041.

111. Pfeiffer, C. M.; Osterloh, J. D.; Kennedy-Stephenson, J.; Picciano, M. F.; Yetley, E. A.; Rader, J. I.; Johnson, C. L. Clin. Chem. 2008, 54, 801–813.

112. (a) Uji, Y.; Motomiya, Y.; Hanyu, N.; Ukaji, F.; Okabe, H. Clin. Chem. 2002, 48, 941–944; (b) Mukai, Y.; Togawa, T.; Suzuki, T.; Ohata, K.; Tanabe, S. J. Chromatogr. B 2002, 767, 263–268; (c) Garcia, A. J.; Apitz-

Castro, R.; J. Chromatogr. B 2002, 779, 359–363.

113. Rusin, O.; Luce, N. N. S.; Agbaria, R. A.; Escobedo, J. O.; Jiang, S. I.; Warner, I. M.; Dawan, F. B.; Lian, K.; Strongin, R. M. J. Am. Chem. Soc. 2004, 126, 438–439; (b) Wang, W.; Rusin, O.; Xu, X.; Kim, K. K.; Escobedo, J. O.; Fakayode, S. O.; Fletcher, K. A.; Lowry, M.; Schowalter, C. M.; Lawrence, C. M.; Fronczek, F. R.; Warner, I. M.; Strongin, R. M. J. Am. Chem. Soc. 2005, 127, 15949–15958; (c) Zhang, X.; Li, C.; Cheng, X.; Wang, X.; Zhang, B. Sens. Act. B 2008, 129, 152–157.

114. (a) Ferguson, E.; Parthasarathy, S.; Joseph, J.; Kalyanaraman, B. J. Lipid Res. 1998, 39, 925–933; (b) Undas, A.; Perla, J.; Lacinski, M.; Trzeciak, W.; Kazmierski, R.; Jakubowski, H. Stroke 2004, 35, 1299–1304.

115. (a) Lee, K.-S.; Kim, T.-K.; Lee, J. H.; Kim, H.-J.; Hong, J.-I. Chem. Commun. 2008, 6173–6175; (b) Chen, H.; Zhao, Q.; Wu, Y.; Li, F.; Yang, H.; Yi, T.; Huang, C. Inorg. Chem. 2007, 46, 11075–1108; (c) Zhang, M.; Yu, M.; Li, F.; Zhu, M.; Li, M.; Gao, Y.; Li, L.; Liu, Z.; Zhang, J.; Zhang, D.; Yi, T.; Huang, C. J. Am. Chem. Soc. 2007, 129, 10322–10323.

116. Bard, A. J. in Electrogenerated chemiluminescence, Marcel Dekker, Inc., New York, 2005; (b) Richter, M. M. Chem. Rev. 2004, 104, 3003–3036; (c) Miao, W. Chem. Rev. 2008, 108, 2506–2553.

117. Shin, I.-S.; Bae, S. W.; Hong, J.-I. Anal. Chem. 2010, 82, 8259-8265; (c) Kim, J. I.; Shin, I.-S.; Kim, H.; Lee, J.-K. J. Am. Chem. Soc. 2005, 127, 1614-1615; (d) Tsuzuki, T.; Tokito, S. Adv. Mater. 2007, 19, 276-280; (e) Barbanate, G. J.; Doeven, E. H.; Kerr, E.; Connell, T. U.; Donnelly, P. S.; White, J. M. Lopes, T. Laird, S. Wilson, D. J. D.; Barnard, P. J.; Hogan, C. F.; Francis, P. S. Chem. Eur. J. 2014, 20, 3322-3332.

118. Chen. K.; Schmittel. M.; Analyst, 2013, 138, 6742-6745.

119. Shin, I.-S.; Kang, Y.-T.; Lee, J.-K.; Kim, T. H.; Kim J. S. Analyst. 2011, 136, 2151–2155

120. James, T. D.; Samankumara Sandanayake, K. R. A.; Shinkai, S. Angew. Chem. Int. Ed. 1994, 33, 2207-2209.

121. Lai, R. Y.; Bard, A. J. J. Phys. Chem. A 2003, 107, 3335-3340.

122. Yang, C. H.; Tai, C. C.; Sun, I. W. J. Mater. Chem. 2004, 14, 947-950.

123. (a) Lowry, M. S.; Bernhard, S. Chem. Eur. J. 2006, 12, 7970-7977.

124. (a) Yang, C.-H.; Su, W.-L.; Fang, K.-H.; Wang, S.-P.; Sun, I.-W. Organometallics 2006, 25, 4514-4519. (b) Woo, H.; Cho, S.; Han, Y.; Chae, W.-S.; Ahn, D.-R.; You, Y.; Nam, W. J. Am. Chem. Soc. 2013, 135, 4771-4787.

125. (a) Fang, K.-H.; Wu, L.-L.; Huang, Y.-T.; Yang, C.-H.; Sun, I.-W. Inorg. Chem. Acta. 2006, 359, 441-450. (b) Frey, J.; Curchod, B. F. E.; Scopelliti, R.; Tavernelli, I.; Rothlisberger, U.; Nazeeruddin, M. K.; Baranoff, E. Dalton. Trans. 2014, 43, 5667-5679.

126. Baskin, S. I.; Brewer, T. G. In Medical Aspects of Chemical and Biological Warfare; Sidell, F., Takafuji, E. T., Franz, D. R., Eds.; TMM Publications: Washington, DC, 1997; Chapter 10, pp 271-286.

127. Warburg, O. Hoppe-Seyler's Z. Physiol. Chem. 1911, 76, 331-346.

128. Kellin, D. Proc. R. Soc. London, Ser. B 1929, 104, 206-251.

129. Vennesland, B.; Comm, E. E.; Knownles, C. J.; Westly, J.; Wissing, F. Cyanide in Biology; Academic Press: London, 1981.

130. Guidelines for Drinking-Water Quality, Clin Pharm World Health

Organization: Geneva. 1996.

131. L. P. Solomonson, B. Vennesland, E. E. Conn, C. J. Knowles, J. Westley, F. Wissing in Cyanide in Biology, Academic Press, London, 1981.

132. Young, C.; Tidwell, L.; Anderson, C. Cyanide: Social, Industrial, and Economic Aspects; Minerals, Metals, and Materials Society: Warrendale, 2001.

133. Licht, S.; Myung, N.; Sun, Y. Anal. Chem. 1996, 68, 954-959.

134. Taheri, A.; Noroozifar, M.; Khorasani-Motlagh, M. J. Electroanal. Chem. 2009, 628, 48-54.

135. Tomasulo, M.; Raymjo, F. M. Org. Lett. 2005, 7, 4633-4636.

136. Yang, Y.-K.; Tae, J. Org. Lett., 2006, 8, 5721-5723.

137. Chung, Y.; Lee, H.; Ahn, K. H. J. Org. Chem. 2006, 71, 9470-9474.

138. Cho, D.-G.; Kim, J.-H.; Sessler, J. L. J. Am. Chem. Soc. 2008, 130, 12163-12167.

139. Lou, X.; Qiang, L.; Qin, J.; Li, Z. ACS Appl. Mater. Interfaces 2009, 1, 2529-2535.

140. Cheng, X.; Tang, R.; Jia, H.; Feng, J.; Qin, J.; Li, Z. ACS Appl. Mater. Interfaces 2012, 4, 4387-4392.

141. Yang, L.; Li, X.; Yang, J.; Qu, Y.; Hua, J. ACS Appl. Mater. Interfaces 2013, 5, 1317-1326.

142. Lin, W.-C.; Fang, S.-K.; Hu, J.-W.; Tsai, H.-S.; Chen, K.-Y. Anal. Chem. 2014, 86, 4648-4652.

143. Sessler, J. L.; Cho, D.-G. . Org. Lett. 2008, 10, 73-75.

144. Ekmekci, Z.; Yilmaz, M. D.; Akkaya, E. U.; Org. Lett. 2008, 10, 461-464.

145. Yang, Z.; Liu, Z.; Chen, Y.; Wang, X.; He, W.; Lu, Y. Org. Biomol. Chem. 2012, 10, 5073.

146. Lin, Q.; Liu, X.; Wei, T.-B.; Zhang, Y.-M. Chem. Asian, J. 2013, 8, 3015-3021.

147. Lee, K.-S.; Kim, H.-J., Kim, G.-H.; Shin, I.; Hong, J.-I. Org. Lett. 2008, 10, 49-51.

148. Chen, X.; Nam, S.-W.; Kim, G.-H.; Song, N.; Jeong, Y.; Shin, I.; Kim S. K.; Kim, J.; Park, S.; Yoon, J. Chem. Commun. 2010, 46, 8953-8955.

149. Lee, C.-H.; Yoon, H.-J.; Shim, J.-S.; Jang, W.-D. Chem. Eur. J. 2012, 18, 4513-1516.

150. Lee, J. H.; Jeong, A. R.; Shin, I.-S.; Kim, H.-J.; Hong, J.-I. Org. Lett. 2010, 12, 764-767.

151. Jung, H. S.; Han, J. H.; Kim, Z. H.; Kang, C.; Kim, J. S. Org. Lett. 2011, 13, 5056-5059.

152. Anzenbacher Jr. P.; Tyson, D. S.; Jursíková, K.; Castellano, F. N. J. Am. Chem. Soc. 2002, 124, 6232-6233.

153. Fillaut, J-L.; Akdas-Kilig, H.; Dean, E.; Latouche, C.; Boucekkine, A. Inorg, Chem. 2013, 52, 4890-4897.

154. Richter, M. M. Chem. Rev. 2004, 104, 3003-3036.

155. Zhan, W.; Bard, A. J. Anal. Chem. 2007, 79, 459-463.

156. Deiss, F.; Lafratta, C. N.; Symer, M.; Blicharz, T. M.; Sojic, N.; Walt, D.

R.; J. Am. Chem. Soc. 2009, 131, 6088-6089.

157. Muzyka, K. Biosens. Bioelectron. 2013, 54, 393-407.

158. Blackburn G. F.; Shah, H. P.; Kenten, J. H; Leland, J. Kamin, R. A.; Link, J.; Peterman, J.; Powell, M. J.; Shah, A.; Talley, D. B. Clin. Chem. 1991, 37, 1534-1539.

159. Bruno, J. G.; Kiel, J. L. Biosens. Bioelectron. 1999, 14, 457-464.

160. Chen, K.; Bats, J. W.; Schmittel, Inorg. Chem. 2013, 52, 12863-12865.

161. Singh, S.; Padovani, D.; Leslie, R. A.; Chiku, T.; Banerjee, R. J. Biol. Chem. 2009, 284, 22457-22466.

162. Chiku, T.; Padonvani, D.; Zhu, W.; Singh, S.; Vitvitsky, V.; Banerjee, R. J. Biol. Chem. 2009, 284, 11601-11612.

163. Shibuya, N.; Tanaka, M.; Yoshida, M.; Ogasawara, Y.; Togawa, T.; Ishii, K.; Kimura, H. Antioxid. Redox. Signal 2009, 11, 703-714.

164. Yang, G.; Wu, L.; Jiang, B.; Yang, W.; Qi, J.; Cao, K.; Meng, Q.; Mustafa, A. K.; Mu, W.; Zhang, S.; Snyder, S. H.; Wang, R. Science 2008, 322, 587-590. (b) Dombkowski, R. A.; Russell, M. J.; Olson, K. R. Am. J. Physiol. Regul. Integr. Comp. Physiol. 2004, 286, R678-R685.

165. (a) Kaneko, Y.; Kimura, Y.; Kimura, H.; Niki, I. Diabetes 2006, 55 1391-1397. (b) Zanardo, R. C. O.; Brancaleone, V.; Disrtutti, E.; Fiorucci, S.; Cirino, G.; Wallace, J. L. FASEB J. 2006, 20, 2118-2120.

166. (a) Eto, K.; Asda, T.; Arima, K.; Makifuchi, T.; Kimura, H. Biochem. Biophys. Res. Commun. 2002, 293, 1485-1488. (b) Kamoun, P.; Belardinelli, M.-C.; Chabli, A.; Lallouchi, K.; Chadefaux-Vekemans, B. Am. J. Med. Genet. A 2003, 116A, 310-311. (c) Yang, W.; Yang, G.; Jia,

X. Wu, L.; Wang, R. J. Physiol. 2005, 569, 519-531.

167. Hannestad, U.; Margheri, S.; Sorbo, B. Anal Biochem. 1989, 178, 394-398.

168. Nagata, T.; Kage, S.; Kimura, K.; Kudo, K.; Noda, M. J. Forensic. Sci. 1990, 35, 706-712.

169. (a) Lei, W.; Dasgupta, P. K. Anal. Chim. Acta 1989, 226, 165-170. (b) Hughes, M. M.; Centelles, M. N.; Moore, K. P. Free Radical Biol. Med. 2009, 47, 1346-1353. (c) Jimenez, D.; Martinez-Manez, R.; Sancenon, F.; Ros-Lis, J. V.; Benito, A.; Soto, J. J. Am. Chem. Soc. 2003, 125, 9000-9001.

170. (a) Lippert, A. R.; New, E. J.; Chang, C. J. J. Am. Chem. Soc. 2011, 133, 10078-10080. (b) Peng, H.; Cheng, Y.; Dai, C. King, A. L. Predmore, B. L.; Lefer, D. J.; Wang, B. Angew. Chem. Int. Ed. 2011, 50, 9672-9675. (c) Yu, F.; Li, P.; Song, P.; Wang, B.; Zhao, J.; Han, K. Chem. Comm. 2012, 48, 2852-2854. (d) Montoya, L. A.; Pluth, M. Chem. Comm. 2012, 48, 4767-4769. (e) Chen, S.; Chen, Z.-J.; Ren, W.; Ai, H.-W. J. Am. Chem. Soc. 2012, 134, 9589-9592.

171. (a) Qian, Y.; Karpus, J.; Kabil, O.; Zhang, S.-Y.; Zhu, H.-L.; Banerjee, R.; Zhao, J.; He, C. Nat. Commun. 2011, 2, 495. (b) Liu, C.; Pan, J.; Li, S.; Zhao, J.; Wu, L. Y.; Berkman, C. E.; Whorton, A. R.; Xian, M. Angew. Chem. Int. Ed. 2011, 50, 10327-10329. (c) Xian, M. Org. Lett. 2012, 14, 2184-2187. (d) Li, X.; Zhang, S.; Cao, J.; Xie, N.; Liu, T.; Yang, B.; He, Q.; Hu, Y. Chem. Comm. 2013, 49, 8656-8658.

172. (a) Cao, X.; Lin, W.; Zheng, K.; He, L. Chem. Comm. 2012, 48, 10529-10531. (b) Liu, T.; Xu, Z.; Spring, D. R. Cui, J. Org. Lett. 2013, 15, 2310-2313. (c) Liu, Y.; Feng, G. Org. Biomol. Chem. 2014, 12, 438-445.

173. (a) Zhan, W.; Bard, A. J. Anal. Chem. 2007, 79, 459-463. (b) Deiss, F.; Lafratta, C. N.; Symer, M.; Blicharz, T. M.; Sojic, N.; Walt, D. R. J. Am. Chem. Soc. 2009, 131, 6088-6089. (c) Muzyka, K. Biosens. Bioelectron. 2013, 54, 393-407.

174. (a) Swanick, K. N.; Ladouuceur, S.; Zysman-Colman, E.; Ding, Z. Chem. Commun. 2012, 48, 3179-3181. (b) Stringer, B. D.; Quan, L. M.; Barnard, P. J.; Wilson, D. J. D.; Hogan, C. F. Organometallics 2014, 33, 4860-4872. (c) Zhou, Y.; Li, W.; Yu, L.; Liu, Y.; Wang, X.; Zhou, M. Dalton Trans. 2015, 44, 1858-1865.

175. (a) Ji, S.; Guo, H.; Yuan, X.; Li, X.; Ding, D.; Gao, P.; Zhao, C. ;Wu, W.; Zhao, J. Org. Lett. 2010, 12, 2876-2879. (b) Guo, H.; Jing, Y.; Yuan, X.; Ji, S.; Zhao, J.; Li, X. Kan, Y. Org. Biomol. Chem. 2011, 9, 3844-3853. (c) Tang, Y.; Yang, H.-R.; Sun, H.-B.; Liu, S.-J.; Wang, J.-X.; Zhao, Q.; Liu, X.-M.; Xu, W.-J.; Li, S.-B.; Huang, W. Chem. Eur. J. 2013, 19, 1311-1319.

3.3. Part III

176. You, Y.; Nam, W. Chem. Soc. Rev. 2012, 41, 7061-7084.

177. You, Y.; Park. S. Y. J. Am. Chem. Soc. 2005, 127, 12438-12439.

178. Lowry, M. S.; Bernhard, S. Chem. Eur. J. 2006, 12, 7970-7977.

179. Ho, C.-L.; Wang, Q.; Lam, C.-S.; Wong, W.-Y.; Ma, D.; Wang, L.; Gao, Z.-Q.; Chen, C.-H.; Cheah, K.-W.; Lin, Z. Chem. Asian. J. 2009, 4, 89-103.

180. Tsuzuki, T.; Shirasawa, N.; Suzuki, T.; Tokito, S. Adv. Mater. 2003, 15, 1455-1458.

181. Lowry, M. S.; Goldsmith, J. I.; Slinker, J. D.; Rohl, R. Pascal, R. A.; Malliaras, Jr. G. G.; Bernhard, S. Chem. Mater. 2005, 17, 5712-5719.

182. (a) Dedeian, K.; Shi, J.; Shepherd, N.; Forsythe, E.; Morton, D. C. Inorg. Chem. 2005, 44, 4445. (b) Yang, C.-H.; Li, S.-W.; Chi, Y.; Cheng, Y.-M.; Yeh, Y.-S.; Chou, P.-T.; Lee, G.-H.; Wang, C.-H.; Su, C.-F. Inorg. Chem. 2005, 44, 7770. (c) P. J. Hay, J. Phys. Chem. A 2002, 106, 1634.

183. Zhou, G.; Ho, C.-L.; Wong, W.-Y.; Wang, Q.; Ma, D.; Wang, L.; Lin, Z.; Marder, T. B.; Beeby, A. Adv. Funct. Mater. 2008, 18, 499-511.

184. Yang, X.; Sun, N.; Dang, J.; Huang, Z.; Yao, C.; Xu, X.; Ho, C.-L.; Zhou, G.; Ma, D.; Zhao, X.; Wong W.-Y. J. Mater. Chem. C. 2013. 1. 3317-3326.

185. (a) Bard, A. J. Electrogenerated Chemiluminescence, Marcel Dekker, New York, 2004; (b) Richter, M. M. Chem. Rev. 2004, 104, 3003-3036.

186. Wei, H.; Wang, E. Luminescence, 2011, 26, 77-85.

187. Kim, J. I.; Shin, I.S.; Kim, H.; Lee, J.-K. J. Am. Chem. Soc. 2005, 127, 1614-1615.

188. Miao, W. Chem. Rev. 2008, 108, 2506.

189. Stringer, B. D.; Quan, L. M.; Bernard, P. J.; Wilson, D. J.; Hogan, C. F. Organometallics 2014, 33. 4860.

Swanick, K. N.; Ladoceur, S.; Zysman-Colman, E.; Ding, Z. Chem. Commun, 2012, 48, 3179.

190. Zhou, Y.; Li, W.; Yu, L.; Liu, Y.; Wang, X.; Zhou, M. Dalton Trans. 2015, 44, 1858.

191. Fernandez-Hernandez, J. M.; Longhi, E.; Cysewski, R.; Polo, F.; Josel, H.-P.; Cola, L. D. Anal. Chem. 2016, 88, 4174.

192. Kerr, E.; Doeven, E. H.; Wilson, D. J. D.; Hogan, C. F.; Francis, P. S. Analyst, 2016, 141, 62.

193. Tsuzuki, T.; Shirasawa, N.; Suzuki, T.; Tokito, S. Adv. Mater. 2003, 15, 1455-1458.

194. Madhu, S.; Basu, S. K.; Jadhav, S.; Ravikanth, M. Analyst 2013, 138, 299−306.

195. Goswami, S.; Manna, A.; Paul, S.; Das, A. K.; Aich, K.; Nandi, P. K. Chem. Commun. 2013, 49, 2912−2914.

196. Bejoymohandas, K. S.; Kumar, A.; Sreenadh, S.; Varathan, E.; Varughese, S.; Subramanian, V.; Reddy, M. L. P. Inorg. Chem. 2016, 55, 3448-3461.

197. Rhee, S. G. Science 2006, 312, 1882-1883.

198. Stone, J. R.; Yang, S. Antioxid. Redox. Signal. 2006, 8. 243-270.

199. Veal, E. A.; Day, A. M.; Morgan, B. A. Mol. Cell 2007, 26, 1-14.

200. Miller, E. W.; Tulyathan, O.; Isacoff, E. Y.; Chang, C. J. Nat. Chem. Biol. 2007, 3. 263-367.

201. Giorgio, M.; Trinei, M.; Migliaccio, E.; Pelicci, P. G. Nat. Rev. Mol. Cell. Biol. 2007, 8, 722-728.

202. Poole, L. B.; Nelson, K. J. Curr. Opin. Chem. Biol. 2008, 12, 18-24.

203. Finkel, T.; Serrano, M.; Blascao, M. A. Nature 2007, 448, 767-774.

204. Balaban, R. S.; Nemoto, S.; Finkel, T. Cell 2005, 120, 483-495.

205. Cutler, R. G. Rejuv. Res. 2005, 8, 138-140.

206. Finkel, T.; Holbrook, N. J. Nature 2000, 408, 239-247.

207. Pi, J. B.; Bai, Y. S.; Zhang, Q.; Wong, V.; Floering L. M.; Daniel, K.; Reece, J. M.; Deeney, J. T.; Andersen M. E.; Corkey, B. E. Colins, S. Diabetes 2007, 56, 1783-1791.

208. Barnham, K. J.; Masters, C. L.; Bush, A. I. Nat. Rev. Drg. Discov. 2004, 3, 205-214.

209. Lin, M. T.; Beal, M. F. Nat. Med. 2006, 12, 1241-1243.

210. Rao, A. V.; Balachandran, B.; Nutr. Neurosci. 2002, 5, 291-309.

211. Miller, E. W.; Albers, A. E.; Pralle, A.; Isacoff, E. Y. Chang, C. J. J. Am. Chem. Soc. 2005, 127, 16652-16659.

212. Dickinson, B. C.; Chang, C. J. J. Am. Chem. Soc. 2008, 130, 9638-9639.

213. Dickinson, B. C.; Huynh, C.; Chang, C. J. J. Am. Chem. Soc. 2010, 132, 5906-5915.

214. Dickinson, B. C.; Peltier, J.; Stone, D.; Schaffer, D. V.; Chang, C. J. Nat. Chem. Biol. 2007, 3, 263-267.

215. Dickinson, B. C.; Chang, C. J. Cell. Metab. 2011, 13, 361-366.

216. Dickinson, B. C.; Tang, Y.; Chang, Z. Y.; Chang, C. J. Chem. Biol. 2011, 174, 1-18.

217. Yang, X.; Sun, N.; Dang, J.; Huang, Z.; Yao, C.; Xu, X.; Ho, C.-L.; Zhou, G.; Ma, D.; Zhao, X.; Wong W.-Y. J. Mater. Chem. C. 2013. 1. 3317-3326.

국문 초록 (Abstract in Korean)

작은 생체분자들을 검출하기 위한 효율적인 화학 센서의 개발은 오랫동안 관련 연구자들에게 큰 관심을 끌어 온 주제이다. 그 중에서도, 전기화학발광을 기반으로 한 화학 센서들은 기존의 분석 방법들에 비해 높은 감도, 좋은 재현 가능성, 그리고 보다 간단한 분석 과정 등의 다양한 장점들을 가지고 있다.

Part I 에서는 인산기를 포함하고 있는 음이온들을 높은 선택성과 감도로 검출할 수 있는 형광 혹은 전기화학발광 화학 감지체의 개발에 대하여 기술하였다. 이러한 연구들을 통해, 우리는 형광 센서를 고안하는 것과 같은 방식을 ECL 분석에 적용할 수 있다는 사실을 확인하였다. 더불어, 이러한 연구들은 ECL 을 기반으로 한 검출 시스템의 높은 감도와 간편성을 보여주었다.

먼저, 피로인산(ppi)에 대한 높은 감도의 센싱을 위하여 쿠마린을 기반으로 한 형광 감지체인 1-2Zn 를 개발하였다. 1-2Zn 는 쿠마린의 도입을 통하여 기존의 나프탈렌 기반의 PPi 센서에 비해 향상된 검출 한계를 보여줌과 동시에 다른 음이온들에 비해 높은 선택성을 보여주었다. 추가적으로, 수용액 상에서 PPi, ATP, 그리고 GTP 를 각각 구별해 낼 수 있는 새로운 화학 감지체인 2-2Zn 를 개발하였다. 각각의 인산기를 포함하고 있는 음이온들에 대한 2-2Zn 의 형광 변화는 엑시머 형성에 의한 구조적 변화와 광유도 전자 전달에 의한 소광 현상 등에 기인한다. 2-2Zn 는 PPi 가 첨가되었을 때 약간의 적색 이동을 보였으며, 반면에 ATP 와 GTP 를 넣어 주었을 때에는 각각 형광의 증가와 소광 현상을 보여주었다.

마지막으로, 파이렌을 기반으로 한 유기인산화합물 신경 작용제에 대한 탐지체 3 을 개발하였다. 탐지체 3 은 분자 내의 고리화 반응을 통해 감도 높은 빠른 검출을 보여주었다. 광발광

연구 외에도, DCP 에 대한 전기화학발광 실험 역시 처음으로 수행되었다. 비록 3 차 아민의 산화에 의해 광유도 전자 전달에 의한 소광 효율이 저하되었고, $Ru(bpy)_3^{2+}$와 같은 다른 알려진 전기화학 발광체들에 파이렌의 전기화학발광 효율이 더 낮음에도 불구하고 신경 작용제들에 대하여 높은 감도로 정량 분석이 가능하였다.

Part II 에서는 고리형 이리듐 착물을 기반으로 하여, 작은 음이온들에 대해 높은 선택성을 가진 전기화학발광 화학 정량계의 개발에 대하여 기술하였다. 높은 ECL 효율을 위하여 적절한 HOMO LUMO 에너지 레벨을 보유한 phenylisoquionline 유닛을 이리듐 착물의 주 리간드로 선택하였다.

호모시스테인과의 선택적인 반응 후에 수반되는 전기화학적 과정을 통한 효율적인 발광을 통한 호모시스테인의 전기화학발광 검출을 위하여 합성탐지체 **4** 가 개발되었다. 이리듐 착물의 주리간드에 위치한 포르밀기는 호모시스테인과의 반응을 통해 고리를 형성하여, 이는 탐지체의 열역학적인 특성과 광물리적 특성의 변화를 유발한다. 99.9% 수용액 상에서 호모시스테인의 양은 0−40 μM 의 범위 내에서 선형 상관관계를 보인다. 전기화학적인 연구와 이론적인 연구를 통하여 이러한 결과들의 기작 과정을 규명하였다. 이러한 전기화학발광 분석법은 호모시스테인의 양에 대한 현장진단을 가능하게 함과 더불어 잠재적으로 심혈관 진단에 대한 조기진단에도 활용될 수 있을 것으로 기대된다.

또한 탐지체 **4** 와 호모시스테인 사이의 반응성을 향상시키기 위하여 추가적으로 전자 주는 기로써의 역할을 할 수 있는 메톡시기가 도입된 탐지체 **5** 와 **6** 이 개발되었다. 특히, 탐지체 **5** 는 탐지체 **4** 와 비교하였을 때 보다 빠른 반응 시간, 더 높은 감도,

그리고 더 높은 발광 증가 비율을 포함한 향상된 성능을 보여주었다. 탐지체 5 에 존재하는 메톡시기는 호모 에너지 레벨을 불안정하게 만들고, 이는 반응 속도의 증가와 초기 화학발광의 완전한 소광을 유발한다. 탐지체 4 에 비해 15 배 정도 낮은 검출 한계와 1.9 배 정도 더 빠른 반응 속도를 보여주었다. 본 연구는 추가적인 치환체를 통하여 에너지 레벨을 조절함으로써, 이리듐 착물을 기반으로 하는 높은 감도와 반응성을 보이는 탐지체를 개발하기 위한 새로운 전략을 제시해 준다.

다음으로, 시안화 이온에 대한 이리듐 착물 기반의 전기화학 탐지체 7 이 고안되어 합성되었다. 탐지체 7 은 페닐 이소퀴놀린를 주 리간드로 하였으며, 시안화 이온에 대한 반응 자리로써 다시안화비닐기를 도입하였다. 시안화 이온이 존재할 때에 선택적으로 탐지체 7 의 붉은 빛의 전기화학발광이 크게 증가하였다. 10 uM 농도의 탐지체 7 은 수용액 상에서 0–0.4 mM 의 범위에서 선형 상관관계를 보여주었다. 또한 표준 첨가법을 통하여 실제 수돗물 내의 시안화 이온의 양을 높은 신뢰성과 재현가능성을 수반하여 정량적으로 분석하는 데에 성공하였다. 또한 이론적인 연구를 통하여 분자의 호모/루모 에너지 레벨과 전자 분포를 예측함으로써 탐지체를 합리적으로 고안하고 기작을 규명하였다.

마지막으로, 황화 이온에 대한 선택적인 센싱을 위해 이리듐 착물 8 을 개발하였다. 탐지체 8 은 불포화 아크릴산에스터와 디나이트로벤젠설포닐(DNBS)기의 두 가지 종류의 반응 자리를 가지고 있다. 불포화 아크릴산에스터 유닛은 황화 이온과 선택적으로 반응하여 청색 이동된 영역에서의 인광과 전기화학발광의 증가를 유발한다. 게다가, DNBS 그룹은 황화 이온과 다른 바이오티올과 반응하여 끊어지는 것으로 잘 알려져 있는 광유발 전자 전달 소광체이다. 탐지체 8 은 한 분자에 두 가지

반응 자리를 도입함으로써 높은 감도와 좋은 선택성을 동시에 보여주었다. 이러한 전기발광기반의 검출방법은 질병의 조기진단을 검사하기 위한 현장진단용 설비를 개발하는 잠재적인 도구가 될 수 있을 것으로 기대한다.

파트 III 에서는 루모 레벨을 조절함으로써 이리듐 기반의 전기화학발광 탐지체를 개발하고 그 기작과정에 대한 연구를 진행하였다. 발광체의 루모 레벨은 ECL 효율과 밀접한 연관성을 가지고 있기 때문에, 분석물에 대한 특정 반응 자리를 통하여 루모 레벨을 조절함으로써 형광 화학센서를 개발하는 방법과는 차별화된 방식으로 ECL 화학센서를 개발하는 것이 가능하다. 우리는 $(ppy)_2Ir(acac)$ 착물을 기본으로 하여 phenylpyridine 에 다양한 부분에 특정 치환체를 도입하여 화학 센서를 개발하고자 하였다.

먼저, 포르밀기를 포함하고 있는 ppy 기반의 3 종류의 이리듐 착물을 개발하였다. 피리딘 고리에 존재하는 포르밀기는 루모 레벨을 강하게 안정화시키며, 추가적으로 도입한 치환기를 통하여 호모-루모 에너지 차이를 유지한 상태에서 에너지 레벨의 수치를 조절하고자 하였다. OMe-acac 착물은 광발광과 전기화학발광에서 다른 신호 변화를 보여주었다. 광발광에서는 명백한 파장대의 변화를 보여준 반면에 전기화학발광에서는 오히려 신호가 감소하는 경향을 보여주었다. 배위되어 있는 이리듐 금속에 대하여 메타 위치에 위치한 전자 주는 기인 메톡시기가 호모, 루모 에너지 레벨을 불안정화 시키며, 이는 전기화학발광 과정에서의 들뜬 상태의 형성을 힘들게 만든다. H-acac 과 Br-acac 착물의 경우 상대적으로 안정화되어 있는 루모 레벨로 인하여 광발광과 전기화학발광에서 비슷한 결과를 보여주었다. 다음으로, 과산화수소에 대한 반응 자리로써 보로네이트기를 다양한 위치에 도입한 이리듐 착물들을 개발하였다. 탐지체 **9** 와 **11** 은

과산화수소를 넣어 주었을 때 노란색에서 녹색으로의 인광 변화를 보였으며, 반면에 탐지체 10 은 같은 조건에서 반대로 녹색에서 노란색으로의 인광 변화를 보여주었다. 탐지체 12 는 9, 11 과 비슷한 인광 변화를 보여주었다. 하지만, 탐지체 9-11 이 벤젠 고리를 변형함으로써 호모 레벨을 중점적으로 변화시킨 것에 비해 탐지체 12 는 피리딘 고리의 변형을 통한 루모 레벨의 변화를 유도하였다. 이러한 과산화수소를 넣어줌에 따른 탐지체 12 의 루모 레벨의 불안정화는 전기화학발광 전자 전달 과정을 방해함으로써 전기화학발광 효율의 저하를 유도하였다. 즉, 탐지체 12 의 전기화학발광 세기는 과산화수소의 첨가에 따라 극적으로 감소하였으며, 광발광 실험에서 비슷한 결과를 보여주었던 탐지체 9-11 과 차별화되는 결과를 보여주었다. 이러한 연구를 통해 일반적인 광발광 탐지체의 개발 방법과 차별화되는, 루모 레벨의 조절을 통한 전기화학발광의 소광에 의한 탐지체를 합리적으로 고안하고 개발할 수 있는 방법을 제시하였다.

주요어: 전기화학적 발광 (ECL), 환형 이리듐 착물, 화학센서, 키모도지미터, 호모시스테인, 시안화 이온, 황화 이온, 과산화수소

감사의 글

2004 년 서울대학교 화학부에 처음 입학하고, 2008 년 대학원에 석박사 통합과정으로 다시 입학한 이래로 참 오랜 세월을 서울대학교에서 지내는 동안, 정말 좋은 사람들을 많이 만난 것 같습니다. 학문적인 조언을 아끼지 않으신 분들도 많았고, 특히 제가 정말 마음이 힘들고 어려웠을 때 옆에서 힘이 되어주고 많은 위로가 되어 준 수많은 어르신 분들과 선후배님들, 그리고 항상 함께 해 준 학부 동기들이 없었다면 절대로 지금처럼 웃는 모습으로 그 어려움들을 이겨낼 수 없었을 것이라고 생각합니다.

먼저, 항상 저와 함께 해 주시는 하나님께 감사드립니다.

대학 생활 내내 부족한 제자를 따뜻하게 지도해 주신 홍종인 교수님께 진심으로 감사드립니다. 학문적인 부분 뿐만이 아니라 신앙적으로도 저의 영적 스승이 되어 주시고 하나님을 알게 해 주셔서 감사합니다. 제가 가장 힘든 시절에 소중한 조언과 기도를 아끼지 않으셨던 김난주 사모님께도 감사드립니다. 또한, 부족한 제 학위 논문을 심사해 주신 정영근 교수님, 박승범 교수님, 이동환 교수님, 그리고 숭실대 신익수 교수님께도 머리 숙여 감사 드립니다.

내가 가장 사랑하는 우리 현주, 널 생각하면 아직도 난 눈에서는 눈물이 나고 한편으론 입가에 미소가 지어진단다. 마지막 순간까지 나에게 진짜 사랑이 무엇인지 알려줘서 정말 고마워. 오빠가 좋은 논문도 내고 졸업도 하는 모습을 제발 죽기 전에 좀 보고 싶다고 그렇게 이야기 했었는데, 오빠가 많이 부족해서 우리 현주 하늘 나라로 가고 나서야 이렇게 논문도 내고 졸업도 하게 되어서 너무 미안해. 그래도 하늘에서 오빠 졸업하는 모습 지켜보면서 누구보다도 더 축하해 줄 거라고 믿는다. 너의 마지막 말처럼 오빠 앞으로 언젠가 현주만큼 좋은 사람도 만나고 보란 듯이 행복하게 잘 살 수 있도록 최대한 노력할게. 많이 보고 싶다. 사랑해.

지금은 실험실을 떠나 쉽게 만날 수 없는 실험실 선배님들, 제가 점점 나이를 먹고 실험실 연차가 찰수록 형님들이 얼마나 그리웠는지 모릅니다. 제 영원한 사수이신 세원이형, 지금은 중국에 계신 우리 경식이형, 술친구 우철이형, 순영이형 재한이형 명기형 종철이형.. 민선 누나, 학부 동기 미애, 실험실 동기 아름이, 다들 잘 지내고 있나 모르겠네. 한분 한분 다 너무 고맙고 보고 싶습니다.

이제는 김교수님이 되신 김성현 박사님, 뱅뱅사거리 대지주 혜영누나, 따뜻한 마음을 가진 동남이형, 선배이자 후배인 새신랑 상욱이형, 어느새 EL 팀의 독보적인 리더가 된 성진이형, 교수님이 직접 인정하신 실험실 공식 애처가 홍철이형 모두들 실험실의 든든한 버팀목들이 되어주셔서 감사합니다. 영원한 04 동기 서영이, 영원한 실험실 운전 기사 동욱이, 항상 고마운 우리 진록이, 든든한 교회 동생 김광명 방장님, 언제나 열심인 재규, 모두들 좋은 결과 있었으면 좋겠습니다. 저보다 먼저 실험실을 나간 석사 후배들 유나, 지연이, 진희, 화용이, 두희형 덕분에 너무 즐거웠고 고마웠습니다.

부족한 선배 밑에서 일하느라 항상 힘들었던 우리 ECL 팀 후배들도 다들 잘됐으면 좋겠습니다. 함께 졸업하는 맏언니 서연이부터 하스스톤은 못하지만 실험은 점점 잘하는 우리 경록이, 유학파 통역병 하영이, 그리고 왠지 벌써 말년차의 포스가 느껴지는 유겸 아빠 태민이까지 참 착하고 성실한 사람들만 우리 팀으로 들어오게 된 것이 얼마나 큰 행운인지 모릅니다. 다들 행복하고 좋은 결과가 있었으면 좋겠습니다.

우리 영남이랑 우리 동선이, 한참 차이나는 늙다리 선배랑 커피도 자주 마셔주고 때로는 말벗도 되어줘서 진심으로 고맙다. 덕분에 말년이 참 즐거웠던 것 같아. 실험적으로도, 그리고 그밖의 외적인 부분에서도 항상 좋은 일만 가득하길. 새로 들어온 신입생들 준호랑 태훈이도 아직 많은 이야기를 나누진 못했지만 실험실 생활 잘 적응하고 멋진 대학원 생활 이어 나갔으면 좋겠다.

마지막으로, 사랑하는 우리 가족들. 할머니, 아빠, 엄마, 그리고 누나에게 가장 큰 감사의 말을 전하고 싶습니다. 항상 과분한 사랑을 주시는 데에도 그 사랑에 보답하지 못하는 것 같아서 항상 죄송한 마음 뿐입니다. 그래도 가족들이 있었기에 지금까지 이렇게 열심히 공부하고 바르게 살아올 수 있었던 것 같습니다. 졸업 후에도 항상 바르고 정직하고 성실하게 살아서 남부럽지 않은 자랑스러운 손자, 아들, 동생이 될 수 있도록 노력하겠습니다.

2017 년 2 월

김훈준 드림